Conception and detection of exotic quantum matter in mesoscopic systems

Dissertation zur Erlangung des naturwissenschaftlichen Doktorgrades der Julius-Maximilians-Universität Würzburg

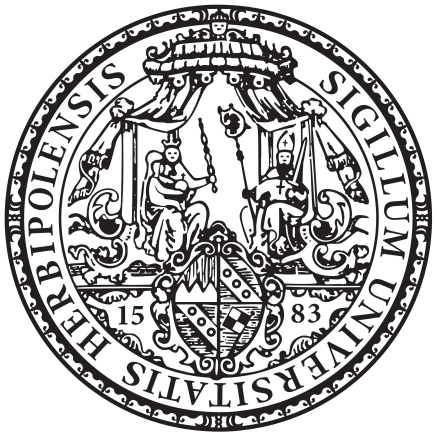

vorgelegt von

Christoph Thomas Fleckenstein

aus Marktheidenfeld

Würzburg 2020

Eingereicht am: .....
bei der Fakultät für Physik und Astronomie

1. Gutachter: .....
2. Gutachter: .....
3. Gutachter: .....
der Dissertation

Vorsitzende(r): .....

1. Prüfer: .....
2. Prüfer: .....
3. Prüfer: .....
im Promotionskolloquium

Tag des Promotionskolloquiums: .....

Doktorurkunde ausgehändigt am: .....

What you get can never be more worthy than how you get there

Niccoló Traverso Ziani
– discussion about democracy –

Zusammenfassung

In der vorliegenden Arbeit untersuchen wir Nanobauteile auf der Basis von topologischen Isolatoren. Diese neue Materialklasse zeichnet sich in erster Linie durch ein isolierendes Inneres aus, während gleichzeitig die Oberfläche leitende Eigenschaften besitzt. Zustände, welche mit diesen leitenden Eigenschaften in Verbindung gebracht werden, können in niedrigster Ordnung durch eine Dirac-Theorie beschrieben werden. Im Falle eines zweidimensionalen topologischen Isolators impliziert das, zusammen mit Zeit-Umkehr Symmetrie, eine helikale Natur dieser Randzustände. Interessante Physik entsteht dann insbesondere, wenn zwei solcher helikalen Randkanalzustände in einer Verengung zusammengeführt werden. Dies hat verschiedene Konsequenzen. Innerhalb der Verengung findet man die gleiche Anzahl an fermionischen Feldern wie man sie auch in einem Quantendraht erwartet. Gleichzeitig besitzt eine solche Konstruktion aber mehr Symmetrien verglichen mit gewöhnlichen Quantendrähten. Außerdem kann eine Verengung in einem zwei-dimensionalen topologischen Isolator auf natürliche Weise helikal kontaktiert werden, so dass spin-aufgelöste Transportmessungen durchgeführt werden können. Diese einzigartige Kombination von Eigenschaften impliziert verschiedenste physikalische Effekte. Wie wir in dieser Arbeit zeigen entsteht in engen Schlitzen, welche in einen homogenen zwei-dimensionalen topologischen Isolator tranchiert werden, eine topologisch supraleitende Phase mit nicht-Abelschen Majorana Moden an den Systemrändern. Diese exotischen Teilchen können mit einem relativ einfachen Transportexperiment nachgewiesen werden, indem man diesen sogenannten Anti-Quantendraht schwach mit einem helikalen Randkanal koppelt und dort die Transportcharakteristiken misst. Die Präsenz von Majorana Moden ist verknüpft mit dem Entstehen von unkonventioneller Supraleitung, insbesondere von sogenannter *odd-frequency* Supraleitung. Wir zeigen, dass dies vielmehr eine allgemeine Erscheinung in derartigen supraleitenden Strukturen ist. Symmetrien sind von elementarer Bedeutung für viele physikalische Effekte. So führt zum Beispiel die natürlich auftretende Ladungs-Konjugation Symmetrie zusammen mit einem zeit-periodischen elektromagnetischen Feld in topologischen Anti-Quantendrähten zu einer topologischen Floquet Nichtgleichgewichts-Phase, welche wiederum durch Transportmessungen detektiert werden kann. Symmetrien spielen auch und insbesondere für Wechselwirkungseffekte eine wichtige Rolle. Hier ist besonders die Existenz eines Dirac-Punktes von großer Bedeutung. In dessen (energetischer) Nähe ist es möglich wechselwirkungs-induzierte Bandlücken zu erzeugen. Anders als Einteilchen-Bandlücken können wechselwirkungs-induzierte Bandlücken zu einer hohen Grundzustandsentartung führen. Diese wiederum ermöglicht die Entstehung komplexer nicht-Abelscher Teilchen, falls zusätzlich supraleitende Ordnung vorhanden ist. Interessanterweise können derartige Vielteilchen-Bandlücken in unserem System schon bei nur schwacher elektronischer Wechselwirkung auftreten. Dieses untypische Verhalten ermöglicht letztendlich die Entstehung von $\mathbb{Z}_4$ parafermionen an Grenzflächen unterschiedlicher Ordnung.

Summary

In this thesis we discuss the potential of nanodevices based on topological insulators. This novel class of matter is characterized by an insulating bulk with simultaneously conducting boundaries. To lowest order, the states that are evoking the conducting behavior in TIs are typically described by a Dirac theory. In the two-dimensional case, together with time-reversal symmetry, this implies a helical nature of respective states. Then, interesting physics appears when two such helical edge state pairs are brought close together in a two-dimensional topological insulator quantum constriction. This has several advantages. Inside the constriction, the system obeys essentially the same number of fermionic fields as a conventional quantum wire, however, it possesses more symmetries. Moreover, such a constriction can be naturally contacted by helical probes, which eventually allows spin-resolved transport measurements.

We use these intriguing properties of such devices to predict the formation and detection of several profound physical effects. We demonstrate that narrow trenches in quantum spin Hall materials – a structure we coin anti-wire – are able to show a topological superconducting phase, hosting isolated non-Abelian Majorana modes. They can be detected by means of a simple conductance experiment using a weak coupling to passing by helical edge states. The presence of Majorana modes implies the formation of unconventional odd-frequency superconductivity. Interestingly, however, we find that regardless of the presence or absence of Majoranas, related (superconducting) devices possess an unconventional odd-frequency superconducting pairing component, which can be associated to a particular transport channel. Eventually, this enables us to prove the existence of odd-frequency pairing in superconducting quantum spin Hall quantum constrictions. The symmetries that are present in quantum spin Hall quantum constrictions play an essential role for many physical effects. As distinguished from quantum wires, quantum spin Hall quantum constrictions additionally possess an inbuilt charge-conjugation symmetry. This can be used to form a non-equilibrium Floquet topological phase in the presence of a time-periodic electro-magnetic field. This non-equilibrium phase is accompanied by topological bound states that are detectable in transport characteristics of the system. Despite single-particle effects, symmetries are particularly important when electronic interactions are considered. As such, charge-conjugation symmetry implies the presence of a Dirac point, which in turn enables the formation of interaction induced gaps. Unlike single-particle gaps, interaction induced gaps can lead to large ground state manifolds. In combination with ordinary superconductivity, this eventually evokes exotic non-Abelian anyons beyond the Majorana. In the present case, these interactions gaps can even form in the weakly interacting regime (which is rather untypical), so that the coexistence with superconductivity is no longer contradictory. Eventually this leads to the simultaneous presence of a $\mathbb{Z}_4$ parafermion and a Majorana mode bound at interfaces between quantum constrictions and superconducting regions.

Contents

1 Introduction and Motivation

The 19th and 20th century were mainly dedicated to the formation of functional industrial societies. With the end of the cold war and ideology induced distortions, this development came to its contemporary summit. Nowadays, societies undergo a similar transformation as in the 19th century. However, rather than changing from a hierarchical to an industrial society, the change happens from an industrial to an information based society. In such a post-industrial society, information eventually becomes the source and currency of economical and political power. Although, there is currently no universally accepted definition of the term information society, it is clear that it comes along with an economical and cultural transition. For the American sociologist Daniel Bell, the informational character of an society is strongly correlated to the number of employees involved in the creation of non-tangible goods. Alain Touraine, research director at the École des Hautes Études en Sciences Sociales in Paris, went beyond that already in 1988 by recognizing that "industrial society had transformed the means of production: post-industrial society changes the ends of production, that is, culture.". What he meant by that becomes clear nowadays. A rapidly increasing number of aspects of modern human life as well as their framing societies are based on the availability and processing of information by intelligent machines. A prominent example of which is the smart phone. Rather than just being an industrial product, with approximately 3.5 billion smartphone users around the globe, it has already become a cultural good, redefining communal life.
An even more profound ongoing cultural change, accompanied with the transformation towards the information society, is the shift of authorities from humans to machines and the development of artificial intelligence. With access to huge pools of information, machines are able to take measured decisions much better than humans. Giving decisional power to machines carries enormous potential, such as for autonomous driving, just to name the tip of the iceberg. Artificial intelligence, constructed from information based learning algorithms, is already able to outperform humans in various disciplines ranging from complex games, such as chess or Go, over image recognition to comprehension and translation of languages. The application list of artificial intelligence and machine learning is long and does not seem to find an end soon. Recently, even applications in theoretical physics have been revealed [CT17].
Processing huge amounts of information is at the heart of all of these 21st century technologies. Progress is therefore fundamentally based on the continuous improvement of hardware components necessary for computations – integrated circuits –. They are built from transistors, clustered to form logical gates on a semiconductor plate, typically called chip. In 1965, G. Moore proposed that the transistor count – the number of transistors that can be placed on a single chip – would double each two years [Moo69]. Together with the so-called Dennard scaling, which proposes constant power density of metal oxid semiconductor field-effect-transistors (MOSFETs), this lead to the anticipation of a chip

performance doubling every 18 months [DGY$^+$74]. Over more than three decades, this anticipation turned out to be roughly correct and chip producers were able to keep up this pace of chip improvement. Around the year 2006, however, Dennard scaling ended. The primary reason for this breakdown is the problem related to the dissipation of waste heat, generated during computations. With an ongoing growing transistor count, more and more transistors are condensed on a single chip and leakage currents threat a "thermal runaway" of the chip. The temporary solution found by chip producing companies to continue the performance scaling of their chips was the development of multi-core processors with still increasing transistor count per core. However, it is obvious that Moore's law can not be continued forever, but will terminate at a natural barrier set by the length scale on which quantum effects render conventional transistors ineffective. This barrier is expected to be hit already within the next decade [Wal16]. Then, the only (conventional) way of improving the computational power of chips, i. e. to use more logical elements, is to increase the area of the chip and thus, eventually also the power consumption. Today, 7% of globally produced electricity is dedicated to computations [ABC17b]. This number is expected to raise up to 13% already within the next decade. The end of Moore's law will even accelerate this development and, in a pessimistic scenario, progress will be substantially slowed down and eventually come to a halt.
Avoiding this scenario to eventuate, new technologies beyond the conventional architecture of the chips have to be explored. This might be achieved by the use of novel materials, such that waste heat production can be significantly reduced and Dennard scaling is regained, or by changing the paradigms of computing as a whole towards *quantum computation*. In a quantum computer, unlike a classical computer, information is stored and processed via qubits, the elementary unit consisting of a generic physical two-level system with states $|0\rangle$ and $|1\rangle$. In contrast to classical computers, quantum computers use entanglement and superposition to perform calculations. By means of that, many quantum algorithms exceed the calculation scope of classical computers by orders of magnitude – a property often coined *quantum supremacy* [BIS$^+$18]. Recently, a very important step towards a generic quantum computer was taken: Google announced to have reached quantum supremacy for the very first time [AAB$^+$19]. With a quantum processor containing 54 superconducting qubits, they solve a task in 200 seconds which would keep the fastest classical supercomputer occupied for around 10000 years to finish. Although, the task itself – producing random numbers – is not particularly useful, it impressively demonstrates that quantum computation is in principle possible and not spoiled by any unknown physical laws. However, for a practically useful quantum computer, that can implement the important quantum algorithms, such as Shor's code [NC00], several obstacles remain to be overcome. They include practical ones, as for instance how to engineer an universal set of gates or how to initialize qubits effectively, but also theoretical ones, such as how to overcome quantum decoherence. Suppressing quantum decoherence typically means to isolate the system from its environment as the main source of decoherence. Perfect isolation is however an illusion and, hence, time-consuming tasks might always be corrupted by decoherence. This problem might be resolved by an alternative approach to quantum computing – *topological quantum computation* [Kit03, NSS$^+$08].
Topological quantum computing uses profound properties of particles called anyons. Anyons are particles that do neither reflect the statistical properties of fermions nor the ones of

bosons, but constitute a third class of particles, strictly defined only in two spatial dimensions. The reason for this restriction is fundamental: 2D systems are peculiar in the sense that the winding of particles around each other is well defined, which is not the case in a three-dimensional system (or higher), where closed trajectories of particles can always be continuously deformed to a point without cutting through other particles [LM77, Wil82a]. This peculiarity of 2D systems eventually allows exotic statistics of emergent particles. The idea of statistics ranges among the fundamental concepts of quantum physics. It emerges from the properties that can be attached to particle wave functions. Under looping one particle around another in a fixed manner (clockwise or counterclockwise), the wave function eventually has to return to its original form up to phase 2θ. In three spatial dimensions, by the topological reasons pointed out above, $\theta = 0, \pi$, which results in two types of particles (statistics): bosons ($\theta = 0$) and fermions ($\theta = \pi$). In 2D, where the winding of particles around each other can be tracked, the statistical angle θ can in principle take any value, which is why the corresponding particles are called anyons [Wil90]. However, not all anyons are useful for topological quantum computations. In particular, *non-Abelian anyons* are desired [NSS$^+$08, Ste08, DSFN15]. Non-Abelian anyons, unlike their Abelian counterparts, live in a degenerate Hilbert space. This has crucial consequences: When a non-Abelian particle is looped around another one, due to the degenerate Hilbert space in which the particles live, the state of the system is not required to return to its initial state, rather it can terminate in any of the states of the degenerate subspace. Thus, the process of looping a non-Abelian particle around another one is mathematically described by an unitary transformation. Notably, up to an (unimportant) Abelian phase, such transformations only depend on the topology of the path taken [WZ84]. The idea behind topological quantum computing is to construct quantum gates out of these unitary transformations. Since this involves adiabatic particle exchange, it is typically coined *braiding* [ZR99, NSS$^+$08]. The outstanding advantage of topological quantum computing is already stated above. For a given configuration of non-Abelian anyons, the resulting state after performing the computation, i. e. after performing braiding operations, does not depend on the details, but only on the topology of the path taken during particle exchange. Hence, computations experience a topological protection at the quantum level. This protection persists as long as the only way of non-trivial unitary evolution (from one degenerate state to another) is a braiding operation and all perturbations on the system have vanishing matrix elements among the different degenerate states.

Fueled by their possibly immense potential for applications in quantum computation, since their first conception in the early eighties, non-Abelian anyons aroused increasing interest. This was especially supported by proposals of non-Abelian states in feasible physical systems, such as fractional quantum Hall systems at filling factor of $\nu = 5/2$ [MR91, LP93, Wen91]. With a mapping to $p_x + ip_y$ SCs, the anyonic states in this system were identified as Ising anyons [GWW91, GWW92, RR96, NW96, RG00] with non-trivial braiding relations [DSFN05]. Subsequently, also other systems, such as Sr_2RuO_4 [DSNT06], $p_x + ip_y$ superfluids of cold atoms [GRA05, TDSN$^+$07] or the A phase of ^{3}He films [Vol94], were proposed to be possible candidates for the realization of $p_x + ip_y$ SCs, hosting non-Abelian states. In particular, it was recognized that Ising anyons constitute topological defects in such kind of superconductors, consequently coined *topological superconductivity*. This terminology obtained an extra flavor with the seminal work by

Kitaev [Kit01], where he proposed the formation of isolated and topologically protected Majorana zero modes in a simple, though rather artificial 1D model, which paved the way for the search of anyons in 1D systems. Some years later, his idea turned out to find application in several physical systems, such as magnetic chains on top of s-wave SCs [NPDBY13, PGvO13, LCD$^+$14] or semiconductor nanowires including SOC with proximity induced superconductivity under the influence of magnetic fields [ORvO10, LSDS10, STL$^+$10, SLTDS10]. The field obtained a boost in 2012, when signatures of Majoranas were announced to be seen in related systems [MZF$^+$12]. Although, a whole pool of possible transport signatures are predicted for Majoranas, ranging from electric-conductance [LLN09, WADB11, PSJA12], noise [BD07, LCL15, Bee15, HBvOO15], thermal conductance [WAM$^+$10, ADH$^+$11, SH16], and ac-Josephson effect [JPA$^+$11, SJPA12, PN12], a conclusive proof for the non-Abelian nature of these low-energy BSs is still missing. Especially, one source of confusion is the discrimination between trivial-Andreev BSs and topological Majorana modes [KMB12, FDTZT18, MST18]. In principle, however, although experimental challenging, topological qubits could be formed from nanowire T-junctions [AOR$^+$11, AHM$^+$16a] and employed for topological quantum computations. Braiding would then be implemented by moving around Majorana modes, either physically, or by a selective changing coupling parameters [SCT11, KPRvO15].
Certainly, 1D topological superconducting systems are just one way to engineer non-Abelian excitations. Other promising ideas are based on more "synthetic" constructions, i. e. combining materials (with maybe contradictory properties) to find interesting effects at their interfaces. Especially, with the advent of TIs [KM05a, KM05b, BHZ06, FKM07, FK07, MB07, KWB$^+$07, KBM$^+$08, Roy09, HXQ$^+$09, XQH$^+$09, KDS11, SND$^+$14, RLD$^+$17], this approach found a new playground. TIs are a class of matter which is characterized by an insulating bulk and metallic edges. They can be classified by topological invariants, depending on the symmetry class of the system [AZ97, Zir96, CTSR16]. For 2D TIs, the presence of edge states can be understood by means of a band-inversion as for instance in quantum wells formed from HgTe/CdTe layers. By virtue of SOC, the edge states of 2D TIs possess helical nature, that is, states with opposite moving direction carry orthogonal spin. This intriguing property, together with their (to good approximation) linear dispersion, allows for a description in terms of a 1D Dirac theory. Kinked mass terms can hence lead to non-trivial BSs [JR76]. In that way, Josephson junctions [FK09, BHM11, HMBG13], but also hetero-junctions built from a ferromagnet and a s-wave SC [Ali12, Bee13], based on a 2D TI, can synthesize a Majorana Kramers pair, Majorana BS, respectively. Interestingly, edge theories can also be particularly useful when it comes to the formation of more complex non-Abelian anyons beyond Majoranas. At the helical edge, interaction induced mass terms can gap out the spectrum in the case of strong interactions [ZK14]. In a hetero-junction with proximity induced s-wave superconductivity, this generates a fourfold ground state degeneracy, enabling the formation of symmetry protected $\mathbb{Z}_4$ parafermions [KYL14, OTMS15]. Similar ideas can be applied to fractional quantum Hall edge states, where the resulting parafermions are topologically protected, but the coexistence of very strong magnetic fields and SCs is required [LBRS12, CAS13, AF16], or even to systems of quantum wires [KL14].
From a theoretical perspective, the concepts introduced above are extremely rich, however many are not experimentally feasible. The vision of a topological quantum computer

rests, on one side, on our understanding of these exotic particles, but certainly also on the accessibility and feasibility of these concepts for experiments. It is therefore of significant importance to find the right frames, ideally connecting the intriguing physics with measurable signatures. This thesis is dedicated to address this task.
Motivated by the developments in the field, we briefly discuss problems in current proposals for the realization of topological superconductivity in nanowires for the formation and detection of the constituent Majorana modes [FDTZT18]. We demonstrate that an alternative realization based on QSH trenches is able to overcome detection problems of Majorana modes by virtue of an unambiguous transport signature when coupled to adjacent helical edge states [FTZCT20]. Related systems, namely superconducting QCs on the basis of a QSH insulator, can exhibit even more exotic particles: When interactions are included, $\mathbb{Z}_4$ parafermions can emerge. While typically, those particles can only form in the case of very strong electron-electron interactions, in our system they are even present for moderate interactions [FTZT19]. Interestingly, recent experiments indicate the presence of such interactions in related nanodevices [SWF$^+$20]. The full comprehensiveness of QSH QCs is certainly not only restricted to the formation of non-Abelian anyons, but extends over various other related topics, such as odd-frequency superconductivity [FZT18], or Floquet topology [FZP$^+$20].
The thesis is organized as follows: In Chap. 2 we give a general overview of the physical concepts that are used throughout the thesis. In particular, we investigate the theory of non-Abelian anyons starting from first principles. We discuss how non-Abelian particles naturally emerge in degenerate 2D quantum theories and derive their intriguing properties. In addition, we outline the abstract formulation of anyon theories and their application to topological quantum computation. Subsequently, we focus on more concrete cases and discuss explicit condensed matter models that serve as hosts for non-Abelian anyons. Towards the end of Chap. 2, we focus on the relation of these particles to exotic types of superconducting pairing. In Chap. 3, we review the fundamental methods that are used in subsequent chapters. We study the theory of Luttinger liquids, describing interacting 1D systems of fermions. We derive all fundamental relations, starting from the formulation of bosonic fields up to the description of spinful Luttinger liquids. Additionally, we inspect RG theory applied to sine-Gordon models. Subsequently, we continue with scattering theory, Green functions in linearly dispersed systems and non-stationary Floquet theory. Chap. 4 is dedicated to the results of the thesis. First, we briefly analyze limiting factors in quantum wires, which are proposed to serve as platform for exotic quantum matter. Next, we move on with the description of QSH QCs, where we demonstrate that such structures might be interpreted as symmetry enriched quantum wires. We investigate the formation of topological superconductivity in QSH anti-wires as well as transport signatures that prove the existence of Majorana end modes. Thereafter, we study the formation and detection of odd-frequency superconductivity in related systems. This is followed by the discussion of Floquet topology. We conclude the chapter examining carefully the formation of $\mathbb{Z}_4$ parafermions in a hetero-junction formed from SCs in combination with an interacting QSH QC. Eventually, we discuss the influence of interactions in recent experiments performed on QSH QPCs. In Chap. 5 we give a summary of all results together with a brief outlook on interesting open questions. Throughout the thesis we use $\hbar = 1$.

2 Non-Abelian anyons

Resolving the elementary constituents of matter is among the most elementary challenges of physics. With the development of quantum mechanics, our understanding of matter experienced a radical change. The quantum mechanical view on the world is basically determined from a handful of fundamental rules, derived from elementary principles. Quantum statistics is at the heart of this paradigmatic change. In three spatial dimensions, it distinguishes two fundamental classes of particles on the basis of simple symmetry arguments. Imagine to have two identical quantum mechanical objects described by a TP wave function $\psi(\mathbf{r}_1, \mathbf{r}_2)$, where $\mathbf{r}_1$ and $\mathbf{r}_2$ represent the positions of particle 1 and 2 in space. Under an exchange of particle 1 and 2 in a, say, counterclockwise manner, the wave function, due to indistinguishability of particle 1 and 2, can only change by a phase, such that the probability density remains unchanged

$$\psi(\mathbf{r}_2, \mathbf{r}_1) = e^{i\theta}\psi(\mathbf{r}_1, \mathbf{r}_2).$$

In a second counterclockwise exchange, along the same line of reasoning, the wave function is required to return to its initial form up to a phase of 2θ

$$\psi(\mathbf{r}_1, \mathbf{r}_2) \to e^{2i\theta}\psi(\mathbf{r}_1, \mathbf{r}_2).$$

In a three dimensional world, the closed loops that the particles have performed undergoing the above exchange processes can always be disentangled and continuously (i. e. without cutting or gluing the world-lines) shrinked to points. Then, obviously, the wave function after the exchange processes cannot be different from the initial wave function, which restricts θ to only two possible values: $\theta = 0$ or $\theta = \pi$, corresponding to bosons and fermions. Numerous (even daily-life) phenomena rest on this simple symmetry property of wave functions in three spatial dimensions. For fermions, it implies the Pauli principle, which eventually explains the existence of metals and ferromagnets [Lan57b, Lan57a, Sto39]. In the case of bosons, it leads, for instance, to superfluidity and superconductivity or Bose-Einstein condensates [Ein24, BCS57, Vol94]. In two spatial dimensions, however, the situation is dramatically different. The notion of one particle wrapping around another one obtains a fundamental new meaning as loops cannot be contracted to points without cutting and gluing. Therefore, winding can be well defined and the state of system is not required to return to its initial form, but is allowed to change by a non-trivial phase. If this phase θ is not 0, nor π, but *any* other value, the particle is coined *anyon* [Wil82a].

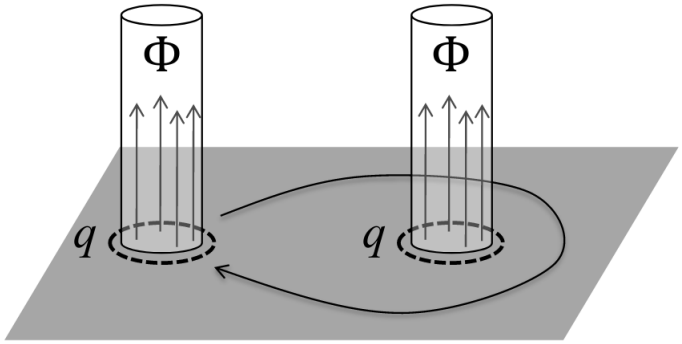

Figure 2.1: Anyons as charge-flux composites: A charge q is bound to a flux, confined to a tube. Reprinted figure from Ref. [LP17].

2.1 Basic concepts

Of course, the formation of anyons requires special conditions and not every particle, which is constrained to live in a 2D world, is a priori an anyon. The notion of anyons can be illustrated by means of a simple toy model [Wil82b, LP17].

Consider a composite particle, built from a charge q which is attached to a locally confined flux Φ (Fig. 2.1). When one such particle encircles another, by virtue of the Aharonov-Bohm effect, the wave function of the system acquires a phase of $e^{2iq\Phi}$ [AB59]. Since the flux is confined to a solenoid, as long as the composite particles do not merge, this phase factor is independent of the specific local details of the path. The exchange statistics is hence described by $R = e^{iq\Phi}$. Especially, for $q\Phi \neq n\pi$ with $n \in \mathbb{Z}$, which might be realized by either fractional charge or fractional flux, these composite particles are anyons, in particular, *Abelian* anyons. The term Abelian relates to the fact that the transformation, describing the exchange process (i. e. R), is a $U(1)$ operation. On the other hand, if the exchange is described by a $U(N)$ operation (with $N > 1$), the corresponding anyons are coined *non-Abelian* as different $U(N)$ operations do not necessarily commute. We will see throughout the next sections that such a $U(N)$ operation is obtained for an exchange of particles in the presence of degeneracies. The best approach to this is to extend our notion of flux. In the above toy model, a magnetic flux was generated by virtue of an electro-magnetic vector potential $\mathbf{A}$

$$\Phi = \oint_{\partial S} \mathrm{d}l\mathbf{A} = \int_S \mathrm{d}\mathbf{S}\ \nabla \times \mathbf{A},$$

where the integral runs over the surface ∂S, the area S of the solenoid in Fig. 2.1, respectively. In the context of the toy model, the flux is therefore a very basic example of a geometric phase (it is acquired along a path due to the presence of $\mathbf{A}$). In a more abstract, though similar way, geometric phases can appear as the "flux" of an abstract vector potential generated for a closed path. This concept of geometric phases was first recognized by Micheal Berry [Ber84, Sim83].

2.2 Abelian and non-Abelian Berry phases

Consider a generic non-degenerate Hamiltonian $H(t)$, subject to the time dependent Schrödinger equation, with the system being in the state $|\psi(t)\rangle$

$$H(t)|\psi(t)\rangle = i\partial_t|\psi(t)\rangle. \tag{2.1}$$

The Hamiltonian is furthermore expected to vary slowly enough such that the adiabatic theorem holds for every point in time [BF28]. We can expand the state of the system in terms of instantaneous eigenstates $|n(t)\rangle$, that satisfy $H(t)|n(t)\rangle = E_n(t)|n(t)\rangle$

$$|\psi(t)\rangle = \sum_n c_n(t)|n(t)\rangle e^{-i\phi_D^n(t)}$$

with the expansion coefficients c_n. n runs over all instantaneous eigenstates and $\phi_D^n(t) = \int_{t_0}^t \mathrm{d}\tau E_n(\tau)$ is a dynamical phase, associated with the time evolution of the system. Using this expansion in Eq. (2.1), after multiplying from the left by $\langle m(t)|$, we obtain an equation for the expansion coefficients $c_n(t)$

$$\partial_t c_m(t) = -\langle m(t)|\partial_t|m(t)\rangle c_m(t) - \sum_{n\neq m} c_m(t)\langle m(t)|\partial_t|n(t)\rangle e^{-i[\phi_D^n(t)-\phi_D^m(t)]}. \tag{2.2}$$

In the absence of degeneracies, the time derivative of the instantaneous eigenstate equation $H(t)|n(t)\rangle = E_n(t)|n(t)\rangle$ for two states $|m(t)\rangle$ and $|n(t)\rangle$ yields

$$\langle m(t)|\partial_t|n(t)\rangle = \langle m(t)|\frac{(\partial_t H(t))}{E_n(t) - E_m(t)}|n(t)\rangle.$$

From the adiabatic theorem, we require

$$\left|\langle m(t)|\left(\partial_t H(t)\right)|n(t)\rangle\right| \ll \frac{|E_n(t) - E_m(t)|}{\Delta T_{nm}},$$

where ΔT_{nm} is a characteristic time scale on which a transition between the states $|m(t)\rangle$ and $|n(t)\rangle$ happens. In the adiabatic limit, $\Delta T_{nm} \to \infty$. Hence, with these assumptions, the second term in Eq. (2.2) cancels out, which yields a simplified equation for the expansion coefficients $c_n(t)$, solved by integration

$$c_n(t) = c_n(0)e^{-\int_{t_0}^t \mathrm{d}\tau\langle n(t)|\partial_\tau|n(t)\rangle}. \tag{2.3}$$

The time dependence in Eq. (2.3) might be parametrized by the trajectory of the particle $|n(t)\rangle \to |n(\mathbf{r}(t))\rangle$. Consequently, we obtain

$$c_n(\mathbf{r}_f) = c_n(\mathbf{r}_i)e^{i\int_{\Gamma_r}\mathbf{dr}\mathbf{A}_n(\mathbf{r})}, \tag{2.4}$$

where $\mathbf{r}_i$ and $\mathbf{r}_f$ are the initial and final vectors along the trajectory Γ_r. The purely real so-called Berry connection $\mathbf{A}_n(\mathbf{r})$ is given by

$$\mathbf{A}_n(\mathbf{r}) = i\langle n(\mathbf{r})|\nabla_{\mathbf{r}}|n(\mathbf{r})\rangle.$$

For a long time it was believed that the geometric phase of Eq. (2.4) can always be removed by a gauge transformation, which is true in the case of an open trajectory Γ_r. Under the gauge transformation $|n'(\mathbf{r})\rangle \to e^{-i\beta(\mathbf{r})}|n(\mathbf{r})\rangle$ with $\beta(\mathbf{r}) \in \mathbb{R}$, the Berry connection changes at every point $\mathbf{A}_n(\mathbf{r}) \to \mathbf{A}'_n(\mathbf{r}) = \mathbf{A}_n(\mathbf{r}) + \nabla_{\mathbf{r}}\beta(\mathbf{r})$. However, the geometric phase $\gamma_n(\Gamma_r) = \int_{\Gamma_r} \mathbf{dr}\mathbf{A}(\mathbf{r})$, acquired along a given path Γ_r, only traces the initial and final points of the gauge field $\beta(\mathbf{r})$

$$\gamma_n(\Gamma_r) \to \gamma'_n(\Gamma_r) = \gamma_n(\Gamma_r) + \left(\beta(\mathbf{r}_f) - \beta(\mathbf{r}_i)\right).$$

An adiabatic evolution along a closed path Γ_r, hence, comes along with a gauge invariant geometric phase. The meaning of this phase becomes clear under the application of Stokes' theorem

$$\gamma_n(\Gamma_r) = \int_{\Gamma_r} \mathbf{dr}\mathbf{A}_n(\mathbf{r}) = \int_{\mathcal{S}} \mathcal{F}^n_{\mu\nu} \mathrm{d}r^\mu \wedge \mathrm{d}r^\nu,$$

where the Berry curvature $F^n_{\mu\nu}$ is defined as

$$F^n_{\mu\nu} = -i\left(\langle\partial_\mu n(\mathbf{r})|\partial_\nu n(\mathbf{r})\rangle - \langle\partial_\nu n(\mathbf{r})|\partial_\mu n(\mathbf{r})\rangle\right) = 2\mathrm{Im}\left[\langle\partial_\mu n(\mathbf{r})|\partial_\nu n(\mathbf{r})\rangle\right]$$

with shorthand notation $|\partial_\mu n(\mathbf{r})\rangle = \frac{d}{dr^\mu}|n(\mathbf{r})\rangle$ and the area $\mathcal{S}$ bounded by the closed curve Γ_r. The Berry curvature behaves like a flux density penetrating through a surface $\mathcal{S}$. As a consequence, the value of the geometric phase, or Berry phase, $\gamma_n(\Gamma_r)$ does not depend on the specific path taken, but on the "flux" encircled. As in our simplified toy model above, a fractional "flux" yields anyonic statistic. This time, however, the "flux" is not related to an electro-magnetic vector potential, but reflects the inner-geometrical properties of the states $|n(r)\rangle$.

The above description of Berry phases in terms of $U(1)$ gauge fields rests on the assumption of a non-degenerate instantaneous eigenspectrum of the corresponding Hamiltonian. The incorporation of degeneracies complicates the above derivation since we cannot use the standard adiabatic theorem anymore, rather a more refined version of the latter is required. This generalization was first presented by Kato in 1950 [Kat50] known as the degenerate adiabatic approximation. He demonstrated that, by slowly varying through parameter space, the system is bound to remain in the same degenerate subspace as long as no crossings between different degenerate subspaces appear along the way. Consider a generic explicitly time-dependent Hamiltonian $H(t)$ with orthonormal instantaneous eigenstates $|n_{g_n}\rangle$, with the index $g_n = 0, 1, ..., d_n - 1$ labeling the different degenerate states within a given eigenspace $\mathcal{H}_n$ of dimension d_n and eigenenergy $E_n(t)$. During the evolution d_n is assumed to be constant. A generic state of such a system can be formulated by [RO10]

$$|\psi(t)\rangle = \sum_n \sum_{g_n} e^{-i\phi^D_n(t)} b_n(t) U^n_{g_n h_n}(t)|n_{g_n}(t)\rangle \tag{2.5}$$

with a dynamical phase $\phi_n^D(t) = \int_{t_0}^t \mathrm{d}\tau E_n(\tau)$. Similar to the non-degenerate case, $b_n(t)$ constitute expansion coefficients among the different subspaces. Additionally, the state can evolve within each subspace, captured by the coefficients $U^n_{h_n g_n}(t)$. Inserting the ansatz of Eq. (2.5) in the time dependent Schrödinger equation and multiplying from the left by $\langle m_{k_m}(t)|$, this yields

$$[\partial_t b_m(t)] U^m_{k_m h_n}(t) + b_m(t) \left[\partial_t U^m_{k_m h_n}(t)\right] = -\sum_n \sum_{g_n} e^{-i(\phi_n^D(t) - \phi_m^D(t))} U^n_{g_n h_n}(t) b_n(t) M^{mn}_{k_m g_n}(t) \tag{2.6}$$

with $M^{mn}_{k_m g_n}(t) = \langle m_{k_m}(t)|\partial_t|n_{g_n}(t)\rangle$. For $m \neq n$, we might rewrite

$$M^{mn}_{k_m g_n}(t) = \langle m_{k_m}(t)| \frac{\partial_t H(t)}{E_n(t) - E_m(t)} |n_{g_n}(t)\rangle.$$

In the degenerate adiabatic approximation, couplings between different eigenspaces $\mathcal{H}_n$ are neglected by the same line of reasoning as in the non-degenerate case. This implies

$$M^{mn}_{k_m g_n}(t) = \delta_{mn} M^{mn}_{k_m g_n}(t) \equiv M^n_{k_n g_n}(t), \quad b_n(t) = b_n(0) \ \forall \ t.$$

Simplification of the indices, using $g_n \to \alpha,\ k_n \to \beta,\ h_n \to \gamma$, produces

$$\partial_t U^n_{\beta\gamma}(t) = -\sum_\alpha M^n_{\beta\alpha}(t) U^n_{\alpha\gamma}(t).$$

The above equation can formally be solved by integration. Using a parametrization along the trajectory Γ_r, we obtain

$$\mathbf{U}^n(\mathbf{r}_f) = \mathcal{W}_n[\Gamma_r]\mathbf{U}^n(\mathbf{r}_i), \tag{2.7}$$

where $\mathbf{U}^n(\mathbf{r}_{f/i})$ is a matrix, containing all the elements $U^n_{\alpha\gamma}(\mathbf{r}_{f/i})$. Furthermore, we define

$$\mathcal{W}_n[\Gamma_r] = \mathcal{T} e^{i\int_{\Gamma_r} \mathbf{dr} \mathcal{A}^n(\mathbf{r})}$$

with the time-ordering operator $\mathcal{T}$ and the non-Abelian Berry connection [WZ84]

$$\mathcal{A}^n_{\alpha\beta}(\mathbf{r}) = i\langle n_\alpha(\mathbf{r})|\nabla_{\mathbf{r}}|n_\beta(\mathbf{r})\rangle.$$

$\mathcal{W}_n[\Gamma_r]$ is often referred to as Wilson loop [ADB14]. From Eq. (2.7) we see that adiabatic evolution in the presence of degeneracies is significantly different than in the non-degenerate case. Instead of a simple $U(1)$ transformation, a $U(d_n)$ transformation appears for a d_n dimensional degenerate subspace. Degenerate adiabatic evolution can therefore change the state of the system among the different degenerate states. This property is the defining ingredient of non-Abelian anyons. Living in a degenerate subspace, when adiabatically interchanged (in a definite manner, meaning clockwise or counterclockwise) they acquire a path dependent geometric $U(d_n)$ transformation that eventually changes their state. Under a local change of basis $|n_\alpha(\mathbf{r})\rangle = \sum_\gamma \chi^n_{\gamma\alpha}(\mathbf{r})|n_\gamma(\mathbf{r})\rangle$ with an unitary matrix

$\boldsymbol{\chi}^n(\mathbf{r})$ a non-Abelian gauge field transforms as

$$\mathcal{A}^n_{\alpha\beta}(\mathbf{r}) \to \mathcal{A}'^n_{\alpha\beta}(\mathbf{r}) = \chi^n_{\alpha\gamma}(\mathbf{r})^* \mathcal{A}^n_{\gamma\delta}(\mathbf{r}) \chi^n_{\delta\beta}(\mathbf{r}) + i\chi^n_{\alpha\gamma}(\mathbf{r})^* \nabla_{\mathbf{r}} \chi^n_{\gamma\beta}(\mathbf{r}).$$

For an infinitesimal small path $\mathbf{dr}$, the non-Abelian Berry phase then transforms up to first order in $\mathbf{dr}$ like

$$e^{i\mathbf{dr}\mathcal{A}^n(\mathbf{r})} \to e^{i\mathbf{dr}\mathcal{A}'^n(\mathbf{r})} \simeq (\boldsymbol{\chi}^n(\mathbf{r}))^\dagger e^{i\mathbf{dr}\mathcal{A}^n(\mathbf{r})} \boldsymbol{\chi}^n(\mathbf{r} - \mathbf{dr}).$$

Along consecutive infinitesimal path steps, neighboring transformations cancel out, which yields the gauge covariance of the Wilson loop along a closed path

$$\mathcal{W}_n[\mathbf{r}_f \leftarrow \mathbf{r}_i] \to \mathcal{W}'_n[\mathbf{r}_f \leftarrow \mathbf{r}_i] = (\boldsymbol{\chi}^n(\mathbf{r}_f))^\dagger e^{i\mathbf{dr}\mathcal{A}^n(\mathbf{r}_f)} \dots e^{i\mathbf{dr}\mathcal{A}^n(\mathbf{r}_i + \mathbf{dr})} e^{i\mathbf{dr}\mathcal{A}^n(\mathbf{r}_i)} \boldsymbol{\chi}^n(\mathbf{r}_i).$$

Hence, for a closed path, the action of an arbitrary gauge transformation is just a local change of basis at the starting point of a given loop. Indeed, since the non-Abelian Berry phase is a $U(d_n)$ transformation, if it would be independent of the basis, it could not have a physical meaning. It would imply that choosing a particular basis to describe a given degenerate subsystem determines the action of the transformation. Observables, related to this geometric phase, would hence as well depend on the basis, which is deeply unphysical. From the above analysis, we see that this is not the case and the non-Abelian Berry phase transforms well under a local change of basis. However, the operational form of the Wilson loop depends on the basis of the starting point in a closed loop, which might not be the same everywhere along the path. Basis independent properties, such as the trace or the eigenvalue spectrum are unaffected by this and, thus, they are the ones that carry intriguing physical information.

2.2.1 Importance of geometric phases for topology

Let us note at this point that, throughout the last decades, geometric phases have become an important tool for the characterization of matter [XCN10, HK10, QZ11]. The reason for this is located in the fact that Berry phases are insensitive to smooth local variations of the path in parameter space. In that sense they are able to capture the topological properties of a given system, which might be interpreted as global geometric phases. This quantized phase remains unchanged upon smooth deformations. In a physical system, described by a many-body Hamiltonian with an energy gap, separating the ground state from all excited states, a smooth deformation can be defined as a change in the Hamiltonian that does not close the gap between ground state and excited states. This principle can be applied to all gapped Hamiltonians, as for instance insulators or SCs [QZ11]. The topological properties of a given system, which are properties of the bulk, can be uniquely related to observable boundary effects by means of the so-called bulk-boundary correspondence [Hal82, Vol94], which itself can be formulated in terms of Wilson loops.

An instructive way to see how this comes about is to investigate the properties of the position operator, projected onto the occupied bands of a generic translational invariant

lattice Hamiltonian. In particular, we are interested in solving the eigenvalue problem

$$\left(\mathcal{P}^{\text{occ}}\hat{x}\mathcal{P}^{\text{occ}} - \frac{\theta}{2\pi}\right)\Psi(\mathbf{x}) = 0,$$

where $\mathcal{P}^{\text{occ}}$ projects to the occupied subspace. $\Psi(\mathbf{x})$ can be expanded in the subspace of occupied Bloch bands

$$\Psi(\mathbf{x}) = \sum_{n=1}^{n_{\text{occ}}} \int \frac{dk}{2\pi} f_{n,k}\psi_k^n(x)$$

with Bloch eigenfunctions $\psi_k^n(x) = e^{ikx}u_k^n(x)$. With periodic boundary conditions in the Brillouin zone, a straight forward calculation yields [ADB14]

$$\sum_{n=1}^{n_{\text{occ}}} \mathcal{W}_{mn}[k + 2\pi \leftarrow k]f_{n,k} = e^{i\theta}f_{m,k}.$$

The eigenspectrum of $\mathcal{P}^{\text{occ}}\hat{x}\mathcal{P}^{\text{occ}}$, hence coincides with the phases of the eigenspectrum of the Wilson loop [Zak89, FK06, ADB14]. Upon smooth deformations, the topological properties of a given Hamiltonian are not changed. We might therefore rewrite the Hamiltonian as a flat-band Hamiltonian with two accumulation points, separating the bands in occupied and empty

$$H_{\text{flat}} = 1 - 2\mathcal{P}^{\text{occ}}. \tag{2.8}$$

Next, we introduce a boundary along x direction, splitting the system in two halves. On one side, $x < 0$, we want all bands to be empty, while on the other side, $x > 0$, we retain Eq. (2.8). This might be expressed as

$$H_{\text{bdr}} = \mathcal{P}^{\text{occ}}V(\hat{x})\mathcal{P}^{\text{occ}} + 1 - \mathcal{P}^{\text{occ}}$$

with $V(\hat{x}) = -1$ for $x > 0$ and $V(\hat{x}) = 1$ for $x < 0$. The boundary spectrum is hence associated with the operator $\mathcal{P}^{\text{occ}}V(\hat{x})\mathcal{P}^{\text{occ}}$. It can be demonstrated that this operator can be smoothly deformed to the projected position operator. This implies that the eigenspectrum of the edge is topologically equivalent to the Wilson loop eigenspectrum as long as the form of the boundary itself does not break the symmetries that protect the bulk spectral flow [FJK11, NS18]. A non-gapped Wilson loop spectrum implies a non-trivial topology of the bulk system that manifests itself as edge modes, connecting empty and occupied bands.

2.3 Anyon models, braiding and topological quantum computing

The fact that the adiabatic exchange of non-Abelian anyons is described by $U(N)$ transformations that do not depend on the details of the path, but only recognize its topology, turns out to be an extremely powerful property. This eventually allows to employ non-Abelian anyons as building-blocks of topological quantum computers, where the ultimate

goal is to design an universal set of quantum gates solely from the $U(N)$ operations that emerge from adiabatic particle exchange. As we will derive below, typically two anyons are not sufficient for this task. Rather, many-anyon system with larger ground state degeneracies are required. This clearly complexifies the description of adiabatic particle exchange, or *braiding*, in terms of non-Abelian Berry phases. However, there is maybe a more elegant, albeit also more formal, approach to describe many-anyon theories that we will review below.

2.3.1 Fusion tree representation of anyon models

Before we write down an explicit anyon model, let us think about the basic requirements that such a model has to obey. For sure, a specific anyon model will always contain different kinds of anyons. In a system with Abelian anyons of kind θ (meaning they acquire a phase of $e^{i\theta}$ when exchanged), necessarily also particles of kind $k^2\theta$ ($k \in \mathbb{N}$) need to exist. The simple reason for those 'higher' particle species is that we might always bring k anyons of kind θ close together, i. e. *fuse* them. When two of such new composite anyons are exchanged, each of the k constituent anyons of composite anyon 1 is exchanged with each constituent of composite anyon 2. The composite anyon can thus be seen as a new anyon of kind $k^2\theta$. This can be captured in general form by fusion rules. For Abelian anyons of kind π/m, they simply read [NSS+08]

$$n^2\frac{\pi}{m} \times k^2\frac{\pi}{m} = (n+k)^2\frac{\pi}{m},$$

where $\times$ denotes the fusion. In the case of non-Abelian anyons, the situation is more subtle. Due to the degeneracy, there might not be an unique way of how non-Abelian anyons can be fused, i. e. how their topological quantum numbers are combined. This is typically expressed by

$$\phi_a \times \phi_b = \sum_c N_{ab}^c \phi_c$$

for anyons of kind a, b and c. Anyons of kind a and b fuse to an anyon of kind c through the *fusion channel* N_{ab}^c whenever $N_{ab}^c \neq 0$. For Abelian anyons, N_{ab}^c is only non-zero for one specific c and zero else, while the theory is non-Abelian if there is at least one combination of a and b such that there are multiple fusion channels with $N_{ab}^c \neq 0$. The fusion multiplicities N_{ab}^c are typically 0 or 1. However, in principle it can also happen that $N_{ab}^c > 1$. This implies multiple distinct ways how a and b can fuse to c.
The different fusion channels might further be used to define the degenerate space in which the anyons live. Since the degeneracy of the system is one-to-one related to the number of possible fusion outcomes, we can define a set of orthogonal states $|ab;c\rangle$ with

$$\langle ab;c|ab;d\rangle = \delta_{cd},$$

spanning the degenerate space, often coined *fusion space* [LP17]. The state $|ab;c\rangle$ refers to a system with two anyons a and b that yield c when fused. In that sense c describes the topological charge of the anyon system formed from a and b. In a naive approach, one could

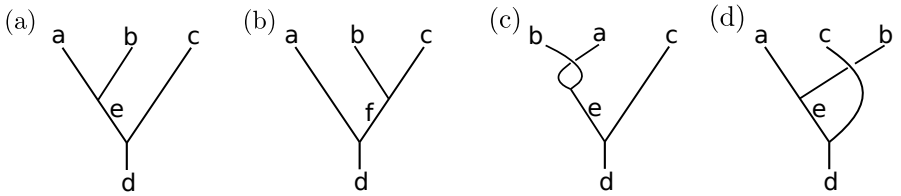

Figure 2.2: (a) Fusion tree diagram of a state $|(ab)c;ec;d\rangle$. Vertical direction defines the time, increasing from top to bottom. Horizontal direction defines space. (b) Fusion tree diagram of $|a(bc);af;d\rangle$. (c) Fusion tree diagram for $|(ba)c;ec;d\rangle$ with interchanged initial positions of particle a and b. (d) Fusion tree diagram for $|(ab)c;ec;d\rangle$ with interchanged initial positions of particle b and c.

suggest the set of states $|ab;c\rangle$ with distinct fusion outcomes to built a topological qubit. This is however not possible. The reason for this is that braiding – the operation that is wanted to determine qubit manipulations – is not able to change the global topological charge. For the system prepared in the state $|ab;c\rangle$, it is hence impossible to ever reach the state $|ab;d\rangle$ (for $d \neq c$) using braiding operations. Thus, two anyon systems are only sufficient to form one ordinary qubit, but not to encode one topological qubit. Instead, more than two anyons are required, such that various different ways of fusion are possible, all with the same final outcome (i. e. same topological charge) and the same fusion order. For instance, in a model with the three anyons a, b and c, a state $|(ab)c;ec;d\rangle$ describes a fusion order where first a and b fuse to e, while subsequently c fuses with e to d, which determines the global topological charge. The fusion tree basis for this model is given by the set of orthonormal states with distinct intermediate fusion outcome e. A convenient way to illustrate such a fusion tree basis state is a fusion tree diagram (see Fig. 2.2 (a)). Each intersection represents one fusion process, where the labeling of the branches gives the fusion input, outcome, respectively. Distinct degenerate states, for our three-anyon model with anyons a, b and c and topological charge d, can be uniquely labeled by the different possible values of e.

Evidently, starting with particles a, b and c, the fusion order described by the states $|(ab)c;\{e\}c;d\rangle$ is not the only possible one, leading to global topological charge d. In another fusion order, where first b is fused with c, the fusion tree basis states would consequently read $|a(bc);a\{f\};d\rangle$. Distinct fusion orders can be interpreted as different bases, that can be related by means of the so called F-matrices, capturing the change in the fusion order

$$|(ab)c;ec;d\rangle = \sum_f (F^d_{abc})_{ef} |a(bc);af;d\rangle, \tag{2.9}$$

where the summation runs over all possible fusion channels given for the fusion of b and c. F-matrices are specific to the anyon model. They can be obtained from consistency equations, known as pentagon equations, which make use of generic cyclic relations [Kit06, RSW09]. The action of a F-matrix is best visualized in a fusion tree diagram. In Fig. 2.2, (a) and (b) are related by a *F-move*, i. e. the application of a F-matrix according to Eq. (2.9). This changes the alignment of the fusion branches, but keeps the initial particle

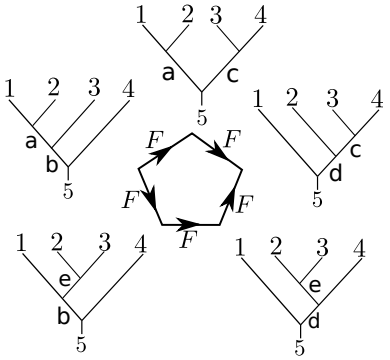

Figure 2.3: Consecutive application of F yields a non-trivial cyclic relation in the case of four anyons. 1, 2, 3, and 4 correspond to the different anyons of the theory with topological charge 5.

configuration as well as the topological charge unchanged. The pentagon equation is a direct consequence of this. Since any F-matrix changes the alignment of only one branch in the fusion tree at a time, consecutive application for four anyons yields a non-trivial cyclic relation. Fig. 2.3 illustrates this generic relation. In terms of formulas, Fig. 2.3 is equivalent to the matrix equation

$$(F^5_{12c})_{ad}(F^5_{a34})_{bc} = \sum_e (F^5_{234})_{ec}(F^5_{1e4})_{bd}(F^5_{123})_{ae}. \tag{2.10}$$

Eq. (2.10) appears to be very cumbersome to be solved in general. Already in the case of the simplest anyon model (discussed in Sec. 2.3.3), where we have two kinds of particles, there are 2^5 different F-matrices. Fortunately, many of them actually correspond to trivial fusion trees such that Eq. (2.10) simplifies and yields a solution for the remaining non-trivial F-matrices. However, this is certainly not always the case.

The fusion tree basis is particularly useful to describe braiding for many-anyon models. As discussed in Secs. 2.1 and 2.2, adiabatic exchange of particles, living in a degenerate space, is accompanied by an unitary transformation. The form of this unitary transformation is given by the non-Abelian Berry phase, capturing an abstract notion of curvature in the corresponding Hilbert space. Furthermore, unitarity implies the existence of a basis in which the transformation will become a diagonal matrix. This basis can be found by using the fusion tree construction of a basis. As all different degenerate states in a many-anyon model with fixed topological charge are labeled by distinct intermediate fusion outcomes, the states diagrammatically represented by Fig. 2.2 (a) and (c) are linearly dependent. In Fig. 2.2 (c), however, anyons a and b are exchanged in a counterclockwise manner. It follows readily

$$|(ba)c; ec; d\rangle = R^e_{ab}|(ab)c; ec; d\rangle, \tag{2.11}$$

where R^e_{ab} is a $U(1)$ phase, describing the exchange process a and b. In contrast to the Abelian case, the non-Abelian exchange not only depends on the types of anyons, but also on their fusion channel e. In the fusion tree basis, R^e_{ab} are consequently the elements of a diagonal matrix R, capturing the action of counterclockwise exchange of

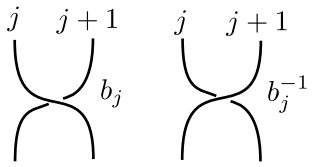

Figure 2.4: Diagrammatic action of the braid group generator b_j on the strands j and $j+1$ and its inverse. The difference between clockwise and counterclockwise exchange of worldlines is illustrated by a cut in the respective worldline.

anyons a and b. Similar to F-matrices, R-matrices can be fully determined from the corresponding anyon model by solving a set of consistency equations, known as hexagon equations [MS89, Kit06, RSW09].
Let us for a moment return to the initial two anyon system formed from anyon a and b. The fusion tree basis of such a system would be similar to the one shown in Fig. 2.2 (a), just that the diagram would end at the intermediate outcome e, with e representing the global topological charge in this scenario. As derived above, the R-matrix, describing an exchange of a and b is diagonal in the basis of Fig. 2.2 (a). As readily seen from Eq. (2.11), application of R yields a $U(1)$ phase and is, thus, not able to flip the value of e. Consequently, two anyons are not enough to encode a topological qubit, as braiding in the two-anyon model (i. e. application of R) is insufficient for computations.
Given a specific basis, braiding of anyons can only take a diagonal form for one pair of anyons. In the above example, with the basis pictorially represented by Fig. 2.2 (a), braiding of anyon a and b is described by the diagonal R-matrix. Evidently, braiding of anyon b and c in the same basis requires more analysis. For that, we first apply F^d_{abc} to change the basis to the fusion order of Fig. 2.2 (b), subsequently we braid b and c in the new basis by applying R, and finally we change back to the initial basis with $\left(F^d_{abc}\right)^{-1}$. The combined action of F and R is often called braid matrix $B_{bc} = \left(F^d_{abc}\right)^{-1} R_{bc} F^d_{abc}$. The resulting state has the diagrammatic form of Fig. 2.2 (d).
Full knowledge of the F and R-matrices in a given many-anyon model allows to efficiently describe all possible braiding operations, as all generators of the corresponding braid group are constructed from F and R matrices.

2.3.2 The braid group

The braid group of N strands $\mathcal{B}_N$ is the group of equivalence classes of braids, formed from the N strands. The group operation is the composition of braids. The generators of the group are the elementary operations, necessary to obtain any group element using the group operation. The braid group $\mathcal{B}_N$ is thus generated by braids b_j describing pairwise exchange of neighboring strands (or world-lines) j and $j+1$ (see Fig. 2.4). Importantly, if b_j constitutes a clockwise exchange of strands, then b_j^{-1} represents a counterclockwise exchange. The braid group $\mathcal{B}_N$ is therefore generated by $N-1$ elementary braiding operations $\{b_1, ..., b_{N-1}\}$ with the mutual relations [NSS+08]

$$b_i b_j = b_j b_i \quad \text{for} \quad |i-j| \geq 2, \qquad b_j b_{j+1} b_j = b_{j+1} b_j b_{j+1} \quad \text{for} \quad 1 \leq j \leq N-1.$$

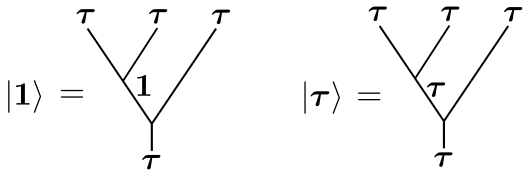

Figure 2.5: Fusion tree basis states for global topological charge $\boldsymbol{\tau}$.

The crucial difference from the permutation group is that $b_j^2 \neq 1$, which implies an infinite number of elements (unlike the permutation group $\mathcal{S}_N$, which has $N!$ elements).

For the abstract three anyon model of the last section with anyons a, b and c, the associated braid group generators are $b_{ab} \equiv R_{ab}$ and $b_{bc} = \left(F^d_{abc}\right)^{-1} R_{bc} F^d_{abc}$. Any braid is built from composites of these generators and their inverse.

2.3.3 Fibonacci anyons

To illustrate this quite abstract analysis, let us discuss a concrete anyon model. The simplest model of anyons to imagine consists of only two fields, one anyon of kind $\boldsymbol{\tau}$ and the vacuum $\mathbf{1}$ [FW02, BHZS05, HZBS07, STL08]. The only non-trivial fusion rule is the fusion of two $\boldsymbol{\tau}$ anyons

$$\boldsymbol{\tau} \times \boldsymbol{\tau} = \mathbf{1} + \boldsymbol{\tau}. \tag{2.12}$$

Explained in words, Eq. (2.12) tells that two $\boldsymbol{\tau}$ particles behave like particle and antiparticle when they fuse to the identity, while in the second fusion channel they behave like a single $\boldsymbol{\tau}$ particle. Based on that fusion rule, repeated associative application shows that the fusion space, i. e. the number of distinct ways to reach final topological charge $\mathbf{1}$ or $\boldsymbol{\tau}$, grows according to the Fibonacci sequence. That is, for a theory consisting of N $\boldsymbol{\tau}$ anyons, fusion yields

$$\bigtimes_N \boldsymbol{\tau} = F_{N-1}\mathbf{1} + F_N\boldsymbol{\tau}$$

with the Fibonacci sequence elements $F_N = F_{N-1} + F_{N-2}$. Where

$$\bigtimes_N \boldsymbol{\tau} = \boldsymbol{\tau} \times \boldsymbol{\tau} \times \ \ldots \ \times \boldsymbol{\tau}$$

denotes the associative fusion of all N fields $\boldsymbol{\tau}$. Let us fix the global topological charge to $\boldsymbol{\tau}$ and the fusion order to that shown in Fig. 2.5. Then, three $\boldsymbol{\tau}$ are able to encode one topological qubit as the fusion space dimension is two ($F_3 = 2$). The 2D fusion tree basis is spanned by the states $|(\boldsymbol{\tau}\boldsymbol{\tau})\boldsymbol{\tau}; \mathbf{1}\boldsymbol{\tau}; \boldsymbol{\tau}\rangle \equiv |\mathbf{1}\rangle$ and $|(\boldsymbol{\tau}\boldsymbol{\tau})\boldsymbol{\tau}; \boldsymbol{\tau}\boldsymbol{\tau}; \boldsymbol{\tau}\rangle \equiv |\boldsymbol{\tau}\rangle$. The solution of the hexagon and pentagon equations for the three $\boldsymbol{\tau}$ model in the basis $(1,0)^T = |\mathbf{1}\rangle$,

$(0,1)^T = |\boldsymbol{\tau}\rangle$ produces [BHZS05, NSS$^+$08]

$$F^{\boldsymbol{\tau}}_{\boldsymbol{\tau}\boldsymbol{\tau}\boldsymbol{\tau}} = \begin{pmatrix} \varphi^{-1} & \varphi^{-1/2} \\ \varphi^{-1/2} & -\varphi^{-1} \end{pmatrix}, \quad R_{\tau\tau} = \begin{pmatrix} e^{-i4\pi/5} & 0 \\ 0 & -e^{-i2\pi/5} \end{pmatrix}, \tag{2.13}$$

where $\varphi = (1+\sqrt{5})/2$ is the golden ratio. Using the definitions in (2.13), we can readily find the generators of the associated braid group

$$b^1_{\boldsymbol{\tau}\boldsymbol{\tau}} = R_{\boldsymbol{\tau}\boldsymbol{\tau}}, \quad b^2_{\boldsymbol{\tau}\boldsymbol{\tau}} = \left(F^{\boldsymbol{\tau}}_{\boldsymbol{\tau}\boldsymbol{\tau}\boldsymbol{\tau}}\right)^{-1} R_{\boldsymbol{\tau}\boldsymbol{\tau}} F^{\boldsymbol{\tau}}_{\boldsymbol{\tau}\boldsymbol{\tau}\boldsymbol{\tau}} = \begin{pmatrix} -e^{-i\pi/5}/\varphi & -ie^{-i\pi/10}/\sqrt{\varphi} \\ -ie^{-i\pi/10}/\sqrt{\varphi} & -1/\varphi \end{pmatrix}, \tag{2.14}$$

where in the basis defined by Fig. 2.5, $b^1_{\boldsymbol{\tau}\boldsymbol{\tau}}$ braids the leftmost two $\boldsymbol{\tau}$'s and $b^2_{\boldsymbol{\tau}\boldsymbol{\tau}}$ the rightmost two. Then, any unitary operation that results from braiding can be represented by composition of $b^1_{\boldsymbol{\tau}\boldsymbol{\tau}}$ and $b^2_{\boldsymbol{\tau}\boldsymbol{\tau}}$ and their inverse. Importantly, to use braiding as building blocks of quantum computations, the ability to construct the required quantum gates, necessary for universal quantum computing [NC00], from the generators of the associated braid group is fundamental. In respect thereof, the Fibonacci anyon theory hides something remarkable. The braid group, generated by $b^1_{\boldsymbol{\tau}\boldsymbol{\tau}}$ and $b^2_{\boldsymbol{\tau}\boldsymbol{\tau}}$, is dense in $SU(2)$ [FW02], which implies that any desired unitary can be approximated to arbitrary accuracy (up to a global phase) using braiding operations. This intriguing property enables Fibonacci anyons to support universal quantum computing solely by braiding and indeed distinguishes them from most other anyon models.

2.3.4 Quantum computing with Fibonacci anyons

Although theoretical possible, from the definitions in (2.14), it is not obvious how to construct useful single- and two-qubit gates from composition of $b^1_{\boldsymbol{\tau}\boldsymbol{\tau}}$ and $b^2_{\boldsymbol{\tau}\boldsymbol{\tau}}$. A convenient method how to find reasonable approximations for specific single qubit gates is a brute force search on a classical computer, that determines all possible braids up to a given length, looking for a braid which resembles the desired unitary in good approximation. The number of possible braids, however, grows exponentially in the length of the braid, which makes this method unfeasible for high-accuracy long braids or two-qubit gates, where the corresponding full Hilbert space (in the Fibonacci case) is already 13. Fortunately, it is possible to find good approximations for single-qubit gates, built from polylogarithmically long braids in the allowed error distance, using iterative algorithms [KSV99, NC00].
Single qubit gates are, however, not adequate for universal quantum computing [NC00]. An important brick of any quantum computer is the entangling of different qubits with two-qubit gates [NC00, BDD$^+$02]. For that, even the techniques used to obtain single qubit gates might not be sufficient anymore. This is the moment to leave aside the brute force method. A neat way to construct two-qubit gates was suggested by Bonesteel *et al.* [BDD$^+$02]. Let us start with a single qubit, formed from three $\boldsymbol{\tau}$ fields, and search for a braid whose action on the Hilbert space corresponds to a braid exchanging two of the three $\boldsymbol{\tau}$ fields, say $\boldsymbol{\tau}$ field 2 and $\boldsymbol{\tau}$ field 3, twice (see Fig. 2.6 (a)). While it is obvious that such a braid can be constructed from applying the corresponding generator of the braid group twice, this is not what we are looking for. Instead, we want to find a combination

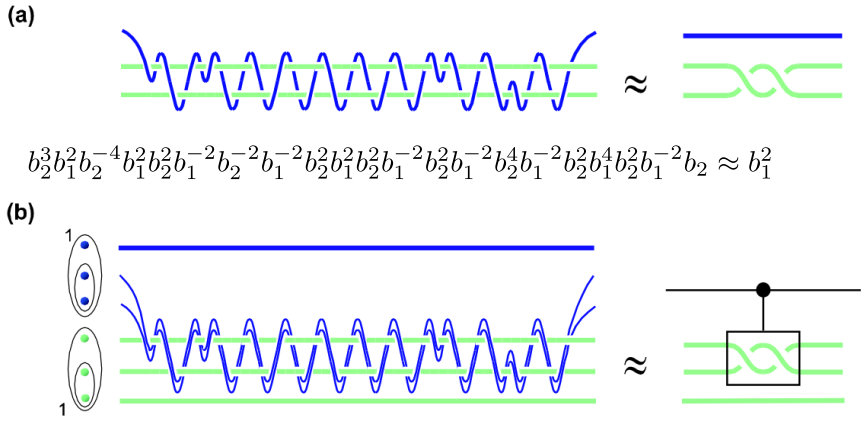

Figure 2.6: Construction of a single- and two-qubit gate. Time flows from left to right. For ease of notation, we have dropped the $\boldsymbol{\tau}$ indices of the braid group generators, i. e. $b^{\nu}_{\boldsymbol{\tau}\boldsymbol{\tau}} \equiv b_\nu$ for $\nu = 1, 2$. (a) Winding the blue $\boldsymbol{\tau}$ field in the given order through the two 'stationary' $\boldsymbol{\tau}$ fields effectively yields an approximate operation on the 'stationary' fields with a distance of $\varepsilon \simeq 2.3 \times 10^{-3}$ from the desired braid. (b) Usage of a second $\boldsymbol{\tau}$ in the winding process produces a controlled-b_1^2 operation. Reprinted figure with permission from Ref. [BHZS05]. Copyright 2020 by the American Physical Society.

of braiding operations that does solely involve the *weaving* of the remaining $\boldsymbol{\tau}$ field (1) around the stationary ones (2 and 3), but not the direct braiding of $\boldsymbol{\tau}$ 2 and 3 [SBF+06]. Finding such a braid in good accuracy is a computationally tractable task (see Fig. 2.6 (a)). The effort is by all means rewarded for the construction of two-qubit gates. Two-qubit gates typically consist of one control qubit and one target qubit. In the target qubit, we aim to execute a tangible operation, depending on the value of the control qubit.

Instead of winding one $\boldsymbol{\tau}$ field around two others, we use the same braiding sequence found for the single-qubit gate, but now, we weave two $\boldsymbol{\tau}$ fields of the control qubit around two $\boldsymbol{\tau}$ fields of the target qubit (see Fig. 2.6 (b)). When the control qubit is in state $|\mathbf{1}\rangle$, the braid is ineffective since we are winding around the vacuum. Then, only a $U(1)$ phase is acquired. However, if the control qubit is in state $\boldsymbol{\tau}$, we can think of the pair of $\boldsymbol{\tau}$ particles as a single $\boldsymbol{\tau}$ particle. Hence, the action of the braid causes the same non-trivial braid as for the single-qubit case and returns a rotation on the target qubit. Thus, the state of the target qubit is modified in dependence of the state of the control qubit and the above scheme represents a *controlled-rotation* gate.

This manual can also be applied to more fundamental gates, such as the controlled-NOT (CNOT) gate. In the first step we find an appropriate single-qubit NOT gate by weaving one $\boldsymbol{\tau}$ in a three $\boldsymbol{\tau}$ system with the remaining stationary $\boldsymbol{\tau}$'s (Fig. 2.7 (b)). Unlike for the controlled-rotation gate, the weaving $\boldsymbol{\tau}$ of the NOT operation is the central $\boldsymbol{\tau}$ of the qubit. If we want to access it from another qubit, we need an injection weave that propagates a $\boldsymbol{\tau}$ particle to the right position, but acts as unity in the computational Hilbert-space, leaving all quantum numbers invariant (Fig. 2.7 (a)). Weaving now two $\boldsymbol{\tau}$ particles from the control qubit in a scheme compiled of injection - NOT - ejection with the $\boldsymbol{\tau}$ particles of the target qubit, this yields an approximation for the desired CNOT gate (see Fig.

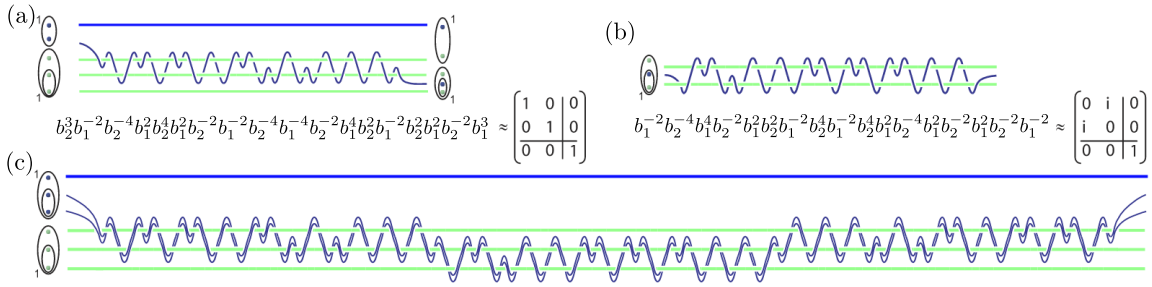

Figure 2.7: (a) Injection weave approximating unity in an error distance of $\varepsilon \simeq 1.5 \times 10^{-3}$. This operation does not change the underlying quantum numbers but injects a field from the control qubit into the target qubit. (b) Braiding scheme that approximates a logical NOT gate in error distance $\varepsilon \simeq 8.5 \times 10^{-4}$. (c) CNOT operation winding two $\boldsymbol{\tau}$ fields of the control qubit through the target qubit. Reprinted figure with permission from Ref. [BHZS05]. Copyright 2020 by the American Physical Society.

2.7 (c)). The distance of the approximate CNOT gate from the true CNOT operation is controlled by the length of the braiding sequence. Higher precision requires more braiding operations in each sequence. For two unitary matrices U and V of dimension n, we can quantify their distance using

$$\varepsilon(U,V) = \sqrt{1 - \frac{|\mathrm{tr}\,(UV^\dagger)\,|}{n}}.$$

If both unitaries are identical up to a global phase $U = e^{i\phi}V$, then $\varepsilon(U,V) = 0$. For a desired error distance ε, it can be shown that the minimum required length of compiled braid group generators scales polynomial in $\log(1/\varepsilon)$ [HRC02, KBS14]. Good approximations for quantum gates can therefore reached within reasonable length of braids.

There are, however, some caveats that spoil the immediate use of Fibonacci anyons for topological quantum computation. One obvious is that the approximation of even simple single qubit gates becomes complicated very soon and requires sequences of many subsequent braiding operations [BHZS05, HZBS07, BBS10]. The approximation of quantum gates also implies a small leakage error in every calculation step, which might become a problem in longer computations. Moreover, another caveat is the missing tensor product structure of the computational Hilbert space. A single qubit requires three Fibonacci anyons to create a computational Hilbert space of dimension 2. Two qubits are consequently encoded from six Fibonacci anyons. The associated fusion space is of dimension 5 in the vacuum sector and 8 in the $\boldsymbol{\tau}$ sector. Qubits and computations, therefore, reside only in a subspace of the fusion space and the remaining part of the fusion space needs to be carefully avoided throughout the computational process. Moreover, the simplicity of the Fibonacci anyon model does by no means correlate with the feasibility of possible models that are able to support them as effective low energy excitations. Indeed, literature provides only a small number of reasonable proposals for Fibonacci anyons in physical systems. Apart from possible realizations in fractional quantum Hall systems at specific fractional filling [RR99], more recent works propose their

existence in artificial lattice models [SCMA15] or domain wall structures formed at the edge of Abelian fractional quantum Hall states [MCA+14][1]. In fact, the complexity of a given anyon model is not necessarily coupled to the complexity of possible systems realizing those anyons in real condensed matter settings. The most prominent example of which are Ising anyons, that might have already been realized in 1D p-wave SCs [Kit01, ORvO10, LSDS10, STL+10, SLTDS10, MZF+12, AHM+16b].

2.3.5 Ising anyons and beyond

Similar to the Fibonacci anyon model, the Ising anyon model contains only one non-Abelian particle $\boldsymbol{\sigma}$. Additionally, however, also an Abelian field $\boldsymbol{\psi}$ is present. The non-trivial fusion rules for this composite Abelian-non-Abelian model are given by [LP17]

$$\begin{aligned} \boldsymbol{\psi} \times \boldsymbol{\psi} &= \mathbf{1}, \\ \boldsymbol{\psi} \times \boldsymbol{\sigma} &= \boldsymbol{\sigma}, \\ \boldsymbol{\sigma} \times \boldsymbol{\sigma} &= \mathbf{1} + \boldsymbol{\psi}. \end{aligned} \tag{2.15}$$

An interpretation of the above fusion rules might be provided by fermions and Majorana particles. Two fermions $\boldsymbol{\psi}$ fuse together to the ground state $\mathbf{1}$, which might be vacuum or, in the case of a p-wave SC, the Cooper-pair condensate. As any fermion can be represented in terms of two Majorana particles, it is clear that three Majorana particles behave in the same way as one Majorana [Maj37]. The third line of (2.15) expresses the non-Abelian nature of Majorana particles: they either fuse to the identity $\mathbf{1}$ or to $\boldsymbol{\psi}$. In the above interpretation, this means that when two Majorana particles are fused, the so formed fermion can either be empty ($\mathbf{1}$) or occupied ($\boldsymbol{\psi}$).

Unlike in the Fibonacci anyon model, the fusion space of the Ising anyon model has a clear tensor product structure. From an associative application of the fusion rules in (2.15) for N fields $\boldsymbol{\sigma}$, we obtain

$$\bigtimes_{N=2n-1} \boldsymbol{\sigma} = 2^{n-1}\boldsymbol{\sigma}, \qquad \bigtimes_{N=2n} \boldsymbol{\sigma} = 2^{n-1}\left(\mathbf{1} + \boldsymbol{\psi}\right), \qquad \forall\ n \in \mathbb{N}. \tag{2.16}$$

Hence, the computational Hilbert space for a given set of qubits exploits the full fusion space. For fixed topological charge, the minimum number of Majorana particles, required to form a topological qubit, is three. In this scenario, the topological charge is forced to be $\boldsymbol{\sigma}$ with the fusion tree basis states $|(\boldsymbol{\sigma}\boldsymbol{\sigma})\boldsymbol{\sigma};\mathbf{1}\boldsymbol{\sigma};\boldsymbol{\sigma}\rangle \equiv |\mathbf{1}\rangle$ and $|(\boldsymbol{\sigma}\boldsymbol{\sigma})\boldsymbol{\sigma};\boldsymbol{\psi}\boldsymbol{\sigma};\boldsymbol{\sigma}\rangle \equiv |\boldsymbol{\psi}\rangle$. The solution to the pentagon and hexagon equations yield [LP17]

$$F^{\boldsymbol{\sigma}}_{\boldsymbol{\sigma}\boldsymbol{\sigma}\boldsymbol{\sigma}} = \frac{1}{\sqrt{2}}\begin{pmatrix} 1 & 1 \\ 1 & -1 \end{pmatrix}, \qquad R_{\boldsymbol{\sigma}\boldsymbol{\sigma}} = e^{-i\pi/8}\begin{pmatrix} 1 & 0 \\ 0 & e^{i\pi/2} \end{pmatrix},$$

where we used the representation $|\mathbf{1}\rangle = (1,0)^T$, $|\boldsymbol{\psi}\rangle = (0,1)^T$. Consequently, the generators

[1] We will discuss the condensed matter realization of non-Abelian anyons in more detail in Sec. 2.4

of the braid group are given by

$$b^1_{\boldsymbol{\sigma\sigma}} = R_{\boldsymbol{\sigma\sigma}}, \qquad b^2_{\boldsymbol{\sigma\sigma}} = \left(F^{\boldsymbol{\sigma}}_{\boldsymbol{\sigma\sigma\sigma}}\right)^{-1} R_{\boldsymbol{\sigma\sigma}} F^{\boldsymbol{\sigma}}_{\boldsymbol{\sigma\sigma\sigma}} = \frac{1}{\sqrt{2}} e^{i\pi/8} \begin{pmatrix} 1 & -i \\ -i & 1 \end{pmatrix}. \tag{2.17}$$

Compared to the Fibonacci case, with the above generators it is now much more obvious how to construct logical quantum gates. In particular, elementary compositions directly lead (up to a global phase) to the Hadamard gate H, the phase gate S and the three Pauli gates X, Y, Z

$$\begin{aligned} H &\sim b^1_{\boldsymbol{\sigma\sigma}} b^2_{\boldsymbol{\sigma\sigma}} b^1_{\boldsymbol{\sigma\sigma}}, \qquad S \sim b^1_{\boldsymbol{\sigma\sigma}} \\ X &\sim b^2_{\boldsymbol{\sigma\sigma}} b^2_{\boldsymbol{\sigma\sigma}}, \quad Y \sim b^1_{\boldsymbol{\sigma\sigma}} b^1_{\boldsymbol{\sigma\sigma}} \left(b^2_{\boldsymbol{\sigma\sigma}}\right)^{-1} \left(b^2_{\boldsymbol{\sigma\sigma}}\right)^{-1}, \quad Z \sim b^1_{\boldsymbol{\sigma\sigma}} b^1_{\boldsymbol{\sigma\sigma}}. \end{aligned}$$

Notably, as opposed to the Fibonacci case, the above gates are exact and now leakage error occurs. Using six $\boldsymbol{\sigma}$ fields, it is furthermore possible to design exact two-qubit gates, such as the CNOT gate, from comparatively simple combinations of braid group generators [Geo08, FDG10].

However, the braid group generators in (2.17) are not able to compile arbitrary unitaries and, unfortunately, the Ising anyon theory has one major weakness. Universal quantum computing requires a fundamental set of gates [NC00]. This set of gates consists of those which are required to build a controlled-controlled-NOT (CCNOT) gate, also called Toffoli gate. Any reversible circuit can then be constructed from Toffoli gates. On the quantum level, designing a Toffoli gate requires Hadamard gates, CNOT gates and T gates, with the property $T^2 = S$ [AGW09]. While it is relatively easy to compile Hadamard and CNOT gates, the Ising anyon model fails to represent the T gate using braiding operations. Thus, quantum computing on the basis of Ising anyons needs to be supplemented by non-topological operations implementing this missing brick [BCNS10]. This in turn requires error-correction, which entails significant computational overhead [Bra06]. Despite this fundamental lack in accessing all relevant quantum gates for universal quantum computing, Ising anyons are still the most promising candidate theory to explore and test the principles of anyonic theories.

On the other hand, the weakness of Ising anyons for universal quantum computing encouraged the investigation of their generalizations. Let us think of the following specific generalization [HWL15, CMA18]

$$\begin{aligned} \boldsymbol{\sigma} \times \boldsymbol{\sigma} &= \sum_{g=0}^{m} \boldsymbol{\psi}_g, \\ \boldsymbol{\psi}_g \times \boldsymbol{\psi}_h &= \boldsymbol{\psi}_{g \oplus h}, \\ \boldsymbol{\psi}_g \times \boldsymbol{\sigma} &= \boldsymbol{\sigma}, \end{aligned} \tag{2.18}$$

where g and h are defined $\mathsf{mod}(m)$. In the case of $m = 1$, the above model is identical to the Ising anyon model of (2.15). If $m > 1$, instead of having one Abelian field as for the Ising anyons, now we have m ($\boldsymbol{\psi}_0$ is identified with the vacuum $\mathbf{1}$). Such a theory is referred to as *parafermion* theory. Eqs. (2.18) imply that now there are $m + 1$ distinct

topological charge sectors. Consecutive associative application of the fusion rules in Eqs. (2.18) for N $\boldsymbol{\sigma}$ particles yields

$$\bigtimes_{N=2n-1} \boldsymbol{\sigma} = (m+1)^{n-1}\boldsymbol{\sigma}, \qquad \bigtimes_{N=2n} \boldsymbol{\sigma} = (m+1)^{n-1}\sum_{g=0}^{m}\boldsymbol{\psi}_g, \qquad \forall\ n \in \mathbb{N}.$$

Compared to Ising anyons, the fusion tree degeneracy is hence increased for $m > 1$. For instance in the case $m = 3$, three $\boldsymbol{\sigma}$ particles provide a large enough space to encode two-qubit gates. However, a striking difference to the case of $m = 1$ is that there is no non-trivial solution to the pentagon and hexagon equations anymore, which complicates a generic description of braiding operations. As such, a theory with the fusion rules (2.18) only obeys projective non-Abelian statistics, that is, the statistics of the particles is not universal but becomes path dependent. This property does not necessarily spoil their use for topological quantum computation. However, the construction of quantum gates from braid group generators becomes model specific [OTMS15, HL16]. Some related models, the so-called metaplectic anyons, even allow for universal quantum computing [HNW13].

2.4 Condensed matter realization of non-Abelian anyons

All conventional matter that we know so far consists of Abelian particles. It is therefore a fair question how, if ever, it is possible to obtain non-Abelian particles when all constituents are Abelian particles. The answer to this highly non-trivial question is twofold. Firstly, it is necessary to set the right frames, that is, as we know from Sec. 2.1, a 2D world, as only there the statistics of particles can deviate from that of fermions and bosons. Secondly, in this 2D world, we need to find a way, such that the relevant excitations are particles with anyonic character, which is not guaranteed in general.

Condensed matter physics equips us with the building blocks to achieve both tasks. Obviously, it is not possible to change the paradigms of space as a whole, however, we can think of a condensed, spontaneously symmetry broken system of atoms that form a crystal. The movement of electrons in such a system would be constrained to the dimensions of the crystal and, for a 2D crystal, the electrons hence experience a 2D world. Still, all the constituent particles are of Abelian nature. This, however, is not always one-to-one related to the nature of the relevant excitations. In particular, strongly interacting systems can drastically reorganize the many-body Fock space and lead to exotic emergent particles.

In this Section, we will shed some light on different models that support non-Abelian anyons as low-energy excitations in various condensed matter systems. Despite the immense comprehensiveness of two dimensional models, such as Kitaev's honeycomb model [Kit06], in view of the scope of the thesis our focus will be set on 1D models. In fact, in one spatial dimension exchange of particles is not well defined. Still, we can define non-Abelian anyons just by their emergent properties. Braiding and related operations, however, always require a second dimension. One of the simplest and simultaneously most fundamental models of such kind is the toy model of the 1D spinless p-wave SC [Kit01].

2.4.1 Splitting the fermion in halves

As starting point, let us think about a single ordinary fermion with a creation operator $\hat{c}$. This fermion might be represented in terms of two Majorana operators as [Maj37]

$$\hat{c} = \frac{1}{2}\left(\hat{\gamma}_1 + i\hat{\gamma}_2\right). \tag{2.19}$$

To ensure the fermionic commutation relations, different Majorana operators obey fermionic anti-commutation

$$\{\hat{\gamma}_j, \hat{\gamma}_k\} = 2\delta_{jk}. \tag{2.20}$$

More importantly, as opposed to usual fermions, the same Majorana operators satisfy

$$\hat{\gamma}_j^\dagger = \hat{\gamma}_j, \qquad \hat{\gamma}_j^2 = 1. \tag{2.21}$$

Up to a global phase, Majorana particles are identical with the non-Abelian Ising anyon field $\boldsymbol{\sigma}$. To see how this relation comes about in the language of fusion, let us consider the fermionic occupation number operator $\hat{n} = \hat{c}^\dagger\hat{c}$. In terms of Majorana modes, we readily obtain

$$\hat{n} = \frac{i}{2}\hat{\gamma}_1\hat{\gamma}_2 + \frac{1}{2}. \tag{2.22}$$

The fermion occupation number operator applied onto an occupation number state yields the two possibilities $\hat{n}|0\rangle = 0|0\rangle$, $\hat{n}|1\rangle = 1|1\rangle$, corresponding to the presence of either 0 or 1 fermion. Consequently, the occupation number states are also eigenstates to the operator $\mathcal{P} = -i\hat{\gamma}_1\hat{\gamma}_2$, which is identified as the fermion parity operator due to

$$\mathcal{P}|0\rangle = |0\rangle, \qquad \mathcal{P}|1\rangle = -|1\rangle. \tag{2.23}$$

In the language of fusion, the product operator $\hat{\gamma}_1\hat{\gamma}_2$ can be seen as the fusion of operators $\hat{\gamma}_1$ and $\hat{\gamma}_2$. The fusion process has two eigenstates $|0\rangle$ and $|1\rangle$, corresponding to the two different possible fusion outcomes. Either the two Majoranas fuse to the vacuum, represented by $\mathbf{1}$ in the fusion language and $|0\rangle$ in the fermion occupation number basis, or to one fermion, depicted by $\boldsymbol{\psi}$, $|1\rangle$, respectively. In that respect, the fusion rules of Majoranas coincide exactly with the ones of the $\boldsymbol{\sigma}$ field in the Ising anyon model, given in Eq. (2.15).

From the identification (2.19), using $\hat{c}^\dagger|0\rangle = |1\rangle$, we further deduce that Majoranas act as creation operators on the manifold $|0\rangle, |1\rangle$, whereas twofold consecutive application of the same Majorana operator leaves the state invariant. This profound property reflects the non-Abelian nature of Majoranas. Note also that the anti-commutation of Majorana operators is not directly related to the R matrix describing a braiding process. Rather it appears as a consequence of (2.21). From

$$\hat{\gamma}_j^2\hat{\gamma}_k = \hat{\gamma}_k\hat{\gamma}_j^2, \qquad \forall j,k,$$

it follows that commutation of two Majoranas must yield a square root of one. As we build the Majorana from a fermion, this root is fixed to +1, producing Eq. (2.20). Since fusion of two Majoranas is captured by the product operator $\hat{\gamma}_j\hat{\gamma}_k$, commutation of Majoranas is an operation that takes place when the two Majoranas are already fused. It happens at the fusion tree level, where the branches of $\hat{\gamma}_j$ and $\hat{\gamma}_k$ are already merged. In contrast to that, braiding operations take place at least one tree level above, where the world-lines of $\hat{\gamma}_j$ and $\hat{\gamma}_k$ are still separated (see Fig. 2.2 (a), (c) and (d)).
Typically, quantum mechanics desires hermitian operators, and single fermionic operators are not expected to appear in any valid Hamiltonian. Provided the theory is based on fermions, hermitian operators are expected to always contain (at least) pairs of Majorana operators. In that sense, we can always describe the system in terms of non-Abelian Majorana particles, however, we expect to find them paired (or fused) to form Abelian particles, but not unpaired. We will see in the following that this expectation is not always guaranteed.

2.4.2 Spinless p-wave superconductors

Consider a 1D system of fermions on a lattice of length L described by the following second-quantized Hamiltonian

$$H_K = \sum_{j=1}^{L-1}\left[-t_K\hat{c}_j^\dagger\hat{c}_{j+1} - \mu\left(\hat{c}_j^\dagger\hat{c}_j - \frac{1}{2}\right) + \Delta\hat{c}_j\hat{c}_{j+1}\right] + \text{h.c.}, \tag{2.24}$$

where $\hat{c}_j^\dagger$ ($\hat{c}_j$) creates (annihilates) a spinless fermion on site j. t_K is a hopping constant, μ a chemical potential and $\Delta = |\Delta|e^{i\theta}$ an induced superconducting gap. Using the transformation of Eq. (2.19) for any lattice fermion

$$\hat{c}_j = \frac{1}{2}e^{-i\theta/2}\left(\hat{\gamma}_{2j-1} + i\hat{\gamma}_{2j}\right), \tag{2.25}$$

we bring the Hamiltonian to the form

$$H_K = \frac{i}{2}\sum_j\left[-\mu\hat{\gamma}_{2j-1}\hat{\gamma}_{2j} + (t_K + |\Delta|)\hat{\gamma}_{2j}\hat{\gamma}_{2j+1} + (-t_K + |\Delta|)\hat{\gamma}_{2j-1}\hat{\gamma}_{2j+2}\right].$$

In principle, the above change of basis can be applied to any system of fermions. The spinless p-wave SC hides something remarkable though.
Let us discuss two limits. First, the trivial case with $|\Delta| = t_K = 0$ and $\mu < 0$. In this scenario, the Hamiltonian simply becomes

$$H_K = -\mu\sum_{j=1}^{L}\left(\hat{c}_j^\dagger\hat{c}_j - \frac{1}{2}\right) = \frac{-i\mu}{2}\sum_{j=1}^{L}\hat{\gamma}_{2j-1}\hat{\gamma}_{2j}.$$

Majorana operators from the same site (i. e. the same fermion $\hat{c}_j$) are paired together and no unpaired Majoranas appear throughout the chain. In the second scenario, let us

fix $|\Delta| = t_K > 0$ and $\mu = 0$. This readily leads to

$$H_K = it_K \sum_{j=1}^{L-1} \hat{\gamma}_{2j}\hat{\gamma}_{2j+1}. \tag{2.26}$$

Now, Majorana modes are paired across different sites. This has a remarkable consequence: In the case of open boundary conditions, the Majorana modes $\hat{\gamma}_1$ and $\hat{\gamma}_{2L}$ are not part of the Hamiltonian anymore. Evidently, they are part of the system though. It is easy to verify

$$\left[it_K \sum_{j=1}^{L-1} \hat{\gamma}_{2j}\hat{\gamma}_{2j+1}, \hat{\gamma}_1 \right] = \left[it_K \sum_{j=1}^{L-1} \hat{\gamma}_{2j}\hat{\gamma}_{2j+1}, \hat{\gamma}_{2L} \right] = 0, \tag{2.27}$$

where $[.,.]$ denotes the commutator. Eq. (2.27) implies that $\hat{\gamma}_1$, $\hat{\gamma}_{2L}$ and the Hamiltonian H_K have a common set of eigenvectors and by applying $\hat{\gamma}_1$ or $\hat{\gamma}_{2L}$ it is not possible to add energy to the system. Ground states are hence characterized by the two unpaired Majorana modes. When we interpret a composition of $\hat{\gamma}_1$ and $\hat{\gamma}_{2L}$ as a single non-local fermion $\hat{d} = (\hat{\gamma}_1 + i\hat{\gamma}_{2L})/2$, then the occupation number operator of this non-local fermion is proportional to an operator describing the fusion of $\hat{\gamma}_1$ and $\hat{\gamma}_2$, $\hat{n}_d = \hat{d}^\dagger\hat{d} = i/2\hat{\gamma}_{2L}\hat{\gamma}_1 + 1/2$. The outcome of the fusion (i. e. the eigenvalues of the operator $-i\hat{\gamma}_1\hat{\gamma}_{2L}$) can take two possible values, corresponding to this non-local fermion being empty or occupied. Both fusion outcomes take the same energy, reflecting the ground state degeneracy.

Let us formulate this in a more precise way. The Hamiltonian of Eq. (2.26) can be rewritten in terms of a new set of fermions $\hat{f}_j = e^{-i\theta/2}(\hat{\gamma}_{2j} + i\hat{\gamma}_{2j+1})/2$

$$H_K = 2t_K \sum_{j=1}^{L_1} \left(\hat{f}_j^\dagger \hat{f}_j - \frac{1}{2} \right). \tag{2.28}$$

Furthermore, since $[\hat{n}_d, H_K] = 0$, we can characterize the eigenstates of the system by occupations of fermions in the bulk $\hat{n}_f = \sum_j^{L-1} \hat{f}_j^\dagger \hat{f}_j$ and (non-local) fermions at the boundary: $|n_f, n_d\rangle$. The ground states of Eq. (2.28) are obviously the ones with $n_f = 0$. However, since $\hat{n}_d$ is not part of the Hamiltonian, we find the two degenerate ground states $|n_f = 0, n_d = 0\rangle = |0\rangle$ and $|n_f = 0, n_d = 1\rangle = |1\rangle$. Importantly, these ground states are also eigenstates to the fermion parity operator $\mathcal{P} = e^{i\pi \sum_j \hat{c}_j^\dagger \hat{c}_j}$ and might be as well represented by equal weight superpositions of all possible states with fixed fermion parity [TPB11, IMR+15]. Then, it can be shown that no local perturbation in the bulk is able to distinguish the different ground states, since in any finite region, for both ground states, the parity can locally be either even or odd. The only way to distinguish between the different ground states are either non-local operators or terms that directly compare the different ends of the wire, i. e. boundary terms.

For instance, in the case of periodic boundary conditions, the extra boundary term in the

Hamiltonian adds the missing fermion to the system

$$H_K = it_K \sum_{j=1}^{L-1} \hat{\gamma}_{2j}\hat{\gamma}_{2j+1} + it_K\hat{\gamma}_{2L}\hat{\gamma}_1 = 2t_K \sum_{j=1}^{L_1} \left(\hat{f}_j^\dagger \hat{f}_j - \frac{1}{2}\right) + 2t_K\left(\hat{n}_d - \frac{1}{2}\right),$$

where the term $it_K\hat{\gamma}_{2L}\hat{\gamma}_1$ attributes different energy to the formerly degenerate ground states. The degeneracy is hence removed, and now the only ground state corresponds to the one with all fermionic states being empty. In that sense, the ends of the wire can be viewed as defects that bind non-Abelian Majorana modes. Removing the defects, by enforcing periodic boundary conditions, also removes the unpaired Majorana modes.
The two limiting cases $|\Delta| = t_K > 0$ and $\mu = 0$ or $|\Delta| = t_K = 0$ and $\mu > 0$ demonstrate that the Hamiltonian of the spinless p-wave superconducting wire supports two distinct *topological* phases. Formally, these phases can be described by a topological invariant [Kit01] showing that the system undergoes a phase transition from topological to trivial at $2t_K = |\mu|$ (for $t_K = |\Delta|$). Consequently, in the whole parameter regime $2t_K > |\mu|$ non-Abelian Majorana modes are bound to the ends of the wire. Away from the point $\mu = 0$, rather than being localized on a single site (1 or $2L$), the Majorana modes acquire a finite decay length and are exponentially localized. The decay length is controlled by the spectral gap (i. e. $\sim |\Delta|$). As the system approaches the phase transition, the spectral gap closes and exactly at $2t_K = |\mu|$ the decay length of the Majorana becomes infinite and boundary modes disappear.

2.4.3 Spin-orbit coupled quantum wires

The spinless nature that Kitaev assumed for the fermions in his model posed a major obstacle that prevented a direct implementation of his idea in more realistic condensed matter systems and so it took almost a full decade until Kitaev's seminal work was transformed into feasible systems. By this time it was recognized that coupling the spin of electrons to their momentum can effectively render them spinless. Then, even ordinary s-wave superconductivity is able to induce topological superconductivity since the Rashba SOC mixes s- and p-wave components of the pairing. An effective model for such a situation is found by SOC quantum wires under the influence of an external magnetic field and proximity induced s-wave superconductivity, described by [ORvO10, LSDS10, STL+10]

$$H_{\mathrm{SOW}} = \int \mathrm{d}x \left[\hat{\Psi}^\dagger(x)\left(\frac{\hat{p}^2}{2m} - \mu(x) + \alpha_S(x)\sigma_x\hat{p} + B(x)\sigma_z\right)\hat{\Psi}(x) + \Delta(x)\hat{\psi}_\uparrow(x)\hat{\psi}_\downarrow(x) + \mathrm{h.c.}\right], \tag{2.29}$$

where σ_j ($j \in x, y, z$) are Pauli matrices acting on spin space and $\hat{\Psi}(x) = (\hat{\psi}_\uparrow(x), \hat{\psi}_\downarrow(x))^T$ are fermionic field operators. $B(x)$ is a magnetic field aligned along z-direction and $\Delta(x)$ constitutes an ordinary s-wave pairing. The Rashba SOC term, $\alpha_S(x)\sigma_x\hat{p}$, couples the spin of the fermions with their moving direction. Microscopically, this term can emerge as a relativistic correction in first order of $(v/c)^2$ (with the speed of light c and the electron group velocity v) as electrons move in a spatially inhomogeneous electric potential [RS15]. In crystals, such terms can naturally appear as the motion of electrons is affected by the total ensemble of atomic cores. The kind and direction of SOC is thereby strongly

dependent on the crystalline symmetries. In modern SOC wires, the direction of Rashba SOC is typically perpendicular to the wire axis.

Applying a BdG transformation [Bog58], we can rewrite Eq. (2.29) to obtain

$$H_{\text{SOW}} = \frac{1}{2}\int \mathrm{d}x \hat{\Psi}^\dagger_{\text{BdG}}(x)\left[\left(\frac{\hat{p}^2}{2m} - \mu(x)\right)\tau_z\sigma_0 + \alpha_S(x)\hat{p}\tau_z\sigma_x + B(x)\tau_0\sigma_z + \Delta(x)\tau_x\sigma_0\right]\hat{\Psi}_{\text{BdG}}(x) \tag{2.30}$$

with the new Pauli matrices τ_j ($j \in x,y,z$) acting in the space of particles and holes and the BdG spinor $\hat{\Psi}_{\text{BdG}}(x) = (\hat{\psi}_\uparrow(x), \hat{\psi}_\downarrow(x), \hat{\psi}^\dagger_\downarrow(x), -\hat{\psi}^\dagger_\uparrow(x))^T$. Furthermore, we use $\sigma_0 = \tau_0 = \mathbb{1}_{2\times 2}$. The BdG transformation is a convenient trick to deal with superconducting systems, where the Hilbert space is doubled by introducing "hole-like" particles. In that way, the Hamiltonian of Eq. (2.29), which is quadratic in fields $\hat{\Psi}(x)$, is transformed into a Hamiltonian of double space, which is linear in new BdG fields $\hat{\Psi}_{\text{BdG}}(x)$. The BdG transformed Hamiltonian of Eq. (2.30) can now be readily diagonalized using appropriate unitary transformations.

Consider the translational invariant case with $\mu(x) = \mu$, $B(x) = B$, $\alpha_S(x) = \alpha_S$ and $\Delta(x) = \Delta$. In this scenario, we can use a mode expansion of the fermionic fields in Eq. (2.30) $\hat{\Psi}_{\text{BdG}}(x) = \sum_k \hat{C}_k e^{ikx}$ with $\hat{C}_k = (\hat{c}_{k,\uparrow}, \hat{c}_{k,\downarrow}, \hat{c}^\dagger_{k,\downarrow}, -\hat{c}^\dagger_{k,\uparrow})^T$ to rewrite the Hamiltonian in momentum space

$$H_{\text{SOW}} = \frac{1}{2}\sum_k \hat{C}^\dagger_k \mathcal{H}_{\text{SOW}}(k)\hat{C}_k, \tag{2.31}$$

where we introduced the Hamiltonian density

$$\mathcal{H}_{\text{SOW}}(k) = \left(\frac{k^2}{2m} - \mu\right)\tau_z\sigma_0 + \alpha_S k\tau_z\sigma_x + B\tau_0\sigma_z + \Delta\tau_x\sigma_0. \tag{2.32}$$

For the case of vanishing superconducting pairing $\Delta = 0$, diagonalization of Eq. (2.32) yields the dispersion relation schematically illustrated in Fig. 2.8. When no magnetic field is applied, the SOC shifts the different spin bands horizontally in momentum space with a crossing at $k = 0$ (Fig. 2.8 (a)). Switching on a magnetic field opens a partial spectral gap around this crossing point (Fig. 2.8 (b)). It furthermore couples states of different spin, which leads to the fact that states at opposite momentum do no longer carry opposite spin, but a small "tilting" is acquired. In particular, when the magnetic field becomes the largest energy scale, as compared to the spin-orbit energy and the chemical potential $B \gg \alpha_S, \mu$, the states of the different branches become more and more polarized along the direction of the magnetic field. In this scenario one of the two bands is displaced in energy by a magnitude of the order of B (see Fig. 2.8 (c)). The effective low-energy physics is then captured by only one of the two bands. In a BdG sense, this band can be described by two states, $|e\rangle$ and $|h\rangle$. In a zeroth order expansion in α_S/B, these two states are spin-z eigenstates, where in the basis of Eq. (2.31) we have

$$|e\rangle = (1,0,0,0)^T, \qquad |h\rangle = (0,0,0,1)^T.$$

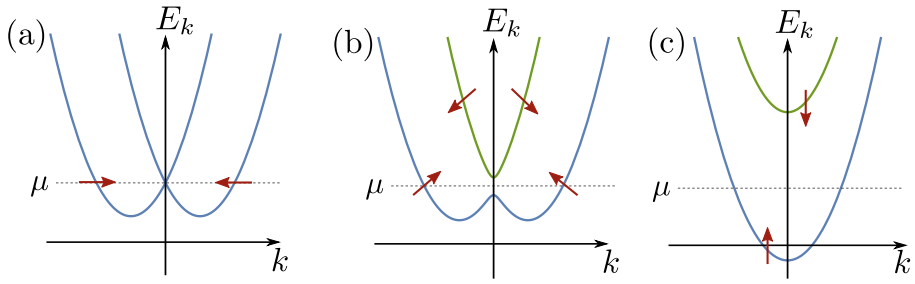

Figure 2.8: Schematic dispersion of energy bands from Eq. (2.31) in three different limits: (a) $B = 0$, (b) $\alpha_S \gg B$ and (c) $B \gg \alpha_S$. In all three panels $\Delta = 0$. The arrows indicate the spin direction of the eigenstates.

Consider now to turn on a s-wave pairing according to the corresponding term in Eq. (2.32). In the subspace of the spin-z eigenstates $|e\rangle$, $|h\rangle$, the matrix elements of s-wave pairing vanish

$$\langle h|\Delta\tau_x\sigma_0|e\rangle = \langle e|\Delta\tau_x\sigma_0|h\rangle = \langle h|\Delta\tau_x\sigma_0|h\rangle = \langle e|\Delta\tau_x\sigma_0|e\rangle = 0.$$

This changes when we include the first order correction in α_S/B to the states $|e\rangle$ and $|h\rangle$. Then, we find [vOPP14]

$$|e\rangle = 1/N_k(1, -\alpha_S k/(2B), 0, 0)^T, \qquad |h\rangle = 1/N_k(0, 0, -\alpha_S k/(2B), 1)^T$$

with $N_k = \sqrt{1 + k^2/(4B^2)}$. Repeating the calculation of the matrix elements of the pairing readily leads to two non-zero elements

$$\langle h|\Delta\tau_x|e\rangle = \langle e|\Delta\tau_x|h\rangle = -\frac{\alpha_S k\Delta}{2BN_k^2}.$$

In the subspace of $|e\rangle$ and $|h\rangle$, the corresponding Hamiltonian density including first order corrections in α_S/B hence resembles to the leading order in k the continuum version of a spinless p-wave superconducting wire discussed in the former section

$$\mathcal{H}_{\mathrm{SOW}}(k) \simeq \left(\frac{k^2}{2m} - \mu\right)\tau_z - \frac{\alpha_S k\Delta}{2BN_k^2}\tau_x.$$

Consequently, at least in the regime where the applied Zeeman field constitutes the largest energy scale, the SOC quantum wire with proximity induced ordinary s-wave superconductivity resembles a topological superconducting phase, hosting non-Abelian Majorana modes at its ends or at phase boundaries. As the phase properties are expected to remain unchanged upon smooth deformations of the Hamiltonian, we do expect to find these topological boundary modes as long as no gap closing appears. Indeed, we can discriminate the topological superconducting phase from the trivial by investigating the spectral properties of Eq. (2.31) corresponding to the eigenvalues of Eq. (2.32), which can be

straightforwardly obtained [ORvO10]

$$E_\pm^2 = B^2 + \Delta^2 + \xi_k^2 + (\alpha_S k)^2 \pm 2\sqrt{B^2\Delta^2 + B^2 + \xi_k^2 + (\alpha_S k)^2 \xi_k^2}$$

with $\xi_k = k^2/(2m) - \mu$. $E_\pm$ has two low-energy points: one around $k = 0$ and another one close to the Fermi momenta following $\xi_k \pm \alpha_S k = 0$. Assuming finite Δ, the gap around the Fermi momenta never closes, however, at $k = 0$, the above expression simplifies and we find that a gap closing appears in E_- for $B = \sqrt{\Delta^2 + \mu^2}$. Hence, we can conclude that for all values of $B > \sqrt{\Delta^2 + \mu^2}$ the system remains in the topological superconducting phase. There, we expect to find Majorana modes, bound to topological defects. Such a defect can be modeled in the simplest fashion by a phase boundary. This might be achieved for instance by a spatial variation of either of the control parameters B, μ or Δ. Let us give a spatial dependence to the applied Zeeman field $B = B(x) = \Delta + bx$, generating a topological defect at $x = 0$. Furthermore, assume to choose $b > 0$ but small enough, such that the relevant length scale l_b on which the spectral properties change follows $l_b \gg 1/k_r$, where k_r are relevant momenta around the low energy points. Then, in an area l_b around $x = 0$, we can approximate the Hamiltonian density of Eq. (2.30) up to linear order in $\hat{p}$, resulting in the Hamiltonian density

$$\mathcal{H}_{\text{SOW,eff}}(x) = \alpha_S \hat{p}\tau_z\sigma_x - \mu\tau_z\sigma_0 + B(x)\tau_0\sigma_z + \Delta\tau_x\sigma_0. \tag{2.33}$$

A convenient way to diagonalize the above Hamiltonian density uses a mapping to the harmonic oscillator. For that, we first square Eq. (2.33) to obtain [ORvO10]

$$\mathcal{H}^2_{\text{SOW,eff}} = (\alpha_S\hat{p})^2 + B(x)^2 + \Delta^2 + 2\Delta B(x)\tau_x\sigma_z - \alpha_S b\tau_z\sigma_y,$$

where the last term appears as a result of the anti-commutator of $\hat{p}$ with the spatially dependent $B(x)$, $\{\alpha_S\hat{p}\tau_z\sigma_x, B(x)\tau_0\sigma_z\} = -\tau_z\sigma_y\alpha_S b$. Upon an unitary transformation U_b, $\mathcal{H}^2_{\text{SOW,eff}}$ becomes diagonal with entries $(\alpha_S\hat{p})^2 + (\Delta \pm B(x))^2 \pm \alpha_S b$. Now, for the case $\Delta - B(x)$, we obtain the Hamiltonian of a harmonic oscillator, whose energy levels are given by $E^2_{n,\pm} = 2\alpha_S b(n + 1/2) \pm \alpha_S b$. Hence, there exists a single zero energy solution $E^2_{0,-}$, where the eigenfunction corresponds to the ground state wave function of the harmonic oscillator. From the respective entries of the unitary U_b we obtain the corresponding BdG operator. This eventually leads to a BS, localized around $x = 0$, of the form

$$\hat{\gamma}(x) = \frac{b}{(\alpha_S\pi)^{1/4}} e^{-bx^2/(2\alpha_S)} \left[f\hat{\psi}_\uparrow(x) + f^*\hat{\psi}^\dagger_\uparrow(x) + f^*\hat{\psi}_\downarrow(x) + f\hat{\psi}^\dagger_\downarrow(x) \right],$$

where $f = (1 + i)/(2\sqrt{2})$. One can readily check that $\hat{\gamma}(x) = \hat{\gamma}^\dagger(x)$, proving the Majorana nature of the computed solution. Evidently, similar constructions of a Majorana solution can be derived for spatial variation of any of the remaining control parameters Δ and μ.

In condensed matter physics, non-Abelian particles, such as the Majorana solution above, appear as effective collective excitations of a system formed from more fundamental particles, which are mostly fermions. Fusion of all non-Abelian particles in a given system is hence required to yield an Abelian total topological charge. For the case of Majorana modes, as evident from Eq. (2.16), this implies an even number of Majorana modes in

any given fermion based system.

The above construction of a topological defect using spatially varying control parameters gives the impression of a single Majorana solution. This is however not true. A second Majorana mode is acquired due to boundary conditions [JR76]. If the space is compactified with periodic boundary conditions, we obtain a second topological defect from the discontinuous jump of the spatially varying control parameter. In the case of open boundary conditions, the second Majorana solution is bound to the topological end of the wire [KL12].

2.4.4 Edge theory hetero-junctions

SOC in combination with ordinary s-wave superconductivity is at the heart of the construction of non-Abelian anyons in condensed matter systems. This eventually condenses in the effective Hamiltonian given in Eq. (2.33). In recent years, similar effective Hamiltonians earned a lot of attention in the context of TIs.

Different from the conventional classes of matter, these novel kind of materials are characterized by an insulating bulk and metallic edges. The first example of such kind of systems was found in 2D systems by the integer and fractional quantum Hall effect, where, due to the presence of strong out of plane magnetic fields, Landau levels form and currents can only propagate along the edges of the sample [KDP80, Hal82, TSG82, Lau83]. The states associated with these currents possess a chiral character. Backscattering is thus exponentially suppressed in the width of the quantum Hall sample leading to an exceedingly precise conductance quantization. The notion of Landau levels as initiator of quantized conductance is convenient. However, as recognized by Haldane, rather than the presence of Landau levels, the breaking of TR symmetry generates non-zero quantized edge conductance. He was able to demonstrate this effect in a gapped lattice model based on Graphene. Thereby, TR symmetry is broken by two terms that mimic a flux. The net flux, however, is kept zero [Hal88]. Still, Haldane demonstrated that a quantized edge conductance exists in his model, provided TR symmetry is broken. However, Haldane's model did not account for the spin of the particles. This gap was eventually closed by Kane and Mele [KM05a, KM05b]. In that, they restored time reversal symmetry, suggesting vanishing edge conductance. Yet, each spin sector separately resembles the Haldane model. As such, helical counter-propagating edge currents are obtained. Unlike for the quantum Hall effect, backscattering is now prevented by TR symmetry. This might appear as a weak point, however, as we will discuss below, it can also evoke interesting physics if we explicitly break TR symmetry and generate backscattering. Inspired by the Kane and Mele model, this phenomenon, called QSH effect, was proposed [BHZ06, FK07, LHQ$^+$08] and realized in different material systems such as HgTe/CdTe quantum wells [KWB$^+$07], InAs/GaSb bilayers [KDS11, SND$^+$14] or Bismuthene on SiC substrates [RLD$^+$17]. Since then, especially the edge states of this novel material class have been subject of intense research.

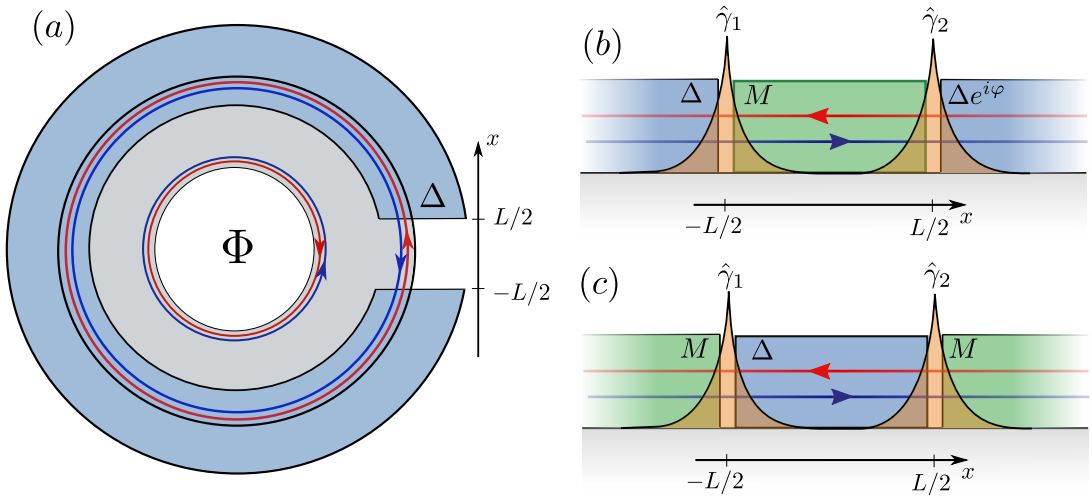

Figure 2.9: (a) Schematic of a Josephson junction based on a QSH ring pierced by a flux. (b) Zoom in of (a). The space dependence of the mass terms is assumed to be $B(x) = M\theta(x + L/2)\theta(L/2 - x)$ and $\Delta(x) = \left[\Delta\theta(-L/2 - x) + \Delta e^{i\varphi}\theta(x - L/2)\right]$. At the interfaces between M and Δ regions, Majorana BSs $\hat{\gamma}_1$ and $\hat{\gamma}_2$ form. (b) Similar junction as in (b) with $M(x) \to \Delta(x)$, $\Delta(x) \to M(x)$ and $\varphi = 0$.

Majorana bound states from superconductor-ferromagnet hetero-junctions

In lowest order, the effective Hamiltonian describing the edge states of a QSH material is given by [WBZ06]

$$H_{\mathrm{QSH}} = \int \mathrm{d}x\ \hat{\Psi}^\dagger(x)\left[v_F \hat{p}\sigma_z\right]\hat{\Psi}(x) \tag{2.34}$$

with $\hat{\Psi}(x) = \left[\hat{\psi}_\uparrow(x), \hat{\psi}_\downarrow(x)\right]^T$. When we proximitize the edge of a QSH insulator with a s-wave SC and expose it to magnetic fields, we end up with a Hamiltonian that is, up to an unitary transformation, identical to the one given in Eq. (2.33) [FK08, FK09]. As opposed to the quantum wire case, we do not need to enforce the slow spatial variation of the control parameters for the validity of the respective effective Hamiltonian. We could hence imagine a hetero-junction, schematically illustrated in Fig. 2.9 (a): a QSH ring pierced by a magnetic flux and proximitized by a s-wave SC for $x < -L/2$ and $x > L/2$ that induces a pairing amplitude in the helical edge states. The SC repels the magnetic field but acquires a phase in the order parameter, which eventually evokes the celebrated Josephson effect [Jos62]. In between the SCs (i. e. for $-L/2 < x < L/2$), the magnetic field enters in the Hamiltonian. Hence, the system is effectively described by the hetero-junction sketched in Fig. 2.9 (b), where the Hamiltonian density takes the same form as in Eq. (2.33), however, with modified spatial dependence $B(x) = M\theta(x+L/2)\theta(L/2-x)$ and $\Delta(x) = \left[\Delta\theta(-L/2 - x) + \Delta e^{i\varphi}\theta(x - L/2)\right]$. At the interfaces between SC and magnetically ordered area, (Majorana) BSs are forming. Finite M leads (in general) to a hybridization, wherefore the low-energy physics can be captured in a two level system. By virtue of PH

symmetry, we find for $L \ll v_F/\Delta$ [FK09]

$$H_{\mathrm{FK}} = 2i\sqrt{D}\Delta\cos(\varphi/2)\hat{\gamma}_1\hat{\gamma}_2 \tag{2.35}$$

with the Majorana operators $\hat{\gamma}_j$ ($j \in 1,2$) and $D = 1/\left[1 + (M\sinh(\kappa L)/\kappa)^2\right]$, where $\kappa = \sqrt{M^2 - \mu^2}$. Let us assume two limits: $M = 0$ and $\kappa L \to \infty$. In the case of $M = 0$, the system restores TR symmetry for the exceptional points $\varphi = n\pi$ with $n \in \mathbb{Z}$. TR symmetry, in turn, enforces Kramers degeneracy. This is realized as the spectrum of Eq. (2.35) touches the bulk spectrum whenever the superconducting phase takes an even multiple of π, while for odd multiples of π, the hybridization vanishes leading to a Kramers pair of Majorana modes. In the case of $M \neq 0$, TR symmetry is always absent. Then, however, hybridization of the two Majorana modes is exponentially suppressed in κL with one Majorana mode bound to each interface of SC and magnetically ordered region (Fig. 2.9 (b)). In this limit, the low-energy physics is insensitive to the specific arrangement of superconducting and magnetic regions as long as proper boundaries between the two can be found. For ease of understanding, in the remainder of this section, we will therefore work with the hetero-junction illustrated in Fig. 2.9 (c) where a single superconducting region is embedded by magnetic regions.

In particular, let us investigate the hetero-junction of Fig. 2.9 (c) from the perspective of ground state degeneracies. While in its present fermionic form, it is not obvious in what way the Hamiltonian obeys a ground state degeneracy, this can be revealed by virtue of *bosonization*.

1D quantum systems of fermions have the remarkable property that they are equivalently described in terms of bosons. Originally, the mapping from fermions to bosons is motivated by electron-electron interactions. The principles that lead to Fermi liquid theory do not apply in 1D and excitations are always of bosonic nature. Pictorially this might be understood from the fact that interacting fermions cannot disperse freely in 1D systems without affecting their neighbors. Then, the relevant excitations are of collective nature, such as density waves, described by bosons. Nowadays, bosonization is a widely used mathematical tool to efficiently describe 1D interacting systems of fermions. For now we are concerned with the physical aspects and consequences of this mapping in the context of non-Abelian anyons. A detailed review of the principles of bosonization will be given in Sec. 3.1.

While the reformulation of 1D fermionic systems in terms of bosons is of particular use when electronic density-density interactions are present, the mapping itself is not restricted to interacting systems and does also apply to the non-interacting case. In particular, the bosonization identity states [Gia03, vDS98]

$$\hat{\psi}_r(x) = \frac{\mathcal{F}_r}{\sqrt{2\pi a}} e^{irk_F x} e^{-i(r\hat{\phi}(x) - \hat{\theta}(x))} \tag{2.36}$$

with $r = \uparrow, \downarrow = +, -$ and the hermitian bosonic field operators $\hat{\phi}(x)$ and $\hat{\theta}(x)$. $\mathcal{F}_r$ are called Klein factors, lowering the number of fermions by one and a is cutoff to avoid divergencies.

The bosonic fields $\hat{\phi}(x)$ and $\hat{\theta}(x)$ obey the commutation relation

$$\left[\hat{\phi}(x), \hat{\theta}(x')\right] = i\pi\theta(x'-x) \tag{2.37}$$

with the Heaviside step function $\theta(x-x')$. Using Eq. (2.36), we can transform Eq. (2.34) into its bosonic form

$$H_{\mathrm{QSH}} = \frac{1}{2\pi}\int \mathrm{d}x \left[\frac{u}{K}\left(\partial_x\hat{\phi}(x)\right)^2 + uK\left(\partial_x\hat{\theta}(x)\right)^2\right]. \tag{2.38}$$

K is a dimensionless parameter capturing the strength of electron-electron interactions and u is a renormalized Fermi velocity. In particular $K=1$ and $u=v_F$ in the non-interacting case, while $K<1$ ($K>1$) for repulsive (attractive) interactions. Starting from Eq. (2.34), we clearly have $K=1$. However, in the perspective of further discussions, it is useful to keep it in the Hamiltonian. Next, we can investigate the mass terms in view of Eq. (2.36)

$$\begin{aligned} H_\Delta &= \int \mathrm{d}x\Delta(x)\left[\hat{\psi}_\uparrow(x)\hat{\psi}_\downarrow(x) + \mathrm{h.c.}\right] = \int \mathrm{d}x \frac{\Delta(x)}{2\pi a}\left[\mathcal{F}_\uparrow\mathcal{F}_\downarrow e^{2i\hat{\theta}(x)} + \mathrm{h.c.}\right], \\ H_\mathrm{B} &= \int \mathrm{d}x B(x)\left[\hat{\psi}^\dagger_\uparrow(x)\hat{\psi}_\downarrow(x) + \mathrm{h.c.}\right] = \int \mathrm{d}x \frac{B(x)}{2\pi a}\left[\mathcal{F}^\dagger_\uparrow\mathcal{F}_\downarrow e^{2i\hat{\phi}(x)}e^{-2ik_F x} + \mathrm{h.c.}\right]. \end{aligned} \tag{2.39}$$

Klein factors do not carry any spatial dependence. Consequently, they do not contribute to the space-time dependence of correlation functions, which is totally controlled by the bosonic fields [Gia03]. In the thermodynamic limit, we can hence ignore the Klein factors in the above equations[2] and obtain

$$H_\Delta = \frac{\Delta}{\pi a}\int_{-L/2}^{L/2} \mathrm{d}x\ \cos\left[2\hat{\theta}(x)\right], \tag{2.40}$$

$$H_\mathrm{B} = H_{\mathrm{B},-} + H_{\mathrm{B},+} = \frac{M}{\pi a}\left[\int_{-\infty}^{-L/2} + \int_{L/2}^{\infty}\right]\mathrm{d}x\ \cos\left[2\hat{\phi}(x) - 2k_F x\right], \tag{2.41}$$

where we used the spatial dependence of $B(x)$ and $\Delta(x)$ as depicted in Fig. 2.9 (c). Here, since the relevant length scales are infinitely long at least for H_B, we require $k_F \to 0$ to obtain H_B as a relevant term. Otherwise, integration renders the energy contribution of H_B irrelevant[3].

The full Hamiltonian of the hetero-junction is compiled by the sum of Eqs. (2.38), (2.40) and (2.41). Our goal is to determine the ground states of this system. On the first sight this gives the impression of a difficult task. However, there are some neat shortcuts. Let us assume to be far away from any boundary of the system, say $x \ll -L/2$. In this region of space, the ground states of the system are determined by H_{QSH} and $H_{\mathrm{B},-}$. The cosine part, $H_{\mathrm{B},-}$, would like to lock the field $\hat{\phi}(x)$ and abandon its spatial dependence $\hat{\phi}(x) \to \hat{\phi}$, such that the eigenvalues of the new phase field $\hat{\phi}$ correspond to the minimum of the cosine potential. Then, also in the kinetic part $\partial_x\hat{\phi} \to 0$. However, Eq. (2.37) implies

[2] This subtle point will be discussed in detail in Sec. 3.1.4

[3] Note that, in general, finite k_F with $k_F \gg 1/L$ leads to a reduction of the overall energy contribution of Eq. (2.41) by (at least) a factor $\sim 1/(k_F L)$.

strong fluctuations in the field $\hat{\theta}(x)$, increasing the kinetic energy. In conclusion, if H_{B} gives the biggest portion to the ground state energy, then, the corresponding states will be characterized by eigenstates of the phase fields $\hat{\phi}$. In contrast, if the kinetic energy term H_{QSH} dominates, ground states will be determined by spatially fluctuating fields $\hat{\phi}(x)$ and $\hat{\theta}(x)$. A systematic way to resolve these competing interests is to use a RG ansatz.
RG theory is a comprehensive fundamental method to obtain the low-energy behavior of a given system[4]. The overall idea is to obtain an insight in low-energy properties of a system by rescaling and integrating out high energy contributions of the partition function. Often times this has to be done perturbatively around a fixed point [Car96, GNT98, Gia03, Fra13]. For our case, this fixed point is given by H_{QSH} and the corresponding Gaussian action, obtained upon a Legendre transformation and a rescaling of the fields $\hat{\phi}(x) \to \tilde{\phi}(x) = 1/(\sqrt{\pi K})\ \hat{\phi}(x)$ and $\hat{\theta}(x) \to \tilde{\theta}(x) = \sqrt{K/\pi}\ \hat{\theta}(x)$. Then, the action of H_{QSH} is found to be

$$S_{\mathrm{QSH}}[\tilde{\phi}] \equiv S_0[\tilde{\phi}] = \frac{1}{2}\int \mathrm{d}x\mathrm{d}t\ \left[\frac{1}{u}(\partial_t\tilde{\phi}(x,t))^2 - u(\partial_x\tilde{\phi}(x,t))^2\right]. \tag{2.42}$$

The perturbation for which we aim to apply the perturbative RG procedure is found by the action of H_{B}

$$S_1[\tilde{\phi}] = g\int \mathrm{d}x u\mathrm{d}t\ \cos\left[\beta\tilde{\phi}(x,t)\right], \tag{2.43}$$

where $\beta = 2\sqrt{\pi K}$ and $g = M/(\pi a u)$. To treat Eq. (2.43) as a perturbation to Eq. (2.42) we need to assume that the coupling constant g is initially small. Now the question to answer is: What is the effective action when only low-energy contributions are included in the partition function? The answer is found by perturbatively integrating out the high energy contributions up to an ultra-violet cutoff. If the system under consideration is renormalizable, which is the case here, the effective action obeys exactly the same structure as the original one but with a new set of coupling constants. This results in a set of differential equations that relate the new coupling constants, after performing the renormalization procedure, to the original ones. For the present case, in first order, we obtain an equation capturing the change in the coupling constant g upon integrating out high energy modes of the portion $\mathrm{d}l$ (where $\mathrm{d}l$ itself is dimensionless) [GNT98]

$$g' = g(1 + (2-d)\mathrm{d}l) \tag{2.44}$$

with the scaling dimension $d = \beta^2/(4\pi)$. Eq. (2.44) results in the differential equation

$$\frac{\mathrm{d}g(l)}{\mathrm{d}l} = (2-d)g(l) \tag{2.45}$$

with the boundary condition $g(l=0) = g$ and the solution $g(l) = e^{2-K}g$. Hence, for $K < 2$, the cosine perturbation introduced by H_{B} becomes more important at lower energies with coupling constants scaling as $g(l) \to \infty$. In this scenario, H_{B} is a RG relevant perturbation.

[4] In this section we are concerned with physical aspects. A more detailed review of RG theory for sine-Gordon models can be found in Sec. 3.1.6.

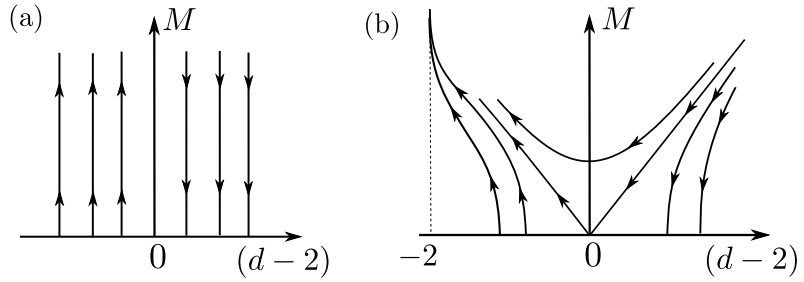

Figure 2.10: Schematic of the RG scaling. The RG flow happens along the direction set by the arrows. Different lines correspond to different initial conditions. (a) RG diagram in first order. (b) RG diagram in second order.

In contrast to that, for $K > 2$, the coupling constant scales as $g(l) \to 0$ and H_{B} is RG irrelevant. Fig. 2.10 (a) depicts this scaling behavior. If we include the second order in our perturbative RG analysis, Eq. (2.45) gets complemented by another differential equation, accounting for a change in the scaling dimensions. Then, the scaling behavior is captured by the set of coupled differential equations

$$\frac{\mathrm{d}g(l)}{\mathrm{d}l} = (2 - d(l))g(l), \qquad \frac{\mathrm{d}d(l)}{\mathrm{d}l} = -Ag^2(l)d^3(l) \tag{2.46}$$

with a numerical real and positive constant A. The solution to the above equation set (2.46) is depicted in Fig. 2.10 (b). Starting with an initially small coupling constant g in the regime $K < 2$, g flows to strong coupling while at the same time $K \to 0$. Typically, the RG flow is not continued forever, but instead it is terminated (in the infrared regime) at the largest characteristic energy scale of the system (such as the energy scale associated with temperature or system size). Lower energy scales are hidden.

Let us now come back to the initial problem of determining the ground states of $H_{\mathrm{QSH}}+H_{\mathrm{B}}$. The RG flow suggests that as we observe the system at low energies, the cosine gains relevance as its coupling constant grows. At the same time, since $K \to 0$, the $(\partial_x\hat{\phi}(x))^2$ contribution to the kinetic energy is RG relevant, while the $(\partial_x\hat{\theta}(x))^2$ contribution becomes RG irrelevant. Therefore we can drop it for the subsequent discussion

$$H_{\mathrm{QSH}} \quad \xrightarrow{\text{RG flow}} \quad H_{\mathrm{QSH,RG}} = \frac{1}{2\pi}\int \mathrm{d}x \frac{u}{K}\left(\partial_x\hat{\phi}(x)\right)^2. \tag{2.47}$$

Obviously, now it is possible to simultaneously minimize the kinetic energy (2.47) and H_{B} from Eq. (2.41) using the phase field ansatz $\hat{\phi}(x) \to \hat{\phi}_-$. Then, the kinetic energy vanishes, while the cosine is minimized when we demand the eigenspectrum of $\hat{\phi}_-$ to span across the different minima of the cosine. Then, we have

$$H_{\mathrm{QSH,RG}} + H_{\mathrm{B},-} \quad \xrightarrow{\hat{\phi}(x)\to\hat{\phi}_-} \quad H_{\mathrm{eff,B},-} = gu\int_{-\infty}^{-L/2} \mathrm{d}x \cos(2\hat{\phi}_-). \tag{2.48}$$

Analogously, for $x \gg L/2$, we obtain

$$H_{\text{eff,B},+} = gu \int_{L/2}^{\infty} \mathrm{d}x \cos(2\hat{\phi}_+)$$

with the phase field $\hat{\phi}_+$.

Naively, the periodicity of the cosine with respect to a shift of $2n\pi$ with $n \in \mathbb{Z}$ in the fields $\hat{\phi}_\pm$ would suggest an infinitely large ground state manifold. However, from the definition of the fermionic fields in Eq. (2.36), for fixed particle number it is clear that $\hat{\phi}_\pm$ is only uniquely defined on $[0, 2\pi[$. Then, on this fixed particle number circle, there are two minima, each of which represent an eigenvalue of the state $|n_{\phi,\pm}\rangle$ with

$$\hat{\phi}_\pm |n_{\phi,\pm}\rangle = \frac{\pi(2n_{\phi,\pm}+1)}{2} |n_{\phi,\pm}\rangle, \tag{2.49}$$

where $n_{\phi,\pm} = 0, 1$ (modulo 2). Eq. (2.49) corresponds to the parametrization $\hat{\phi}_\pm = (\pi/2)(2\hat{n}_{\phi,\pm}+1)$ with the integer valued operator $\hat{n}_{\phi,\pm}$ with $\hat{n}_{\phi,\pm}|n_{\phi,\pm}\rangle = n_{\phi,\pm}|n_{\phi,\pm}\rangle$. $H_{\text{B},\pm}$ induces a magnetic order in the system. Hence, from a physical viewpoint, a ground state degeneracy of two for each ordered region is a reasonable result. The different states represent the two different values ($\pm$) the magnetization can take along a fixed direction.

Let us now extend the above discussion and include the superconducting regime. Deep inside the superconducting regime ($x \sim 0$), we can draw the same line of reasoning as for the magnetically ordered regions. Provided $K > 1/2$ with initially small coupling constant $\delta_\Delta = \Delta/(\pi a u)$, H_Δ constitutes a RG relevant perturbation and scales to strong coupling. In second order we find that also K is rescaled, where this time $K \to \infty$. This renders $(u/K)(\partial_x \hat{\phi})^2$ in the kinetic part (H_{QSH}) RG irrelevant and leads to the effective low-energy Hamiltonian

$$H_{\text{eff},\Delta} = \delta_\Delta u \int_{-L/2}^{L/2} \mathrm{dx} \cos(2\hat{\theta}) = \delta_\Delta u L \cos(2\hat{\theta}) \tag{2.50}$$

with the phase field $\hat{\theta}$.

In total, the effective Hamiltonian is then compiled from the three parts $H_{\text{eff,B},\pm}$ and $H_{\text{eff},\Delta}$, resulting in

$$H_{\text{eff,tot}} = \delta_\Delta u L \cos(2\hat{\theta}) + gu \int_{-\infty}^{-L/2} \mathrm{d}x \ \cos(2\hat{\phi}_-) + gu \int_{L/2}^{\infty} \mathrm{d}x \cos(2\hat{\phi}_+). \tag{2.51}$$

Naively, one could now suppose that the total ground state manifold is just given by the multiplication of the degeneracies of the different constituent parts, i. e. $2 \times 2 \times 2 = 8$. However, this conjecture is not correct as it disregards the commutation relations of the phase fields induced by Eq. (2.37)

$$\left[\hat{\phi}_+, \hat{\theta}\right] = 0, \qquad \left[\hat{\phi}_-, \hat{\theta}\right] = i\pi. \tag{2.52}$$

Hence, $\hat{\theta}$ and $\hat{\phi}_-$ cannot have a common set of eigenstates and ground states of each

ordered region are not immediately also ground states of the composite system. Still, we know that Eq. (2.51) holds all information about the low-energy spectrum. Moreover, using (2.52), straightforward calculations yield

$$\left[H_{\text{eff,tot}}, e^{i\hat{\phi}_\pm}\right] = \left[H_{\text{eff,tot}}, e^{i\hat{\theta}}\right] = 0.$$

This implies that neither $e^{i\hat{\phi}_\pm}$ nor $e^{i\hat{\theta}}$ projects the system out of the eigenspace of $H_{\text{eff,tot}}$. However, since $[e^{i\hat{\phi}_-}, e^{i\hat{\theta}}] \neq 0$, they cannot be used at the same time to characterize the ground states. Instead, we have to find a maximum set of operators that commute with the Hamiltonian and among each other. Typically, there are different operator sets that fulfill these requirements and it is usually only a matter of choice which one to pick. For us, the two possible sets are found by either $\{e^{i\hat{\phi}_+}, e^{i\hat{\theta}}\}$ or $\{e^{i\hat{\phi}_-}, e^{i\hat{\phi}_+}\}$. Note that we could always complement these sets by operators $e^{i2\hat{\theta}}$ or $e^{i2\hat{\phi}_\pm}$, however, such operators only carry the eigenvalue -1. Thus, they are not able to discriminate among different ground states and cannot be relevant for their characterization.

Let us choose for convenience $\{e^{i\hat{\phi}_-}, e^{i\hat{\phi}_+}\}$. If we demand no additional boundaries in the system (upon space compactification), the phase fields $\hat{\phi}_-$ and $\hat{\phi}_+$ originate from the same magnetic region, which implies that they cannot be independent. Rather, either of the two fields is sufficient to characterize the ground states. However, by virtue of (2.52), we can not equal the two fields. Instead, we require

$$\hat{\phi}_+ = \hat{\phi}_- + \hat{Q}, \tag{2.53}$$

where the operator $\hat{Q}$ ensures (2.52) with

$$\left[\hat{Q}, \hat{\theta}\right] = -i\pi. \tag{2.54}$$

$\hat{Q}$ has a profound physical interpretation as the charge trapped between the two magnetically ordered regions. This is understood by means of the basic bosonization identity relating the spatial derivative of the field $\hat{\phi}(x)$ and the charge density $\hat{\rho}(x)$, $\partial_x\hat{\phi}(x) = -\pi\hat{\rho}(x)$ [vDS98, Gia03]. Thus, in the region $-L/2 < x < L/2$, we obtain

$$\int_{-L/2}^{L/2} \mathrm{d}x\ \hat{\rho}(x) = \frac{-1}{\pi}\int_{-L/2}^{L/2} \mathrm{d}x\ \partial_x\hat{\phi}(x) = \frac{1}{\pi}\left(\hat{\phi}(-L/2) - \hat{\phi}(L/2)\right) = \frac{1}{\pi}\left(\hat{\phi}_- - \hat{\phi}_+\right) = -\frac{\hat{Q}}{\pi}.$$

While $\hat{Q}$ itself does not commute with the effective Hamiltonian, $e^{i\hat{Q}}$ does. The eigenspectrum of $e^{i\hat{Q}} = e^{i\pi\hat{n}_Q}$ is determined from Eqs. (2.49) and (2.53) to be ± 1 with the corresponding eigenstates $|n_Q\rangle$ with $n_Q = 0, 1$. This readily allows for the identification of $e^{i\hat{Q}}$ with the fermion parity operator $\mathcal{P}$.

Either of the three operators, $e^{i\hat{\phi}_-}$, $e^{i\hat{\phi}_+}$, $e^{i\hat{Q}} = \mathcal{P}$, is sufficient to discriminate among different ground states, yielding a two-fold degeneracy. Interestingly, in analogy to the Kitaev chain model, also in this quite abstract approach, the fermion parity operator appears as the profound generator of degeneracy.

Notably, the above approach is not only comprehensive to determine ground states, but

also to obtain the corresponding non-Abelian BS operators. As we expect them to live in the ground state manifold, it is obvious that they should not project the system out of the same. Hence, they are expected to commute with the effective Hamiltonian of Eq. (2.51). Consequently, they can only be formed from non-trivial operators that obey the same property, i. e. $e^{i\hat{\phi}_\pm}$ and $e^{i\hat{\theta}}$. Moreover, they should satisfy the Majorana conditions of Eqs. (2.20) and (2.21) and act as creation operators on the ground state manifold.
For that, let us investigate the action of $e^{i\hat{\theta}}$ on the ground states $|n_Q\rangle$. Using the commutation relation of Eq. (2.54), we straightforwardly obtain

$$\begin{aligned} e^{i\pi\hat{n}_Q}\left(e^{i\hat{\theta}}|n_Q\rangle\right) &= e^{i\pi(n_Q+1)}\left(e^{i\hat{\theta}}|n_Q\rangle\right), \\ e^{i\pi\hat{n}_Q}\left[\left(e^{i\hat{\theta}}\right)^2|n_Q\rangle\right] &= e^{i\pi\hat{n}_Q}\left[e^{2i\hat{\theta}}|n_Q\rangle\right] = e^{i\pi(n_Q)}\left(e^{2i\hat{\theta}}|n_Q\rangle\right). \end{aligned}$$

This readily allows the identifications

$$e^{i\hat{\theta}}|n_Q\rangle = |n_Q+1\rangle, \qquad \left(e^{i\hat{\theta}}\right)^2|n_Q\rangle = |n_Q+2\rangle = |n_Q\rangle.$$

Thus, operators $\propto e^{i\hat{\theta}}$ act as creation operators on the ground state manifold with the property $(e^{i\hat{\theta}})^2 \propto \mathbb{1}$. This strongly suggest to utilize $e^{i\hat{\theta}}$ for the construction of interface Majorana operators. Solely $e^{i\hat{\theta}}$ is, however, not sufficient as we expect to obtain a single Majorana mode bound to each interface, where we demand the different Majoranas to anti-commute. To incorporate the anti-commutation relations, we need to include $e^{i\hat{\phi}_-}$ and $e^{i\hat{\phi}_+}$. This leads to the interface operators [CAS13]

$$\hat{\gamma}_1 = e^{i\pi/2}e^{-i\hat{\theta}}e^{-i\hat{\phi}_-}, \qquad \hat{\gamma}_2 = e^{i\hat{\theta}}e^{i\hat{\phi}_+} \tag{2.55}$$

with the mutual property $\hat{\gamma}_1\hat{\gamma}_2 = -\hat{\gamma}_2\hat{\gamma}_1$, while $\hat{\gamma}_1^2 = \hat{\gamma}_2^2 = \mathbb{1}$.
Let us investigate the operators of (2.55) against the background of fusion. We could imagine to adiabatically shrink the length of the superconducting region and bring the two Majoranas closer together until they fuse as $L \to 0$. The result of this fusion process is

$$\hat{\gamma}_1\hat{\gamma}_2 = e^{-i\pi/2}e^{i\hat{Q}} \equiv -i\mathcal{P}.$$

In the same way as for the Kitaev model based on lattice fermions (see Eqs. (2.22) and (2.23)), fusion of Majorana particles produces the operator that generates the ground state manifold, namely fermion parity. The different outcomes of the fusion process are then equivalent to the distinct eigenstates of $\mathcal{P}$.

Parafermions

The excessive use of formalism in the above discussion might raise the impression of using a sledgehammer to crack a nut. The formation of Majorana modes can be decently demonstrated already on the single particle fermionic level without too much formalism.

However, when we want to understand the formation of more complex anyons, in particular parafermions, the fermionic picture is not sufficient any more. This is the regime where the above formalism expands its comprehensiveness.

Let us recapitulate the properties of parafermions from their fusion rules, given in (2.18). Instead of 2 distinct fusion outcomes, such as for the Majoranas or Ising anyons, fusion of two particular parafermions yields m (with $m > 2$) different fusion outcomes, implying a degeneracy of m in the presence of two parafermions. For Majoranas, the non-Abelian nature condenses in the relation $\hat{\gamma}^2 = \mathbb{1}$ (with the Majorana $\hat{\gamma}$). Then, Majorana operators act as creation operators on the degenerate manifold. The straightforward generalization of this property in the presence of m ground states naturally yields

$$\hat{\chi}_j^m = \mathbb{1}, \tag{2.56}$$

where the application of the parafermion operator $\hat{\chi}_j$ projects from a given ground state $|n_j\rangle$ to $|n_j + 1\rangle$, while the m-fold application of $\hat{\chi}_j$ leaves the state invariant. This cyclic relation then also implies

$$\hat{\chi}_j^\dagger = \hat{\chi}_j^{m-1}. \tag{2.57}$$

Moreover, from $\hat{\chi}_j^m \hat{\chi}_k = \hat{\chi}_k \hat{\chi}_j^m$, we deduce the exchange relation of two parafermion operators to yield a m-th root of 1

$$\hat{\chi}_j \hat{\chi}_k = \hat{\chi}_k \hat{\chi}_j e^{(2i\pi/m)\mathrm{sign}(k-j)}. \tag{2.58}$$

By virtue of the above relation, we coin these particles $\mathbb{Z}_m$ parafermions [CAS13, OTMS15, AF16]. Note also that, while for the Majorana it is easy to find a modest descriptive representation in terms of fermions, similar considerations yield much more cumbersome relations for parafermions [CO14, CMSS18]. Accordingly, finding physical fermion based models supporting parafermionic excitations is also significantly harder. However, with the discussion of the last section, we are provided with the appropriate tools to directly construct $\mathbb{Z}_m$ parafermions.

Let us reiterate the SC-ferromagnet hetero-junction of the last section. The topological ground state degeneracy was basically evoked by virtue of cosine potentials. In particular, the interplay between $\cos(2\hat{\theta})$ and $\cos(2\hat{\phi}_\pm)$ provokes a two-fold ground state degeneracy, sufficient for the formation of two Majoranas, bound at the interfaces. In view of this awareness, the most logical step towards a m-fold ground state degeneracy is to recycle the above model with replacing $\cos(2\hat{\phi}_\pm) \to \cos(m\hat{\phi}_\pm)$. This scenario produces the effective Hamiltonian

$$H^m_{\mathrm{eff,tot}} = gu \int_{-\infty}^{-L/2} \mathrm{d}x \cos(m\hat{\phi}_-) + gu \int_{L/2}^{\infty} \mathrm{d}x \cos(m\hat{\phi}_+) + \delta_\Delta uL \cos(2\hat{\theta}). \tag{2.59}$$

Instead of 2 minima within $[0, 2\pi[$, each region, ordered according to $\cos(m\hat{\phi}_\pm)$, produces m minima. When we demand no additional boundaries in the system, we can again characterize the different ground states from eigenstates of the operator $\mathcal{P} = e^{i\hat{Q}} = e^{i(\hat{\phi}_+ - \hat{\phi}_-)}$. $\mathcal{P}$ still commutes with the Hamiltonian, however, now it comes along with m distinct

eigenvalues and eigenstates. Let us use the parametrization $\hat{\phi}_\pm = (\pi/m)(2\hat{n}_{\phi,\pm} + 1)$ with the integer valued operator $\hat{n}_{\phi,\pm}$ taking the m eigenvalues $0, ..., m-1$ (modulo m). Then, consequently, we obtain

$$\mathcal{P}|n_Q\rangle = e^{i(2\pi/m)n_Q}|n_Q\rangle \qquad \text{with} \quad \mathcal{P} = e^{i\hat{Q}} = e^{i(2\pi/m)(\hat{n}_{\phi,+}-\hat{n}_{\phi,-})} = e^{i(2\pi/m)\hat{n}_Q},$$

where we introduced the operator $\hat{n}_Q = \hat{n}_{\phi,+} - \hat{n}_{\phi-}$ with the eigenvalues $n_Q = 0, ...m-1$ (modulo m). The so formed m-fold ground state degeneracy offers room for non-Abelian particles with the properties of Eqs. (2.56-2.58). Along the lines of the Majorana case, we can construct them, utilizing the set of non-trivial operators that commute with the effective Hamiltonian of Eq. (2.59). With the commutation relations of (2.52), we can readily derive

$$\left[H^m_{\text{eff,tot}}, e^{i\hat{\phi}_\pm}\right] = \left[H^m_{\text{eff,tot}}, e^{i(2/m)\hat{\theta}}\right] = 0.$$

Note that, due to the increased multiplicity m of the fields $\hat{\phi}_\pm$, already the exponential of the $2/m$-th fraction of $i\hat{\theta}$ commutes with the Hamiltonian. With (2.52) it is then straightforward to demonstrate that $e^{i(2/m)\hat{\theta}}$ acts as a creation operator on the ground states $|n_Q\rangle$

$$e^{i(2\pi/m)\hat{n}_Q}\left(e^{i(2/m)\hat{\theta}}|n_Q\rangle\right) = e^{i(2\pi/m)(\hat{n}_Q+1)}\left(e^{i(2\pi/m)\hat{\theta}}|n_Q\rangle\right) = e^{i(2\pi/m)(\hat{n}_Q+1)}|n_Q+1\rangle.$$

This leads to the interface operators

$$\hat{\chi}_1 = e^{i\pi(m-1)/m}e^{-i(2/m)\hat{\theta}}e^{-i\hat{\phi}_-}, \qquad \hat{\chi}_2 = e^{i(2/m)\hat{\theta}}e^{i\hat{\phi}_+}$$

with the mutual relations

$$\hat{\chi}_2\hat{\chi}_1 = \hat{\chi}_1\hat{\chi}_2 e^{(2/m)[\hat{\theta},\hat{\phi}_-]} = \hat{\chi}_1\hat{\chi}_2 e^{-i(2/m)\pi}.$$

More importantly, we obtain the desired non-Abelian properties due to

$$\hat{\chi}_1^m = \hat{\chi}_2^m = \mathbb{1}.$$

Again, fusion of two $\mathbb{Z}_m$ parafermions yields the operator that generates the ground state manifold

$$\hat{\chi}_2\hat{\chi}_1 = e^{i\pi(m-1)/m}\mathcal{P},$$

where the distinct fusion outcomes correspond to the m distinct eigenstates of $\mathcal{P}$.

Let us now investigate how an effective Hamiltonian of the kind (2.59) might physically emerge. For the simplest case, $m = 2$, the mapping of Eq. (2.36) implies the equivalence (up to Klein factors) of single particle fermionic mass terms and $\cos(2\hat{\phi}(x))$ in the bosonic language. Evidently, each fermionic field operator contributes $+1$ $\hat{\phi}(x)$ in the argument of the cosine. Consequently, to design a $\cos(m\hat{\phi}(x))$ with $m > 2$, we require at least m fermionic field operators. If we demand an overall even number of fermionic fields in

each term of the Hamiltonian, such terms are $m/2$-particle interaction terms. Then, the simplest extension of the $m = 2$ case is given by $m = 4$. In the fermionic language, such a term corresponds to the so-called *correlated TP backscattering* [WBZ06, OTMS15]

$$H_{\text{2pbs}} = g_{\text{2pbs}} \int \mathrm{d}x \, \left(\hat{\psi}_{\uparrow}^{\dagger}(x) \hat{\psi}_{\uparrow}^{\dagger}(x+a) \hat{\psi}_{\downarrow}(x+a) \hat{\psi}_{\downarrow}(x) + \text{h.c.} \right), \tag{2.60}$$

where a small shift a is required to prevent Pauli principle annihilation. As opposed to SP backscattering, in the presence of TP backscattering, TR symmetry is only spontaneously broken. From that point of view, H_{2pbs} seems to be compatible with the elementary symmetries of QSH insulators. However, since it scatters two $\uparrow$ particles in two $\downarrow$ particles, it furthermore requires broken axial spin symmetry [WBZ06, SRvOG12, OTMS15]. Given these conditions, it can be demonstrated that H_{2pbs} is generated in a second order RG analysis from only ordinary density-density interaction terms [OTMS15].
In principle, one could imagine similar terms generating cosines with even higher multiplicities m. However, there are some caveats. First of all, the scaling dimension d of a term like $\cos(m\hat{\phi}(x))$ is given by

$$d(m) = \frac{m^2 K}{4}.$$

Thus, in an one-loop RG approach, we find that $\cos(m\hat{\phi}(x))$ is RG relevant provided

$$K < \frac{8}{m^2}.$$

For the case of $m = 4$, this produces $K < 1/2$, which already implies strong repulsive electron-electron interactions. Moreover, even if K can be tuned to small enough values, such that $m > 4$ terms become RG relevant, the $m = 4$ term would (in a RG sense) grow with the fastest rate as $d(m = 4) < d(m > 4)$. Assuming initially small coupling constants of the same order of magnitude, it follows that after the RG flow is stopped at the largest characteristic energy scale of the system, the $m = 4$ term most likely constitutes the dominant contribution to the low-energy effective Hamiltonian. Ground states will hence be ordered according to the minima of the $m = 4$ term.
However, even $m = 4$ has a catch when it comes to the formation of $\mathbb{Z}_4$ parafermions. In contrast to Majoranas, which are topologically protected, $\mathbb{Z}_4$ parafermions are only symmetry protected. A breaking of TR symmetry leads to the collapse of parafermionic modes into Majoranas [CMA18]. Such a TR breaking term is for instance given by a magnetic impurity in y-direction, $\sim \delta(x) \sin(2\hat{\phi}(x))$, which splits the formerly degenerate minima of the $\cos(4\hat{\phi}(x))$ in two groups. Then a simultaneous minimization of $\sin(2\hat{\phi}(x))$ and $\cos(4\hat{\phi}(x))$ leads to only two global minima. This finding is related to an important work by Fidkowski and Kitaev, in which they prove that the only non-trivial zero-mode, based on 1D fermionic systems, is a Majorana [FK11]. Although this seems to rule out even the possibility of symmetry protected parafermions, we have to keep in mind that the edge states of QSH insulators are emerging as a consequence of the topological properties of a 2D system. The surrounding vacuum is then non-trivial, wherefore such systems are not constrained by Fidkowski and Kitaev's classification [CAS13]. On the other hand,

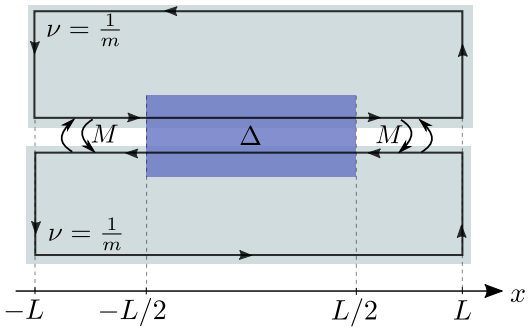

Figure 2.11: Schematic illustration of a hetero-junction formed from two coupled fractional quantum Hall systems with filling factor $\nu = 1/m$.

a breaking of TR symmetry leads to topological trivial vacuum. Then, Fidkowski and Kitaev's prove applies and interface BSs turn into Majorana modes.

A workaround to this limitation is to utilize edge states of 2D topological systems that are not symmetry protected. In that way, topologically non-trivial vacuum is not bound to the presence of symmetries. Then, non-Abelian anyons beyond the Majorana can also emerge as topologically protected excitations [CAS13, AF16]. The most prominent example of such a state of matter is the fractional quantum Hall effect, supporting chiral edge states of fractionally charged quasi-particles [STG99].

To construct parafermions as BSs at the interfaces between gaps of different character, a single chiral edge state is insufficient since it cannot be gapped out. Instead, two counter-propagating modes are required. For fractional quantum Hall systems we therefore need to consider a system sketched in Fig. 2.11: Two adjacent fractional quantum Hall systems, each with filling factor $\nu = 1/m$ are proximitized to each other and to a SC. In the region of the SC ($-L/2 < x < L/2$) particles of each edge assemble into Cooper pairs forming a superconducting gap at the edge. Outside the superconducting region ($-L < x < -L/2$ and $L/2 < x < L$), wave function overlap leads to ordinary backscattering. Similar to the edge states of QSH insulators, such a composite system can be described in terms of a bosonic Hamiltonian. The kinetic part becomes [Wen04, CAS13]

$$H_{\mathrm{FQH}} = \frac{m v_F}{2\pi} \int \mathrm{d}x \left[\left(\partial_x \hat{\phi}(x) \right)^2 + \left(\partial_x \hat{\theta}(x) \right)^2 \right],$$

where the fields $\hat{\phi}(x)$ and $\hat{\theta}(x)$ now obey

$$\left[\hat{\phi}(x), \hat{\theta}(x') \right] = i \frac{\pi}{m} \theta(x' - x).$$

Neglecting Klein factors, the mass terms of ordinary backscattering and superconducting

order are found to be described by

$$\begin{aligned} H_{\mathrm{M}} &\sim M\left[\int_{-L}^{-L/2}+\int_{L/2}^{L}\right]\mathrm{d}x\ \cos(2m\hat{\phi}(x)), \\ H_{\Delta} &\sim \Delta\int_{-L/2}^{L/2}\mathrm{d}x\ \cos(2m\hat{\theta}(x)). \end{aligned}$$

For the case of $m = 1$, the Hamiltonian describes integer quantum Hall systems and the emergent BSs are Majoranas. For $m > 1$, the BSs carry parafermionic character. The major difference of this approach with respect to QSH based junctions is that emergent $\mathbb{Z}_m$ parafermions are now topologically protected excitations. This happens as we cannot find any local order parameter that distinguishes between the m different ground states as long as we remain in the $\nu = 1/m$ phase. In this scenario, rather than the internal instability of parafermions, the major obstacle to be overcome is the experimental realization as the formation of a fractional quantum Hall phase typically requires very strong out-of-plane magnetic fields. This in turn collides with the required presence of superconducting order.

2.5 Relation of anyons and unconventional superconductivity

2.5.1 Time as label for the classification of paired states

All the above realizations of anyonic excitations rest on the presence of superconductivity. However, conventional superconducting order, as described by BCS theory [BCS57], is not sufficient. Instead, unconventional p-wave type superconductivity is required. By virtue of such pairing, non-Abelian BSs form at phase boundaries, where the field operators of these particles necessarily carry information about the incorporated superconducting order. In the BdG language, they are built from electron- and hole-like states, while in the language of bosonization, they contain the pinned field $\hat{\theta}$ as an ambassador of superconducting order. The intriguing properties of non-Abelian anyons are thus deeply related to unconventional superconductivity. Let us shed some light on this link.

Superconducting order is expressed in terms of anomalous correlation functions for two fermions $\hat{\psi}_{\alpha,a}(\boldsymbol{r},t)$ and $\hat{\psi}_{\beta,b}(\boldsymbol{r}',0)$ at the space-time coordinates $(\boldsymbol{r},t)$, $(\boldsymbol{r}',0)$, respectively [LB19]

$$G_{\alpha\beta,ab}(\boldsymbol{r},\boldsymbol{r}',t) = \langle \mathcal{T}\hat{\psi}_{\alpha,a}(\boldsymbol{r},t)\hat{\psi}_{\beta,b}(\boldsymbol{r}',0)\rangle. \tag{2.61}$$

$\mathcal{T}$ constitutes a time-ordering operator, indicating that operators that follow it are to be ordered with increasing time arguments from right to left. $\langle ...\rangle$ denotes a many-body expectation value. If $G_{\alpha\beta,ab}(\boldsymbol{r},\boldsymbol{r}',t) \neq 0$, we name the corresponding thermodynamic ground state a *paired* state. More formally, a paired state of a matter field operator $\hat{O}$ is defined such that $\langle\hat{O}\rangle = 0$, yet the anomalous correlation function $\langle\hat{O}(1)\hat{O}(2)\rangle \neq 0$, but obeys a long-range order in terms of the labels 1 and 2 [LB19].

Let us now think of the time ordered Green function of a Majorana particle $\gamma(\boldsymbol{r},t)$ bound

to an interface such that $\boldsymbol{r} = 0$ is fixed for all times

$$G(t) = \langle \mathcal{T} \hat{\gamma}^\dagger(0,t)\gamma(0,0)\rangle.$$

From the defining property of Majorana excitations, $\hat{\gamma}^\dagger(\boldsymbol{r},t) = \hat{\gamma}(\boldsymbol{r},t)$, we deduce that $G(t)$ is equivalently describing the pairing of Majoranas. In particular, this pairing has the intriguing property to be odd in time [TSN12, AT13]

$$G(t) = -G(-t),$$

which follows directly from the definition of time-ordering irrespectively of the Majorana nature of the operators [HWB15, KSBT17, LB19]. The Majorana carries no further quantum numbers, such as spin or orbital degrees of freedom. Hence, time constitutes the only label that is able to give a classifying character to the symmetry of the pairing. In particular, the odd-time character implies that the pairing only happens delayed in time but never at equal times. This is in stark contrast to conventional paired states, such as the BCS pairing, which is always even in time.

Paired states of matter are among the most fascinating physical effects. Beside the fundamental aspects, the interest in such states of matter is also fueled by possible groundbreaking technological applications. While conventional paired states (where the term conventional mostly refers to BCS type pairing) is fairly understood today, this does not equally apply to unconventional pairing. The unconventional odd-in-time character of paired states was first proposed in the context of spin 1 superconducting states in He^3 [Ber74]. At the time, Berezinskii recognized that time, in the same way as space, spin or orbital degrees of freedom, complements the notion of Pauli's principle. That is, for a paired state of fermions, the anomalous correlation function of Eq. (2.61) has to be an odd function upon exchange of all labels. In the conventional case $G_{\alpha\beta,ab}(\boldsymbol{r},\boldsymbol{r'},t)$ is even in time. This means that pairing can also happen at $t = 0$ and Pauli principle is provided by the remaining quantum numbers. If, on the other hand, $G_{\alpha\beta,ab}(\boldsymbol{r},\boldsymbol{r'},t)$ is an odd function of t, time is among the determinative labels. This further implies that pairing cannot happen locally in time.

Odd-time, or equivalently in Fourier space *odd-frequency*, pairing has many profound physical consequences. First of all, it implies that the equal-time pairing amplitude vanishes. Hence, paired particles are not found at the same space-time coordinate. In the case of electrons, this mitigates Coulomb repulsion, wherefore strongly interacting systems might condensate in an odd-frequency paired state [CMT93]. Moreover, odd-frequency paired states can behave quite exotic in heterojunctions to normal metals [TG07, TTG07], conventional superconductors [TGKU07] or ferromagnets [BVE01, BVE05]. In particular, they can coexist with ferromagnetic order. This happens as odd-frequency pairing allows in turn for equal spin pairing. Then, ferromagnetic order is ineffective in splitting up the Cooper pairs. Along the same lines of reasoning, external magnetic fields are not repelled by odd-frequency states, leading to an anomalous paramagnetic Meißner effect [YTN11, LLM17]. Returning to non-Abelian anyons, the required p-wave superconductivity, necessary for topological superconductivity, is an effectively even orbital pairing. Often times it is generated from ordinary s-wave superconductivity by virtue of SOC.

Then, the pairing carries a strong even orbital equal spin component, which naturally promotes its odd-frequency character and eventually allows (odd-frequency) Majorana modes to appear.

2.5.2 Berezinskii classification of pairing

Symmetry is a central cornerstone in the theory of pairing that dictates the properties of the corresponding condensate and goes back to the fundamental concepts of quantum statistics. Let us concentrate specifically on superconducting pairing, built from two fermions according to Eq. (2.61). For two fermions, Pauli principle enforces anti-symmetry under exchange of all quantum numbers. This translates one-to-one to the pairing amplitude. Under permutation of all labels, $G_{\alpha\beta,ab}(\boldsymbol{r},\boldsymbol{r}',t)$ has to behave anti-symmetric [LB19]

$$(\mathcal{S}\mathcal{O}P^*T^*)\,G_{\alpha\beta,ab}(\boldsymbol{r},\boldsymbol{r}',t)\,(\mathcal{S}\mathcal{O}P^*T^*)^{-1} = G_{\beta\alpha,ba}(\boldsymbol{r}',\boldsymbol{r},-t) = -\Delta_{\alpha\beta,ab}(\boldsymbol{r},\boldsymbol{r}',t), \quad (2.62)$$

where $\mathcal{S}$ and $\mathcal{O}$ permute the spins α and β, orbits a and b, respectively. P^* and T^* interchange the relative space and time coordinates. Note that the latter two operations are not equivalent to total space and time inversion, but merely permute relative coordinates. T^* is hence not the same as TR, which would actually convert $G_{\alpha\beta,ab}(\boldsymbol{r},\boldsymbol{r}',t)$ into $G^\dagger_{\alpha\beta,ab}(\boldsymbol{r},\boldsymbol{r}',t)$.
Most conveniently, the anti-symmetry of Eq. (2.62) is expressed using anomalous Green functions. This has the advantage that we can get rid of the time-ordering operator $\mathcal{T}$, appearing in Eq. (2.61). Instead, we use the *retarded* (R) and *advanced* (A) Green function, which directly relate to a given time-ordering. In Fourier space, they are defined by

$$G^{R/A}_{\alpha\beta,ab}(\boldsymbol{r},\boldsymbol{r}',\omega) = \int \mathrm{d}t\; e^{i(\omega\pm i0^+)t} G^{R/A}_{\alpha\beta,ab}(\boldsymbol{r},\boldsymbol{r}',t)$$

with

$$G^{R}_{\alpha\beta,ab}(\boldsymbol{r},\boldsymbol{r}',t) = -i\theta(t)\langle\{\hat{\psi}_{\alpha,a}(\boldsymbol{r},t),\hat{\psi}_{\beta,b}(\boldsymbol{r}',0)\}\rangle$$

and the mutual relation

$$G^{R}_{\alpha\beta,ab}(\boldsymbol{r},\boldsymbol{r}',t) = \Big(G^{A}_{\alpha\beta,ab}(\boldsymbol{r}',\boldsymbol{r},-t)\Big)^\dagger.$$

In that way, the symmetry constraint of Eq. (2.62) translates into [Ber74]

$$G^{R}_{\alpha\beta,ab}(\boldsymbol{r},\boldsymbol{r}',\omega) = -G^{A}_{\alpha\beta,ab}(\boldsymbol{r}',\boldsymbol{r},-\omega). \quad (2.63)$$

3 Methods

3.1 Luttinger liquid theory

Systems of interacting quantum particles are among the most challenging, but likewise also among the most interesting and comprehensive problem sets in modern physics. The systematic description of interacting systems requires elaborated techniques, which we will discuss in detail in this section for 1D interacting fermions.
In fact, dimensionality plays a key role in the description of interacting systems. In particular, it was recognized by Landau [Lan57b, Lan57a] that (most often) electron-electron interactions are only accorded a minor role in two or higher dimensional systems. This happens as excitations are long-living quasi-particles that are still fermionic in nature. The presence of interactions can then be incorporated using a perturbative approach. In one dimension a similar ansatz generically fails and perturbation theory yields divergencies [Gia03]. The reason for this failure originates from the fact that relevant excitations are drastically different in 1D: Instead of individual quasi-particles, only collective excitations are to be expected. Pictorially, this can be understood as, in the presence of interactions, non of the 1D fermions can propagate freely without affecting its neighbors. Therefore relevant excitations carry collective character with an overall *bosonic* nature. This peculiarity was recognized early on by Tomonaga [Tom50]. Still it took a journey of over 30 years and the contribution and refinements of many famous authors until *bosonization* of 1D fermions was entirely understood [Lut63, Hal81a, Hal81b].

3.1.1 Bosonization

In this section, we reiterate the mapping of 1D interacting fermions to free bosons. The section mainly follows the seminal review by von Delft and Schoeller [vDS98] and Giamarchi's book [Gia03]. Bosonization wants to map a system of interacting fermions onto a system of free bosons. This is generically only possible if the system of electrons obeys a linear energy dispersion like

$$H_0 = \sum_{k,r=R,L} (r v_F k - k_F)\, \hat{c}^\dagger_{r,k} \hat{c}_{r,k} \tag{3.1}$$

with the fermionic creation and annihilation operators $\hat{c}^\dagger_{r,k}$ and $\hat{c}_{r,k}$ of species $r = (R, L) = (+, -)$, characterizing right- (R) and left-moving (L) particles. Under these conditions, all PH excitations are only dependent on the relative momentum q (see Fig. 3.1 (a)). Thus, collective PH operators of the form

$$\hat{b}_{r,q} \sim \sum_k \hat{c}^\dagger_{r,k+q} \hat{c}_{r,k} \tag{3.2}$$

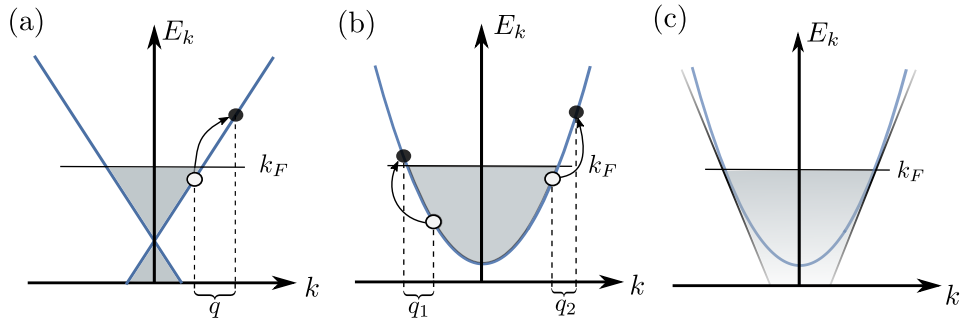

Figure 3.1: Schematic of PH excitations for a linear dispersed theory (a) and quadratic spectrum (b). (c) Illustrates the linearization of a quadratic model around the Fermi energy. Filled circles denote particles, while empty circles illustrate holes.

are associated with the same dispersion relation as the fermions of Eq. (3.1). Hence, instead of describing the system in terms of the fermionic operators $\hat{c}^\dagger_{r,k}$ and $\hat{c}_{r,k}$, we can equivalently rewrite the theory in terms of the operators $\hat{b}_{r,q}$ and $\hat{b}^\dagger_{r,q}$. As we will derive below, these collective electron-hole excitations carry a bosonic character, which one might already deduce as they are built from a product of two fermionic operators.

Such a reorganization of the many particle Fock space strongly relies on the linearity of the spectrum. For non-linearly dispersed systems, PH symmetry is typically absent and the spectrum of the fermionic Hamiltonian is not expected to coincide with the one found for the operators $\hat{b}_{r,q}$. Fig. 3.1 (b) sketches the situation for a quadratic theory. Although the illustrated PH excitation processes have the same excitation energy, they come along with a different momentum transfer $|q_1| \neq |q_2|$. In this case, bosonization of the model is still possible, however it is insufficient to solve interacting many-particle problems as the mapping produces yet another interacting model, now in terms of bosons. Still, if we are concerned with the low-energy physics around the Fermi level, we can linearize the spectrum around k_F and obtain a free-boson theory describing the low-energy properties of the model (Fig. 3.1 (c)). This goes hand in hand with a momentum cutoff that truncates high-energy states, which are not compatible with this approximation. The role of curvature can be included perturbatively, however the low-energy properties remain unchanged [Hal81b].

For either case (purely linear spectrum or approximately linear spectrum around k_F) the fermionic fields are given by a mode expansion around the Fermi surface[1]

$$\hat{\psi}_r(x) = \frac{e^{irk_F x}}{\sqrt{L}} \sum_k e^{irkx} \hat{c}_{r,k}. \tag{3.3}$$

[1] Technically, this representation is only entirely correct for the purely linear spectrum. However we will stick to this representation for the subsequent sections and postpone the detailed discussion to Sec. 3.1.5.

3.1.2 Bosonic reorganization of the Fock space

The rewriting of a linear dispersed theory in terms of operators of the kind (3.2) is based on a reorganization of the many-particle Fock space. The entire Fock space F spanned by the set of operators $\{\hat{c}^\dagger_{r,k}, \hat{c}_{r',k'}\}$ can be generically decomposed as a sum of N-particle Hilbert spaces $F = \sum_{\oplus N} \mathcal{H}_N$, where each Hilbert space $\mathcal{H}_N$ has a defined total particle number N as well as defined chiral particle numbers N_R and N_L. A generic state of a given Hilbert space $\mathcal{H}_N$ can hence be represented like

$$|N\rangle = f(\{\hat{c}^\dagger_{r,k}\hat{c}_{r,k'}\})|N\rangle_0, \tag{3.4}$$

where $|N\rangle_0$ defines the ground state (i. e. the absence of excitations) in the presence of N particles and $f(\{\hat{c}^\dagger_{r,k}\hat{c}_{r,k'}\})$ is an arbitrary function that only depends on bilinear combinations of fermionic operators. Given that, in the next step one has to demonstrate that these bilinear combinations of fermionic operators are indeed of bosonic nature and that the corresponding space, spanned by this set of operators, is complete. However, before we go on with that, let us clarify the meaning of finite N-particle states against the background of unbounded spectra.

Fermionic normal ordering

Unbounded spectra lead to a number of unphysical divergencies. This is most evident from the particle number operator

$$\hat{N}_r = \sum_k \hat{c}^\dagger_{r,k}\hat{c}_{r,k}, \tag{3.5}$$

counting the number of occupied states below a given Fermi level. The Fermi sea contributes an infinitely large number, which would produce a divergent particle number regardless of the value of k_F.

There are different schemes to regularize such unphysical divergencies and retain physically meaningful quantities. The most common method of which is *normal ordering*. For that, let us introduce the vacuum state $|0\rangle_0$ as the many-particle state where all the states below the Dirac point ($k_F = 0$) are occupied and all the states above the Dirac point are empty. $|0\rangle_0$ serves as a reference state relative to which we define the occupations of all other states in F. In particular, let us define normal ordering, denoted by ${}^*_*\hat{O}^*_*$ for an operator $\hat{O}$, so that

$${}^*_*\hat{O}^*_* = \hat{O} - {}_0\langle 0|\hat{O}|0\rangle_0. \tag{3.6}$$

The subtraction of the expectation value of $\hat{O}$ with respect to the reference state $|0\rangle_0$ now yields a finite value for expectation values on states $|N\rangle_0$ with excess particle number N.

Bosonic operators

Keeping this in mind, let us now introduce the operators

$$\hat{b}^\dagger_{r,q} = \frac{i}{\sqrt{n_q}} \sum_k \hat{c}^\dagger_{r,k+q} \hat{c}_{r,k}, \qquad \hat{b}_{r,q} = \frac{-i}{\sqrt{n_q}} \sum_k \hat{c}^\dagger_{r,k-q} \hat{c}_{r,k}.$$

For a system of length L, all momenta are quantized. In particular, we have $q = (2\pi/L)n_q$ with the positive integer $n_q \in \mathbb{Z}^+$. $\hat{b}^\dagger_{r,q}$ and $\hat{b}_{r,q}$ consist of all possible PH excitations of fixed momentum q. In that sense, they might be interpreted as creation and annihilation operators of momentum q. Moreover, note that for $q \neq 0$, ${}^*_*\hat{b}_{r,q}{}^*_* \equiv \hat{b}_{r,q}$ and ${}^*_*\hat{b}^\dagger_{r,q}{}^*_* \equiv \hat{b}^\dagger_{r,q}$. This implies that $\hat{b}_{r,q}$ as well as $\hat{b}^\dagger_{r,q}$ are well behaved and no divergencies appear. Consequently, also the product of $\hat{b}_{r,q}$'s ($\hat{b}^\dagger_{r,q}$'s) is well behaved and we readily find

$$\left[\hat{b}^\dagger_{r,q}, \hat{b}^\dagger_{r',q'}\right] = \left[\hat{b}_{r,q}, \hat{b}_{r',q'}\right] = 0.$$

The commutator of $\hat{b}_{r,q}$ with $\hat{b}^\dagger_{r',q'}$ is more subtle. Straightforward manipulations, using the standard fermionic commutation relations, yield

$$\left[\hat{b}_{r,q}, \hat{b}^\dagger_{r',q'}\right] = \delta_{rr'} \frac{1}{\sqrt{n_q n_{q'}}} \sum_k \left(\hat{c}^\dagger_{r,k+q-q'} \hat{c}_{r,k} - \hat{c}^\dagger_{r,k+q} \hat{c}_{r,k+q'} \right). \tag{3.7}$$

For the case $q \neq q'$, the above product of fermionic operators is again well behaved. Shifting $k \to k - q'$ in the second term readily allows to subtract them from each other without ambiguity to yield zero. If however $q = q'$, Eq. (3.7) consists of divergent operators and we first have to construct normal ordered expressions. With the definition of Eq. (3.6) we obtain

$$\begin{aligned} \left[\hat{b}_{r,q}, \hat{b}^\dagger_{r',q'}\right] = \delta_{rr'}\delta_{qq'} \sum_k \frac{1}{n_q} \Big\{ & {}^*_*\hat{c}^\dagger_{r,k}\hat{c}_{r,k}{}^*_* - {}^*_*\hat{c}^\dagger_{r,k+q}\hat{c}_{r,k+q}{}^*_* \\ & + {}_0\langle 0|\hat{c}^\dagger_{r,k}\hat{c}_{r,k}|0\rangle_0 \; - \; {}_0\langle 0|\hat{c}^\dagger_{r,k+q}\hat{c}_{r,k+q}|0\rangle_0 \Big\}. \end{aligned} \tag{3.8}$$

The first two terms on the right hand side do not produce divergent expectation values anymore and cancel as evident with using $k' = k + q$ in the second term. The terms in the second line of Eq. (3.8) essentially count all occupied states up to $k = 0$, $k = -q$, respectively. Thus,

$${}_0\langle 0|\hat{c}^\dagger_{r,k}\hat{c}_{r,k}|0\rangle_0 \; - \; {}_0\langle 0|\hat{c}^\dagger_{r,k+q}\hat{c}_{r,k+q}|0\rangle_0 = \frac{1}{n_q} \left(\sum_{n_k=-\infty}^{0} - \sum_{n_k=-\infty}^{-n_q} \right) = 1,$$

leading to

$$\left[\hat{b}_{r,q}, \hat{b}^\dagger_{r',q'}\right] = \delta_{rr'}\delta_{qq'}. \tag{3.9}$$

The above result is a crucial cornerstone of bosonization as it complements the bosonic commutation relations of the operators $\hat{b}_{r,q}$ and $\hat{b}_{r',q'}$, built solely from linear combina-

tions of PH excitations. Moreover, it once more illuminates the fundamental role of the unbounded nature of the spectrum. Without this unboundedness, Eq. (3.9) would just yield zero and no bosonic reorganization of the Fock space would be possible. Eq. (3.9) belongs to the family of *anomalous commutators*, that yield non-zero values only in the presence of an unbounded spectrum (i. e. for infinitely many particles) [GNT98]. Such commutators play a central role in physics. A prominent example is, for instance, the so-called *chiral anomaly*, where an anomalous non-conservation of the chiral particle number appears in the presence of electro-magnetic fields [Adl69, BJ69]. In particular, the electro-magnetic response involves commutators that are closely related to the one of Eq. (3.9).

As stated earlier, it is obvious that any state $|N\rangle$ of the Hilbert space $\mathcal{H}_N$ can be constructed from bilinear combinations of fermionic operators (see Eq. (3.4)). Remarkably, this quite generic statement can be refined and formulated on the basis of the operators $\hat{b}^\dagger_{r,q}$. In particular, the following statement holds [vDS98]:

> For every $|N\rangle$, there exists a function $f(\hat{b}^\dagger)$ of $\hat{b}^\dagger$'s such that $|N\rangle = f(\hat{b}^\dagger)|N\rangle_0$. i. e. the $\hat{b}^\dagger$'s, acting on $|N\rangle_0$, span the complete N-particle Hilbert space $\mathcal{H}_N$.

This means that any state $|N\rangle \equiv |N;\{m_q\}\rangle$ is fully characterized by the number of particles N and the set of PH operations $\{m_q\}$ induced by $f(\hat{b}^\dagger)$. Assuming the correctness of the above assertion, we can rigorously express all fermionic operators by combinations of $\hat{b}^\dagger_{r,q}$ and $\hat{b}_{r',q'}$. In particular, we can reformulate the Hamiltonian of Eq. (3.1) in terms of bosons.

Straightforward manipulations yield

$$\left[H_0, \hat{b}^\dagger_{r,q}\right] = v_F r q \hat{b}_{r,q}, \tag{3.10}$$

implying that if $|E\rangle$ is an eigenstate to H_0 with eigenvalue E, then $\hat{b}^\dagger_{r,q}|E\rangle$ is also an eigenstate of H_0 with eigenvalue $E + v_F q$. Furthermore, since H_0 commutes with the normal ordered particle number operator ${}^*_*\hat{N}_r{}^*_*$ (see Eq. (3.5)), any N-particle ground state $|N\rangle_0 = |N;0\rangle$ is also an eigenstate of H_0. Assuming periodic boundary conditions with respect to length L, momenta are quantized according to $q = (2\pi/L)n_q$ with integers n_q. This implies the expectation value[2]

$${}_0\langle N|H_0|N\rangle_0 = \frac{2\pi v_F}{L}\sum_r \sum_{n_{q,r}=1}^{N_r} n_{q,r} = \sum_r \frac{\pi v_F}{L} N_r(N_r+1). \tag{3.11}$$

Combining the implications of Eqs. (3.10) and (3.11) together with the assertion that the bosonic operators $\hat{b}^\dagger_{r,q}$ acting on $|N;0\rangle$ span the entire N-particle Hilbert space $\mathcal{H}_N$, we can conclude

$$H_0 = \sum_{r,q\neq 0} v_F r q \; \hat{b}^\dagger_{r,q}\hat{b}_{r,q} + \frac{v_F\pi}{L}\sum_r {}^*_*\hat{N}_r{}^*_*({}^*_*\hat{N}_r{}^*_* + 1). \tag{3.12}$$

[2]For ease of understanding, we assume $N_r > 0$. However, the result also holds for $N_r < 0$.

This is a remarkable result. The Hamiltonian, which is quadratic in fermionic operators, is also quadratic in terms of bosonic operators (which means quatric in fermionic operators). This awareness is at the heart of bosonization.

Boson fields and the bosonization identity

On the basis of the bosonic operators $\hat{b}^\dagger_{r,q}$ and $\hat{b}_{r,q}$, we can now define bosonic fields as

$$\hat{\varphi}^\dagger_r(x) = \sum_{q>0} \frac{r}{\sqrt{n_q}} e^{irqx} \hat{b}^\dagger_{r,q} e^{-aq/2}, \qquad \hat{\varphi}_r(x) = \sum_{q>0} \frac{r}{\sqrt{n_q}} e^{-irqx} \hat{b}_{r,q} e^{-aq/2}, \tag{3.13}$$

where a is small real and positive regularization parameter to avoid divergencies due to the unbounded spectrum and keep track of the correct bosonic and fermionic commutation relations. In principle, a should be sent to zero at some point of a given calculation to undo this modification[3]. In the following, it will be useful to work with the hermitian combination of the bosonic fields in (3.13)

$$\hat{\phi}_r(x) = \hat{\varphi}_r(x) + \hat{\varphi}^\dagger_r(x) = \sum_{q>0} \frac{r}{\sqrt{n_q}} \left(e^{-iqrx} \hat{b}_{r,q} + e^{iqrx} \hat{b}^\dagger_{r,q} \right) e^{-aq/2}.$$

The operator $\hat{\phi}_r(x)$ takes a central role in most of the elementary bosonization relations such as for the normal ordered (chiral) electron density. With the fermionic field operators of Eq. (3.3), we obtain

$$\begin{aligned} \hat{\rho}_r(x) &= {}^*_*\hat{\psi}^\dagger_r(x)\hat{\psi}_r(x){}^*_* = \frac{1}{L}\sum_q e^{irqx} \sum_k {}^*_*\hat{c}^\dagger_{r,k-q} c_{r,k}{}^*_* \\ &= \frac{1}{L}\sum_{q>0} i\sqrt{n_q} \left({}^*_* e^{irqx} \hat{b}_{r,q} - e^{irqx} \hat{b}^\dagger_{r,q} {}^*_* \right) + \frac{1}{L}\sum_k {}^*_*\hat{c}^\dagger_{r,k}\hat{c}_{r,k}{}^*_* \\ &\overset{a\to 0}{=} \frac{1}{2\pi} {}^*_*\partial_x\hat{\phi}_r(x){}^*_* + \frac{1}{L} {}^*_*\hat{N}_r{}^*_*. \end{aligned} \tag{3.14}$$

Since ${}^*_*\partial_x\hat{\phi}_r(x){}^*_* \equiv \partial_x\hat{\phi}_r(x)$, normal ordering is irrelevant for this part and henceforth we drop it for the chiral fields. Note also that, here, normal ordering renders a obsolete, which is why the identification holds for $a \to 0$. In a more field theoretical approach on can get by without normal ordering and instead use a *point splitting* ansatz [vDS98] ${}^*_*\hat{\psi}^\dagger_r(x)\hat{\psi}_r(x){}^*_* \to \hat{\psi}^\dagger_r(x)\hat{\psi}_r(x-ia)$, where divergent terms appear as $a \to 0$.

Similar manipulations as in (3.14) allow us to express the Hamiltonian of Eq. (3.12) in

[3] Note that introducing a finite a is not the same as normal ordering. However, as we will see below when deriving the bosonic form of the fermionic fields, un-normal ordered bosonic expressions are only well defined for finite a. A detailed discussion about this cutoff can be found in Refs. [Hal81b] and [Gia03].

terms of the bosonic fields $\hat{\phi}_r(x)$. Up to an unimportant constant, we obtain

$$\begin{aligned} H_0 &= \sum_r \frac{v_F}{2\pi} \int_{-L/2}^{L/2} \mathrm{d}x \ \left(\partial_x \hat{\phi}_r(x)\right)^2 + \sum_r \frac{\pi v_F}{L} {}^*_* \hat{N}_r {}^*_*{}^2 \\ &= v_F \pi \int_{-L/2}^{L/2} \mathrm{d}x \left(\hat{\rho}_R^2(x) + \hat{\rho}_L^2(x)\right). \end{aligned} \tag{3.15}$$

To derive the second line, we made use of the relation (3.14) and the periodicity of $\hat{\phi}_r(x)$ on the length L.

Next, let us derive the last missing brick – the fermionic field operator in terms of bosonic fields – complementing the fundamental bosonization relations. Form the definition of the bosonic operators $\hat{b}_{r,q}$ and the fermionic field operators of Eq. (3.3), we straightforwardly obtain

$$\left[\hat{b}_{r,q}, \hat{\psi}_{r'}(x)\right] = \delta_{rr'} \alpha_q(x) \hat{\psi}_r(x),$$

where $\alpha_q(x) = (i/\sqrt{n_q}) e^{irqx}$. Now, since $\hat{b}_{r,q}|N;0\rangle = 0$, the above commutator implies that $\hat{\psi}_r(x)|N;0\rangle$ is an eigenstate of $\hat{b}_{r,q}$ with eigenvalue $\alpha_q(x)$. This in turn promotes the formulation of $\hat{\psi}_r(x)|N;0\rangle$ as a boson coherent state

$$\hat{\psi}_r(x)|N\rangle_0 = \exp\left[\sum_{q>0} \alpha_q(x) \hat{b}_{r,q}^\dagger\right] \mathcal{F}_r \hat{\lambda}_r(x)|N;0\rangle = e^{ir\hat{\varphi}^\dagger(x)} \mathcal{F}_r \hat{\lambda}_r(x)|N;0\rangle, \tag{3.16}$$

where we made use of (3.13). The operator $\mathcal{F}_r$ is a so-called Klein factor. Its purpose is to lower the number of fermions by one. Only then we are allowed to equate left and right side of Eq. (3.16)[4]. Strictly speaking, the identification $\exp\left[\sum_{q>0} \alpha_q(x) \hat{b}_{r,q}^\dagger\right] = ir\hat{\varphi}_r(x)$ is only valid for vanishing regularization parameter $a = 0$, implying that no normal order related problems appear here.

The phase operator $\hat{\lambda}_r(x)$ can be derived from the definition of fermionic fields in combination with the expectation value $\langle N;0|\mathcal{F}_r^\dagger \hat{\psi}_r(x)|N;0\rangle = \lambda_r(x)$. This yields, for periodic boundary conditions ($q = (2\pi/L)n_q$)

$$\hat{\lambda}_r(x) = \frac{1}{\sqrt{L}} e^{irk_F x} e^{ir(2\pi x/L) {}^*_* \hat{N}_r {}^*_*}.$$

Now, from the action of $\hat{\psi}_r(x)$ on a generic state $|N, \{m_q\}\rangle$, we find its final form to be

$$\hat{\psi}_r(x) = \frac{\mathcal{F}_r}{\sqrt{L}} e^{irk_F x} e^{ir(2\pi x/L) {}^*_* \hat{N}_r {}^*_*} e^{ir\hat{\varphi}_r^\dagger(x)} e^{ir\hat{\varphi}_r(x)} = \frac{\mathcal{F}_r}{\sqrt{2\pi a}} e^{irk_F x} e^{ir(2\pi x/L) {}^*_* \hat{N}_r {}^*_*} e^{ir\hat{\phi}_r(x)}.$$

In the last step, we have redone normal ordering of the boson field exponentials to obtain a more compact form. This requires the presence of a small cutoff a according to (3.13). Subsequently, instead of using directly the chiral fields $\hat{\phi}_r(x)$, it makes sense to introduce

[4] We will discuss the role of Klein factors in more detail in Sec. 3.1.4

a new set of canonical fields $\hat{\phi}(x)$ and $\hat{\theta}(x)$, defined by

$$\begin{aligned}\hat{\phi}(x) &= -\frac{1}{2}\left(\hat{\phi}_R(x)+\hat{\phi}_L(x)\right)-\frac{\pi x}{L}\left({}^{*}_{*}\hat{N}_R{}^{*}_{*}+{}^{*}_{*}\hat{N}_L{}^{*}_{*}\right),\\ \hat{\theta}(x) &= \frac{1}{2}\left(\hat{\phi}_R(x)-\hat{\phi}_L(x)\right)+\frac{\pi x}{L}\left({}^{*}_{*}\hat{N}_R{}^{*}_{*}-{}^{*}_{*}\hat{N}_L{}^{*}_{*}\right)\end{aligned}$$

with the mutual commutation relation

$$\left[\hat{\phi}(x),\frac{1}{\pi}\partial_{x'}\hat{\theta}(x')\right]=i\delta(x-x'), \tag{3.17}$$

which suggests the field $(1/\pi)\partial_x\hat{\theta}(x)$ as the canonically conjugate momentum of $\hat{\phi}(x)$. In the canonical representation, the fermionic field operators take the form

$$\hat{\psi}_r(x)=\frac{\mathcal{F}_r}{\sqrt{2\pi a}}e^{irk_Fx}e^{-i(r\hat{\phi}(x)-\hat{\theta}(x))}. \tag{3.18}$$

The advantage of the canonical representation is mainly their simplified relation to electron density operators [Gia03]

$$\partial_x\hat{\phi}(x)=-\pi\left(\hat{\rho}_R(x)+\hat{\rho}_L(x)\right),\qquad \partial_x\hat{\theta}(x)=\pi\left(\hat{\rho}_R(x)-\hat{\rho}_L(x)\right). \tag{3.19}$$

This allows a convenient formulation of H_0 (Eq. (3.15))

$$H_0=\frac{v_F}{2\pi}\int_{-L/2}^{L/2}\mathrm{d}x\left[\left(\partial_x\hat{\phi}(x)\right)^2+\left(\partial_x\hat{\theta}(x)\right)^2\right].$$

3.1.3 Bosonizing interactions

So far, we have merely been concerned with bosonizing a free fermionic theory. Although this is interesting from the mathematical and conceptional point of view, if that was the scope of bosonization, its potential for application would be very limited. Fortunately, the power of bosonization unfolds not before density-density interactions are considered. For either chirality, there are two possible density-density interaction terms that can arise[5]

$$H_{\text{int}}=\int_{-L/2}^{L/2}\mathrm{d}x\ \left[g_2\hat{\rho}_R(x)\hat{\rho}_L(x)+\frac{g_4}{2}\left(\hat{\rho}_R(x)\hat{\rho}_R(x)+\hat{\rho}_L(x)\hat{\rho}_L(x)\right)\right].$$

For ease of understanding, we assume homogeneous interactions here. There is a hidden subtlety though: in the current form, Pauli principle enforces the g_4 term to vanish. g_4 interactions are hence only expected to appear non-local in space, however, for demonstration purposes we shall keep it here in its present form. With the definitions of (3.19) it is straightforward to demonstrate that also (and in particular) interaction terms are

[5] Luttinger liquids are typically introduced with four interaction terms with coupling constants g_1-g_4. Thereby, g_1 and g_3 are non-density-density interactions and eventually enter the Hamiltonian only for specific conditions. In view of the subsequent chapters, which regard mainly helical systems, these terms need extra requirements that are not met in this thesis.

quadratic in bosonic fields. The full Luttinger liquid Hamiltonian including interactions then becomes [Gia03]

$$H_{\mathrm{LL}} = H_0 + H_{\mathrm{int}} = \frac{1}{2\pi}\int_{-L/2}^{L/2} \mathrm{d}x \ \left[\frac{u}{K}\left(\partial_x \hat{\phi}(x)\right)^2 + uK\left(\partial_x \hat{\theta}(x)\right)^2\right], \tag{3.20}$$

where

$$u = v_F\sqrt{(1+g_4/(2\pi v_F))^2 - (g_2/(2\pi v_F))^2}, \qquad K = \sqrt{\frac{1+g_4/(2\pi v_F) - g_2/(2\pi v_F)}{1+g_4/(2\pi v_F) + g_2/(2\pi v_F)}}. \tag{3.21}$$

Thereby, u can be interpreted as a renormalized Fermi velocity and K is a dimensionless parameter characterizing the type and strength of interactions. In the absence of interactions we clearly have $K = 1$ and $u = v_F$. For repulsive interactions we have $g_4, g_2 > 0$, which implies $K < 1$, whereas for attractive interactions the opposite happens, $g_4, g_2 < 0$, leading to $K > 1$.

The Hamiltonian of Eq. (3.20) is the most commonly used Hamiltonian to describe 1D interacting (Dirac) fermions. Even for $K \neq 1$, it describes a theory of free bosons. In fact, with the gauge transformation $\hat{\phi}(x) \to \tilde{\phi}(x) = \hat{\phi}(x)/\sqrt{K}$ and $\hat{\theta}(x) \to \tilde{\theta}(x) = \sqrt{K}\hat{\theta}(x)$, keeping the canonical commutation relations of Eq. (3.17) invariant, we obtain the standard Hamiltonian of a free boson theory [Gia03].

This changes when we consider interaction terms that do not resemble in a quadratic form when rewritten in terms of bosons, which happens to be the case for most non-density-density interactions. For the above theory, the simplest term that shows such a behavior is a hybridization term of a right-moving and a left-moving fermion (named H_{B} for the helical QSH system in the former chapter, see Eq. (2.39))

$$H_{\mathrm{B}} = \int_{-L/2}^{L/2} \mathrm{d}x \ B\left[\hat{\psi}_R^\dagger(x)\hat{\psi}_L(x) + \mathrm{h.c.}\right] = \int_{-L/2}^{L/2} \mathrm{d}x \ \frac{B}{2\pi a}\left[\mathcal{F}_R^\dagger \mathcal{F}_L e^{2i\hat{\phi}(x)} e^{-2ik_F x} + \mathrm{h.c.}\right], \tag{3.22}$$

where we used Eq. (3.18). The exponentials of the field $\hat{\phi}(x)$ in the above equation give rise to infinite orders of $\hat{\phi}(x)$, so that the resulting theory, formed from $H_{\mathrm{LL}} + H_{\mathrm{B}}$, now describes a massive bosonic theory.

In its present form, Eq. (3.22) is not particularly tangible, which is mainly due to the emerging combination of Klein factors. Indeed, often times Klein factors are tacitly excluded from the discussion, leading to simpler forms of non-density-density interactions that are easier to treat as they are now purely of bosonic nature [Gia03]. However, neglecting Klein factors is a subtle point, worth to be discussed in more detail.

3.1.4 On the role of Klein factors

In general, Klein factors $\mathcal{F}_\eta$ are necessary to complement the action of a fermionic field $\hat{\psi}_\eta(x)$, expressed in terms of bosonic fields, onto a given N-particle state. In particular, they lower (raise) the number of η-fermions, N_η, by one. For a general state, composed of PH excitations $|N;\{m_q\}\rangle = f(\{\hat{b}_\eta^\dagger\})|N;0\rangle = f(\{\hat{b}_\eta^\dagger\})|N_1,...,N_\eta,...N_M;0\rangle_0$ (with M distinct

fermion species), this yields

$$\mathcal{F}_\eta^\dagger|N\rangle = f(\{\hat{b}_\eta^\dagger\})\hat{c}_{N_\eta+1}^\dagger|N_1,...,N_\eta,...,N_M;0\rangle = f(\{\hat{b}_\eta^\dagger\})\hat{T}_\eta|N_1,...,N_\eta+1,...,N_M;0\rangle,$$
$$\mathcal{F}_\eta|N\rangle = f(\{\hat{b}_\eta^\dagger\})\hat{c}_{N_\eta}|N_1,...,N_\eta,...,N_M;0\rangle = f(\{\hat{b}_\eta^\dagger\})\hat{T}_\eta|N_1,...,N_\eta-1,...,N_M;0\rangle,$$

where $\hat{c}_{N_\eta+1}^\dagger$ ($\hat{c}_{N_\eta}$) creates (annihilates) a fermion in the lowest empty (full) level of species η. Furthermore, we used that $\mathcal{F}_\eta$ commutes with all bosonic operators. The operator $\hat{T}_\eta$ counts the number of minus signs picked up when commuting the fermionic operators $\hat{c}_{N_\eta}^\dagger$ ($\hat{c}_{N_\eta}$) to the appropriate position to create (annihilate) a fermion of kind η

$$\hat{T}_\eta = (-1)^{\sum_{\bar{\eta}=1}^{\eta-1}\hat{N}_{\bar{\eta}}}.$$

Then, $\mathcal{F}_\eta$ might as well be represented as

$$\mathcal{F}_\eta = \sum_{N_1,..N_M}\sum_{\{m_q\}}|N_1,...,N_\eta-1,...,N_M;\{m_q\}\rangle\langle N_1,...,N_\eta,...,N_M;\{m_q\}|\hat{T}_\eta.$$

Klein factors do not yield any space or time dependence of measurable quantities. Those are completely captured by the bosonic fields. Thus, in the thermodynamic limit, where one particle more or less does not change the overall properties of the system, the action of $\mathcal{F}_\eta$ is determined by $\hat{T}_\eta$. In this limit, it follows for the thermodynamic properties of terms like Eq. (3.22) applied to a generic state of the Hilbert space

$$\begin{aligned}\mathcal{F}_R^\dagger\mathcal{F}_L|N_L,N_R;\{m_q\}\rangle &= (-1)^{N_L-1}|N_L-1,N_R+1;\{m_q\}\rangle \sim (-1)^{N_L-1}|N_L,N_R;\{m_q\}\rangle,\\ \mathcal{F}_L^\dagger\mathcal{F}_R|N_L,N_R;\{m_q\}\rangle &= -\mathcal{F}_R\mathcal{F}_L^\dagger|N_L,N_R;\{m_q\}\rangle \sim (-1)^{N_L-1}|N_L,N_R;\{m_q\}\rangle.\end{aligned}$$

This implies that, in the thermodynamic limit, we can identify the Klein factors with a Majorana-like operator $\mathcal{F}_\eta^\dagger, \mathcal{F}_\eta \to \hat{\gamma}_\eta$ and factorize them (in the corresponding order). This in turn allows us to rewrite Eq. (3.22) as a cosine [Gia03]. Klein factors then just yield an overall sign, which can be absorbed in the coupling constant.

3.1.5 Spinless, spinful and helical Luttinger liquids

So far, we have mainly been concerned with bosonizing a linear theory consisting of one unspecific right- and left-mover. Physically, there are (at least) two different scenarios where such assumptions are reasonable: (i) In a system of 1D non-relativistic spinless interacting fermions with large k_F and (ii) for a 1D system of interacting relativistic fermions (see Fig. 3.1 (a) and (c)).
In the first case, the theory needs to be linearized around the Fermi level to allow for a valid description in terms of bosons. However, we have to keep in mind that the so constructed right- and left-moving fermionic fields originate from the same physical fermion $\hat{\psi}(x)$

$$\hat{\psi}(x) = \hat{\psi}_R(x) + \hat{\psi}_L(x) = e^{ik_Fx}\tilde{\psi}_R(x) + e^{-ik_Fx}\tilde{\psi}_L(x), \tag{3.23}$$

where we used the definition of Eq. (3.3) and defined the slowly varying fields $\tilde{\psi}_r(x) =$

$1/\sqrt{L}\sum_k e^{irkx}\hat{c}_{r,k}$. Thus, the (physical) fermion density is complemented by oscillating contributions, typically called Friedel oscillations [Gia03]

$$\hat{\rho}(x) = {}^{*}_{*}\hat{\psi}(x)^{\dagger}\hat{\psi}(x){}^{*}_{*} = \sum_r {}^{*}_{*}\tilde{\psi}^{\dagger}_r(x)\tilde{\psi}_r(x){}^{*}_{*} + e^{-2ik_F x}\tilde{\psi}^{\dagger}_R(x)\tilde{\psi}_L(x) + \text{h.c.}.$$

Away from half filling (i. e. for large k_F) the Hamiltonian of Eq. (3.20) is still valid since those terms oscillate according to $4k_F$ (remember that the Hamiltonian is quadratic in density operators). Hence, in this scenario, they do not contribute energy to the system and can be neglected in the Hamiltonian.

For the second scenario of 1D relativistic fermions, no such extra terms appear. Here, physical fermions are represented as a vector $\hat{\psi}(x) = \left(\hat{\psi}_R(x), \hat{\psi}_L(x)\right)^T$. Thus, for any value of k_F the electron density is just given by

$$\hat{\rho}(x) = \sum_r {}^{*}_{*}\hat{\psi}^{\dagger}_r(x)\hat{\psi}_r(x){}^{*}_{*}.$$

With relabeling the indices $R \to \uparrow$, $L \to \downarrow$, this case literally corresponds to the helical system of a QSH edge.

Remarkably, the scope of bosonization goes even beyond these two cases and is able to elegantly describe *spinful* interacting fermions. While this is clear for the kinetic part of the Hamiltonian, where we find $H_{0,\text{SLL}} = H_{0,\uparrow} + H_{0,\downarrow}$ with

$$H_{0,\nu} = \frac{v_F}{2\pi}\int_{-L/2}^{L/2} \mathrm{d}x \left[\left(\partial_x\hat{\phi}_\nu(x)\right)^2 + \left(\partial_x\hat{\theta}_\nu(x)\right)^2\right],$$

dependent on the fields of each spin sector $\hat{\phi}_\nu(x), \hat{\theta}_\nu(x)$ ($\nu = \uparrow, \downarrow$), it is much less obvious when interactions are considered. Then, we also obtain density-density interaction terms that act non-diagonal in the spin sectors

$$\begin{aligned} H_{\text{int}} = &\sum_\nu \int_{-L/2}^{L/2} \mathrm{d}x \ \left[g_{2\parallel}\hat{\rho}_{R,\nu}(x)\hat{\rho}_{L,\nu}(x) + g_{2\perp}\hat{\rho}_{R,\nu}(x)\hat{\rho}_{L,-\nu}(x)\right] \\ &+ \sum_r\sum_\nu \int_{-L/2}^{L/2} \mathrm{d}x \ \left[\frac{g_{4\parallel}}{2}\hat{\rho}_{r,\nu}(x)\hat{\rho}_{r,\nu}(x) + \frac{g_{4\perp}}{2}\hat{\rho}_{r,\nu}(x)\hat{\rho}_{r,-\nu}(x)\right]. \end{aligned} \tag{3.24}$$

However, as the theory is still quadratic in density operators, we can find an unitary transformation that diagonalizes the combined Hamiltonian $H_{\text{SLL}} = H_{0,\text{SLL}} + H_{\text{int}}$. This leads to a new set of bosonic fields, coined charge (ρ) and spin (σ) fields

$$\hat{\phi}_\nu(x) = \frac{1}{\sqrt{2}}\left(\hat{\phi}_\uparrow(x) + \nu\hat{\phi}_\downarrow(x)\right), \qquad \hat{\theta}_\nu(x) = \frac{1}{\sqrt{2}}\left(\hat{\theta}_\uparrow(x) + \nu\hat{\theta}_\downarrow(x)\right)$$

with $\nu = (\rho, \sigma) = (+, -)$. The terminology "charge" and "spin" fields is not only by chance but carries a genuine physical meaning. The charge sector ρ contains information about the full fermion density (current) as for instance $\partial_x\hat{\phi}_\rho = -\pi/\sqrt{2}(\hat{\rho}_\uparrow(x) + \hat{\rho}_\downarrow(x))$, while the spin sector tracks the relative density (current), i. e. the net spin. Rewritten in these new

fields, the Hamiltonian of the spinful Luttinger liquid becomes diagonal

$$H_{\mathrm{SLL}} = H_{0,\mathrm{SLL}} + H_{\mathrm{int}} = \frac{1}{2\pi} \sum_{\nu=\sigma,\rho} \int_{-L/2}^{L/2} \mathrm{d}x \left[\frac{u_\nu}{K_\nu} \left(\partial_x \hat{\phi}_\nu(x) \right)^2 + u_\nu K_\nu \left(\partial_x \hat{\theta}_\nu(x) \right)^2 \right] \quad (3.25)$$

with different Luttinger parameter and velocity for each sector

$$u_\nu = v_F \sqrt{(1 + g_{4\nu}/(2\pi v_F))^2 - (g_{2\nu}/(2\pi v_F))^2}, \quad K_\nu = \sqrt{\frac{1 + g_{4\nu}/(2\pi v_F) - g_{2\nu}/(2\pi v_F)}{1 + g_{4\nu}/(2\pi v_F) + g_{2\nu}/(2\pi v_F)}}, \quad (3.26)$$

where $g_{2\nu} = g_{2\parallel} + \nu g_{2\perp}$ and $g_{2\nu} = g_{4\parallel} + \nu g_{4\perp}$ ($\nu = (\rho, \sigma) = (+, -)$). In a (1D) quantum wire of spinful fermions, there is usually no reason why $g_{2\perp}$ should be different from $g_{2\parallel}$ and, thus, typically one assumes $K_\sigma = 1$. The opposite extreme would be $g_{2\parallel} = 0$ while $g_{2\perp} \neq 0$, which yields $K_\sigma = 1/K_\rho$. K_ρ, in turn, has the same parameter range as the Luttinger parameter of a spinless or helical Luttinger liquid: $0 < K_\rho < 1$ for repulsive interactions and $K_\rho > 1$ for attractive interactions.

Spinful Luttinger liquids are not only useful to describe interacting spinful fermions in a quantum wire. They might, for instance, as well be used to capture the physics of interacting helical edge states, a situation that arises when two edges of a QSH system are brought close to each other in QSH QPCs or QCs. For such a system, in contrast to quantum wires, K_σ is typically expected to be larger than one since intra-edge interactions ($g_{2\perp}$ and $g_{4\parallel}$) are expected to dominate over inter-edge interactions ($g_{2\parallel}$ and $g_{4\perp}$). The deviation of K_σ from one can have important implications. In particular, as we will see in Sec. 4.6, it allows new types of interaction terms, acting in the σ sector, to become relevant in a RG sense.

3.1.6 Perturbative renormalization group theory for sine-Gordon models

RG theory constitutes a cornerstone method of modern many-body field theory that finds application in various different areas and forms. A general introduction of the topic is far beyond the scope of this thesis, which is why we will focus only on the specific application of RG theory to sine-Gordon models following Refs. [GNT98, Gia03, Mal13]. A more general approach can for instance be found in Ref. [Sha94, Car96, Fra13].

The basic idea behind RG theory is to derive an effective low energy theory via integrating out the high energy parts of a given partition function and rescaling of the result. In this way one obtains insight how operators behave when only low energies are considered. Thereby, any RG procedure always follows the same three steps: (i) integrating out high energy modes, (ii) rescaling of momenta and (iii) renormalization of the fields. Let us be more concrete on this. Consider a generic partition function in momentum space

$$Z = \int \prod_{|\boldsymbol{k}| \leq \Lambda} \mathrm{d}\hat{\phi}(\boldsymbol{k}) \; e^{-S[\hat{\phi}(\boldsymbol{k})]}, \quad (3.27)$$

where $\boldsymbol{k} = (k, \omega/v)^T$ is a 2D momentum-frequency vector in Euclidean space (i. e. imag-

inary time) and Λ is a high energy cutoff[6]. Let us assume we are only interested in the low-energy properties of the above partition function, say for $|\boldsymbol{k}| < \Lambda/s$ with $s > 1$. This suggests to split $\hat{\phi}(\boldsymbol{k})$ in two parts: the *slow-* and the *fast-modes*

$$\begin{aligned} \hat{\phi}_< &= \hat{\phi}(\boldsymbol{k}) \quad \text{for } 0 < |\boldsymbol{k}| < \Lambda/s, \\ \hat{\phi}_> &= \hat{\phi}(\boldsymbol{k}) \quad \text{for } \Lambda/s < |\boldsymbol{k}| \leq \Lambda. \end{aligned} \tag{3.28}$$

By assumption we are only interested in measurable properties of the slow fields $\hat{\phi}_<(\boldsymbol{k})$. Our goal is, thus, to find an effective action that only takes into account those slow modes and reproduces all the low-energy correlation functions. With the split up of (3.28), the action is expected to take the form

$$S[\hat{\phi}_<, \hat{\phi}_>] = S_0[\hat{\phi}_<] + S_0[\hat{\phi}_>] + S_1[\hat{\phi}_<, \hat{\phi}_>], \tag{3.29}$$

where S_0 is of quadratic form in its argument and, as we will explicitly demonstrate below, separates into slow and fast parts. S_1 is a generic contribution to S without this property. For the partition function, we straightforwardly obtain

$$Z = \int \prod_{0 \leq |\boldsymbol{k}| < \Lambda/s} \mathrm{d}\hat{\phi}(\boldsymbol{k}) \prod_{\Lambda/s \leq |\boldsymbol{k}| < \Lambda} \mathrm{d}\hat{\phi}(\boldsymbol{k}) \; e^{-S_0[\hat{\phi}_<]} e^{-S_0[\hat{\phi}_>]} e^{-S_1[\hat{\phi}_<, \hat{\phi}_>]}.$$

A simple reorganization leads to an effective action $S_{\text{eff}}[\hat{\phi}_<]$, taking into account only the slow fields

$$Z = \int \prod_{0 \leq |\boldsymbol{k}| < \Lambda/s} \mathrm{d}\hat{\phi}(\boldsymbol{k}) \; e^{-S_0[\hat{\phi}_<]} Z_{0>} \langle e^{-S_1[\hat{\phi}_<, \hat{\phi}_>]} \rangle_{0>} \equiv \int \prod_{0 \leq |\boldsymbol{k}| < \Lambda/s} \mathrm{d}\hat{\phi}(\boldsymbol{k}) \; e^{S_{\text{eff}}[\hat{\phi}_<]},$$

where we used

$$\langle \mathcal{O} \rangle_{0>} = \frac{1}{Z_{0>}} \int \prod_{\Lambda/s \leq |\boldsymbol{k}| < \Lambda} \mathrm{d}\hat{\phi}(\boldsymbol{k}) \; \mathcal{O} \; e^{-S_0[\hat{\phi}_>]}.$$

As $Z_{0>}$ merely is a multiplicative constant, we can safely drop it for the subsequent discussion of the effective action and define [GNT98]

$$S_{\text{eff}}[\hat{\phi}_<] = S_0[\hat{\phi}_<] - \ln \left[\langle e^{-S_1[\hat{\phi}_<, \hat{\phi}_>]} \rangle_{0>} \right]. \tag{3.30}$$

$S_{\text{eff}}[\hat{\phi}_<]$ now captures the low energy behavior of the system, where the role of the high energy modes is formally incorporated in the logarithm. The RG transformation is, however, more than just the definition of an effective action. In particular, the central goal is to obtain an insight in how the system changes upon the above mode elimination. In doing so, the problem is that one cannot directly compare the effective action with the original one as they are each defined on a different kinematic region. To remedy this defect, we

[6] Working in imaginary time has the advantage that scalars in momentum-frequency space are given by $k^2 + \omega^2/u^2$. This implies for $|\boldsymbol{k}| < \Lambda$ that k and ω are bounded. In Minkovski space, $|\boldsymbol{k}|$ is still bounded, however, k and ω are individually unbounded, leading to complications in integrations.

need to rescale the momenta in the effective action $\boldsymbol{k} \to \boldsymbol{k}' = s\boldsymbol{k}$ to retrieve the original cutoff Λ. Finally, to avoid the trivial effects of multiplicative constants, we rescale the fields $\hat{\phi}(\boldsymbol{k}'/s) \to \hat{\phi}'(\boldsymbol{k}'/s) = \xi_s^{-1}\hat{\phi}(\boldsymbol{k}'/s)$, where we choose ξ_s such that a certain coupling in the quadratic part of the action has a fixed coefficient.

This choice is not only by chance. The quadratic part of the action certainly takes a special role, that is to say, it constitutes a fixed point under the RG transformation. Let us shine some light on this important point. RG transformations define a mapping of actions defined in the same phase space. Equivalently, the initial action might be interpreted as a point in coupling constant space. Successive RG transformations then induce this point to change or *flow* in the same space. In that sense, fixed point actions are the ones that reproduce themselves and do not flow under the three-step RG transformation. Actions with this property are separable in momenta, i. e. they do not contain parts that mix different shells defined by $|\boldsymbol{k}| = \mathsf{const}.$. As evident from Eqs. (3.29) and (3.30), in case the action only contains separable parts ($S_1[\hat{\phi}_<, \hat{\phi}_>] = 0$), the effective action reproduces exactly the initial one.

Let us be more specific on that and consider the action of the free Luttinger liquid Hamiltonian. Legendre transformation of Eq. (3.20) leads to the Lagrangian

$$\mathcal{L} = \int \mathrm{d}x \left[\frac{1}{2u} \left(\partial_t \tilde{\phi}(x,t) \right)^2 - \frac{u}{2} \left(\partial_x \tilde{\phi}(x,t) \right)^2 \right],$$

where the fields $\tilde{\phi}(x,t)$ are related to the ones in Eq. (3.20) by $\tilde{\phi}(x,t) = 1/\sqrt{K\pi}\hat{\phi}(x,t)$. After integration by parts, we obtain in imaginary time $\tau = -it$

$$S_0[\tilde{\phi}] = \frac{1}{2} \int \mathrm{d}^2x \ \tilde{\phi}(\boldsymbol{x}) \nabla_x^2 \tilde{\phi}(\boldsymbol{x}), \tag{3.31}$$

where $\mathrm{d}^2x = u\mathrm{d}\tau\mathrm{d}x$, $\nabla_x^2 = \partial_x^2 + 1/u^2\partial_\tau^2$ and $\boldsymbol{x} = (x, u\tau)^T$. Now we can split the field $\tilde{\phi}(x,\tau)$ in slow and fast oscillating parts

$$\tilde{\phi}(\boldsymbol{x}) = \tilde{\phi}_<(\boldsymbol{x}) + \tilde{\phi}_>(\boldsymbol{x}), \tag{3.32}$$

where

$$\tilde{\phi}_<(\boldsymbol{x}) = \int_{|\boldsymbol{q}|<\Lambda/s} \frac{\mathrm{d}^2q}{(2\pi)^2} \tilde{\phi}(\boldsymbol{q}) e^{i\boldsymbol{q}\boldsymbol{x}}, \qquad \tilde{\phi}_>(\boldsymbol{x}) = \int_{\Lambda/s \le |\boldsymbol{q}| < \Lambda} \frac{\mathrm{d}^2q}{(2\pi)^2} \tilde{\phi}(\boldsymbol{q}) e^{i\boldsymbol{q}\boldsymbol{x}} \tag{3.33}$$

with $\boldsymbol{q} = (q, \omega/u)^T$. Using Eq. (3.32) in (3.31), this yields

$$S_0[\tilde{\phi}] = S_0[\tilde{\phi}_<] + S_0[\tilde{\phi}_>] + 2S_0[\tilde{\phi}_<, \tilde{\phi}_>],$$

where

$$S_0[\tilde{\phi}_<, \tilde{\phi}_>] = \frac{1}{2} \int \mathrm{d}^2x \ \tilde{\phi}_>(\boldsymbol{x}) \nabla_x^2 \tilde{\phi}_<(\boldsymbol{x}).$$

Using the expansions of Eq. (3.33), one line of straightforward calculation produces $S_0[\tilde{\phi}_<, \tilde{\phi}_>] = 0$. Thus, the action of the free Luttinger liquid separates in fast and slow

modes. Upon the three-step RG transformation, the partition function changes only by a global constant, leaving all coupling constants invariant. The free Luttinger liquid, hence constitutes a fixed point in RG sense.

This changes when we additionally consider a bosonic mass term with an action like[7]

$$S_1[\tilde{\phi}] = \int \mathrm{d}^2x \; g\cos[\beta\tilde{\phi}(\boldsymbol{x})]. \tag{3.34}$$

Evidently, $S_1[\tilde{\phi}]$ does not separate in fast and slow modes under the expansions of Eqs. (3.32) and (3.33). Instead, the cosine produces infinite orders of mixed terms. In this scenario, the effective action is formally given by Eq. (3.30). It is obvious that the second term is difficult to treat if one desires an exact analytical result for the effective action. However, for small coupling constants g, we can capture the effect of the second term in good approximation by an expansion in powers of g. In a second order expansion we obtain [GNT98]

$$S_{\text{eff}}[\tilde{\phi}_<] = S_0[\tilde{\phi}_<] + \langle S_1[\tilde{\phi}_<, \tilde{\phi}_>]\rangle_{0>} - \frac{1}{2}\left(\langle S_1^2[\tilde{\phi}_<, \tilde{\phi}_>]\rangle_{0>} - \langle S_1[\tilde{\phi}_<, \tilde{\phi}_>]\rangle_{0>}^2\right) + \mathcal{O}(g^3). \tag{3.35}$$

Let us estimate the first order correction around the fixed point. With Eq. (3.34) we have

$$\langle S_1[\tilde{\phi}_<, \tilde{\phi}_>]\rangle_{0>} = \frac{g}{2}\sum_{\sigma=\pm}\int \mathrm{d}^2x \; \exp\left[i\beta\sigma\tilde{\phi}_<(\boldsymbol{x})\right]\langle\exp\left[i\beta\sigma\tilde{\phi}_>(\boldsymbol{x})\right]\rangle_{0>}.$$

For s close to one (but $s > 1$), the above average yields

$$\langle\exp\left[i\beta\sigma\tilde{\phi}_>(\boldsymbol{x})\right]\rangle_{0>} = 1 - \frac{\beta^2}{4\pi}\mathrm{d}l + \mathcal{O}(\mathrm{d}l^2)$$

with $\mathrm{d}l = -\ln(s)$. Thus, in first order approximation, we obtain an effective action like

$$S_{\text{eff}}^{(1)}[\tilde{\phi}_<] = S_0[\tilde{\phi}_<] + g\left(1 - \frac{\beta^2}{4\pi}\mathrm{d}l\right)\int \mathrm{d}^2x \; \cos\left[\beta\tilde{\phi}_<(\boldsymbol{x})\right]. \tag{3.36}$$

Now, to compare Eq. (3.36) to the original action we need to rescale all momenta in the opposite direction. If we want to preserve the scalar product $\boldsymbol{k}\boldsymbol{x}$, this implies $\boldsymbol{x} \to \boldsymbol{x}/s \simeq \boldsymbol{x}(1 + \mathrm{d}l)$. Likewise, in first order, $\int \mathrm{d}^2x \to (1 + 2\mathrm{d}l)\int \mathrm{d}^2x$ and $\nabla_x^2 \to (1 - 2\mathrm{d}l)\nabla_x^2$. Thus, upon this transformation the Gaussian part $S_0[\tilde{\phi}_<]$ remains invariant. The mass term, however, appears with a new coupling constant

$$g' = g\left[1 + \left(2 - \frac{\beta^2}{4\pi}\right)\mathrm{d}l\right]. \tag{3.37}$$

The above equation might be reformulated in differential form using the dimensionless

[7] Note that here g has the dimension of momentum as $\mathrm{d}^2x = u\mathrm{d}\tau\mathrm{d}x$

coupling constant $z = g/\Lambda$

$$\frac{\mathrm{d}z(l)}{\mathrm{d}l} = \left(2 - \frac{\beta^2}{4\pi}\right) z(l).$$

Let us interpret this result. With decreasing the energetic scale that we assume to be relevant for the theory, the coupling constant of a given cosine perturbation can either grow, in case $\beta^2/(4\pi) < 2$, or shrink when $\beta^2/(4\pi) > 2$. If we obtain a growing coupling constant, it means that the given perturbation gains relevance as we observe lower energies. Hence, we coin such a perturbation a *RG relevant perturbation*. Likewise, terms that flow to vanishing coupling constants under the three-step RG transformation are *RG irrelevant*. Typically, the solution to Eq. (3.37) is visualized as a scaling portrait in the $z - \beta$ plane. As β is not renormalized in first order, this produces a rather trivial picture, shown in Fig. 2.10 (a). This changes when we include the second order terms of Eq. (3.35) in the discussion. Upon similar, albeit more sophisticated calculations as done for the first order, we derive a second differential equation, which this time describes the flow of β. In combination with first order, this produces a system of coupled differential equations

$$\frac{\mathrm{d}z(l)}{\mathrm{d}l} = [2 - d(l)]\, z(l), \qquad \frac{\mathrm{d}d(l)}{\mathrm{d}l} = -\frac{12\pi}{\Lambda^3} z^2(l) d^3(l)$$

with the replacement $d(l) = \beta^2(l)/(4\pi)$. The trajectories of the solution are schematically illustrated in Fig. 2.10 (b). Similar to the first order approximation, $d(l) = 2$ constitutes a special point in parameter space. Let us therefore discuss the trajectories in the vicinity of this point. There, two separatrices , $\pm 1/\sqrt{2}(d(l) - 2) \equiv \pm\kappa$, divide the parameter space in three regimes: (i) weak-coupling, for $z(l) \leq \kappa$ and $d(l) > 2$, (ii) strong-coupling, for $z(l) \leq -\kappa$ and $d(l) < 2$, and (iii) crossover regime, for $-z(l) < \kappa < z(l)$. In the weak-coupling regime, $z(l)$ flows to a stable fixed point with $z(l) \to 0$. In contrast, in the strong-coupling regime $z(l) = 0$ constitutes an unstable fixed point. Here, the RG flow promotes $z(l) \to \infty$, while at the same time $\beta(l) \to 0$. In the third regime, the crossover regime, no fixed points exist at all.
Hence, for the crossover and the strong-coupling regime, one could anticipate the RG flow to continue forever. This, however, would imply that only infinitely low energies are considered to participate in the theory. In reality, this is of course not the case. Therefore, the RG flow needs to be stopped at the largest energy scale set by the system, such as temperature or system size. Energies below these characteristic energy scales are hidden.

3.2 Scattering theory and quantum transport

Obtaining insight in the profound physical properties of a given system is a core discipline of physics. Pictorially speaking, the typical protocol to approach this task is to "throw" something on the system and observe the response. A convenient ansatz for that is to couple the system of interest to particle reservoirs and perform quantum transport measurements. Thereby, the response of the system is controlled by the scattering matrix. By virtue of the deep connection between the scattering matrix and the Hamiltonian of a given

system, the characteristics obtained from such measurements often times carry revealing and instructive information. The physical quantity of interest for such a measurement is the current operator.

Let us assume a mesoscopic system based on fermions that acts as a scatterer when connected to N_r macroscopic reservoirs. The fermions of each reservoir α are described by field operators $\hat{\psi}_\alpha(x,t)$[8]. Depending on whether we are dealing with relativistic or non-relativistic electrons, $\hat{\psi}_\alpha(x,t)$ takes a different form. While in the non-relativistic case $\hat{\psi}_\alpha(x,t)$ sums up right- and left-moving components (see Eq. (3.23)), in the relativistic case, $\hat{\psi}_\alpha(x,t)$ has a spinor structure. Moreover, also the current operators are different in both cases. However, as we have seen already against the background of bosonization, linearization provides a valid and comprehensive approximation of the systems behavior around the Fermi surface, provided k_F is large enough[9]. Thus, a system of non-relativistic fermions might be approximated around the Fermi surface by a linear (Dirac-like) theory. Under these assumptions, the current operator of (a relativistic or non-relativistic) fermionic lead α is given by [Mos11]

$$\hat{I}_\alpha(t) = \frac{e}{2\pi} \int\int \mathrm{d}E\mathrm{d}E' e^{i(E-E')t} \left[\hat{b}^\dagger_\alpha(E)\hat{b}_\alpha(E') - \hat{a}^\dagger_\alpha(E)\hat{a}_\alpha(E')\right], \tag{3.38}$$

where $\hat{a}^\dagger_\alpha(E)$ ($\hat{b}^\dagger_\alpha(E)$) creates an incident (scattered or outgoing) electron at energy E in lead α[10]. When we assume the mesoscopic scatterer not to affect the equilibrium properties of the reservoirs, we obtain the measurable current that flows into lead α as the quantum-statistical average of Eq. (3.38) $I_\alpha = \langle \hat{I}_\alpha \rangle$. Let us assume that the reservoirs are adiabatically connected to the scattering region and no correlations appear among electrons of different reservoirs. Then, for the incoming particles, which are assumed to be equilibrium particles, averaging yields

$$\langle \hat{a}^\dagger_\alpha(E)\hat{a}_\beta(E') \rangle = \delta_{\alpha\beta}\delta(E-E')f_\alpha(E)$$

with the Fermi-Dirac distribution $f_\alpha(E) = (1 + e^{(E-\mu_\alpha)/(k_B T_\alpha)})^{-1}$. Here, k_B is the Boltzmann constant, T_α the temperature and μ_α the chemical potential of lead α. In contrast, particles associated with the operators $\hat{b}^\dagger_\alpha(E)$ and $\hat{b}_\alpha(E)$ are scattered and are, thus, in general non-equilibrium particles. However, by virtue of the scattering matrix $S_{\alpha\beta}(E)$, we can relate the outgoing operators $\hat{b}^\dagger_\alpha(E)$, $\hat{b}_\alpha(E)$ to all incoming operators via

$$\hat{b}_\alpha(E) = \sum_{\beta=1}^{N_r} S_{\alpha\beta}(E)\hat{a}_\beta(E).$$

[8] For ease of understanding, we assume 1D reservoirs and connections to the scattering region.

[9] A more rigorous derivation of this statement starting from the definition of the current operator can for instance be found in Ref. [Mos11].

[10] We have switched here the notation from right- and left-moving to incident and outgoing as right- and left-moving loses meaning in the presence of many leads.

Thus, averaging the outgoing contributions in Eq. (3.38) yields

$$\langle \hat{b}_\alpha^\dagger(E)\hat{b}_\alpha(E')\rangle = \delta(E-E')\sum_{\beta=1}^{N_r}|S_{\alpha\beta}(E)|^2 f_\beta(E).$$

Now, together with the unitarity of the scattering matrix, $\sum_{\beta=1}^{N_r}|S_{\alpha\beta}(E)|^2 = 1$, we find the insightful formula [Bü86, Bü92]

$$I_\alpha = \frac{e}{2\pi}\int \mathrm{d}E \sum_{\beta=1}^{N_r}|S_{\alpha\beta}(E)|^2\left(f_\beta(E)-f_\alpha(E)\right).$$

Let us assume small voltage differences among different reservoirs $\mu_\alpha = \mu_0 + eV_\alpha$ with $eV_\alpha \ll \mu_0$ and $T_\alpha = T_0$ for all α. Having $|eV_\alpha| \ll k_B T_\alpha$ we can approximate the Fermi distributions around μ_0 by

$$f_\alpha(E) = f_0(E) - eV_\alpha\frac{\partial f_0(E)}{\partial E} + \mathcal{O}(V_\alpha^2),$$

where $f_0(E)$ is the Fermi distribution with chemical potential μ_0 and temperature T_0. With recognizing $\lim_{T_0\to 0}\partial_E f_0(E) = -\delta(E-\mu_0)$, we obtain the conductance as [Bü86, Bü92]

$$G_{\alpha\beta} = \frac{\mathrm{d}I_\alpha}{\mathrm{d}V_\beta} = \frac{e^2}{2\pi}|S_{\alpha\beta}(\mu_0)|^2. \tag{3.39}$$

It is clear that the above conductance formula can only hold in two scenarios: first, for vanishingly small applied bias $eV_\alpha \to 0$ or, second, for a finite applied bias, when the energy dependence of the scattering matrix around μ_0 is negligible, $S_{\alpha\beta}(E) \simeq S_{\alpha\beta}(\mu_0)$.

3.2.1 Relation of Hamiltonian and transfer matrix

Next, let us shine some light on the question why quantum transport measurements, i. e. measurements of the scattering matrix elements, carry profound physical information of the system properties. Let us therefore consider an arbitrary effectively 1D time-independent Hamiltonian linear in momentum like

$$H = \int_{-L/2}^{L/2}\mathrm{d}x\ \hat{\Psi}^\dagger(x)\left[A\hat{p}_x + V(x)\right]\hat{\Psi}(x) \tag{3.40}$$

with the fermionic field operators $\hat{\Psi}^\dagger(x)$ and $\hat{\Psi}(x)$ being $2N_r$ dimensional spinors, $\hat{\Psi}(x) = \left(\hat{\psi}_{1,a}(x),\hat{\psi}_{1,b}(x)...,\hat{\psi}_{N_r,a}(x),\hat{\psi}_{N_r,b}(x)\right)$ consisting of N_r different kinds, each of which having an "incoming" (a) and "outgoing" (b) field. $V(x)$ and A are Hermitian $2N_r \times 2N_r$ matrices capturing all present single particle potentials. We strive to diagonalize Eq. (3.40). Thus, we need to solve the associated single particle problem $[A\hat{p}_x + V(x)]\Psi(x) = E\Psi(x)$.

By virtue of the linearity in $\hat{p}_x$, we find the solution by integration

$$\Psi(x) = U(x, x_0)\Psi(x_0), \tag{3.41}$$

where we defined the transfer matrix

$$U(x, x_0) = \hat{S}_{\leftarrow} \exp\left[\frac{i}{v_F}\int_{x_0}^{x} \mathrm{d}x' A^{-1}\left(E - V(x')\right)\right] \tag{3.42}$$

with the spatial-ordering operator $\hat{S}_{\leftarrow}$, ordering all appearing spatial coordinates ascending from right to left. Now, let us couple each of the $2N_r$ different fermions to a lead. We demand that also the leads are well approximated by a Hamiltonian that is linear in momentum. This implies continuity of the wave functions at the interfaces between system and leads. Lead fermions in the regime $x < -L/2$ are thus connected to the ones for $x > L/2$ by $U(L/2, -L/2)$. Upon linear transformations, the transfer matrix can easily be transformed into the scattering matrix. Thus, scattering matrices contain all the profound information about the Hamiltonian of the system. Knowledge about the transfer or scattering matrix determines all fermionic correlations, captured by the Green function.

3.2.2 McMillan Green function

Green functions describe the fundamental correlations of many-body theory. Indeed, by virtue of Wick's theorem, any N-point correlation function (for a system described by a quadratic Hamiltonian) can eventually be decomposed into a collection of two-point correlation functions, i. e. Green functions or *propagators* [Wen04]. In general, the Green function is the solution of a given differential equation exposed to the delta inhomogeneity. This rather unspecific condition allows for several solutions, implying that the Green function is not unique, which eventually gives rise to the physically motivated *retarded* and *advanced* Green functions, that describe forward or backward temporal correlations. Let us explicitly monitor how this ambiguity emerges. Retarded (R) and advanced (A) fermionic Green functions are defined as

$$G^{\nu}(x, x', t) = -\nu i\theta(\nu t)\langle\{\hat{\Psi}(x, t), \hat{\Psi}^{\dagger}(x', 0)\}\rangle,$$

where $\nu = (R, A) = (+, -)$. $\{...,...\}$ is the anti-commutator and $\hat{\Psi}(x, t)$ is a fermionic field operator annihilating a fermion at position x at time t. In Fourier space, we obtain

$$G^{\nu}(x, x', \omega) = \int \mathrm{d}t\; e^{i(\omega \pm i0^{+})t} G^{\nu}(x, x', t). \tag{3.43}$$

Then, all Green functions are determined from two defining equations

$$\left[\omega - \mathcal{H}(x, \hat{p}_x)\right] G^{\nu}(x, x', \omega) = \delta(x - x'), \qquad G^{\nu}(x, x', \omega)\left[\omega - \mathcal{H}(x', \hat{p}_{x'})\right] = \delta(x - x'), \tag{3.44}$$

where $\mathcal{H}(x, \hat{p}_x)$ is the Hamiltonian density of the system. For any $x \neq x'$, the above equations imply that Green functions might be represented in terms of eigenfunctions of

$\mathcal{H}(x,\hat{p}_x)$ and its transposed $\bar{\mathcal{H}}(x',\hat{p}_{x'}) = \mathcal{H}^T(x',-\hat{p}_{x'})$[11] with the eigenvalue ω [McM68]

$$G^\nu_{\alpha\beta}(x,x',\omega) = \sum_{i,j} a^\nu_{ij}\phi_{i,\alpha}(x,\omega)\tilde{\phi}_{j,\beta}(x',\omega), \tag{3.45}$$

where we demand $\mathcal{H}(x,\hat{p}_x)\phi_j(x,\omega) = \omega\phi_j(x,\omega)$ and $\bar{\mathcal{H}}(x',\hat{p}_{x'})\tilde{\phi}_j(x',\omega) = \omega\tilde{\phi}_j(x,\omega)$. The index j characterizes the different linearly independent eigenfunctions. The indices α and β specify the α-th and β-th component of the corresponding eigenfunction. a^ν_{ij} are expansion coefficients yet to be determined. With inserting Eq. (3.45) in (3.44), we readily see that any combination of eigenfunctions solves the problem for $x \neq x'$. The implementation of the delta distribution on the right hand sides of (3.44) requires more care. Imagine a Hamiltonian density of the form

$$\mathcal{H}(x,\hat{p}_x) = \sum_{\ell=0}^{k} A_\ell \hat{p}_x^\ell, \tag{3.46}$$

where A_ℓ are generic Hermitian $n\times n$ matrices[12] for a given spinor basis of dimension n. Integration of (for instance) the left equation in (3.44) from $x'-\varepsilon$ to $x'+\varepsilon$ in the limit $\varepsilon\to 0$ yields the k determining equations

$$\lim_{\varepsilon\to 0}\left[\partial_x^{k-1}G(x,x',\omega)\big|_{x=x'+\varepsilon} - \partial_x^{k-1}G(x,x',\omega)\big|_{x=x'-\varepsilon}\right] = -(i)^k A_k^{-1}, \tag{3.47}$$

$$\lim_{\varepsilon\to 0}\left[\partial_x^{k-j}G(x,x',\omega)\big|_{x=x'+\varepsilon} - \partial_x^{k-j}G(x,x',\omega)\big|_{x=x'-\varepsilon}\right] = 0, \quad \text{for } 1<j\leq k. \tag{3.48}$$

The above equations set $n^2\times k$ additional conditions on the Green function. In particular, in the limit $\varepsilon\to 0$, they specify the x' dependence for an assumed x dependence. Let us slightly rewrite Eq. (3.45)

$$G^\nu_{\alpha\beta}(x,x',\omega) = \sum_{i,j} a^\nu_{ij}\phi_{i,\alpha}(x,\omega)\tilde{\phi}_{j,\beta}(x',\omega) \equiv \sum_i \phi_{i,\alpha}(x,\omega)g^\nu_{i,\beta}(x',\omega), \tag{3.49}$$

where we defined $g^\nu_{i,\beta}(x',\omega) = \sum_j a^\nu_{ij}\tilde{\phi}_{j,\beta}(x',\omega)$. Now, to obtain a discontinuous jump in $\partial_x^{k-1}G^\nu(x,x',\omega)$ we use the ansatz

$$G^\nu_{\alpha\beta}(x,x',\omega) = G^{\nu,<}_{\alpha\beta}(x,x',\omega)\theta(x-x') + G^{\nu,>}_{\alpha\beta}(x,x',\omega)\theta(x'-x), \tag{3.50}$$

where each part is of the form of Eq. (3.49)

$$G^{\nu,</>}_{\alpha\beta}(x,x',\omega) = \sum_i \phi_{i,\alpha}(x,\omega)g^{\nu,</>}_{i,\beta}(x',\omega)$$

[11] Here, transposing acts also on the operators. If we think of transposing only as a matrix operation, we need to set $\hat{p}_{x'}\to -\hat{p}_{x'}$, which would yield $\mathcal{H}^T(x',\hat{p}_{x'})$.

[12] For convenience, we assume A_ℓ to be independent of x for $\ell\neq 0$. Instead, for having $A_\ell \equiv A_\ell(x)$ also for $\ell\neq 0$, we need to replace the Hamiltonian density by $\mathcal{H}(x,\hat{p}_x)\to\sum_{\ell=0}^k\{A_\ell(x),\hat{p}_x^\ell\}$ to preserve hermicity.

with $g^{\nu,</>}_{i,\beta}(x',\omega) = \sum_j a^{\nu,</>}_{ij} \tilde{\phi}_{j,\beta}(x',\omega)$. The differential equation, defined by Eq. (3.46), produces $n \times k$ linearly independent solutions $\phi_i(x,\omega)$ (with $i \in 1,...n \times k$). On the other hand, our ansatz of Eq. (3.50) gives $2n^2 \times k$ free (x' dependent) parameters $g^{</>}_{j,\beta}(x',\omega)$. However, from Eqs. (3.47) and (3.48), we obtain only $n^2 \times k$ determining equations. Thus, the Green function is underdetermined by a factor of 2. In the end, it is this ambiguity that allows the definition of different Green functions, such as retarded, advanced or causal.
To resolve the underdetermination, additional conditions are required. Those can be obtained from boundary behavior of the Green function. The retarded Green function is defined in the upper half complex plane (see Eq. (3.43)). If we assume an infinitesimal dissipation in the leads, we have $\lim_{x\to\pm\infty} G^R(x,x',\omega + i0^+) = 0$. This gives a selection rule how to distribute the eigenfunctions in the two regimes $x > x'$ and $x < x'$ and exactly yields the missing factor of 2. In the literature, such boundary conditions are often called *outgoing wave boundary conditions* [KT00, HBY10, CBT15].
Let us now assume the scattering problem of the former section. The scatterer is defined by Eq. (3.40) and for $x < -L/2$ and $x > L/2$ we assume the presence of leads. In either lead, the form of the scattering states is easily determined using the ansatz of incoming and outgoing states. Together with outgoing wave boundary conditions and the continuity of wave functions at each interface, this yields the retarded Green function in the leads, $G^R(x_0,x_0',\omega)$ at the lead coordinates x_0 and x_0'. Now, by virtue of the linearity of Eq. (3.40) and the resulting transfer matrix (Eqs. (3.41) and (3.42)), we get access to the Green function for any set of coordinates x and x'

$$G^R(x,x',\omega) = U(x,x_0)G^R(x_0,x_0',\omega)\tilde{U}^T(x',x_0'), \tag{3.51}$$

where $\tilde{U}^T(x',x_0')$ is the transfer matrix associated with $\tilde{\mathcal{H}}(x,\hat{p}_x)$. Eq. (3.51) can be extremely useful when it comes to the characterization of electronic correlations in complex scattering systems, where the explicit form of the wave functions is cumbersome but the general solution, formulated in terms of transfer matrices, is not.

3.2.3 Non-stationary scattering theory

So far, the main focus has been set on time-independent Hamiltonians. Especially for scattering theory, time-independence is necessary as all the above derivation requires energy conservation, which is induced by time translation invariance of the system. For explicitly time-dependent Hamiltonians, this is clearly not provided. However, there is a class of Hamiltonians that constitute a hybrid case, namely, time-periodic Hamiltonians [Shi65]. For such systems, energy is not conserved in general, however, discrete time translational invariance implies energy conservation up to multiples of the driving frequency.

Blueprint of Floquet theory

Let us briefly sketch the theory of time-periodic systems following Ref. [EA15]. Consider a generic T-periodic Hamiltonian $\mathcal{H}(x,t) = \mathcal{H}(x,t+T)$. Because of the explicit time dependence of $\mathcal{H}(x,t)$, the system is described by the time dependent Schrödinger equation

$$i\partial_t\psi(x,t) = \mathcal{H}(x,t)\psi(x,t). \tag{3.52}$$

The time-periodicity of $\mathcal{H}(x,t)$ implies that the probability density of corresponding eigenstates is also invariant under time-translation by T. Hence, eigenfunctions of Eq. (3.52) are given by

$$\psi_\alpha(x,t) = e^{-i\epsilon_\alpha t} u_\alpha(x,t) \qquad \text{with} \qquad u_\alpha(x,t+T) = u_\alpha(x,t).$$

Inserting the above ansatz in Eq. (3.52), this readily produces an eigenvalue problem for the so-called *quasi-energy operator* $\mathcal{Q}(x,t) = \mathcal{H}(x,t) - i\partial_t$,

$$\mathcal{Q}(x,t) u_\alpha(x,t) = \epsilon_\alpha u_\alpha(x,t). \tag{3.53}$$

Thereby, the Floquet states $u_\alpha(x,t)$ form a complete set of orthonormal states in an extended Hilbert space $\mathcal{R} \otimes \mathcal{L}_T$, formed from the Hilbert space $\mathcal{R}$ of square integrable functions on the configuration space and the space $\mathcal{L}_T$ of time-periodic functions with period $T = 2\pi/\Omega$. Thus, we can expand

$$u_\alpha(x,t) = \sum_{n=-\infty}^{\infty} \sum_k c^n_{\alpha,k} \varphi_k(x) e^{in\Omega t}, \tag{3.54}$$

where the functions $\varphi_k(x)$ ($e^{in\Omega t}$) form a complete orthonormal set of states in $\mathcal{R}$ ($\mathcal{L}_T$). The expansion (3.54) readily implies that ϵ_α is only defined up to multiples of Ω as evident from a shift of the index n. Henceforth, we use the notation $\varphi_k(x)e^{in\Omega t} \equiv |\varphi_k, n\rangle\rangle$ and $u_\alpha(x,t) = |u_\alpha(x,t)\rangle\rangle$. Then, we define the inner product in $\mathcal{R} \otimes \mathcal{L}_T$ as

$$\langle\langle \varphi_j, m | \varphi_k, n \rangle\rangle = \frac{1}{T} \int_0^T \mathrm{d}t \; \langle \varphi_j | \varphi_k \rangle e^{i(n-m)\Omega t} = \delta_{kj}\delta_{nm}$$

with the standard inner product $\langle ... | ... \rangle$ defined on $\mathcal{R}$. The expansion coefficients $c^n_{\alpha,k}$ represent an unitary map from $\varphi_k(x)e^{in\Omega t}$ to $u_\alpha(x,t)$. Thus, also the states $u_\alpha(x,t)$ form a complete set in $\mathcal{R} \otimes \mathcal{L}_T$[13]. Using Eq. (3.54) in (3.53) and multiplying from the left by $\mathbb{1} = \sum_{l,m} |\varphi_l, m\rangle\rangle\langle\langle \varphi_l, m|$, this yields an effectively time-independent infinite dimensional eigenvalue problem for the Floquet expansion coefficients $c^m_{\alpha,l}$

$$\sum_{n=-\infty}^{\infty} \sum_k \langle \varphi_l | \mathcal{Q}_{n,m} | \varphi_k \rangle c^n_{\alpha,k} = \epsilon_\alpha c^m_{\alpha,l}, \tag{3.55}$$

where we defined

$$\mathcal{Q}_{n,m} = \frac{1}{T} \int_0^T \mathrm{d}t \; \mathcal{H}(x,t) e^{i(n-m)\Omega t} + \delta_{nm} n\Omega.$$

[13] Note that for each $t \in [0,T[$ there is one extended Hilbert space $\mathcal{R} \otimes \mathcal{L}_T$. This will become important for the time-evolution operator

Next, let us investigate the time-evolution operator. Generically, for explicitly time dependent Hamiltonians, time-evolution is described by

$$K(t,t_0) = \mathcal{T}\exp\left[-i\int_{t_0}^{t} \mathrm{d}t' \mathcal{H}(x,t')\right].$$

With the special properties of Floquet Hamiltonians being periodic in time T, we readily find

$$K(nT,0) = K(T,0)^n, \qquad K(t+T,0) = K(t,0)K(T,0).$$

In particular, note that in general $K(t,0)$ does not commute with $K(T,0)$ except at times $t = nT$. Let us be more specific about the form of $K(t_f,t_i)$. The time dependence of a generic state is governed by the Floquet modes (3.54). Thus, at time t, a generic state might be represented as

$$\psi(x,t) = \sum_\alpha d_\alpha e^{-i\epsilon_\alpha t}|u_\alpha(x,t)\rangle\rangle$$

with time independent expansion coefficients d_α. Then, consequently, the time-evolution operator, capturing the time propagation from t_i to t_f, must be given by

$$K(t_f,t_i) = \sum_\alpha e^{-i\epsilon_\alpha(t_f-t_i)}|u_\alpha(x,t_f)\rangle\rangle\langle\langle u_\alpha(x,t_i)|. \tag{3.56}$$

Although the above relation looks similar to the time-evolution in a stationary system, there is a subtle difference. Namely, the Floquet states $|u_\alpha(x,t)\rangle\rangle$ do not built an orthogonal set of states at different times t. Hence, in general, Eq. (3.56) cannot be represented as the matrix exponential of a time-independent Hamiltonian. However, the Floquet states are by definition periodic in time T. Thus, for a time propagation by a full period T we can replace t_f with $t_i + T$. Consequently, $|u_\alpha(x,t_f)\rangle\rangle \equiv |u_\alpha(x,t_i)\rangle\rangle$, so that

$$K(t_i+T,t_i) = \sum_\alpha e^{-i\epsilon_\alpha(t_f-t_i)}|u_\alpha(x,t_i)\rangle\rangle\langle\langle u_\alpha(x,t_i)| \equiv \exp\left[-iTH_F(x,t_i)\right],$$

where $H_F(x,t_i)$ is the so-called time-independent Floquet Hamiltonian

$$H_F(x,t_i) = \sum_\alpha \epsilon_\alpha |u_\alpha(x,t_i)\rangle\rangle\langle\langle u_\alpha(x,t_i)|.$$

Note that, in a certain sense, there is an analogy of Floquet theory to Bloch theory of crystals. In Bloch theory, discrete translational invariance leads to a Bloch Hamiltonian where momentum is only defined up to multiples $2\pi/a_L$ with a lattice spacing a_L. In Floquet theory, something similar happens due to discrete time translational invariance. However, instead of momentum, now energy is only defined up to multiples of $\Omega = 2\pi/T$. The analogy of the Bloch Hamiltonian, describing the motion of fermions in the crystal, is the Floquet Hamiltonian, responsible for time-translations by a full period.

Floquet scattering theory

The fact that energy is conserved up to multiples of the driving frequency allows for a modified formulation of stationary scattering theory for Floquet systems [MB02]. Let us consider a time-periodic scatterer, adiabatically connected to stationary leads. Since energy is well defined in each lead, the current operator of Eq. (3.38) is still valid. For reasons that will become clear below, it is convenient to change to frequency space. This produces [Mos11]

$$\hat{I}_\alpha(\omega) = e \int \mathrm{d}E \left[\hat{b}^\dagger_\alpha(E)\hat{b}_\alpha(E+\omega) - \hat{a}^\dagger_\alpha(E)\hat{a}(E+\omega)\right].$$

Now, as opposed to the stationary case, the energy of electrons can change by multiples of the driving frequency while passing the scatterer. Thus,

$$\hat{b}_\alpha(E) = \sum_{n=-\infty}^{\infty} \sum_{\beta=1}^{N_r} S_{F,\alpha\beta}(E, E_n)\hat{a}_\beta(E_n)$$

with a similar relation for $\hat{b}^\dagger_\alpha(E)$. $S_{F,\alpha\beta}(E, E_n)$ represents the Floquet scattering matrix, describing all possible transitions from incoming to outgoing fermions with a change in energy from E to $E_n = E + n\Omega$. Notably, while scattered, the energy of the fermions cannot change by any other value than the $n\Omega$. Under performing a quantum-statistical averaging, this leads to the average current [Mos11]

$$\langle \hat{I}_\alpha(\omega)\rangle = I_\alpha(\omega) = \sum_{l=-\infty}^{\infty} 2\pi\delta(\omega - l\Omega) I_{\alpha,l},$$

where

$$I_{\alpha,l} = \frac{e}{2\pi} \int \mathrm{d}E \left[\sum_{\beta=1}^{N_r} \sum_{n=-\infty}^{\infty} S^\dagger_{F,\alpha\beta}(E_n, E) S_{F,\alpha\beta}(E_l, E_n) f_\beta(E_n) - \delta_{l0} f_\alpha(E)\right].$$

An important implication of the two above equations is that even in the absence of thermal or voltage differences between the leads, a dynamical scatterer generates an alternating time-dependent current

$$I_\alpha(t) = \sum_{l=-\infty}^{\infty} e^{-il\Omega t} I_{\alpha,l}.$$

Of course, when averaging over time, all oscillating contributions vanish, leaving behind only the time-independent current $I_{\alpha,0}$. Since also the Floquet scattering matrix has to obey unitarity, we find an intuitively clear expression for the time-independent current [Mos11]

$$I_{\alpha,0} = \frac{e}{2\pi} \int \mathrm{d}E \sum_{\beta=1}^{N_r} \sum_{n=-\infty}^{\infty} \left[|S_{F,\alpha\beta}(E_n, E)|^2 f_\beta(E) - |S_{F,\beta\alpha}(E_n, E)|^2 f_\alpha(E)\right].$$

The current into lead α is determined by the difference of two electron flows. The first consists of the sum of various electrons scattered from all leads β into lead α. The second describes the flow of electrons incident from lead α into leads β. Notably, the probabilities $|S_{F,\alpha\beta}(E_n, E)|^2$ and $|S_{F,\beta\alpha}(E_n, E)|^2$ are not necessarily equivalent. In particular, such a situation is given for an inversion asymmetric scatterer. Then, even in the absence of voltage or temperature differences between the leads, a time-independent current can appear, known as a *quantum pump* [Mos11].
When we assume spatial inversion symmetry of the scatterer, quantum pumps are absent. Then, a time-independent current is generated only in the presence of voltage or temperature differences. For small voltage differences, similar to the stationary case, the conductance matrix is determined by the scattering matrix [ABC17a]

$$G_{\alpha\beta} = \frac{\mathrm{d}I_{\alpha,0}}{\mathrm{d}V_\beta} = \frac{e^2}{2\pi} \sum_{n=-\infty}^{\infty} |S_{F,\alpha\beta}(E_n, E)|^2. \tag{3.57}$$

Obtaining insight in the quantum transport characteristics of a dynamical scatterer requires knowledge of the infinite dimensional Floquet scattering matrix. For that, we need to solve Eq. (3.55), which can become a very formidable task as we are dealing with infinite dimensional matrices. Formally, electrons can change their energy while being scattered by any multiple n of energy quanta Ω. However, in practice, the transmission probability converges to zero as $n \to \pm\infty$. Thus, there is a $n_{\max}$ such that transmission probabilities for absorbing/emitting $n_{\max} + 1$ energy quanta is negligible for a given accuracy. This is generically the case if the amplitude of a dynamic scattering potential δU is much smaller than $n_{\max}\Omega$. Then, the matrix elements connecting the different sectors where $\delta n > n_{\max}$ in the (quasi-) Schrödinger equation (3.55) become negligible. This leads to an effective equation with only $2n_{\max} + 1$ sectors, centered around $n = 0$.

4 Quantum spin Hall quantum constrictions as a novel platform for exotic quantum matter

4.1 Limitations of spin-orbit coupled quantum wires

With the proposal of Majorana end modes in quantum wires [ORvO10, LSDS10, STL$^+$10] and promising subsequent experiments [MZF$^+$12], the search for non-Abelian anyons in condensed matter systems reached a new level. Since then, the fast developing field was fueled by rapid improvements of experimental samples leading to exciting experimental signatures [CAJ$^+$15, AHM$^+$16b]. During this process, however, it was recognized that it is by far not a trivial task to discriminate among truly non-Abelian particles and trivial low-energy Andreev BSs. Indeed, in real systems, it is very likely that both, Majoranas and low energy Andreev BSs, can appear and continuously transform into each other. Such a situation is for instance generated when the control parameters, that are able to bring the system to the topological regime, carry a significant spatial dependence. For SOC quantum wires, those control parameters are given by the externally applied magnetic field B, the chemical potential μ and the induced superconducting pairing amplitude Δ. While it is unlikely that the magnetic field varies significantly on the length scale of the quantum wire, this cannot be a priori assumed for μ and Δ. In modern SOC quantum wire samples, the SC is grown as a (partial) shell on top of the wire, covering only a portion of the full wire [CAJ$^+$15, AHM$^+$16b]. Thus, the proximity induced pairing amplitude is expected to vary significantly throughout the wire. While this is in principle not a problem for the topological properties of the system, it can lead to the formation of non-topological Majorana modes that are localized at one end of the wire only. The missing topological protection then leads to strong hybridization of these non-topological Majorana modes, which in turn destroys their non-Abelian nature. However, in some circumstances, these non-topological Majorana modes yield similar signatures as compared to topological ones so that discriminating them from each other is somewhat elusive. Typically, low-energy modes in these systems are associated with exponentially protected Majorana modes. However, an increasing number of works indicate that this strict assignment must be relaxed, especially in the presence of spatially varying potentials [KMB12, FDTZT18, MZST18]. Consequently, also the believed characteristic quantized zero-energy peak in the local conductance as a signature of topological Majorana modes looses its significance. Throughout the last years, a number of proposals were suggested to overcome this obstacle [LSDS18, VNAW19, ZS20], however, so far no conclusive experimental evidence was reached.

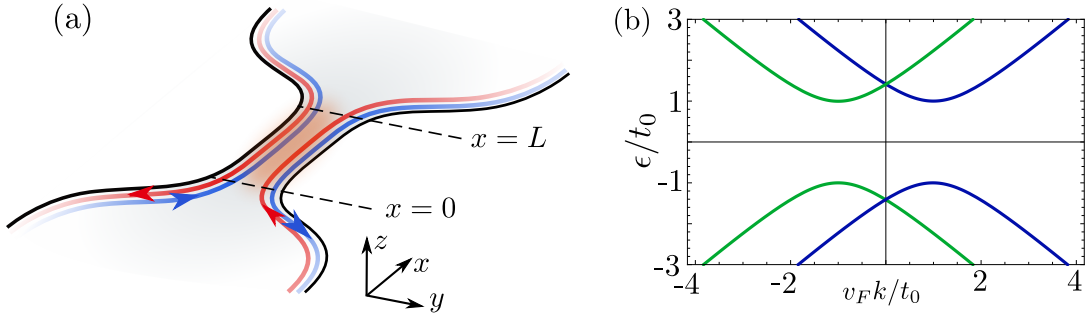

Figure 4.1: (a) Schematic of a QC of length L based on a QSH insulator. (b) Spectrum of an infinitely long QSH QC including all TR invariant SP processes. Different colors represent states with orthogonal spin. ϵ denotes energy eigenvalues of the Schrödigner equation.

4.2 The quantum spin Hall quantum constriction – a symmetry-enriched quantum wire

The difficulties emerging in quantum wire based topological SCs are manifold. Even despite the fact that spatially varying potentials complicate the readout of Majorana associated signals, proving the existence of Majoranas in quantum wires is cumbersome. The main reason for complications is naturally given by the fact that true quantum wires are only *quasi* 1D objects and the Hamiltonian of Eq. (2.29) constitutes only an approximation. In true quantum wires, higher sub-bands exist and contribute to the physics at low energies [HTZC$^+$17, WAvH$^+$19]. Moreover, even for the simplified purely 1D Hamiltonian, detection schemes suffer from the absence of symmetries in the wire and, particularly, in the leads.

Fortunately, topological superconductivity is not exclusively attached to SOC wires, but may also be realized in various other hybrid systems, ranging from atomic chains placed on s-wave SCs [NPDBY13, PGvO13, LCD$^+$14] over quantum Hall based systems [FGSJ18] to hetero-junctions on the basis of 2D TIs [FK09]. Among those, from the perspective of present symmetries, in particular 2D TI based hetero-junctions are interesting. Taking into account only the low-energy effective Hamiltonian describing the surface states, 2D TIs possess TR and chiral symmetry. Spin and propagation direction are intimately related by TR symmetry, which in principle allows for new spin-selective detection schemes. However, on the other hand, such hetero-junctions drastically lack experimental feasibility mainly due to difficulties in realizing ferromagnetic ordering at the helical edge.

Interestingly and largely overlooked, helical edge based devices can realize topological superconductivity and even more exotic phenomena also in the absence of ferromagnetic ordering. The enabling requirement is the presence of a second helical edge, so that both edges can hybridize and interact. Such a device – a *QSH QC* – unites the best properties of two worlds. Consider the device sketched in Fig. 4.1 (a). The edge states of a QSH insulator are guided into a narrow constriction. Within the constriction, $0 < x < L$, the system can be interpreted as a linearized version of a spinful quantum wire. Clearly, the device obeys the same number of fermionic fields, while at the same time, due to the linear dispersion, the system naturally possesses a charge-conjugation symmetry. Outside

the constricted region, isolated helical edge states provide an intimate relation of spin and propagation direction. This enables a whole new variety of insightful spin-selective transport experiments.
Consider an infinitely extended QC. Then, we retain momentum as an eligible quantum number. In good approximation, the kinetic part of the system is described by two copies of H_{QSH} (Eq. (2.34)) with opposite helicity

$$H_p = \int_{-\infty}^{\infty} \mathrm{d}x\ \mathcal{H}_p(x) = \int_{-\infty}^{\infty} \mathrm{d}x \sum_{\nu,\sigma} \hat{\psi}^\dagger_{\nu,\sigma}(x)(-iv_F\sigma\nu\partial_x - \mu)\hat{\psi}_{\nu,\sigma}(x), \tag{4.1}$$

where $\hat{\psi}_{\nu,\sigma}(x)$ are annihilating fermionic fields carrying spin-index $\sigma \in \{\uparrow,\downarrow\} = \{+,-\}$ and edge-index $\nu \in \{1,2\} = \{+,-\}$; μ acts as a chemical potential and v_F is the Fermi velocity. Let us assume the constriction to be narrow enough to provide a finite overlap of wave functions from states of different edges. In the presence of TR symmetry, two SP terms emerge [TK09, LBRT11, LPBL16, Dol11, SRvOG12]

$$H_{t_0} = \int_{-\infty}^{\infty} \mathrm{d}x\ \mathcal{H}_{t_0}(x) = \int_{-\infty}^{\infty} \mathrm{d}x\ t_0(x) \sum_{\sigma} \left[\hat{\psi}^\dagger_{1,\sigma}(x)\hat{\psi}_{2,\sigma}(x) + \mathrm{h.c.}\right], \tag{4.2}$$

$$H_{t_c} = \int_{-\infty}^{\infty} \mathrm{d}x\ \mathcal{H}_{t_0}(x) = \int_{-\infty}^{\infty} \mathrm{d}x\ t_c(x) \sum_{\nu} \left[\nu\hat{\psi}^\dagger_{\nu,\uparrow}(x)\hat{\psi}_{-\nu,\downarrow}(x) + \mathrm{h.c.}\right]. \tag{4.3}$$

While Eq. (4.2) describes a hybridization of fermionic states with the same spin associated to different edges and does not require further symmetry breaking with respect to H_p, Eq. (4.3) is only finite if axial spin symmetry is absent and takes the role of an effective SOC across the constriction [WBZ06]. Using $t_0(x) = t_0$ and $t_c(x) = t_c$, the spectrum associated with $H_0 = H_p + H_{t_0} + H_{tc}$ is depicted in Fig. 4.1 (b). Notably, either parameter regime $\epsilon > 0$ and $\epsilon < 0$ shares essential ingredients with the spectrum of a SOC quantum wire. In this sense, QSH QCs, including relevant SP scattering terms, might be interpreted as symmetry enriched SOC quantum wires. As we will see below, the additional symmetries that the system obeys with respect to ordinary quantum wires have important physical consequences not only in the SP picture but, particularly, when interactions are considered. Then, despite the fact that the linear dispersion increases the scope of bosonization, the existence of a Dirac point becomes of fundamental importance for the relevance of bosonic mass terms.

4.3 Topological superconductivity in quantum spin Hall anti-wires

Let us now explore how the above properties of such devices can be used to create and unambiguously detect topologically protected Majorana modes. To invoke topological superconductivity in quantum wires, despite SOC, superconducting order as well as a Zeeman field are required. Since QSH QCs possess very similar spectral properties as compared to SOC quantum wires, we can guess that such a device will similarly acquire a topological phase in the presence of s-wave superconductivity and Zeeman coupling as well.
Adding both contributions to the Hamiltonian, we obtain $H = H_p + H_{t_0} + H_{t_c} + H_{\mathrm{B}} + H_{\Delta}$,

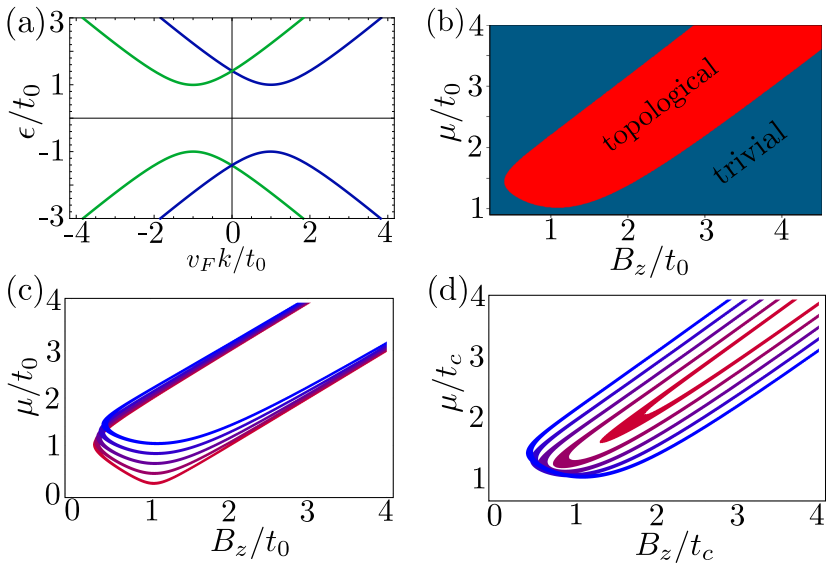

Figure 4.2: (a) Spectrum of H_0. The different colors represent states with orthogonal spin. (b) Phase diagram as function of μ and B_z (under the choice $t_0 = t_c = 1$, $\Delta/t_0 = 0.3$, $v_F = 1$). (c) Dependence of the topological phase on t_c. The different curves correspond to $t_c/t_0 = 0.2, 0.4, 0.6, 0.8, 1.0$ (red to blue), $\Delta = 0.3t_0$, $t_0 = 1$, $v_F = 1$. (d) Dependence of the topological phase on t_0. The curves correspond to $t_0/t_c = 0.2, 0.4, 0.6, 0.8, 1$ (red to blue), $\Delta/t_c = 0.3$, $t_c = 1$, $v_F = 1$.

where

$$H_{\mathrm{B}} = \int_{-\infty}^{\infty} \mathrm{d}x\ \mathcal{H}_B(x) = \int_{-\infty}^{\infty} \mathrm{d}x\ B_z(x) \sum_{\nu,\sigma} \sigma \hat{\psi}^{\dagger}_{\nu,\sigma}(x) \hat{\psi}_{\nu,\sigma}(x), \tag{4.4}$$

$$H_{\Delta} = \int_{-\infty}^{\infty} \mathrm{d}x\ \mathcal{H}_{\Delta}(x) = \int_{-\infty}^{\infty} \mathrm{d}x\ \Delta(x) \sum_{\nu} \left[\hat{\psi}^{\dagger}_{\nu,\uparrow}(x) \hat{\psi}^{\dagger}_{\nu,\downarrow}(x) + \mathrm{h.c.} \right]. \tag{4.5}$$

The gyro-magnetic factor for the edge states is predicted to be $g \sim 10$ [SPAW18] for typical QSH materials so that magnetic fields compatible with the presence of superconductivity are sufficient for our purposes.

Indeed, for the translational invariant case where all coupling constants are x-independent, we find that the corresponding Hamiltonian undergoes a topological phase transition, indicated by a gap-closing and reopening depending on the control parameters μ and B_z (see Fig. 4.2 (b)). The coupling strength t_c that appears in Eq. (4.3) hardly affects the topological parameter regime (see Fig. 4.2 (c)). However, it controls the magnitude of the gaps in the topological regime and therefore the decay length of possible low-energy BSs in the presence of boundaries. By contrast, Eq. (4.2) has less influence on the magnitude of the gaps, but strongly affects the shape of the topological regime (Fig. 4.2 (d)). While a concrete estimation of the magnitude of t_0 is difficult, it is clear that it can be tuned up to the magnitude of the bulk gap, by reducing the width of the constriction [MB07].

There are different possible schemes how a QSH QC with the above properties could be realized in the laboratory. The natural straightforward way would be, of course, to cut

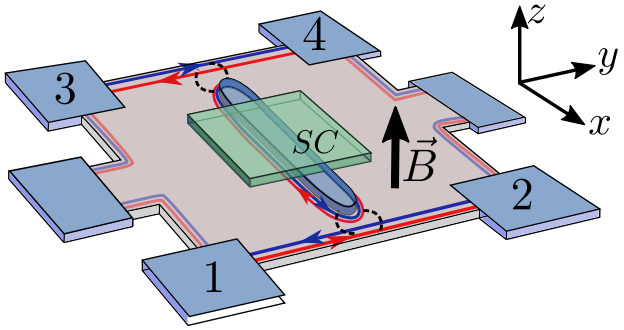

Figure 4.3: Schematic illustration of the system: A QSH anti-wire, covered by a s-wave SC under the influence of a magnetic field weakly coupled to helical edge states at the boundary of the QSH stripe.

out a constriction from a 2D TI stripe as shown in Fig. 4.1 (a). Yet another, maybe more powerful design can be found by carving narrow trenches in an elsewhere homogeneous QSH insulator. Henceforth we call such a structure *anti-wire* (see Fig. 4.3). In that way, natural boundaries would directly be given to the system. Moreover, such a method could have the advantage that, once it is possible to construct a single trench, the positioning of many such trenches is most likely straightforward. Therefore, such systems possess a natural scalability, that is of importance when it comes to quantum computing. Since different anti-wires emerge from the same underlying 2D system, it is possible to tune their coupling strength via external gate voltages applied between two anti-wires. Hence, the link between the two anti-wires might be changed from an insulating (chemical potential inside the bulk gap of the 2D TI) to a conducting (chemical potential inside the conduction band) region, allowing for controllable fusion of the Majoranas at the end of different anti-wires.

4.3.1 Majorana end modes in quantum spin Hall anti-wires

As numerously discussed in this thesis, boundaries take an outstanding role in topological systems. In particular, 1D topologically superconducting systems are characterized by Majorana zero modes, bound at each end of the system. To investigate the presence of topological BSs, boundaries are thus inevitable. Therefore, henceforth we focus on a QSH anti-wire with a finite length L[1]. To model boundaries, it is convenient to consider the additional Hamiltonian density

$$\mathcal{H}_T(x) = T_b\left[\delta(x)+\delta(x-L)\right]\sum_\sigma\left[\hat{\psi}^\dagger_{1,\sigma}(x)\hat{\psi}_{2,\sigma}(x)+\text{h.c.}\right], \tag{4.6}$$

which describes a strong hybridization of states from different sides of the anti-wire at $x = 0$ and $x = L$. Then, in the limit $T_b \to \infty$, the system within $0 < x < L$ becomes completely isolated from the outside world, forming an autonomous anti-wire. Such a decoupling comes along with the formation of boundary conditions for the involved fields.

[1] All coupling constants are assumed to be x-independent for the extend of the anti-wire.

Consider the kinetic part of the Hamiltonian including impurity scattering at $x = 0$ and $x = L$

$$\tilde{H}_p = \int \mathrm{d}x \sum_{\nu,\sigma} \hat{\psi}^\dagger_{\nu,\sigma}(x)(-iv_F\sigma\nu\partial_x)\hat{\psi}_{\nu,\sigma}(x) + T_b \int \mathrm{d}x\,[\delta(x)+\delta(x-L)] \sum_\sigma \left[\hat{\psi}^\dagger_{1,\sigma}(x)\hat{\psi}_{2,\sigma}(x) + \mathrm{h.c.}\right]. \tag{4.7}$$

We can formally diagonalize the Hamiltonian (4.7) with eigenfunctions from the associated SP problem

$$\tilde{h}_p(x)\Psi(x) = \epsilon\Psi(x), \tag{4.8}$$

where $\tilde{h}_p(x) = -iv_F\eta_z\sigma_z\partial_x + T_b[\delta(x)+\delta(x-L)]\,\eta_x\sigma_0$ with Pauli matrices η_j, σ_j ($j \in \{x,y,z\}$) acting on edge-, spin-space, respectively, and the basis $\Psi(x) = (\psi_{1,\uparrow}(x), \psi_{1,\downarrow}(x), \psi_{2,\uparrow}(x), \psi_{2,\downarrow}(x))^T$. In vicinity ε close to the impurities with $\varepsilon \to 0$, Eq. (4.8) is solved by

$$\Psi(-\varepsilon) = e^{T_b\eta_y\sigma_z}\Psi(\varepsilon), \quad \Psi(L+\varepsilon) = e^{-T_b\eta_y\sigma_z}\Psi(L-\varepsilon).$$

In the limit $T_b \to \infty$, this results in the boundary conditions

$$\psi_{1,\sigma}(0) = i\psi_{2,\sigma}(0), \quad \psi_{1,\sigma}(L) = -i\psi_{2,\sigma}(L).$$

They are satisfied by the functions $\psi_{\nu,\sigma,q}(x) = -i\psi_{-\nu,\sigma,q}(-x)$ with $\psi_{\nu,\sigma,q}(x) = (1/\sqrt{L})\exp[iqx]$ and the quantization condition $q = (\pi/L)(n_q - 1/2)$. By applying an expansion of the fermionic fields in terms of the functions $\psi_{\nu,\sigma,q}(x)$, namely $\hat{\psi}_{\nu,\sigma}(x) = \sum_q \psi_{\nu,\sigma,q}(x)\hat{c}_q$, we obtain the boundary conditions for the fields to be

$$\hat{\psi}_{\nu,\sigma}(x) = -i\hat{\psi}_{-\nu,\sigma}(-x). \tag{4.9}$$

Clearly, from the quantization of q, the fields need to be anti-periodic with respect to $2L$

$$\hat{\psi}_{\nu,\sigma}(L) = -\hat{\psi}_{\nu,\sigma}(-L).$$

Now, we can use Eq. (4.9) to specify the Hamiltonian of an anti-wire of length L. Generically, the anti-wire Hamiltonian is given by

$$H_{\mathrm{AW}} = \int_0^L \mathrm{d}x\,[\mathcal{H}_p(x) + \mathcal{H}_{t_0}(x) + \mathcal{H}_{t_c}(x) + \mathcal{H}_B(x) + \mathcal{H}_\Delta(x)]\,.$$

Inserting Eq. (4.9) reduces the number of fermionic fields by a factor of two, but likewise also leads to an unfolded Hamiltonian of double system size, including non-local contributions

$$\begin{aligned} H_{\mathrm{AW}} &= \frac{1}{2}\int_{-L}^{L} \mathrm{d}x\,\hat{\Phi}^\dagger(x)\big[-iv_F\partial_x + \tau_z\sigma_z B_z + \tau_z\sigma_0\mu + \tau_z\sigma_x\ \mathrm{sign}(x)t_c\big]\hat{\Phi}(x) \\ &- \frac{1}{2}\int_{-L}^{L} \mathrm{d}x\,\Phi^\dagger(x)\big[\tau_x\sigma_y\Delta + i\ \mathrm{sign}(x)t_0\big]\hat{\Phi}(-x), \end{aligned} \tag{4.10}$$

where τ_j ($j \in \{x,y,z\}$) are Pauli matrices acting on PH space and[2]

$$\hat{\Phi}(x) = (\hat{\psi}_{1,\uparrow}(x), \hat{\psi}_{2,\downarrow}(x), \hat{\psi}^\dagger_{1,\uparrow}(x), \hat{\psi}^\dagger_{2,\downarrow}(x))^T.$$

Our goal is to determine the eigenfunctions $U_\epsilon(x)$ with energy eigenvalue ϵ of the Hamiltonian density in Eq. (4.10), which at first sight seems to be a cumbersome task since H_{AW} contains non-local contributions. However, we can overcome its non-locality by the ansatz

$$U_\epsilon(x) = u_\epsilon(x)\theta(x) + v_\epsilon(-x)\theta(-x), \tag{4.11}$$

where $u_\epsilon(x)$ and $v_\epsilon(x)$ are spinors in the given basis. From the continuity of the solutions $U_\epsilon(x)$ at $x = 0$ as well as from the anti-periodicity of the system with respect to $2L$, the solution needs to obey the boundary conditions $u_\epsilon(0) = v_\epsilon(0)$ and $u_\epsilon(L) = -v_\epsilon(L)$. The SP problem associated with Eq. (4.10) becomes equivalent to the set of equations for the functions $u_\epsilon(x)$ and $v_\epsilon(x)$

$$\big[-iv_F\partial_x s_z\tau_0\sigma_0 + s_0\tau_z\sigma_z B_z + s_0\tau_z\sigma_0\mu + s_z\tau_z\sigma_x t_c - s_x\tau_x\sigma_y\Delta + s_y\tau_0\sigma_0 t_0\big]\chi_\epsilon(x) = \epsilon\chi_\epsilon(x), \tag{4.12}$$

where we defined the basis function $\chi_\epsilon(x) = (u_\epsilon(x), v_\epsilon(x))^T$ and the Pauli-matrices s_j acting on the space spanned by $u_\epsilon(x)$ and $v_\epsilon(x)$. The general solution of (4.12) can be found by integration

$$\chi_\epsilon(x) \;=\; M_\epsilon(x,x_0)\chi_\epsilon(x_0), \tag{4.13}$$

where

$$\begin{aligned} M_\epsilon(x,x_0) \;&=\; \exp\Big[\int_{x_0}^{x} \mathrm{d}x' \frac{i}{v_F} s_z\tau_0\sigma_0\big(\epsilon - (s_0\tau_z\sigma_z B_z + s_0\tau_z\sigma_0\mu + s_z\tau_z\sigma_x t_c \\ &-\; s_x\tau_x\sigma_y\Delta + s_y\tau_0\sigma_0 t_0)\big)\Big]. \end{aligned}$$

Not every energy ϵ is compatible with the boundary conditions. For the topological phase, however, in the limit $L \to \infty$, there should be a decaying solution for $\epsilon \to 0$ of the form $\Gamma(0) = (\zeta(0), \zeta(0))$ (i. e. fulfilling the BCs at $x = 0$). Thus, in this limit, Eq. (4.13) turns into an eigenvalue problem for $\zeta(0)$ of the form

$$\lim_{L\to\infty} M_0(L,0)\Gamma(0) \stackrel{!}{=} 0. \tag{4.14}$$

If we further demand the solution to be a Majorana, we require
$\zeta(0) = \big(f(0), g(0), f^*(0), g^*(0)\big)^T$. For $\epsilon = 0$, PH symmetry implies

$$\hat{\varrho} M_0(x,x')\hat{\varrho}^{-1} = M_0(x,x')$$

[2] Note that now edge and spin space are somewhat merged in the new basis. For convenience, we associate the Pauli matrices σ_j with $j \in \{x,y,z\}$ to this new space.

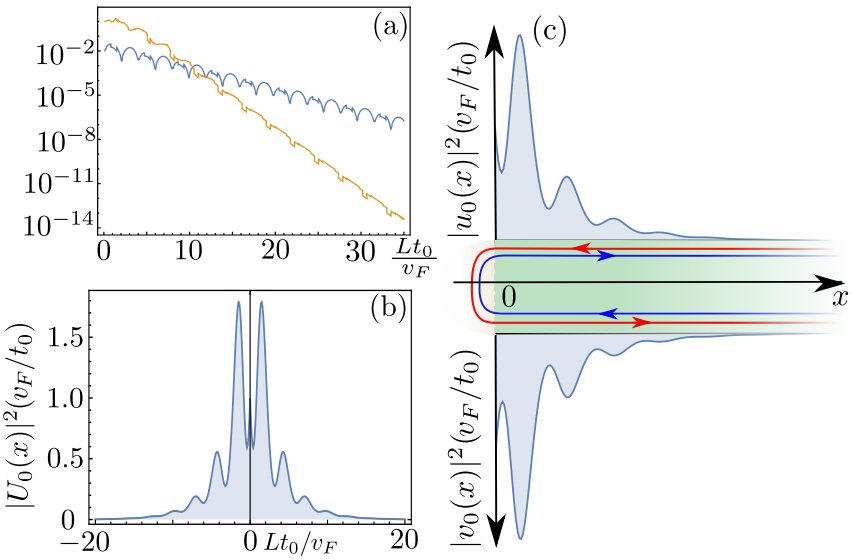

Figure 4.4: (a) λ_M (yellow) and $\delta\Gamma_{\lambda_M}$ (blue) as a function of L. (b) $|U_0(x)|^2$ according to Eq. (4.11) with $U_0(0) = \nu_\lambda$. (c) Schematic illustration of the probability distribution in the (folded) anti-wire. The parameters of the calculation are: $B/t_0 = 0.6$, $\mu/t_0 = \sqrt{2}$, $\Delta/t_0 = 0.3$, $t_c = t_0 = 1$, $v_F = 1$.

with the PH symmetry operator $\hat{\varrho}$. Thus, demanding the Majorana solution for $\zeta(0)$, implies that $\zeta(x)$ obeys Majorana form for any point x.

For finite L, Eq. (4.14) does not hold anymore. However, we expect to find an approximate Majorana solution that tends exponentially towards the true Majorana solution upon increasing L. This means that $M_0(L,0)$ possesses an eigenvalue $\lambda_M \sim \exp(-\alpha L)$ ($\alpha \in \mathbb{R}^+$) whose corresponding eigenvector ν_{λ_M} fulfills the BC at $x = 0$. Its deviation from the Majorana solution should thereby be exponentially suppressed. It can be measured with

$$\delta\Gamma_{\lambda_M} = \frac{1}{2}\|s_0(\mathbb{1} - \tau_x\sigma_0)\mathrm{Re}[\nu_{\lambda_M}] + s_0(\mathbb{1} + \tau_x\sigma_0)\mathrm{Im}[\nu_{\lambda_M}]\|.$$

Indeed, we find that such a solution exists in the topological regime (see Fig. 4.4 (a)). The probability density associated to this wave function is illustrated in Fig.4.4 (b,c).

4.3.2 Conductance properties and unambiguous detection of Majorana zero-modes

Interestingly, the anti-wire setup shown in Fig. 4.3 allows us to perform novel transport experiments that are impossible for quantum wire based systems. When the anti-wire is brought in proximity to other boundaries of the surrounding 2D TI sample, a weak coupling between outer helical edge states and anti-wire develops that allows for spin-resolved transport experiments. The only adjustment to model such an open system is to

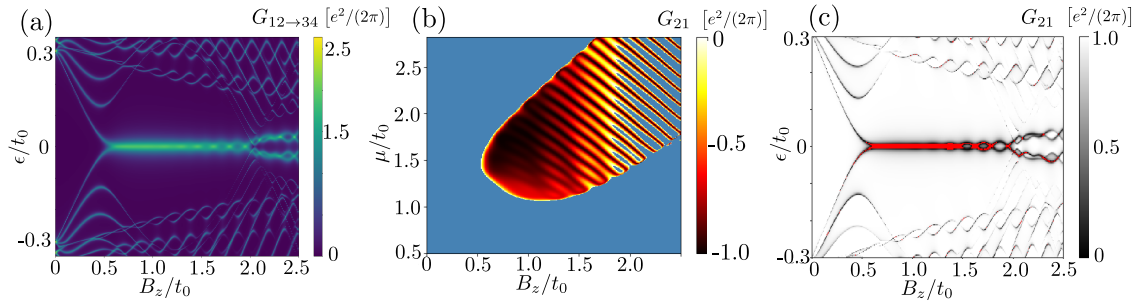

Figure 4.5: (a) Two-terminal conductance as function of energy ϵ and Zeeman field B_z. (b-c) Multi-terminal conductance between contacts 1 and 2 with respect to Fig. 4.3 (a), as a function of μ and B_z (b), ϵ and B_z (c), respectively. In (b), all values $G_{21} > 0$ are colored in blue. In (c), all values $G_{21} < 0$ are colored in red. Other parameters of the plots are: $L = 20 v_F/t_0$, $\Delta/t_0 = 0.3$, $\mu/t_0 = \sqrt{2}$ ((a) and (c)), $\epsilon = 0$ (b), $t_0 = t_c = 1$ $v_F = 1$. For computational reasons, the delta distribution, separating the anti-wire from the leads, is replaced with its step function series $\delta_a(x) = \mathsf{rect}(x/a)/a$ with $a = 0.1$. Moreover, $T_b/t_0 = 1.5$ for (a-b) and $T_b/t_0 = 2$ for (c).

keep the amplitude T_b in Eq. (4.6) finite. Then, the full Hamiltonian reads

$$H_{\text{open}} = \int_{-\infty}^{+\infty} \mathrm{d}x[\mathcal{H}_p(x) + \mathcal{H}_T(x)] + \int_0^L \mathrm{d}x\,[\mathcal{H}_{t_0}(x) + \mathcal{H}_{t_c}(x) + \mathcal{H}_\Delta(x) + \mathcal{H}_B(x)],$$

where the kinetic terms for $x < 0$ and $x > L$ describe the two outer helical edges.

There are two distinct transport regimes that yield potentially interesting physical insight. The first one is the two-terminal conductance, obtained when contacts 1 and 2 of Fig. 4.3 (a), as well as 3 and 4, are each coupled to reservoirs with local chemical potentials μ_{12} and μ_{34}, respectively. For small voltage differences $eV = \mu_{12} - \mu_{34}$, the two-terminal conductance can then be calculated in terms of elements of the corresponding scattering matrix (see Eq. (3.39)). Note, however, that contact 1 and 2, as well as 3 and 4, are treated as the *same* lead. Then, incident particles of such a combined lead, let us call it lead 12, can thus only be transmitted to lead 34 or reflected back into lead 12. In this sense, transmission from contact 1 to contact 2 is ill-defined. This suggests to define reflections and transmission only with respect to the leads 12 and 34 (instead of 1 2 3 and 4). Note that such composed helical edge leads might be interpreted as spinful quantum wire leads. According to the notation of Eq. (3.39), the reflection coefficients carry an extra index, which now characterizes the edge into which incident particles get reflected/transmitted. This eventually results in the conductance

$$G_{12\to34} = \frac{\mathrm{d}I_{12}}{\mathrm{d}V_{12}} = \frac{e^2}{2\pi}\left[2 + \sum_{j\in1,2}\left[|r^{\mathrm{eh}}_{12,12,\,j}|^2 - |r^{\mathrm{ee}}_{12,12,\,j}|^2\right]\right], \tag{4.15}$$

where $r^{\mathrm{e}\nu}_{12,12,\,j}$ are normal ($\nu = \mathrm{e}$) and Andreev reflection amplitudes ($\nu = \mathrm{h}$) in lead 12 and edge j. Note also that, since hole-like particles carry opposite charge with respect to electrons, their contributions to the conductance enter with opposite sign. The elements

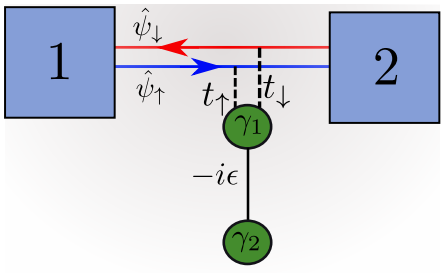

Figure 4.6: Schematic illustration of a Majorana mode side-coupled to a helical edge.

of the scattering matrix are computed numerically by integration of H_{open}. Fig. 4.5 (a) shows the two-terminal conductance as a function of excitation energy ϵ and applied Zeeman field B_z. Whenever an anti-wire BS is on resonance, a peak in the two-terminal conductance emerges. From that, it is also clearly visible where the system enters (leaves) the topological phase, indicated by a forming (resolving) prominent zero energy peak in the two-terminal conductance.

Even though clearly visible, such a signature is not sufficient as a proof for the associated BS to be a Majorana. Instead, a signature exclusively attached to the Majorana is desirable. We show below that such a signature exists in our setup. It is related to the multi-terminal conductance between contacts 1 and 2 of Fig. 4.3 (a). In this scenario, contacts 1 and 2 are treated as independent leads. Then, we restore the notation of Eq. (3.39)

$$G_{21} = \frac{\mathrm{d}I_2}{\mathrm{d}V_1} = \frac{e^2}{2\pi}\left[|t_{21}^{\mathrm{ee}}|^2 - |t_{21}^{\mathrm{eh}}|^2\right], \tag{4.16}$$

where $t_{21}^{\nu\nu'}$ is the transmission amplitude of a ν' particle from lead 1 to a ν particle in lead 2. G_{21} can either take positive or negative values, depending on which scattering process dominates. Below we demonstrate that a negative signal at zero energy can be unambiguously associated with a Majorana BS. Figs. 4.5 (b-c) show that, when the anti-wire is in the topological phase and features Majoranas at its ends, the multi-terminal conductance G_{21} at zero-energy is indeed negative. Moreover, Fig. 4.5 (c) shows that the negative signal (highlighted in red) is prominently seen at zero energy. There are, however, also some scattering events at non-zero energy with the same property, which implies that the negative signal alone is not sufficient as a proof for the presence of a Majorana.

Evidently, the above model is rather complicated to study analytically. However, since we are interested in condensing the transport properties that are related to topological Majorana modes, forming at the ends of the anti-wire, it is convenient to employ a simpler toy model, capturing the essential physics. To this end, we use the model schematically depicted in Fig. 4.6. A single helical edge, described by the Hamiltonian density $\mathcal{H}_p(x)$ of Eq. (4.1) (with $\nu = 1$), is coupled to the Majorana mode, say $\hat{\gamma}_1 = \hat{d} + \hat{d}^\dagger$ with the fermionic creation (annihilation) operators $\hat{d}^\dagger$ ($\hat{d}$), via the tunneling Hamiltonian (at $x = 0$)

$$H_c = \sum_\sigma t_\sigma \left[\hat{\gamma}_1 \hat{\psi}_{1\sigma}(0) + \text{h.c.}\right].$$

The spin-dependent coupling constants t_σ account for the spin-texture of the Majorana mode [PASJ17, CSH+18]. Such a coupling between anti-wire Majorana mode and helical edge is reasonable since TR symmetry is absent in the anti-wire, and no symmetry constraints exist. The second Majorana mode is $\hat{\gamma}_2 = i\hat{d} - i\hat{d}^\dagger$. While $\hat{\gamma}_2$ is not directly coupled to the helical edge, it can (weakly) hybridize with $\hat{\gamma}_1$ via

$$H_d = -i\frac{\epsilon_d}{2}\hat{\gamma}_1\hat{\gamma}_2.$$

The actual setup requires the presence of a Zeeman field. Thus, it is reasonable to include it as well in the nearby helical edges of the toy model. Then, in total, the Hamiltonian of the toy model is given by $H_{\mathrm{TM}} = H_p(\nu = 1) + H_{\mathrm{B}}(\nu = 1) + H_c + H_d$. To determine the transport properties according to Eq. (4.16), we need to compute the scattering matrix of the system. In particular, we are interested in the conducting properties of the helical edge that passes by the anti-wire. Thus, we need to reformulate the scattering problem so that we obtain determining equations for the eigenstates in the helical edge. To this end, let us first rewrite H_{TM} like

$$H_{\mathrm{TM}} = \frac{1}{2}\int \mathrm{d}x\ \tilde{\Psi}^\dagger(x) h_{\mathrm{TM}}(x)\tilde{\Psi}(x) \tag{4.17}$$

with $\tilde{\Psi}(x) = (\hat{\psi}_\uparrow(x), \hat{\psi}_\downarrow(x), \hat{\psi}^\dagger_\uparrow(x), \hat{\psi}^\dagger_\downarrow(x), \hat{d}, \hat{d}^\dagger)^T$ and the replacement

$$h_{\mathrm{TM}}(x) = v_F \begin{pmatrix} -i\partial_x - \frac{\mu}{v_F} + \frac{B_z}{v_F} & 0 & 0 & 0 & t_\uparrow(x) & t_\uparrow(x) \\ 0 & i\partial_x - \frac{\mu}{v_F} - \frac{B_z}{v_F} & 0 & 0 & t_\downarrow(x) & t_\downarrow(x) \\ 0 & 0 & -i\partial_x + \frac{\mu}{v_F} - \frac{B_z}{v_F} & 0 & -t_\uparrow(x) & -t_\uparrow(x) \\ 0 & 0 & 0 & i\partial_x + \frac{\mu}{v_F} + \frac{B_z}{v_F} & -t_\downarrow(x) & -t_\downarrow(x) \\ t_\uparrow(x) & t_\downarrow(x) & -t_\uparrow(x) & -t_\uparrow(x) & \frac{\epsilon_d}{v_F} & 0 \\ t_\uparrow(x) & t_\downarrow(x) & -t_\uparrow(x) & -t_\uparrow(x) & 0 & -\frac{\epsilon_d}{v_F} \end{pmatrix},$$

where $t_\sigma(x) = (t_\sigma/v_F)\delta(x)$. To diagonalize Eq. (4.17), we expand $\tilde{\Psi}(x)$ in eigenfunctions of the Hamiltonian density

$$\tilde{\Psi}(x) = \sum_{k,d} U_{k,d}(x)\hat{\chi}_{k,d} \tag{4.18}$$

with matrices $U_{k,d}(x)$ and fermionic annihilation operators $\hat{\chi}_{k,d} = (\hat{C}_k, \hat{C}_d)^T$ with $\hat{C}_k = (\hat{c}_{\uparrow,k}, \hat{c}_{\downarrow,k}, \hat{c}^\dagger_{\uparrow,k}, \hat{c}^\dagger_{\downarrow,k})$ and $\hat{C}_d = (\hat{c}_d, \hat{c}^\dagger_d)$. Inserting Eq. (4.18) in Eq. (4.17), this yields

$$H_{\mathrm{TM}} = \frac{1}{2}\sum_{k,k',d,d'} \hat{\chi}_{k',d'} \int \mathrm{d}x\ U^\dagger_{k',d'}\Xi(x)\ U_{k,d}(x)\hat{\chi}_{k,d},$$

where we defined

$$\Xi(x) = \begin{pmatrix} h_p^B(x) & \eta\delta(x) \\ \eta^\dagger\delta(x) & \epsilon_d\sigma_z \end{pmatrix}$$

with

$$h_p^B(x) = -iv_F\partial_x\tau_0\sigma_z - \mu\tau_z\sigma_0 + B_z\tau_z\sigma_z$$

and

$$\eta = \begin{pmatrix} t_\uparrow & t_\downarrow & -t_\uparrow & -t_\uparrow \\ t_\uparrow & t_\downarrow & -t_\uparrow & -t_\uparrow \end{pmatrix}^T.$$

When the columns of $U_{k,d}(x)$ are formed by orthogonal eigenfunctions of $\Xi(x)$, the problem becomes diagonal. Hence, we need to search for functions $(\Phi_k(x), \Phi_d)$, such that

$$\begin{pmatrix} h_p^B(x)\Phi_k(x) + \eta\delta(x)\Phi_d \\ \eta^\dagger\Phi_k(0) + \epsilon_d\sigma_z\Phi_d \end{pmatrix} = \epsilon \begin{pmatrix} \Phi_k(x) \\ \Phi_d \end{pmatrix}, \tag{4.19}$$

where in the second row, we performed the integration of Eq. (4.17) right away as it contains no differential forms. From Eq. (4.19), we obtain an equation for the solutions $\Phi_k(x)$ by solving the second row for Φ_d and inserting the result in the first one

$$h_p^B(x)\Phi_k(x) + \delta(x)\eta \begin{pmatrix} \frac{1}{\epsilon-\epsilon_d} & 0 \\ 0 & \frac{1}{\epsilon+\epsilon_d} \end{pmatrix} \eta^\dagger\Phi_k(0) = \epsilon\Phi_k(x). \tag{4.20}$$

This equation might be solved in the following way [PKA16]. When $x \neq 0$ the equation reduces to $h_p^B(x)\Phi_k(x) = \epsilon\Phi_k(x)$ which is solved by plane waves. Moreover, the δ-distribution implies a discontinuous jump of the solutions at $x = 0$. Hence, for $x > 0$, $x < 0$ and $x = 0$, the solution takes different values. This can be incorporated by the ansatz

$$\Phi_k(x) = (\Phi_k^e(x), \Phi_k^h(x)) \tag{4.21}$$

with

$$\Phi_k^e(x) = \begin{pmatrix} (\bar{\phi}_\uparrow^e + \mathrm{sign}(x)\delta\phi_\uparrow^e)e^{i(k+B_z-\mu)x} \\ (\bar{\phi}_\downarrow^e + \mathrm{sign}(x)\delta\phi_\downarrow^e)e^{-i(k+B_z+\mu)x} \end{pmatrix}, \Phi_k^h(x) = \begin{pmatrix} (\bar{\phi}_\uparrow^h + \mathrm{sign}(x)\delta\phi_\uparrow^h)e^{i(k-B_z+\mu)x} \\ (\bar{\phi}_\downarrow^h + \mathrm{sign}(x)\delta\phi_\downarrow^h)e^{-i(k-B_z-\mu)x}, \end{pmatrix} \tag{4.22}$$

where

$$\bar{\phi}_{\uparrow/\downarrow}^{e/h} = (\phi_{\uparrow/\downarrow,2}^{e/h} + \phi_{\uparrow/\downarrow,1}^{e/h})/2, \tag{4.23}$$

$$\delta\phi_{\uparrow/\downarrow}^{e/h} = (\phi_{\uparrow/\downarrow,2}^{e/h} - \phi_{\uparrow/\downarrow,1}^{e/h})/2. \tag{4.24}$$

Thereby, the indices 1 and 2 refer to the lead to which the corresponding scattering state amplitudes are adiabatically connected to. Integration of Eq. (4.20) using Eqs. (4.21-

4.24), from $x = 0^-$ to $x = 0^+$, this results in

$$-iv_F \begin{pmatrix} \sigma_z & 0 \\ 0 & \sigma_z \end{pmatrix} \begin{pmatrix} \phi^e_{\uparrow,2} - \phi^e_{\uparrow,1} \\ \phi^e_{\downarrow,2} - \phi^e_{\downarrow,1} \\ \phi^h_{\uparrow,2} - \phi^h_{\uparrow,1} \\ \phi^h_{\downarrow,2} - \phi^h_{\downarrow,1} \end{pmatrix} + \frac{1}{2}\eta \begin{pmatrix} \frac{1}{\epsilon-\epsilon_d} & 0 \\ 0 & \frac{1}{\epsilon+\epsilon_d} \end{pmatrix} \eta^\dagger \begin{pmatrix} \phi^e_{\uparrow,2} + \phi^e_{\uparrow,1} \\ \phi^e_{\downarrow,2} + \phi^e_{\downarrow,1} \\ \phi^h_{\uparrow,2} + \phi^h_{\uparrow,1} \\ \phi^h_{\downarrow,2} + \phi^h_{\downarrow,1} \end{pmatrix} = 0. \tag{4.25}$$

Eq. (4.25) can now be reorganized such that we obtain the scattering matrix.

$$\begin{pmatrix} \phi^e_{\downarrow,1} \\ \phi^h_{\downarrow,1} \\ \phi^e_{\uparrow,2} \\ \phi^h_{\uparrow,2} \end{pmatrix} = S \begin{pmatrix} \phi^e_{\uparrow,1} \\ \phi^h_{\uparrow,1} \\ \phi^e_{\downarrow,2} \\ \phi^h_{\downarrow,2} \end{pmatrix}$$

with

$$S = \begin{pmatrix} R_{11} & T_{12} \\ T_{21} & R_{22} \end{pmatrix}$$

and

$$R_{\nu\nu'} = \begin{pmatrix} r^{ee}_{\nu\nu'} & r^{he}_{\nu\nu'} \\ r^{eh}_{\nu\nu'} & r^{hh}_{\nu\nu'} \end{pmatrix}, \quad T_{\nu\nu'} = \begin{pmatrix} r^{ee}_{\nu\nu'} & r^{he}_{\nu\nu'} \\ r^{eh}_{\nu\nu'} & r^{hh}_{\nu\nu'} \end{pmatrix}.$$

The scattering amplitudes are given by

$$r^{ee}_{\nu\nu} = r^{hh}_{\nu\nu} = -r^{eh}_{\nu\nu} = -r^{he}_{\nu\nu} = \frac{t_\uparrow t_\downarrow \epsilon}{\epsilon(t_\uparrow^2 + t_\downarrow^2 - iv_F\epsilon) + iv_F\epsilon_d^2},$$

$$t^{ee}_{21} = t^{hh}_{21} = \frac{t_\uparrow^2 \epsilon}{\epsilon(t_\uparrow^2 + t_\downarrow^2 - iv_F\epsilon) + iv_F\epsilon_d^2} - 1, \qquad t^{eh}_{21} = t^{he}_{21} = \frac{-t_\uparrow^2 \epsilon}{\epsilon(t_\uparrow^2 + t_\downarrow^2 - iv_F\epsilon) + iv_F\epsilon_d^2}, \tag{4.26}$$

$$t^{ee}_{12} = t^{hh}_{12} = \frac{t_\downarrow^2 \epsilon}{\epsilon(t_\uparrow^2 + t_\downarrow^2 - iv_F\epsilon) + iv_F\epsilon_d^2} - 1, \qquad t^{eh}_{12} = t^{he}_{12} = \frac{-t_\downarrow^2 \epsilon}{\epsilon(t_\uparrow^2 + t_\downarrow^2 - iv_F\epsilon) + iv_F\epsilon_d^2}, \tag{4.27}$$

where ϵ is the energy at which the scattering process takes place.

For ϵ being sufficiently close to $\pm\epsilon_d$, we find that $t_\uparrow > t_\downarrow$ implies $G_{21} < 0$ (compare to Eq. (4.16) and (4.26)). This property essentially emerges as a consequence of spin-momentum-locking at the helical edge. Notably, $G_{21} < 0$ implies $G_{12} > 0$ (which is related to the elements (4.27)) and, likewise, for the opposite scenario with $t_\uparrow < t_\downarrow$, we obtain $G_{21} > 0$ but $G_{12} < 0$. We can test the validity of our simple toy model against this property by numerically computing the conductance G_{21} and G_{12} in the full model. The result is shown in Fig. 4.7. While for G_{21} there is a dominant negative signal around $\epsilon = 0$, for G_{12} no such signal is obtained, but instead $G_{21} > 0$. This confirms the validity of the employed toy model for low energies.

Remarkably, note that the scattering matrix elements and, as a consequence, also the conductances are independent of the values of μ and B_z as both parameters do not open

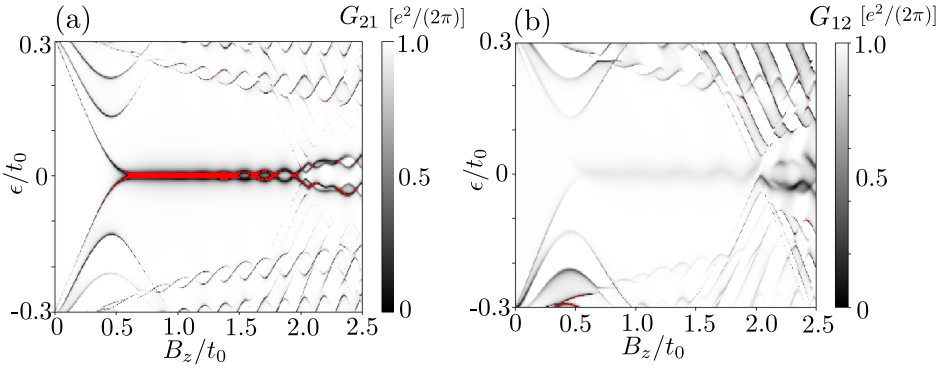

Figure 4.7: Non-local conductance's G_{21} (a) and G_{12} (b) as a function of energy ϵ. The parameters are the same as given in Fig. 4.5 (c). All negative values are colored in red.

spectral gaps within the helical edge states passing by the anti-wire. In the presence of B_z, the symmetry protection against impurity scattering is lost as the Zeeman term breaks TR symmetry. This, however, does not influence the universality of our result as impurity scattering should affect electronic states in the same way as hole-like states. Hence, even though the transmission amplitudes might be reduced due to impurity scattering, the ratio $|t^{ee}_{\nu\nu}|/|t^{eh}_{\nu\nu}|$ is expected to be (on average) constant. Hence, also the non-local conductance G_{21} (G_{12}) is not expected to loose its qualitative information (based on its sign) in the presence of impurity scattering. Moreover, long mean free path have been reported in the new generation of QSH systems [BSH+18]. This implies a low level of impurity scattering. Thus, in conclusion, as long as we couple to a single Majorana (at any energy), where the coupling constant has a spin texture which is not polarized perpendicular to the spin quantization axis [3], either G_{21} or G_{12} has to be negative.

Now, we want to extract the particularity of a Majorana *zero-mode*. To do so, let us first extend the simple toy model for higher energies by replacing the hybridization Hamiltonian H_d by the Hamiltonian of a spin-less p-wave SC (Eq. (2.24)). We assume the tunneling to happen only on the first site. Then, the corresponding tunneling Hamiltonian can be written as

$$H_c = \int \mathrm{d}x \sum_{\sigma=\uparrow,\downarrow} \left[t_\sigma \delta(x) \hat{\psi}^\dagger_\sigma(x) \hat{c}_1 + \mathrm{h.c.} \right].$$

For the combined system, $H_{\mathrm{TM}} = H_p(\nu = 1) + H_{\mathrm{B}}(\nu = 1) + H_c + H_K$, we can numerically compute the scattering matrix along the lines of the above derivation. The corresponding conductance results for G_{21} are shown in Fig. 4.8 (a). Again, for the topological regime of the Kitaev chain, $|\mu| < 2t_K$, where we expect to find topological Majorana modes bound to the ends of the chain, a prominent negative signal is obtained in the non-local conductance G_{21}. However, even higher energy states (in particular close to $\mu = 0$) can also return negative conductance G_{21}. Let us try to understand this result on the level of the toy model Hamiltonian. For the present case, the full Hamiltonian might be written

[3] In the anti-wire, with both Zeeman field and spin-flip scattering, spin-directions are not preserved. Hence, it is not possible to have a Majorana spin-texture perpendicular to the z-axis.

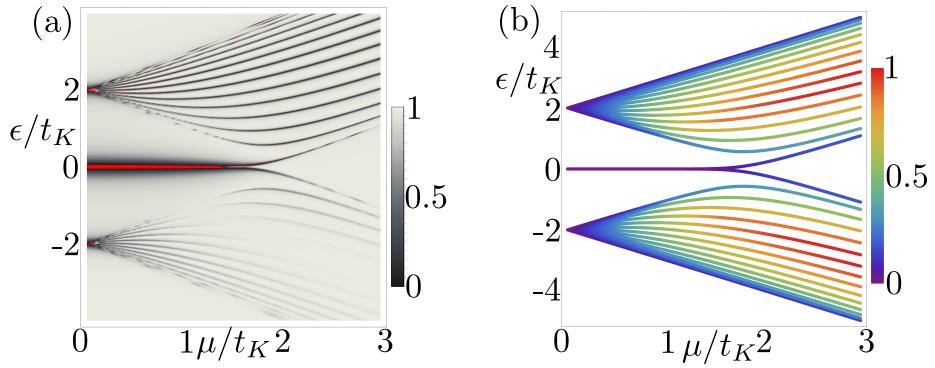

Figure 4.8: (a) Non-local conductance G_{21} in units of $e^2/(2\pi)$ for a helical edge, side-coupled to a Kitaev chain a function of the chemical potential μ in the chain and energy ϵ. Negative values are colored red. (b) Eigenstates of the Kitaev chain as a function of the system parameters μ and ϵ. The color code represents the absolute difference of electronic ($\zeta^{(e)}_{\alpha,1}$) and hole-like wave function ($\zeta^{(h)}_{\alpha,1}$) at the first site of the chain normalized to the maximum value reached for all eigenstates indexed by α. Further parameters of the plots are: $t_K = \Delta = 0.5$, the number of sites is $N = 15$.

in the form

$$H^{\mathrm{K}}_{\mathrm{TM}} = \frac{1}{2}\int \mathrm{d}x\ \tilde{\Psi}^\dagger(x) \begin{pmatrix} h_p^B(x) & \Gamma(x) \\ \Gamma^\dagger(x) & h_K \end{pmatrix} \tilde{\Psi}(x) \tag{4.28}$$

with the Hamiltonian density of the Kitaev chain h_K[4] and the basis

$$\tilde{\Psi}(x) = (\hat{\psi}_\uparrow(x), \hat{\psi}_\downarrow(x), \hat{\psi}^\dagger_\uparrow(x), \hat{\psi}^\dagger_\downarrow(x),\ \hat{c}_1, \hat{c}^\dagger_1, \ldots, \hat{c}_N, \hat{c}^\dagger_N).$$

Moreover, $\Gamma(x)$ is the Hamiltonian density of the coupling Hamiltonian H_c, which can be written as

$$H_c = \frac{1}{2}\int \mathrm{d}x\ (\hat{\psi}^\dagger_\uparrow(x), \hat{\psi}^\dagger_\downarrow(x), \hat{\psi}_\uparrow(x), \hat{\psi}_\downarrow(x))\Gamma(x) \begin{pmatrix} \hat{c}_1 \\ \hat{c}^\dagger_1 \\ \vdots \\ \hat{c}^\dagger_N \end{pmatrix}$$

with

$$\Gamma(x) = \delta(x) \begin{pmatrix} t_\uparrow & 0 & 0 & \ldots & \ldots & 0 \\ t_\downarrow & 0 & 0 & \ddots & & 0 \\ 0 & -t_\uparrow & 0 & & \ddots & 0 \\ 0 & -t_\downarrow & 0 & \ldots & \ldots & 0 \end{pmatrix}.$$

[4] With Hamiltonian density of the Kitaev chain we just mean the matrix elements of Eq. (2.24) in the given basis divided by the system size

We can now apply an unitary transformation to Eq. (4.28) that diagonalizes h_K

$$F = \begin{pmatrix} \mathbb{1} & 0 \\ 0 & U_K \end{pmatrix}.$$

Then, Eq. (4.28) becomes

$$H_{\mathrm{TM}}^{\mathrm{K}} = \frac{1}{2}\int \mathrm{d}x\ \tilde{\Psi}^\dagger(x) F \begin{pmatrix} h_p^B(x) & \Gamma(x)U_K \\ U_K^\dagger \Gamma^\dagger(x) & U_K^\dagger h_K U_K \end{pmatrix} F^\dagger \tilde{\Psi}(x).$$

Since U_K diagonalizes h_K, it is formed from the eigenstates of h_K

$$U_K = (\zeta_1, \zeta_2, \ldots \zeta_{2N}),$$

where $\zeta_\alpha = (\zeta_{\alpha,1}^{(e)}, \zeta_{\alpha,1}^{(h)}, ..., \zeta_{\alpha,N}^{(e)}, \zeta_{\alpha,N}^{(h)})^T$ (with the number of sites N) are column vectors with the property $h_K\zeta_\alpha = \epsilon_\alpha\zeta_\alpha$. Thus, the transformed coupling Hamiltonian contains the elements of the eigenfunctions at the first site. Consequently, in a low energy approximation around an eigenenergy ϵ_α of h_K, the coupling only happens to the first site of the corresponding eigenstate ζ_α. If we want to preserve PH symmetry, it also has to connect to its PH partner at $-\epsilon_\alpha$, $\hat{\varrho}\zeta_\alpha$ with the PH operator $\hat{\varrho} = \mathbb{1} \otimes \sigma_x \hat{K}$, where $\hat{K}$ denotes complex conjugation. Then, the effective Hamiltonian reads

$$H_\alpha = \frac{1}{2}\int \mathrm{d}x\ \tilde{\Psi}_\alpha^\dagger(x) \begin{pmatrix} h_p^B(x) & \Gamma_\alpha(x) \\ \Gamma_\alpha(x) & \epsilon_\alpha\sigma_z \end{pmatrix} \tilde{\Psi}_\alpha(x) \tag{4.29}$$

with the basis $\tilde{\Psi}_\alpha = (\hat{\psi}_\uparrow(x), \hat{\psi}_\downarrow(x), \hat{\psi}_\uparrow^\dagger(x), \hat{\psi}_\downarrow^\dagger(x), \hat{d}_\alpha, \hat{d}_\alpha^\dagger)$ where $\hat{d}_\alpha^\dagger$ creates a fermion in the Kitaev chain at energy ϵ_α. The coupling matrix $\Gamma_\alpha(x)$ is given by

$$\Gamma_\alpha(x) = \delta(x) \begin{pmatrix} t_\uparrow\zeta_{\alpha,1}^{(e)} & t_\downarrow\zeta_{\alpha,1}^{(e)} & -t_\uparrow\zeta_{\alpha,1}^{(h)} & -t_\downarrow\zeta_{\alpha,1}^{(h)} \\ t_\uparrow\zeta_{\alpha,1}^{(h)*} & t_\downarrow\zeta_{\alpha,1}^{(h)*} & -t_\uparrow\zeta_{\alpha,1}^{(e)*} & -t_\downarrow\zeta_{\alpha,1}^{(e)*} \end{pmatrix}^T.$$

This effectively corresponds to the coupling to a particle $\chi = \zeta_{\alpha,1}^{(e)*} d_\alpha^\dagger + \zeta_{\alpha,1}^{(h)} \hat{d}_\alpha$. In particular, for $\zeta_{\alpha,1}^{(e)} \equiv \zeta_{\alpha,1}^{(h)} = 1$, it corresponds to the side-coupled Majorana toy model.

Now, we solve the scattering problem defined by the effective Hamiltonian of Eq. (4.29) and use the result to compute the conductance G_{21}. The results are depicted in Fig. 4.9 (a-c) as a function of $\zeta_{\alpha,1}^{(e)}$ and $\zeta_{\alpha,1}^{(h)}$, which we parametrize by $\zeta_{\alpha,1}^{(e)} = (1/N)\cos(\xi)$ and $\zeta_{\alpha,1}^{(h)} = (1/N)\sin(\xi)$ (we omit a complex phase since the result is completely independent of it). Since $\zeta_{\alpha,1}^{(e/h)}$ only represent the eigenfunction at the first site of the Kitaev chain, N can differ from 1. In particular, for spatially spread eigenfunctions N is a large number. For this case, N effectively renormalizes the coupling constants $t_\uparrow$ and $t_\downarrow$.

A negative conductance G_{21} (on resonance i.e. $\epsilon = \epsilon_\alpha$) is reached when $\delta\zeta = ||\zeta_{\alpha,1}^{(e)}| - |\zeta_{\alpha,1}^{(h)}|| < \kappa$. This explains why there are scattering events away from zero-energy (where the corresponding wave function is not expected to be particularly close to the Majorana

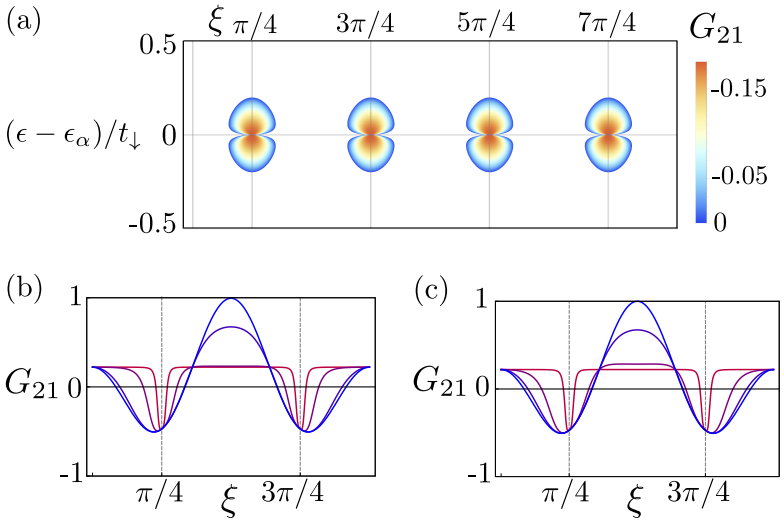

Figure 4.9: (a) Conductance G_{21} around the energy $\epsilon_\alpha = 0$ as a function of $\zeta^{(e)}_{\alpha,1} = 1/N\cos(\xi)$ and $\zeta^{(h)}_{\alpha,1} = 1/N\sin(\xi)$ ($N = 1$). $t_\uparrow = 1.2t_\downarrow$ with $t_\downarrow = 0.2$. (b-c) Non-local conductance G_{21} for the coupling to a generic eigenstate of a PH symmetric system $\chi = \zeta^{(e)}_{\alpha,1}\hat{d}_\alpha + \zeta^{(h)*}_{\alpha,1}\hat{d}^\dagger_\alpha$ on resonance $\epsilon = \epsilon_\alpha$. In (b) $N = 1$, while $\epsilon_\alpha/t_\uparrow = 2,\ 0.2,\ 0.02$, and 0.002 (blue to red). In (c) $\epsilon_\alpha/t_\uparrow = 0.002$, while $N = 100,\ 10,\ 5,\ 1$ (blue to red). Further parameters are $t_\downarrow = (3/5)t_\uparrow$ with $t_\uparrow = 0.5$.

form) that yield a negative non-local conductance value (compare to Figs. 4.5 (b-c) and 4.8 (a)). From the numerical side, we can confirm our above analysis by computing κ for each eigenstate of the Kitaev chain and compare it against the obtained conductance G_{21}. The results are depicted in Fig. 4.8 (a) and (b). Whenever the eigenstates of the Kiteav chain are sufficiently close to the Majorana form (at the first site), G_{21} returns a negative signal. For $\mu = 0$, all the eigenstates satisfy the Majorana condition and so $G_{21} < 0$ throughout the spectrum. Increasing μ leads to a finite κ for most of the states and consequently the negative signal is lost. The topological Majorana modes at zero-energy preserve their Majorana form until eventually $\mu/t_K \to 2$. Throughout this regime, a prominent negative signal is produced by G_{21}.

Away from zero-energy (for $\mu \neq 0$), the threshold κ (to see negative G_{21}) is in general not particularly small and not directly related to the magnitude of the coupling constants $t_\uparrow$ and $t_\downarrow$ (see Fig. 4.9 (b)).

An exclusion to that ambiguity is the behavior close to $\epsilon_\alpha = 0$. There, the parameter regime in which we find negative conductance (with fixed N, $t_\uparrow$, and $t_\downarrow$) becomes sharply centered around the Majorana case so that $\kappa \to 0$ (see Fig. 4.9). This, in turn, implies that a mid-gap state ($\epsilon_\alpha \to 0$) that produces a negative G_{21} has to be a Majorana excitation, i.e. it has to be *self-adjoint*. At zero energy, the negative signal is thus an unambiguous signature of an isolated Majorana mode. Effectively, this important result rests on two fundamental assumptions: (i) the helical nature of the QSH edge leads, and (ii) the fact that the topological Majorana modes couple differently to spin-up and spin-down states. This is reasonable since the spin perpendicular to the spin quantization axis of the leads cannot be a good quantum number in the presence of both, Zeeman field and SP scattering

terms in the QSH QC.
Of course, the effects that complicate the story in the quantum wire case, such as spatially varying potentials, can also affect the spectral properties in the anti-wire system. However, in our system we are equipped with a tool to discriminate among (topological) Majorana modes and trivial Andreev BSs by means of a simple conductance experiment.
Moreover, this conductance regime (G_{21}) cannot only serve as an indicator of the Majorana, rather it even contains profound physical information regarding the superconducting pairing. In particular, $G_{21} < 0$ implies that there is a transport channel in which incoming electrons are transmitted as holes. In combination with spin-momentum locking at the helical edge, this then implies the creation of an *equal spin* Cooper pair in the superconducting condensate. As we will subsequently derive, a symmetry analysis shows that such Cooper pairs typically have (partially) an *odd-frequency* character.

4.4 Formation and detection of odd-frequency superconductivity

As discussed in Sec. 2.5, there is deep physical connection between non-Abelian anyons and unconventional superconductivity. However, the relation is unilateral. The presence of unconventional superconductivity is a necessary yet not sufficient condition for the presence of Majorana modes. In that sense, proving the existence of unconventional superconductivity in a physical system does not imply the presence of Majorana modes, however, it may qualify this system as a potential platform for the latter. Since we know already that QSH QCs are a suitable platform for topological superconductivity, we also expect to find unconventional superconductivity. However, the interesting question, that is yet to be answered, is whether one can directly detect the presence of unconventional superconductivity in those system, regardless of the presence or absence of Majorana modes.
In what follows, we address this question systematically and demonstrate that a direct detection of unconventional superconductivity is indeed accessible for QSH QCs. Thereby, we closely follow the derivations and results presented in Ref. [FZT18]. In particular, we will explicitly compute the pairing amplitudes for the different superconducting symmetry classes and show that specific multi-terminal conductance experiments can prove the presence of odd-frequency superconductivity, generated by the QSH QC in combination with ordinary proximity induced s-wave superconductivity. To this end, we apply the formalism discussed in Sec. 3.2.2. This enables us to efficiently compute all fermionic two-point correlation functions.
More specifically, we find that the QSH QC, including all TR invariant SP scattering terms, generates unconventional (odd-frequency) non-local equal spin-triplet pairing across the hetero-junction. The equal spin nature of this pairing term, in turn, implies CAR amplitudes, i. e. the transmission of an incoming electron as a hole. While it is not uncommon to obtain CAR processes in hetero-junctions [MBB06], in QSH based systems, they are typically related to TR symmetry breaking terms [CBT15]. Moreover, the experimental verification of CAR scattering processes, via multi-terminal conductances, can be challenging. This happens as CAR processes compete with EC processes that typically dominate over CAR [MBB06]. In this scenario, since EC contributes with an opposite sign to the

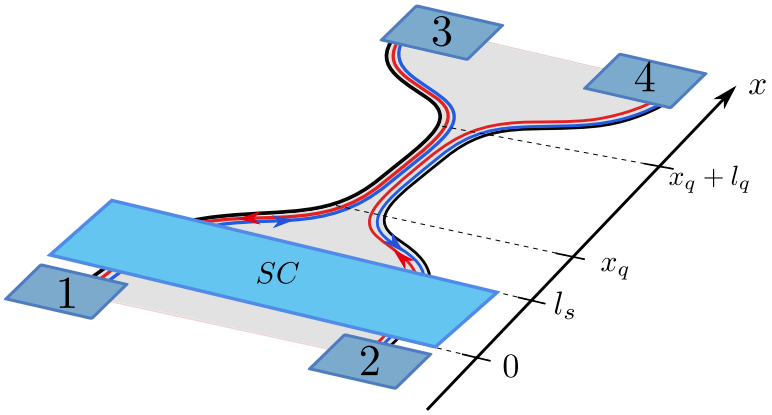

Figure 4.10: Schematic of a QSH QC in proximity to a s-wave SC.

multi-terminal conductance, the latter cannot be used to indicate the presence of CAR. Interestingly, this is not the case for QSH QCs. Instead, CAR dominates over EC for a large regime in parameters space. This ultimately facilitates the proof of the presence of unconventional superconductivity by means of simple conductance experiments.

4.4.1 Scattering state Green function for quantum spin Hall quantum constrictions

The system we investigate is a slightly modified version of the anti-wire setup: a QC, described by Eqs. (4.1-4.3) in proximity to an ordinary s-wave SC (see Fig. 4.10). The SP scattering terms are modeled as step functions, extending over the length l_q. Likewise, the SC is placed outside the constricted region over the length l_s. For the scheme shown in Fig. 4.10, we have $\Delta(x) = \Delta\theta(x)\theta(l_s - x)$, $t_0(x) = t_0\theta(x - x_q)\theta(x_q + l_q - x)$ and $t_c(x) = t_c\theta(x - x_q)\theta(x_q + l_q - x)$ with $\theta(x)$ the Heaviside function. For the subsequent discussion, it is convenient to formulate the (SP) Hamiltonian in compact form

$$\begin{aligned}\mathcal{H}(x) &= -iv_F\partial_x\eta_z\tau_z\sigma_z - \mu(x)\eta_0\tau_z\sigma_0 + \Delta(x)\eta_0\tau_x\sigma_0 \\ &+ t_0(x)\eta_x\tau_z\sigma_0 + t_c(x)\eta_y\tau_z\sigma_y,\end{aligned} \tag{4.30}$$

where we use the basis $\hat{\Phi}(x) = \left(\hat{\Psi}_1(x), \hat{\Psi}_2(x)\right)^T$ with

$$\hat{\Psi}_\lambda(x) = (\hat{\psi}_{\lambda,\uparrow}(x), \hat{\psi}_{\lambda,\downarrow}(x), \hat{\psi}^\dagger_{\lambda,\downarrow}(x), -\hat{\psi}^\dagger_{\lambda,\uparrow}(x))^T. \tag{4.31}$$

Note that, for reasons that will become clear throughout the next sections, by Eq. (4.31) we use a different basis as compared to former sections. The Pauli matrices η_i, τ_i and σ_i with $i \in \{x, y, z\}$ act on edge, PH and spin space.

Our goal is to determine the symmetries of the superconducting pairing amplitudes. For that, we ultimately need to compute the anomalous propagator. From Sec. 3.2.2, we know that this can be done in a convenient way upon solving the SP scattering problem defined

by the first order differential Schrödinger equation $\mathcal{H}(x)\Phi(x) = \omega\Phi(x)$. From

$$\partial_x\Phi(x) \quad = \quad \frac{i}{v_F}[h(x) + \eta_z\tau_z\sigma_z\omega]\Phi(x)$$

with

$$h(x) = \eta_z\tau_z\sigma_z[\mu(x)\eta_0\tau_z\sigma_0 - \Delta(x)\eta_0\tau_x\sigma_0 - t_0(x)\eta_x\tau_z\sigma_0 - t_c(x)\eta_y\tau_z\sigma_y],$$

we find the general solution

$$\Phi(x) = \mathcal{S}_{\leftarrow}U(x, x_0)\Phi_0(x_0), \tag{4.32}$$

where

$$U(x, x_0) = \exp\left[\frac{i}{v_F}\int_{x_0}^{x} \mathrm{d}x\,(h(x) + \eta_z\tau_z\sigma_z\omega)\right]. \tag{4.33}$$

In Eq. (4.32), $\hat{S}_{\leftarrow}$ is a spatial-ordering operator. As we only apply piecewise constant potentials, we can neglect $\hat{S}_{\leftarrow}$ whenever the integration runs within a homogeneous section. The continuity of the wave functions at each interface allows us to rewrite the scattering problem, defined by the Hamiltonian (4.30), in terms of transfer matrices

$$\Phi_{\text{right},k}(x_q + l_q) = U_t(x_q + l_q, x_q)U_0(x_q, l_s)U_{SC}(l_s, 0)\Phi_{\text{left},k}(0), \tag{4.34}$$

where the transfer matrices $U_t(x_t, x_t')$, $U_0(x_0, x_0')$ and $U_{SC}(x_{SC}, x_{SC}')$ are defined according to Eq. (4.33) in the bounds $\{x_t, x_t'\} \in [x_q, x_q + l_q]$, $\{x_0, x_0'\} \in [l_s, x_q]$, and $\{x_{sc}, x_{sc}'\} \in [0, l_s]$ (see also Fig. 4.10). The form of the vectors $\Phi_{\text{left},k}(x)$ and $\Phi_{\text{right},k}(x)$ are fixed by spin momentum locking, together with the basis of Eq. (4.31)[5]. However, we still need to select a channel for an incident particle, whose amplitude we fix to unity [ADH+11]. In that way, we obtain eight linearly independent scattering states denoted by the index $k \in [1, ..., 8]$. They are classified according to the incoming amplitude: incoming electron/hole from the right/left from lead $1, 2, 3, 4$. An incoming particle $\chi \in \{e, h\}$ from lead λ can be reflected as an electron with amplitude $r^{\chi e}_{\lambda'\lambda}(\omega)$ or as a hole with amplitude $r^{\chi h}_{\lambda'\lambda}(\omega)$ into edge λ'. Likewise, transmission is possible with an amplitude $t^{\chi e}_{\lambda'\lambda}(\omega)$ and $t^{\chi h}_{\lambda'\lambda}(\omega)$. One half of the scattering states, $\Phi_{\text{left},1-4}(x)$, represent a particle incident from the left. At $x = 0$ we have

$$\begin{aligned}
\Phi_{\text{left},1}(0) &= \left(1, r^{ee}_{11}(\omega), r^{eh}_{11}(\omega), 0, t^{ee}_{21}(\omega), 0, 0, t^{eh}_{21}(\omega)\right)^T, \\
\Phi_{\text{left},2}(0) &= \left(0, r^{he}_{11}(\omega), r^{hh}_{11}(\omega), 1, t^{he}_{21}(\omega), 0, 0, t^{hh}_{21}(\omega)\right)^T, \\
\Phi_{\text{left},3}(0) &= \left(0, t^{ee}_{12}(\omega), t^{eh}_{12}(\omega), 0, r^{ee}_{22}(\omega), 1, 0, r^{eh}_{22}(\omega)\right)^T, \\
\Phi_{\text{left},4}(0) &= \left(0, t^{he}_{12}(\omega), t^{hh}_{12}(\omega), 0, r^{he}_{22}(\omega), 0, 1, r^{hh}_{22}(\omega)\right)^T.
\end{aligned} \tag{4.35}$$

They are connected by the transfer matrices to the corresponding outgoing modes at

[5] Note that the labeling of states with "right" and "left" does not relate to their propagation direction. Rather, it describes whether a state is associated with the region right- or leftmost of the scatterer.

$x = x_q + l_q$

$$\begin{aligned}
\Phi_{\text{right},1}(x_q+l_q) &= \left(t^{ee}_{31}(\omega),0,0,t^{eh}_{31}(\omega),0,t^{ee}_{41}(\omega),t^{eh}_{41}(\omega),0\right)^T,\\
\Phi_{\text{right},2}(x_q+l_q) &= \left(t^{he}_{31}(\omega),0,0,t^{hh}_{31}(\omega),0,t^{he}_{41}(\omega),t^{hh}_{41}(\omega),0\right)^T,\\
\Phi_{\text{right},3}(x_q+l_q) &= \left(t^{ee}_{32}(\omega),0,0,t^{eh}_{32}(\omega),0,t^{ee}_{42}(\omega),t^{eh}_{42}(\omega),0\right)^T,\\
\Phi_{\text{right},4}(x_q+l_q) &= \left(t^{he}_{32}(\omega),0,0,t^{hh}_{32}(\omega),0,t^{he}_{42}(\omega),t^{hh}_{42}(\omega),0\right)^T.
\end{aligned}$$

Each transmission amplitude has to be multiplied by a phase factor containing the position, energy and chemical potential. Since such phases neither change the transport properties, nor enter in the lead Green function (for a convenient choice of initial parameters), we can safely absorb these phases in the amplitudes.

A complementary set of yet another four independent scattering states is built from states describing an incident particle from the right $\Phi_{\text{right},5-8}(x)$

$$\begin{aligned}
\Phi_{\text{right},5}(x_q+l_q) &= \left(r^{ee}_{33}(\omega),1,0,r^{eh}_{33}(\omega),0,r^{ee}_{43}(\omega),r^{eh}_{43}(\omega),0\right)^T,\\
\Phi_{\text{right},6}(x_q+l_q) &= \left(r^{he}_{33}(\omega),0,1,r^{hh}_{33}(\omega),0,r^{he}_{43}(\omega),r^{hh}_{43}(\omega),0\right)^T,\\
\Phi_{\text{right},7}(x_q+l_q) &= \left(r^{ee}_{34}(\omega),0,0,r^{eh}_{34}(\omega),1,r^{ee}_{44}(\omega),r^{eh}_{44}(\omega),0\right)^T,\\
\Phi_{\text{right},8}(x_q+l_q) &= \left(r^{he}_{34}(\omega),0,0,r^{hh}_{34}(\omega),0,r^{he}_{44}(\omega),r^{hh}_{44}(\omega),1\right)^T.
\end{aligned}$$

Their transmitted counterparts leftmost to the scatterer read

$$\begin{aligned}
\Phi_{\text{left},5}(0) &= \left(0,t^{ee}_{13}(\omega),t^{eh}_{13}(\omega),0,t^{ee}_{23}(\omega),0,0,t^{eh}_{23}(\omega)\right)^T,\\
\Phi_{\text{left},6}(0) &= \left(0,t^{he}_{13}(\omega),t^{hh}_{13}(\omega),0,t^{he}_{23}(\omega),0,0,t^{hh}_{23}(\omega)\right)^T,\\
\Phi_{\text{left},7}(0) &= \left(0,t^{ee}_{14}(\omega),t^{eh}_{14}(\omega),0,t^{ee}_{24}(\omega),0,0,t^{eh}_{24}(\omega)\right)^T,\\
\Phi_{\text{left},8}(0) &= \left(0,t^{he}_{14}(\omega),t^{hh}_{14}(\omega),0,t^{he}_{24}(\omega),0,0,t^{hh}_{24}(\omega)\right)^T.
\end{aligned} \tag{4.36}$$

Each scattering problem of the form of Eq. (4.34), is therefore a 8×8 linear eigenvalue problem. The complexity of the propagators $U_t(x,x')$, however, requires a numerical treatment of the problem.

Having solved the scattering problem, we can construct the scattering state Green function by applying the formalism described in Sec. 3.2.2. From Eq. (3.45), we know that any Green function of the hetero-junction can be represented in the form

$$G^{R/A}_{n,m}(x,x',\omega) = \sum_{i,j} a^{R/A}_{i,j}(\omega)\phi_{i,n}(x,\omega)\tilde{\phi}_{j,m}(x',\omega),$$

where R and A label retarded and advanced Green function, respectively. $\phi_{i,n}(x,\omega)$,

$\tilde{\phi}_{j,m}(x',\omega)$ are the n-th, m-th, component of the i-th, j-th eigenstate[6]. The indices i,j run over all independent scattering states. Furthermore, Eq. (3.47) enforces a discontinuity of the Green functions as $x \to x'$

$$\lim_{\varepsilon\to 0}\left[\hat{G}^{R/A}(x'+\varepsilon,x',\omega)-\hat{G}^{R/A}(x'-\varepsilon,x',\omega)\right]=-\frac{i}{v_F}\eta_z\tau_z\sigma_z. \tag{4.37}$$

A promising ansatz that is able to implement this discontinuous jump looks like

$$G^{R/A}_{\alpha\beta}(x,x',\omega)=G^{R/A,<}_{\alpha\beta}(x,x',\omega)\theta(x-x')+G^{R/A,>}_{\alpha\beta}(x,x',\omega)\theta(x'-x),$$

where each part is of the form of Eq. (3.49)

$$G^{R/A,<\!/\!>}_{\alpha\beta}(x,x',\omega)=\sum_i \phi_{i,\alpha}(x,\omega)g^{<\!/\!>}_{i,\beta}(x',\omega)\equiv\sum_{i,j}a^{R/A,<\!/\!>}_{i,j}(\omega)\phi_{i,n}(x,\omega)\tilde{\phi}_{j,m}(x',\omega).$$

However, Eq. (4.37) is not sufficient to determine all x- and x'-independent coefficients $a^{R/A}_{i,j}(\omega)$. For that, we additionally need to include the assumed boundary behavior of the Green function. If we aim for the retarded Green function, and we assume an infinitesimal dissipation in the leads, this yields the additional condition

$$\lim_{x\to\pm\infty} G^R(x,x',\omega+i0^+)=0. \tag{4.38}$$

The latter condition implies a selection rule how the eigenfunctions need to be split up in the two groups $x<x'$ and $x>x'$ and eventually allows us to fully determine the retarded Green function.

Now, let us be more explicit. From Eq. (3.51), we know that, while having access to the transfer matrix of the system, it is sufficient to determine the Green function in a single set of points x_0, x_0'. Subsequently, obtaining the Green function at any given other set of points x,x' is a matter of matrix multiplications.

For our system, a convenient choice for an initial set of points is given (for instance) anywhere in the left leads $x,x'<0$. There, the wave functions are reasonably simple so that their boundary behavior is clear. Indeed, as no gap-inducing parameters are present in the leads, the wave functions are characterized by plane waves $\sim\exp[\pm i\omega x]$[7]. Thereby, right-moving particles carry a + sign, while left-moving particles obey a minus sign in the exponent. The correct boundary behavior for the retarded Green function, following Eq. (4.38), is thus obtained by using the states of (4.36) for $x<x'$ and the ones of (4.35) for $x>x'$. Thus, we have

[6] Note that $\tilde{\phi}_{j,m}(x',\omega)$ are eigenstates of the transposed Schrödinger equation.

[7] Here, we are only interested in the behavior as a function of ω and neglect possible dependence on the chemical potential.

$$\begin{aligned}\hat{G}^{R,>}(x,x',\omega) &= \Phi_{\text{left},1}(x,\omega)g_1^T(x',\omega)+\Phi_{\text{left},2}(x,\omega)g_2^T(x',\omega)\\ &+ \Phi_{\text{left},3}(x,\omega)g_3^T(x',\omega)+\Phi_{\text{left},4}(x,\omega)g_4^T(x',\omega), \qquad (4.39)\\ \hat{G}^{R,<}(x,x',\omega) &= \Phi_{\text{left},5}(x,\omega)g_5^T(x',\omega)+\Phi_{\text{left},6}(x,\omega)g_6^T(x',\omega)\\ &+ \Phi_{\text{left},7}(x,\omega)g_7^T(x',\omega)+\Phi_{\text{left},8}(x,\omega)g_8^T(x',\omega) \qquad (4.40)\end{aligned}$$

with the unknown vectors $g_j^T(x',\omega)$. Furthermore, the eigenstates $\Phi_{\text{left},j}(x)$ are given by

$$\Phi_{\text{left},j}(x) = U_0(x,0)\Phi_{\text{left},j}(0).$$

Inserting Eqs. (4.39) and (4.40) into Eq. (4.37), this results in a linear equation system for the vectors $g_j(x',\omega)$. Finally, reinserting the solution into Eqs. (4.39) and (4.40), we obtain the retarded Green function leftmost of the scattering region ($x,x'<0$). In general, it consists of four blocks

$$G^R(x,x',\omega) = \begin{pmatrix} G_{11}^R(x,x',\omega) & G_{21}^R(x,x',\omega)\\ G_{12}^R(x,x',\omega) & G_{22}^R(x,x',\omega)\end{pmatrix}.$$

Each $\hat{G}^R_{\lambda\lambda'}(x,x',\omega)$ is itself a 4×4 matrix, representing the intra-edge Green function for $\lambda=\lambda'$ and inter-edge Green function for $\lambda\neq\lambda'$, respectively. Leftmost of the scattering region $x,x'<0$, we find

$$G_{11}^R(x,x',\omega) = \frac{-i}{v_F}\begin{pmatrix} e^{\frac{i}{v_F}\delta x(\mu+\omega)}\theta(\delta x) & 0 & 0 & 0\\ e^{-\frac{i}{v_F}\overline{x}(\mu+\omega)}r_{11}^{ee} & e^{-\frac{i}{v_F}\delta x(\mu+\omega)}\theta(-\delta x) & 0 & e^{-\frac{i}{v_F}(\delta x\mu+\overline{x}\omega)}r_{11}^{he}\\ e^{\frac{i}{v_F}(\delta x\mu-\overline{x}\omega)}r_{11}^{eh} & 0 & e^{\frac{i}{v_F}\delta x(\mu-\omega)}\theta(-\delta x) & e^{\frac{i}{v_F}\overline{x}(\mu-\omega)}r_{11}^{hh}\\ 0 & 0 & 0 & e^{-\frac{i}{v_F}\delta x(\mu-\omega)}\theta(\delta x)\end{pmatrix}, \qquad (4.41)$$

$$G_{22}^R(x,x',\omega) = \frac{-i}{v_F}\begin{pmatrix} e^{-\frac{i}{v_F}\delta x(\mu+\omega)}\theta(-\delta x) & e^{-\frac{i}{v_F}\overline{x}(\mu+\omega)}r_{22}^{ee} & e^{-\frac{i}{v_F}(\delta x\mu+\overline{x}\omega)}r_{22}^{he} & 0\\ 0 & e^{\frac{i}{v_F}\delta x(\mu+\omega)}\theta(\delta x) & 0 & 0\\ 0 & 0 & e^{-\frac{i}{v_F}\delta x(\mu-\omega)}\theta(\delta x) & 0\\ 0 & e^{\frac{i}{v_F}(\delta x\mu-\overline{x}\omega)}r_{22}^{eh} & e^{\frac{i}{v_F}\overline{x}(\mu-\omega)}r_{22}^{hh} & e^{\frac{i}{v_F}\delta x(\mu-\omega)}\theta(-\delta x)\end{pmatrix}, \qquad (4.42)$$

$$G_{21}^R(x,x',\omega) = \frac{-i}{v_F}\begin{pmatrix} 0 & 0 & 0 & 0\\ 0 & e^{-\frac{i}{v_F}\overline{x}(\mu+\omega)}t_{12}^{ee} & e^{-\frac{i}{v_F}(\delta x\mu+\overline{x}\omega)}t_{12}^{he} & 0\\ 0 & e^{\frac{i}{v_F}(\delta x\mu-\overline{x}\omega)}t_{12}^{eh} & e^{\frac{i}{v_F}\overline{x}(\mu-\omega)}t_{12}^{hh} & 0\\ 0 & 0 & 0 & 0\end{pmatrix}, \qquad (4.43)$$

and

$$G^R_{12}(x,x',\omega) = \frac{-i}{v_F}\begin{pmatrix} e^{\frac{-i}{v_F}\overline{x}(\mu+\omega)}t^{ee}_{21} & 0 & 0 & e^{-\frac{i}{v_F}(\delta x\mu+\overline{x}\omega)}t^{he}_{21} \\ 0 & 0 & 0 & 0 \\ 0 & 0 & 0 & 0 \\ e^{\frac{i}{v_F}(\delta x\mu-\overline{x}\omega)}t^{eh}_{21} & 0 & 0 & e^{\frac{i}{v_F}\overline{x}(\mu-\omega)}t^{hh}_{21} \end{pmatrix} \tag{4.44}$$

with $\delta x = x - x'$ and $\overline{x} = x + x'$. Furthermore, we dropped the ω dependence of the scattering amplitudes to save space. Finally, the Green function at any desired set of points x and x' can be obtained from the above Green function according to Eq. (3.51) just by matrix multiplication with the SP propagators of the system, defined in Eq. (4.33).

4.4.2 Symmetries of superconducting pairing amplitudes

Each of the above blocks possesses the general structure

$$\hat{G}^R_{\lambda\lambda'}(x,x',\omega) = \begin{pmatrix} \hat{G}^R_{\lambda\lambda',ee}(x,x',\omega) & \hat{G}^R_{\lambda\lambda',eh}(x,x',\omega) \\ \hat{G}^R_{\lambda\lambda',he}(x,x',\omega) & \hat{G}^R_{\lambda\lambda',hh}(x,x',\omega) \end{pmatrix}.$$

While $\hat{G}^R_{\lambda\lambda',ee}(x,x',\omega)$ and $\hat{G}^R_{\lambda\lambda',hh}(x,x',\omega)$ constitute the normal part of the Green function, the anomalous parts, $\hat{G}^R_{\lambda\lambda',eh}(x,x',\omega)$ and $\hat{G}^R_{\lambda\lambda',he}(x,x',\omega)$, carry all information about the superconducting pairing. In particular, in the absence of superconducting order, those correlation functions typically vanish. As a basic example, consider the above Green function in the left lead. We can decompose each block (Eqs. (4.41-4.44)) into normal and anomalous parts. Then, the anomalous parts depend on the different electron-hole reflection coefficients. Although there is no explicit superconducting order present for $x, x' < 0$, the correlation function can still recognize the proximity effect since electron-hole reflection amplitudes (i. e. the Cooper-pair creation amplitudes) are non-zero in the presence of superconductivity elsewhere in the scattering region.
More importantly, the form of the anomalous Green function contains profound information about the symmetries of the superconducting pairing. According to the Berezinskii classification of pairing amplitudes (see Sec. 2.5.2), the pairing amplitudes have to be anti-symmetric under exchange of *all* constituent labels. In our system, pairing is labeled by four quantities: the edge indices, the spatial coordinates, spin, and frequency (or time). In what follows, we are only interested in intra-edge pairing, i. e. $\lambda = \lambda'$. This effectively reduces the number of labels to three: frequency, spin, and orbit.
For the basis we have picked in Eq. (4.31), we can directly illustrate the spin-texture of the pairing with the decomposition into Pauli matrices

$$G^R_{\lambda\lambda,eh}(x,x',\omega) = f^R_{\lambda\lambda,0}(x,x',\omega)\sigma_0 + f^R_{\lambda\lambda,j}(x,x',\omega)\sigma_j,$$

where $j \in \{x,y,z\}$. $f^R_{\lambda\lambda,0}(x,x',\omega)$ is the singlet (S) component of the pairing, relating to the anti-symmetric spin configuration $(\uparrow\downarrow - \downarrow\uparrow)$. Likewise, the triplet (T) components relate to the symmetric spin configuration with $f^R_{\lambda\lambda,z}(x,x',\omega)$ with $(\uparrow\downarrow + \downarrow\uparrow)$, and the equal spin pairing $f^R_{\lambda\lambda,\uparrow\uparrow} = f^R_{\lambda\lambda,x}(x,x',\omega) - if^R_{\lambda\lambda,y}(x,x',\omega)$, $f^R_{\lambda\lambda,\downarrow\downarrow} = f^R_{\lambda\lambda,x}(x,x',\omega) + if^R_{\lambda\lambda,y}(x,x',\omega)$, having $\uparrow\uparrow$, $\downarrow\downarrow$ configuration, respectively. The Berezinskii symmetry constraint of Eq.

(2.63) now translates to the different spin components like

$$f^R_{\lambda\lambda,0}(x,x',\omega) = f^A_{\lambda\lambda,0}(x',x,-\omega), \tag{4.45}$$
$$f^R_{\lambda\lambda,j}(x,x',\omega) = -f^A_{\lambda\lambda,j}(x',x,-\omega) \tag{4.46}$$

with $j \in \{x,y,z\}$. Here, $f^A_{\lambda\lambda,l}(x',x,\omega)$ ($l \in \{0,x,y,z\}$) are the singlet and triplet components of the advanced pairing amplitudes derived from the advanced Green function. We can further decompose the symmetry requirements of Eqs. (4.45) and (4.46) into orbital and frequency symmetries. Therefore, we split up the pairing amplitudes in even and odd orbital parts

$$f^R_{\lambda\lambda,l}(x,x',\omega) = \zeta^{R,+}_{\lambda\lambda,l}(x,x',\omega) + \zeta^{R,-}_{\lambda\lambda,l}(x,x',\omega) \tag{4.47}$$

with even (E) and odd (O) parts defined as $\zeta^{R,\pm}_{\lambda\lambda,l}(x,x',\omega) = 1/2(f^R_{\lambda\lambda,l}(x,x',\omega) \pm f^R_{\lambda\lambda,l}(x',x,\omega))$. To ensure Eqs. (4.45) and (4.46), the symmetries in ω are then required to be

$$\zeta^{R,\pm}_{\lambda\lambda,0}(x,x',\omega) = \pm\zeta^{A,\pm}_{\lambda\lambda,0}(x,x',-\omega), \tag{4.48}$$
$$\zeta^{R,\pm}_{\lambda\lambda,j}(x,x',\omega) = \mp\zeta^{A,\pm}_{\lambda\lambda,j}(x,x',-\omega), \tag{4.49}$$

where $j \in \{x,y,z\}$ and $\zeta^{A,\pm}_{\lambda\lambda,j}(x,x',-\omega)$, $\zeta^{A,\pm}_{\lambda\lambda,0}(x,x',-\omega)$ are the even and odd orbital parts of the advanced pairing amplitudes. Eq. (4.48) and (4.49) describe all possible symmetry classes, that are, coined in the order frequency, spin, orbit as: ESE ($\zeta^{R,+}_{\lambda\lambda,0}(x,x',\omega)$), OSO ($\zeta^{R,-}_{\lambda\lambda,0}(x,x',\omega)$), ETO ($\zeta^{R,-}_{\lambda\lambda,j}(x,x',\omega)$) and OTE ($\zeta^{R,+}_{\lambda\lambda,j}(x,x',\omega)$).

4.4.3 Non-local odd-frequency pairing

The absence of translational invariance in hetero-structures inevitably leads to a mixture of even and odd orbital parts in the pairing amplitudes. Moreover, spin-momentum locking of helical edge states implies the formation of triplet pairing. In combination, we thus deduce that, by construction, ETO and OTE pairing amplitudes are expected to appear. In bare superconducting QSH hetero-junctions, triplet pairing exists only in the form of the amplitude $f^R_{\lambda\lambda,z}(x,x',\omega)$ corresponding to the spin configuration ($\uparrow\downarrow + \downarrow\uparrow$). Spin sensitive conductance measurements are ineffective in discriminating this triplet amplitude from their singlet counterparts. This dilemma resolves if equal spin pairing is present in the hetero-junction. Then, there is a transport process, namely CAR across the junction, which is usually suppressed by spin-momentum locking [AGC$^+$10], that is directly related to the injection of a Cooper pair with $\uparrow\uparrow$ ($\downarrow\downarrow$) spin texture. Typically, equal spin pairing is generated at the helical edge in the presence of TR breaking ferromagnetic ordering [CBT15]. Interestingly, in our setup, we can design an equal spin pairing in the absence of TR breaking terms, just by means of a QSH QC. This is possible, due to the simultaneous presence of the two TR invariant SP coupling terms, given in Eqs. (4.2) and (4.3). In particular, Eq. (4.2) leads to Andreev BSs between SC and QSH QC (see Fig. 4.10), that extend over both edges. Additionally, Eq. (4.3) mixes $\uparrow$ and $\downarrow$ fermions across the edges. In combination with Eq. (4.2), this eventually allows for $\uparrow\uparrow$- and $\downarrow\downarrow$-pairing in a single edge.

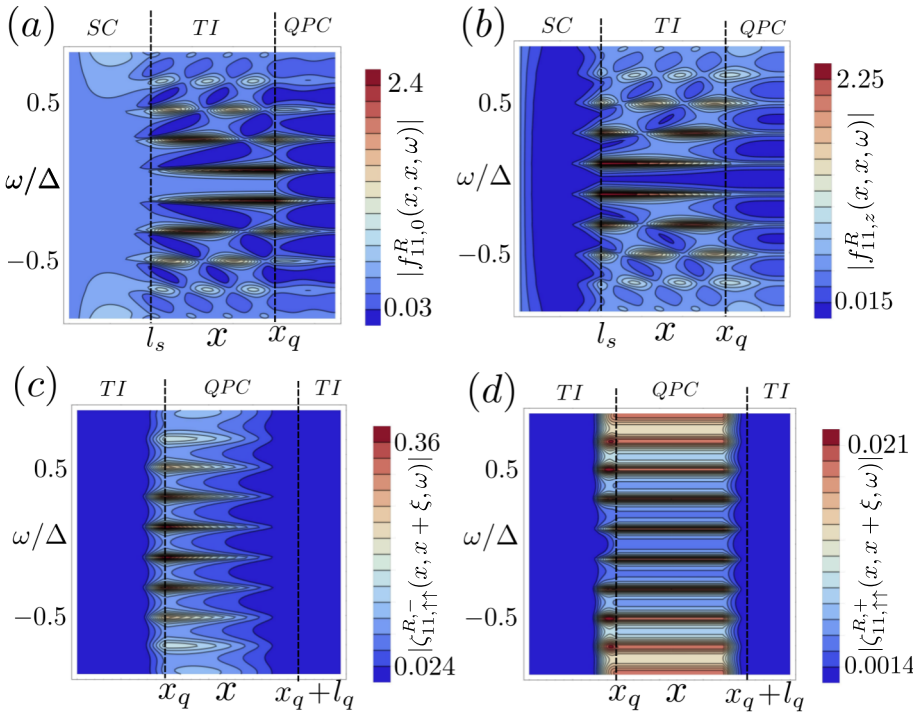

Figure 4.11: Superconducting pairing in the hetero-junction of Fig. 4.10 as a function of position x and energy ω. (a) and (b) illustrate the local singlet and triplet ($\uparrow\downarrow + \downarrow\uparrow$) pairing, while (c) and (d) show the even- and odd-frequency equal spin pairing with $x' = x+\xi$ and $\xi = 0.5\xi_\Delta$. We use the parameters: $\mu = 0$, $t_0/\Delta = t_c/\Delta = 0.4$, $l_s = 4\xi_\Delta$, $l_q = 3\xi_\Delta$ and $x_q = 10\xi_\Delta$ with $\xi_\Delta = \frac{v_F}{\Delta}$. Reprinted figure with permission from Ref. [FZT18]. Copyright 2020 by the American Physical Society.

To demonstrate this effect, we proceed with the calculation of the pairing amplitudes. We apply Eq. (3.51), with $G^R(x_0, x_0', \omega)$ for $x_0,\ x_0' \to 0^-$ [8] and the transfer matrices of Eq. (4.33) and calculate the amplitudes $f^R_{11,j}(x,x,\omega)$ with $j \in \{0,\ z\}$ and $x \in [0, x_q + l_q]$ (see Fig. 4.11 (a) and (b)). As $x = x'$, we naturally compute the even orbital parts of the pairing, ESE and OTE. Notably, in contrast to SC-ferromagnet hetero-junctions at the helical edge, we find that local equal spin correlations are totally suppressed throughout the whole junction so that $f^R_{11,\sigma\sigma}(x,x,\omega) = 0$. Typically, local equal spin pairing is related to the amplitude of electron-electron (hole-hole) reflection $r^{ee}_{11}(\omega)$ ($r^{hh}_{11}(\omega)$), which is suppressed by TR symmetry in our system. Interestingly however, non-local equal spin correlations are generated in the form of $f^R_{11,\sigma\sigma}(x, x+\xi, \omega)$ with $x \in [0, x_q + l_q - \xi]$. The results are shown in Fig. 4.11 (c) and (d). We find a non-local equal spin pairing $f^R_{11,\sigma\sigma}(x, x+\xi, \omega)$ in the system, whenever there is at least one point χ with $\chi \in [x, x+\xi]$ that belongs to the constricted region. This is realized in two scenarios: (i) When at least one of the two spatial coordinates of the corresponding correlation function is part of the constriction, i.

[8] Strictly speaking, $x_0 = x_0'$ is ill-defined in the Green function. Instead, we have to choose $x_0 = x_0' \pm 0^+$. Here, we pick $x_0 = x_0' + 0^+$. In particular, a chosen order should be kept also when using Eq. (3.51) to compute the Green function in another set of points as the transfer matrices are not able to account for the discontinuous jumps that appear in the Green function as $x \to x'$.

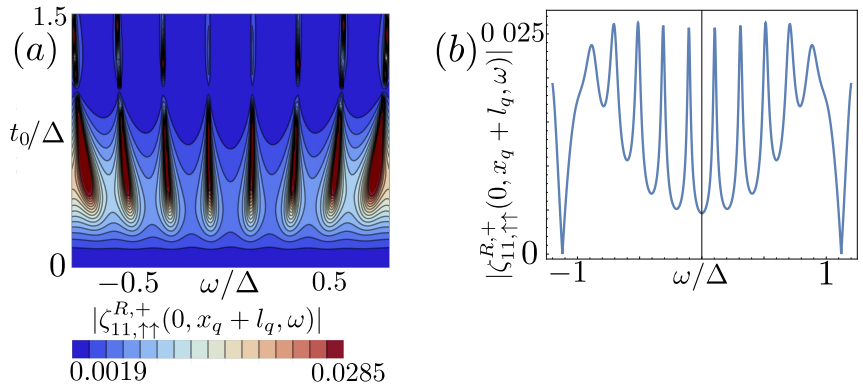

Figure 4.12: (a) OTE part of the pairing amplitude $|f^R_{11,\uparrow\uparrow}(0, x_q + l_q, \omega)|$ as a function of coupling strength $t_0/\Delta = t_c/\Delta$ and energy ω/Δ. (b) Line cut from (a) for $t_0/\Delta = t_c/\Delta = 0.4$ and the other parameters given in Fig. 4.11. Reprinted figure with permission from Ref. [FZT18]. Copyright 2020 by the American Physical Society.

e. $x, x + \xi \in [x_q, x_q + l_q]$ (see Fig. 4.11 (c) and (d)). (ii) When the pairing happens across the whole constriction (Fig. 4.12). In both cases, even- and odd-frequency parts appear. Importantly, the presence of *both* SP coupling terms (Eqs. (4.2) and (4.3)) is crucial for finite non-local equal spin pairing amplitudes at a single edge (Fig. 4.13).
Typically, the presence of Andreev BSs enhances the odd-frequency components of the pairing [LB19]. Indeed, also our system possesses an increased non-local pairing $f^R_{11,\uparrow\uparrow}(0, x_q + l_q, \omega)$, whenever the energy of an Andreev BS is matched (see Fig. 4.12). Note, in particular, that the energy of Andreev BSs can be controlled by a superconducting phase shift applied between the SC at edge 1 and 2. Especially, for a shift of π (mod 2π), this energy becomes zero for one Andreev BS that is then turned into a Kramers pair of Majoranas, bound in between the SCs and the constricted region [LPBL16].
In general, we obtain that the non-local equal spin pairing across the junction is equally composed of OTE and ETO parts. This turns out to be a very generic result, originating from spin-momentum locking. As the retarded Green function implements time-ordering, non-local equal spin pairing from $x = 0$ to $x' = x_q + l_q$ represents a correlation acting forward in time and forward in space, while correlations from $x = x_q + l_q$ to $x' = 0$ describe the corresponding process backward in space. For a defined pairing amplitude ($f^R_{\lambda\lambda,\uparrow\uparrow}(0, x_q + l_q, \omega)$ or $f^R_{\lambda\lambda,\downarrow\downarrow}(0, x_q + l_q, \omega)$) at the helical edge, only one of the two processes is finite due to spin-momentum locking. This behavior inverts as x and x' are exchanged. Consequently, Eq. (4.47) implies that ETO and OTE pairing necessarily appear with equal amplitudes.

4.4.4 Transport signatures

The spin-momentum locking at the helical edge equips us with an observable that is directly related to the non-local equal spin pairing: the CAR process. However, CAR processes compete with EC processes. Since both processes contribute with opposite charges to the overall current, they enter with an opposite sign in the corresponding

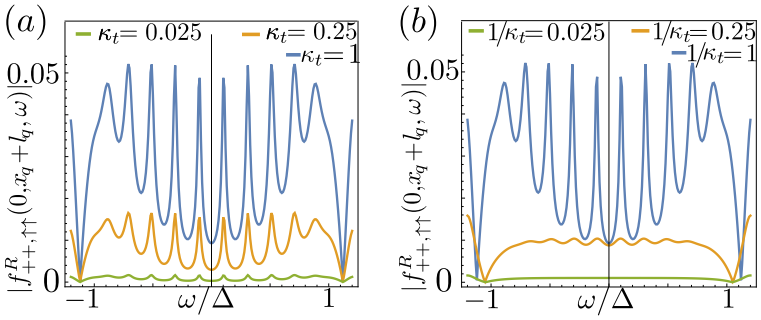

Figure 4.13: Non-local $\uparrow\uparrow$-pairing as a function of ω for different amplitudes of SP scattering. We introduce the dimensionless parameter ratio $\kappa_t = t_c/t_0$. Other parameters are the same as in Fig. 4.11. Reprinted figure with permission from Ref. [FZT18]. Copyright 2020 by the American Physical Society.

conductance. To read out whether CAR processes contribute to the tunneling for a given scatterer, this requires CAR to dominate over EC. Only then, the non-local conductance provides evidence for such kind of scattering.

For concreteness, the non-local differential conductance we are interested in is $G_{31}(\omega)$, measuring the transmission between contacts 1 and 3 of Fig. 4.10 at excitation energy ω. By definition $G_{31}(\omega)$ is given as the differential change of the current at contact 3, when a voltage V_1 is applied at contact 1 (see also Eq. (3.39))

$$G_{31}(\omega) = \frac{e^2}{2\pi}\left(|t^{ee}_{31}(\omega)|^2 - |t^{eh}_{31}(\omega)|^2\right).$$

If EC processes dominate, which is typically the case, no evidence for CAR is obtained from $G_{31}(\omega)$. In turn, a negative non-local conductance $G_{31}(\omega)$ is only possible if CAR processes are finite. Unfortunately, most often this is not the case [MBB06]. Especially not at the helical edge, where CAR is additionally assigned to the creation of an equal spin Cooper pair [CBT15].

In that respect, superconducting QSH QCs possess two major advantages: First, they provide non-local odd-frequency equal spin pairing across the junction in a TR invariant manner, directly related to $t^{eh}_{31}(\omega)$. Second, as the constriction involves the second edge by virtue of the SP hybridization terms, there are now three open channels available for EC. As a consequence, this yields a reduced rate $t^{ee}_{\lambda\lambda'}(\omega)$ for each individual channel. The combination of those two effects leads to a domination of CAR over EC in a large domain of parameter space and eventually produces a non-local conductance $G_{31}(\omega) < 0$ (Fig. 4.14). Notably, unlike other proposals, in superconducting QSH QCs nearly no fine-tuning is needed in order to measure CAR. Moreover, comparing Figs. 4.12 and 4.14 (a), we notice that the presence of Andreev BSs leads to an enhanced (or resonant) CAR that is signaled as a dip in the non-local conductance.

So far, we have excluded the influence of a finite chemical potential from the discussion by choosing $\mu = 0$. However, finite chemical potential can play an important role for the detection of CAR processes in the junction. In particular, we find that finite μ yields an

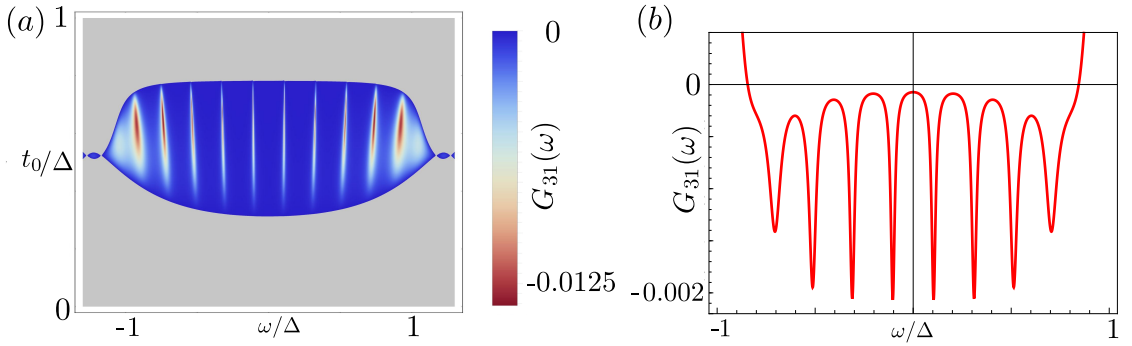

Figure 4.14: (a) Non-local conductance $G_{31}(\omega)$ in units of $e^2/(2\pi)$ for the setup shown in Fig. 4.10 with the parameters of Fig. 4.11. In the gray area we obtain $G_{31}(\omega) > 0$, while in the colored region we have $G_{31}(\omega) < 0$. (b) Line cut for $t_0/\Delta = 0.4$. Reprinted figure with permission from Ref. [FZT18]. Copyright 2020 by the American Physical Society.

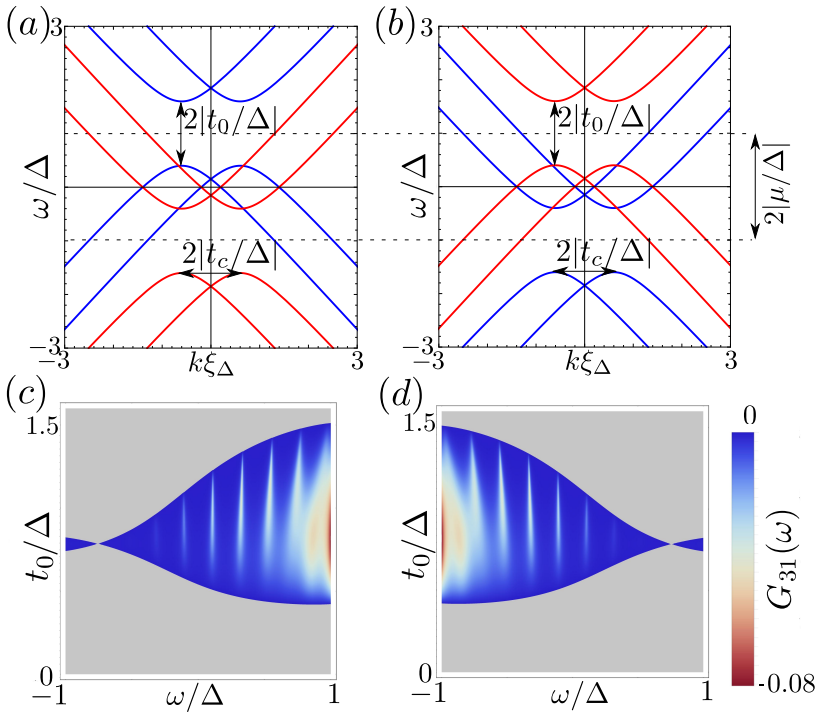

Figure 4.15: (a)-(b) Dispersion relation of the QPC with the parameters $t_0/\Delta = t_c/\Delta = 0.6$, and $\mu/\Delta = -1$ in (a) and $\mu/\Delta = 1$ in (b). Electron-like excitations are shown in blue, hole-like excitations in red. (c)-(d) Non-local conductance $G_{31}(\omega)$ in units of $e^2/(2\pi)$ for the parameters $l_s = 3\xi_\Delta$, $l_q = 2\xi_\Delta$, $x_q = 9\xi_\Delta$ and $\mu/\Delta = -1$ in (c), $\mu/\Delta = 1$ in (d) with $\xi_\Delta = v_F/\Delta$. Reprinted figure with permission from Ref. [FZT18]. Copyright 2020 by the American Physical Society.

asymmetry of the non-local conductance signature $G_{31}(\omega)$ with respect to $\omega \to -\omega$ (see Fig. 4.15 (c) and (d)): with positive chemical potential, negative excitation energies are favored to for enhancing CAR over EC and vice versa. An explanation for this effect might be found on the basis of the dispersion relation of the (infinitely long) QSH QC (Fig. 4.15 (a) and (b)). While the forward scattering H_{t_c} (Eq. (4.3)) is insensitive to μ, the net effect of the spin-preserving scattering H_{t_0} (Eq. (4.2)) is reduced by finite chemical potential. Moreover, since μ acts in the opposite way to electron- and hole-like excitations, we can emphasize or suppress backscattering on electron- and hole-like states using excitation energies $\omega \neq 0$. To eventually obtain $G_{31}(\omega) < 0$, it is important to maximize $t^{eh}_{\nu\nu'}$ (i. e. the transmission of incident electronic states as hole-like particles) and likewise suppress $t^{ee}_{\nu\nu'}$. Comparing this against Fig. 4.15 (a) and (b), we see that the favorable regime for positive chemical potential is given by negative excitation energies and vice versa. Then, hole-like states can freely propagate through the constriction, while the transmission of electronic states is exponentially suppressed. Certainly, the full complexity of the problem is not completely captured in this simplified picture. Interestingly however, it is indeed consistent with our numerical results (see Fig. 4.15 (c)-(d)).

4.5 Floquet topology

Odd-frequency superconductivity and the related topological superconductivity constitute just two examples for how QSH QCs can provide a novel and comprehensive platform for exotic quantum matter. Indeed, the symmetries that are present in such devices allow a whole family of fascinating physical effects. Yet another interesting example emerges in the context of Floquet theory [FZP+20]. Actually, topological superconductivity is a stationary phase of matter. Interestingly, however, such a phase can be imitated in QSH QCs with a time-periodic non-stationary Hamiltonian completely without the use of superconductivity. To this end, the role of superconductivity is replaced by an oscillating electro-magnetic field. Of course, superconducting systems obey PH symmetry, which is not expected to be found in the absence of superconducting order. However, QSH QCs are equipped with a similar symmetry, namely, charge-conjugation. Thus, any state at energy ϵ has a counterpart with the same quantum numbers at $-\epsilon$ (see Fig. 4.1 (b)). Hence, if we excite negative energy states by a fixed energy, say Ω, they can hybridize with their counterpart at positive energy and open a hybridization gap. The resulting spectrum obeys similar properties as induced by superconductivity with the difference that no pairing is present. In other words, using an oscillating electro-magnetic field, we generate a conduction-valence band symmetry centered around quasi-energy $\epsilon = \Omega/2$ that imitates PH symmetry. Similar ideas have been employed for quantum wires as well [TLK17, KMP+19], however, there the existence of a suitable valence band is not justified as no supporting symmetries are present.

For small amplitudes eA of the electro-magnetic field (with electron charge e), the interesting physics happens around the drive-induced conduction-valence band symmetric points at quasi-energy $\epsilon = \Omega/2 \,(\mathrm{mod}\ \Omega)$. Around those quasi-energy values, hybridization gaps of amplitude $\propto |eA|$ are formed. Similar to the static case, an additionally applied Zeeman field B_z competes with the drive-induced gap. This eventually leads to a gap

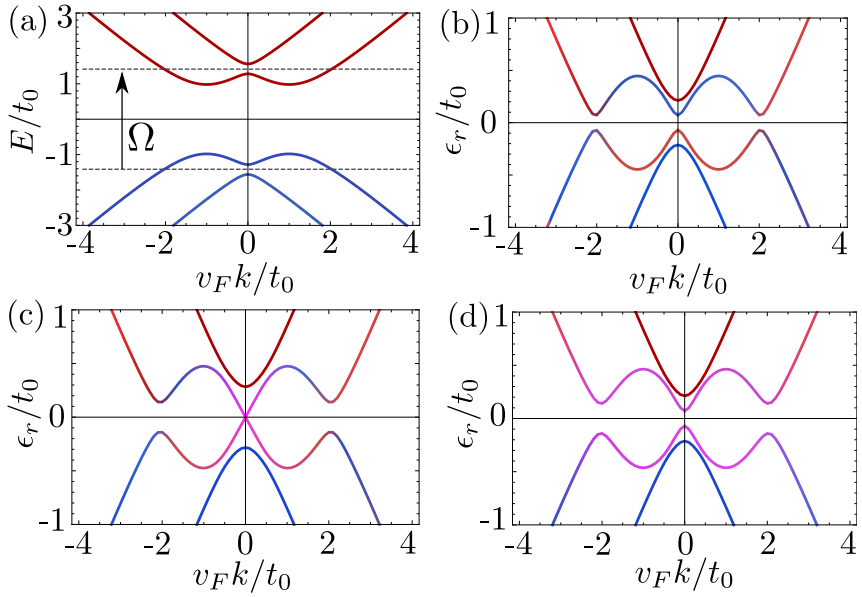

Figure 4.16: (a) QSH QC eigenvalue spectrum with additional Zeeman field. The coupling induced by external electromagnetic radiation with resonant frequency $\Omega = 2\sqrt{t_c^2 + t_0^2}$ ($t_0 = t_c$) is also shown by means of the arrow. (b)-(d) Quasi-energy spectrum $\epsilon_r = \epsilon - \Omega/2$ of the effective quasi-energy operator based on the extended Floquet-Hilbert space with (b) $eA/B_z = 0.5$, (c) $eA/B_z = 1$, (d) $eA/B_z = 2$. The topological phase is characterized by $0 < eA/B_z < 1$. The colors in the spectra (b-d) function as a guide to the eye to visualize band inversion. Reprinted figure with permission from Ref. [FZP+20]. Copyright 2020 by the American Physical Society.

closing-reopening, which indicates the topological phase transition in the Floquet spectrum. In accordance with the stationary case, the Floquet topological phase, found on resonance for $0 < eA/B_z < 1$, is accompanied by topological Floquet BSs at the end of the QSH QC. Although such states share similarities with non-Abelian Majorana modes – their stationary counterparts – they can only obey non-Abelian properties for very specific conditions [KL13, TLK17].
Interestingly, if the time-periodic part of the Hamiltonian is limited to the constricted region, so that fermion distributions are well defined in the isolated helical edge leads, the presence of Floquet topological BSs can be detected by means of standard transport experiments.
In what follows, we closely follow the results presented in Ref. [FZP+20]

4.5.1 Time-periodically driven quantum spin Hall quantum constrictions

The system we investigate is given by a QSH QC with the kinetic part given by Eq. (4.1). We furthermore assume the presence of all TR invariant SP scattering processes, described by Eqs. (4.2) and (4.3), as well as Zeeman field like Eq. (4.4). The so generated spectrum (for a translational invariant QSH QC, i. e. $t_0(x) = t_0$, $t_c(x) = t_c$ and $B_z(x) = B_z$) is depicted in Fig. 4.16 (a). The presence of a natural charge conjugation symmetry in our system suggests the possibility to engineer topological properties related to this symmetry

with a periodically driven external electro-magnetic field. The Hamiltonian associated with the driving is

$$H_{\mathrm{A}}(t) = \int_{\infty}^{\infty} \mathrm{d}x\ \hat{\Psi}^{\dagger}(x)(-eA\cos(\Omega t)\eta_z\sigma_z)\hat{\Psi}(x), \tag{4.50}$$

where we use the basis $\hat{\Psi}(x) = (\hat{\psi}_{\uparrow,1}(x), \hat{\psi}_{\downarrow,1}(x), \hat{\psi}_{\uparrow,2}(x), \hat{\psi}_{\downarrow,2}(x))^T$. η_z and σ_z are Pauli-matrices, acting on edge- and spin-space. Eq. (4.50) is able to induce a non-equilibrium topological phase transition. The most constructive way to understand such a dynamical transition is to apply the Shirley-Floquet theory of periodically driven systems, described in Sec. 3.2.3. Then, the problem boils down to the computation of the *effective* quasi-energy operator of the full Hamiltonian $H_F = H_p + H_{t_0} + H_{t_c} + H_{\mathrm{B}} + H_{\mathrm{A}}(t) = H_{\mathsf{stat}} + H_{\mathrm{B}} + H_{\mathrm{A}}(t)$.

The quasi-energy operator Q and the associated quasi-stationary Schrödinger equation are defined in Eq. (3.55)[9]. With the cosine drive of Eq. (4.50), the quasi-energy operator has only three non-zero contributions, resulting in an infinite dimensional tridiagonal matrix. The stationary part of the Hamiltonian can be directly identified with the diagonal elements of Q

$$Q_{n,n} = H_{\mathsf{stat}} + H_{\mathrm{B}} + n\Omega. \tag{4.51}$$

The time-periodic part of the Hamiltonian, $H_{\mathrm{A}}(t)$, produces elements on the two semi-diagonals

$$Q_{n,n+1} = Q_{n,n-1} = \frac{1}{2}\int_{-\infty}^{\infty} \mathrm{d}x(-eA)\hat{\Psi}^{\dagger}(x)\eta_z\sigma_z\hat{\Psi}(x). \tag{4.52}$$

Each diagonal block $Q_{n,n}$ is separated by an energy Ω from its neighboring blocks, where the different blocks are coupled by $Q_{n,n\pm1}$. Since, for the QSH QC, there are positive as well as negative energy states and the spectrum is unbounded[10], we will find degeneracies among different diagonal blocks. If, additionally, the matrix elements that capture a connection between the eigenstates of the different blocks are non-zero, a hybridization gap forms (see Fig. 4.16 (b)).

More explicitly, the Fermi field operators in the constricted region read $\hat{\Psi}(x) = \sum_k \hat{C}_k e^{ikx}$ with creation operators $\hat{C}_k = (\hat{c}_{k\uparrow1}, \hat{c}_{k\downarrow1}, \hat{c}_{k\uparrow2}, \hat{c}_{k\downarrow2})^T$. We apply an unitary transformation U such that H_{stat} becomes diagonal. The new creation operators $\hat{D}_k = U\hat{C}_k$ are then associated with the eigenvalues $\pm E(\pm k) = \pm\sqrt{t_0^2 + (t_c \pm kv_F)^2}$ (see Fig. 4.16 (a)). In particular, let us denote $\hat{d}_k^{\pm\pm}$ as the fermion with eigenvalue $\pm E(\pm k)$. In terms of those

[9] We work in a second-quantized picture here. Q thus represents the second-quantized operator with respect to the one defined in Eq. (3.55).

[10] Strictly speaking, the spectrum is bounded by the magnitude of the bulk bandgap. The physics discussed in this section thus requires energy scales that are significantly smaller than this bandgap.

transformed fermions $\hat{D}_k$, H_B and $Q_{n,n\pm1}$ become in the basis $\hat{D}_k = \left(\hat{d}_k^{--}, \hat{d}_k^{-+}, \hat{d}_k^{+-}, \hat{d}_k^{++}\right)$

$$\begin{aligned} H_\mathrm{B} &= \sum_k \hat{D}_k^\dagger [B_0(k)\tau_0\sigma_x + \frac{B_1(k)(\tau_x\sigma_x - \tau_y\sigma_y)}{2} + \frac{B_2(k)(\tau_x\sigma_x + \tau_y\sigma_y)}{2}]\hat{D}_k, \\ Q_{n,n\pm1} &= \sum_k \hat{D}_k^\dagger [\frac{\Delta_0(k)\tau_x(\sigma_0 - \sigma_z)}{2} + \frac{\Delta_0(-k)\tau_x(\sigma_0 + \sigma_z)}{2} \\ &+ \frac{\Delta_1(k)(\tau_z\sigma_0 - \tau_z\sigma_z)}{2} - \frac{\Delta_1(-k)(\tau_z\sigma_0 + \tau_z\sigma_z)}{2}]\hat{D}_k \end{aligned} \tag{4.53}$$

with $\Delta_0(k) = -eA|t_0|/\sqrt{t_0^2 + (t_c + kv_F)^2}$ and $\Delta_1(k) = -eA(t_c + kv_F)/\sqrt{t_0^2 + (t_c + kv_F)^2}$. The explicit k-dependence of B_0 ,B_1 and B_2 can be derived analytically but is too lengthy to be presented here. However, these parameters obey $B_0,\ B_1,\ B_2 \propto B_z$. In the resonant case with $\Omega = 2\sqrt{t_c^2 + t_0^2}$ (see Fig. 4.16 (a)), drive-induced non-equilibrium gaps are opened around the degenerate points in the eigenvalue spectrum of the quasi-energy operator (see Fig. 4.16). The magnitudes of these gaps are controlled by the corresponding matrix elements. Provided $eA, B_z \ll \Omega$, matrix elements describing the coupling between states that are separated by at least Ω in quasi-energy can be safely neglected for quasi-energies close to the resonance point. This eventually yields the effective quasi-energy operator

$$Q_\mathrm{eff} = \sum_k \tilde{D}_k^\dagger \begin{pmatrix} E(-k) & B_0(k) & \Delta_0(-k) & 0 \\ B_0(k) & E(k) & 0 & \Delta_0(k) \\ \Delta_0(-k) & 0 & -E(-k)+\Omega & B_0(k) \\ 0 & \Delta_0(k) & B_0(k) & -E(k)+\Omega \end{pmatrix} \tilde{D}_k,$$

where $\tilde{D}_k = \left(\hat{d}_k^{+-}, \hat{d}_k^{++}, \hat{d}_k^{--}, \hat{d}_k^{-+}\right)^T$. Remarkably, on resonance ($\Omega = 2\sqrt{t_c^2 + t_0^2}$) at quasi-energy $\epsilon = \Omega/2$, we find a gap-closing and reopening around $eA = B_z$, indicating a topological phase transition in the Floquet spectrum (Fig. 4.16 (b-d)). Even for driving frequencies that are not perfectly on resonance, but shifted by an imbalance $\delta\Omega$, i. e. $\Omega = 2(\sqrt{t_0^2 + t_c^2} - \delta\Omega)$, we still find a similar behavior, however, now the gap-closing and reopening takes place at Zeeman field strength

$$B_z = \pm\sqrt{(eA)^2 + (\delta\Omega)^2(1 + (t_c/t_0)^2)}. \tag{4.54}$$

In that sense, the imbalance $\delta\Omega$ takes a similar role as the chemical potential does for the formation of topological superconducting phases in the stationary case of a SOC quantum wire or a QSH anti-wire. Here, however, the necessary condition is that Ω is larger than the SP induced gaps, so that valence band states can be excited to conduction band states and hybridize (compare to Fig. 4.16 (a)).

4.5.2 Transport properties and topological Floquet bound states

Next, let us investigate a system schematically depicted in Fig. 4.17 (a). If the periodically driven electro-magnetic field acts only locally in the constricted region, Fermi distributions are well defined in the leads. Then, for the structure shown in Fig. 4.17 (a), the phase

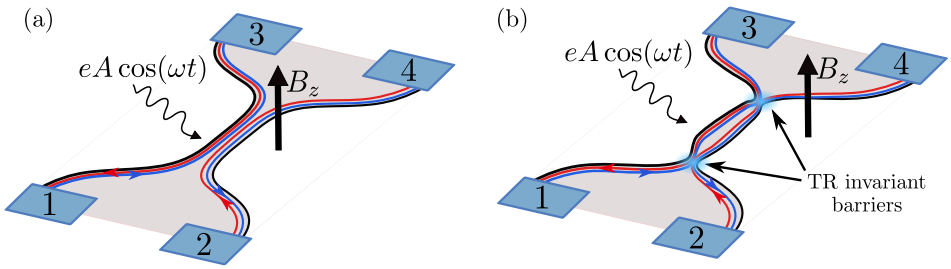

Figure 4.17: (a) Schematic sketch of the system: a QSH QC (a) without TR invariant barriers and (b) with TR invariant barriers at the ends of the constriction. (b) corresponds to the anti-wire setup of Sec. 4.3. In both scenarios, the QSH QC is exposed to electro-magnetic radiation, while in the leads no time dependent terms appear. Reprinted figures with permission from Ref. [FZP+20]. Copyright 2020 by the American Physical Society.

transition derived above can be detected by means of photon-assisted transport. For simplicity, we assume the potentials in the constriction to be step functions $t_0(x) = t_c(x) = t_0\theta(x)\theta(L-x)$. This assumption is valid, provided the Fermi wave length λ_F is much smaller than the smoothing length L_s that describes the build-up of the constriction potentials which itself should be smaller than L. Hence, we require $\lambda_F \ll L_s \ll L$[11]. Moreover, also the driven electro-magnetic field is modeled in terms of step functions, extending over the area of the constriction, $eA(x,t) = eA(t)\theta(x)\theta(L-x)$.
The conducting properties can be accessed upon solving the SP scattering problem of the hetero-junction defined by

$$\mathcal{Q}(x)|\nu(x)\rangle = \epsilon|\nu(x)\rangle. \tag{4.55}$$

$\mathcal{Q}(x)$ is the associated SP quasi-energy operator with respect to Eqs. (4.51) and (4.52), where we now use the x-dependent SP scattering potentials. Eq. (4.55) can be formally solved by integration. For that, we first rewrite the eigenvalue problem as

$$P\partial_x|\nu(x)\rangle = \frac{i}{v_F}(\epsilon - \mathcal{Q}_1(x))|\nu(x)\rangle$$

with $P = \mathbb{1}_\infty\eta_z\sigma_z$ and $\mathcal{Q}_1(x) = \mathcal{Q}(x) + iv_F P\partial_x$. Upon integration, we find the (infinite dimensional) transfer matrix associated with the driven QSH QC

$$M(L,0) = \exp\left[\int_0^L \mathrm{d}x \frac{i}{v_F} P^{-1}(\epsilon - \mathcal{Q}_1(x))\right].$$

An incoming mode can be scattered in any sector with photon number m and lead index j. However, transitions including high numbers of photons are considerably less probable and the reflection-/transmission-amplitudes $r^m_{jj}(\epsilon)$, $t^m_{jj'}(\epsilon)$ vanish with increasing photon

[11] Note that our result is not explicitly dependent on the exact shape of the potentials in the constriction. Rather, as we will show below, it gives a measure for the Floquet topological properties of the constriction. Those are expected to be independent of the exact shape of the potentials as long as we keep $eA, B_z \ll \Omega$.

number m. This allows us to compute the conductance with only a finite number $\overline{m}$ of harmonics by extracting the matrix $M_{\overline{m}}(L,0) = \exp\left[i/v_F \int_0^L \mathrm{d}x\ P_{\overline{m}}^{-1}(\epsilon - \mathcal{Q}_{1,\overline{m}}(x))\right]$ out of the infinite dimensional matrix $M(L,0)$.

The approximate transfer matrix $M_{\overline{m}}(L,0)$ defines a $4(2\overline{m}+1)$ dimensional scattering problem. To solve it, we need to propose appropriate incoming and outgoing states $\psi^{\alpha}_{\mathrm{in},\overline{\mathrm{m}}}(x)$, $\psi^{\alpha}_{\mathrm{out},\overline{\mathrm{m}}}(x)$ (with the lead index α). Since our scattering problem possesses a spatial symmetry with respect to the center of the QSH QC, the Floquet scattering matrix is expected to reflect this symmetry, so that $S_{F,\beta\alpha}(E_n,E) = S_{F,\alpha\beta}(E_n,E)$ [Mos11]. Thus, we only need to find half of all scattering amplitudes. For that, we choose to work with incoming states for $x<0$ (lead index 1 and 2 in Fig. 4.17) and outgoing states for $x>L$ (lead index 3 and 4 in Fig. 4.17). In the approximation up to photon number $\overline{m}$, those are given by

$$\begin{aligned}
\psi^{\alpha}_{\mathrm{in},\overline{\mathrm{m}}}(x) &= M^{p}_{\overline{m}}(x,0)\left[D_{\overline{m},\alpha} + \mathbb{1}_{\overline{m}\times\overline{m}}\frac{(\eta_0\sigma_0 - \eta_z\sigma_z)}{2}S_{\overline{m},\alpha}\right],\\
\psi^{\alpha}_{\mathrm{out},\overline{\mathrm{m}}}(x) &= M^{p}_{m}(x,0)\left[\mathbb{1}_{\overline{m}\times\overline{m}}\frac{(\eta_0\sigma_0 + \eta_z\sigma_z)}{2}S_{\overline{m},\alpha}\right]
\end{aligned}$$

with

$$\begin{aligned}
S_{\overline{m},1} &= (t^{\overline{m}}_{31}(\epsilon), r^{\overline{m}}_{11}(\epsilon), t^{\overline{m}}_{21}(\epsilon), t^{\overline{m}}_{41}(\epsilon), \ldots, t^{-\overline{m}}_{31}(\epsilon), r^{-\overline{m}}_{11}(\epsilon), t^{-\overline{m}}_{21}(\epsilon), t^{-\overline{m}}_{41}(\epsilon))^T,\\
S_{\overline{m},2} &= (t^{\overline{m}}_{32}(\epsilon), t^{\overline{m}}_{12}(\epsilon), r^{\overline{m}}_{22}(\epsilon), t^{\overline{m}}_{42}(\epsilon), \ldots, t^{-\overline{m}}_{32}(\epsilon), t^{-\overline{m}}_{12}(\epsilon), r^{-\overline{m}}_{22}(\epsilon), t^{-\overline{m}}_{42}(\epsilon))^T,\\
D_{\overline{m},\alpha} &= \sum_{l=1}^{4}\delta_{l,\alpha^2}\hat{e}^{(2\overline{m}+1)}_{\overline{m}+1}\otimes\hat{e}^{(4)}_{l},
\end{aligned}$$

where $\hat{e}^{(4)}_l$ are (4 dimensional) Cartesian basis vectors associated with the operators $\hat{C}_k$, while $\hat{e}^{(2\overline{m}+1)}_{\overline{m}+1}$ is a $(2\overline{m}+1$ dimensional) Cartesian basis vector associated to photon space. $\alpha\in\{1,2\}$ defines the lead index for incoming particles. The matrix $M^{p}_{\overline{m}}(x,0)$ is the transfer matrix calculated from the system without the potentials of the constriction, i.e.

$$M^{p}_{\overline{m}}(x,0) = \exp\left[\int_0^x \mathrm{d}x\frac{i}{v_F}P^{-1}_{\overline{m}}(\epsilon - \mathcal{Q}^{p}_{\overline{m}})\right]$$

with the matrix elements $[\mathcal{Q}^{p}_{\overline{m}}]_{k,l} = \delta_{k,l}k\omega$ for $|k|\leq|\overline{m}|$. The scattering amplitudes $r^{m}_{\alpha\alpha}(\epsilon)$ and $t^{m}_{\alpha\beta}(\epsilon)$ describe scattering processes that take into account an absorption (emission) of m photons, i. e. $r^{m}_{\alpha\alpha}(\epsilon) = r_{\alpha\alpha}(\epsilon + m\Omega,\epsilon)$.

Their values are obtained upon solving $M_{\overline{m}}(L,0)\psi^{\alpha}_{\mathrm{in},\overline{\mathrm{m}}}(0) = \psi^{\alpha}_{\mathrm{out},\overline{\mathrm{m}}}(L)$. Then, the different conductances can be obtained from Eq. (3.57). In particular, we identify two interesting transport regimes: (i) the local linear conductance in a single lead, given by

$$G^{\overline{m}}_{\alpha}(\epsilon) = \frac{e^2}{2\pi}[1 - \sum_{m=-\overline{m}}^{\overline{m}}|r^{m}_{\alpha\alpha}(\epsilon)|^2]. \tag{4.56}$$

(ii) The two-terminal conductance in both leftmost leads. Similar to the stationary case,

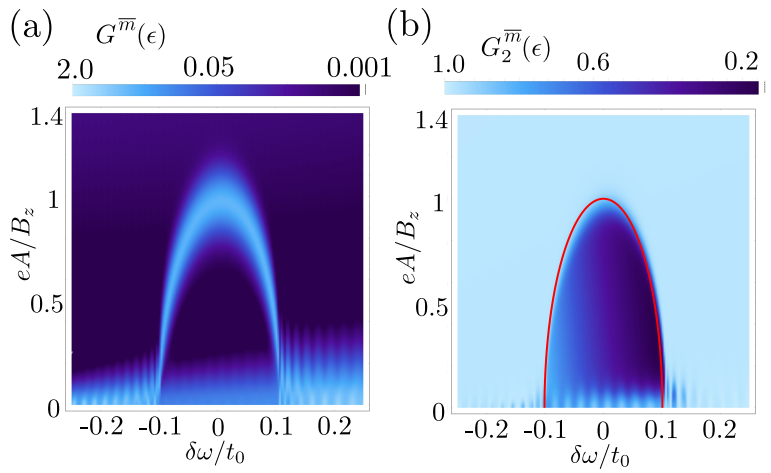

Figure 4.18: (a) Two terminal conductance evaluated from Eq. (4.57) and (b) four terminal conductance from Eq. (4.56) in units of $e^2/(2\pi)$ for quasi-energy $\epsilon = \sqrt{t_0^2 + t_c^2} - \delta\Omega$ and driving frequency $\Omega = 2(\sqrt{t_0^2 + t_c^2} - \delta\Omega)$. Additional parameters are $L = 27\ v_F/\gamma_0$, $\overline{m} = 10$, $v_F = 1$ and $t_0 = t_c = 1$. The red line corresponds to the gap-closing-reopening of the effective quasi-energy operator (Eq. (4.54)) indicating the topological phase transition. Reprinted figure with permission from Ref. [FZP+20]. Copyright 2020 by the American Physical Society.

in the latter case, contact 1 and 2 are treated as one lead 12. Again, scattering amplitudes are additionally labeled according to the edge into which they get reflected/transmitted (compare to Eq. (4.15)). Hence, we obtain for the two-terminal conductance

$$G^{\overline{m}}(\epsilon) = \frac{e^2}{2\pi}[2 - \sum_{m=-\overline{m}}^{\overline{m}} \sum_{j\in 1,2} |r^m_{12,12,\ j}(\epsilon)|^2]. \tag{4.57}$$

The results for the four-terminal ($G^{\overline{m}}_\alpha(\epsilon)$) as well as the two-terminal conductance ($G^{\overline{m}}(\epsilon)$) are shown in Fig. 4.18 (a)-(b). Both are evaluated for $\epsilon_r = 0$ with $\epsilon_r = \epsilon - \Omega/2$ and $\Omega = 2(\sqrt{t_0^2 + t_c^2} - \delta\Omega)$. For the case of vanishing driving amplitude eA, the conductance approaches its stationary value. By turning on a finite eA, small Floquet hybridization gaps are forming. In the regime $eA \ll (v_F/L)$, the decay length of the associated Floquet modes is expected to be larger than the length of the constriction. This results in an oscillating pattern, emerging from Fabry-Pérot resonances. Driving amplitudes in the regime $(v_F/L) < eA \ll \Omega$ block the two-terminal transport through the constriction. This results in zero conductance for sufficiently large constriction potentials (Fig. 4.18 (a)). Finite conductance is only restored close to the phase transition (see the light-blue curve). There, the spectral Floquet gap around $k = 0$ closes and allows a finite transmission through the constriction.

In case of a four terminal measurement, the two phases are more prominently separated: In the trivial phase, the conductance is fixed to $e^2/(2\pi)$ per channel, which implies the absence of backscattering in the channel of the incoming state. In this regime, TR symmetric processes dominate the physics and backscattering in the same channel is strongly

suppressed. When the system undergoes the Floquet topological transition by crossing the red line of Fig. 4.18 (b), perfect conductance quantization is lost since the scattering is dominated by the TR breaking Zeeman field. Then, the conductance significantly differs from $e^2/(2\pi)$. This unusual reflection is a direct consequence of a topological boundary state forming at the ends of the constriction at quasi-energy $\epsilon = \Omega/2$.

In topological systems, typically, distinct topological phases are distinguishable also in the two-terminal sector, such as it is for instance the case for SOC quantum wires or even QSH anti-wires, the stationary (superconducting) counterpart of the current model. This is different here. Topological and trivial regime produce exactly the same transport signature in the two-terminal sector for both phases. The reason for the indistinguishability of the topologically distinct phases in this transport sector is inbuilt in the particular coupling to the leads: Each helical edge is strongly coupled to the constricted region, however, only to half of the channels. This selective coupling directly affects the visibility of the topological phase. A convenient way to understand how this comes about is to investigate the complementary detection scheme shown in Fig. 4.17 (b). Additionally to the setup discussed before, we add TR invariant barriers of length L_{bar} and strength T_b at each end of the constriction. These barriers are described by the Hamiltonian

$$H_{\mathsf{barrier}} = T_b \Big[\int_{-L_{\mathsf{bar}}}^{0} \mathrm{d}x + \int_{L}^{L+L_{\mathsf{bar}}} \mathrm{d}x \Big] \Psi^\dagger(x) \eta_x \sigma_0 \Psi(x).$$

The resulting Hamiltonian exactly corresponds to the anti-wire model of the Sec. 4.3. The inclusion of the barriers has two effects: (i) The coupling to the leads is suppressed by a factor $\exp(-T_b L_{\mathsf{bar}}/v_F)$. (ii) The upper and lower helical edges merge at the barrier. Likewise, in the constriction, the developing boundary conditions for increasing barrier strength lead to a well defined eigenspectrum of the QSH QC. Then, as far as the two-terminal conductance is concerned, the weak coupling to the leads allows us to resolve these eigenstates. The results are shown in Fig. 4.19 (a-b). For weak coupling (see Fig. 4.19 (a)) the localized eigenstates within the QPC region are clearly visible in the two terminal conductance. In fact, around $eA/B_z = 1$, the Floquet gap closes and the system enters the topological phase for $eA/B_z < 1$, where a topological mid-gap state is formed. Note that as $eA \to 0$ yet another transition appears as the system becomes effectively static in this limit.

For finite eA, the physics is dominated by tunneling processes. This leads to an enhanced transmission, whenever the energy of the incoming particles matches a quasi-energy level in the weakly coupled driven anti-wire. For decreasing barrier strength T_b, the visibility of the topological BS is reduced as the system gets more and more coupled to each helical edge separately (Fig. 4.19 (b)). Then, a prominent signature is found in the conductance of an isolated helical edge as compared to the combined signal of two edges. Indeed, stronger coupling increases the visibility of the topological mid-gap state in the four-terminal conductance, where it appears as a finite reflection into the same channel at the resonant frequency (Fig. 4.19 (c-d)). This reflection can be interpreted as a direct consequence of the Floquet topological BSs that form at the ends of the driven anti-wire as we will subsequently demonstrate.

Having solved the scattering problem, we can visualize these topological BSs for the quasi-

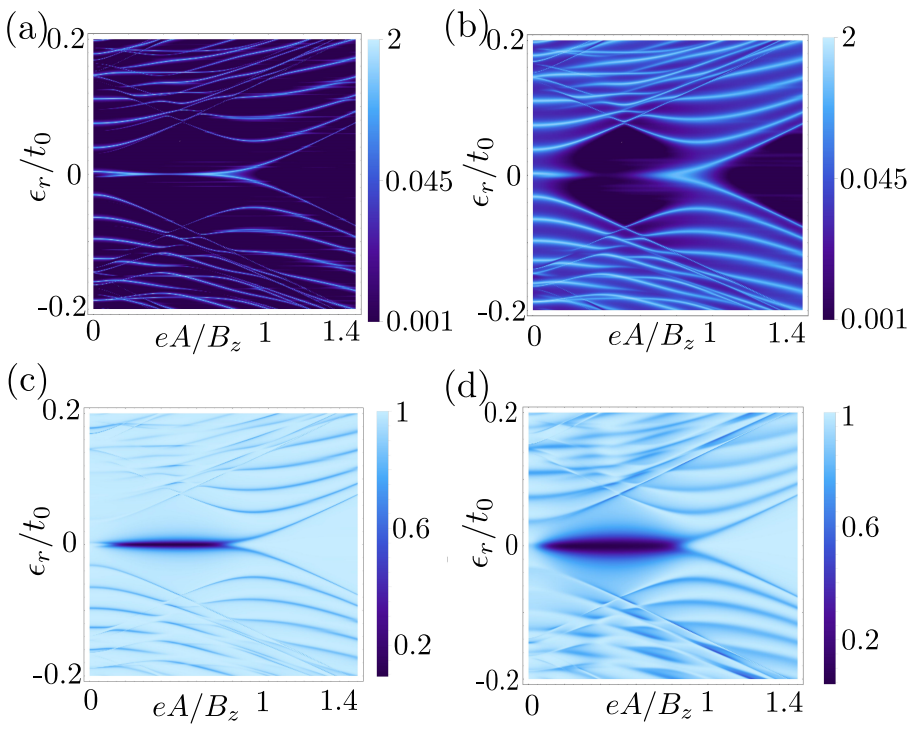

Figure 4.19: (a-b) Two-terminal and (c-d) four-terminal conductance in units of $e^2/(2\pi)$ through a decoupled QPC under the influence of driven electro-magnetic vector field eA. $\epsilon_r = \epsilon - \Omega/2$, $\Omega = 2\sqrt{t_0^2 + t_c^2}$, $L = 120\ v_F/t_0$, $L_{\text{bar}} = 1/2\ v_F/t_0$, $v_F = 1$, $\overline{m} = 5$, $t_0 = t_c$, $t_0 = 0.5$, $eA = 0.1$. Further parameter choices are (a) $T_b/t_0 = 10$, (b) $T_b/t_0 = 6$, (c) $T_b/t_0 = 6$, and (d) $T_b/t_0 = 4$. Reprinted figure with permission from Ref. [FZP+20]. Copyright 2020 by the American Physical Society.

open case with strong barriers, i. e. $T_b \gg t_0, t_c$. However, as we are working within the framework of an open system, we find a solution to the scattering problem for any ϵ and thus, strictly speaking, the notion of a BSs is not well defined in such systems. However, we can label a particular solution a BS when there is a local maximum that grows as the gap-inducing parameters, T_b, t_0 and t_c, are increased [FKTTZ18]. This ensures that such a state becomes a true BS with vanishing decay length in the limit of infinite gap strength. For our time-dependent problem, the solutions to the time-dependent Schrödinger equation are generically given by

$$\Psi_{\epsilon}^{\overline{m}}(x,t) = e^{-i\epsilon t} \sum_{m=-\overline{m}}^{\overline{m}} u_{\epsilon,m}^{\overline{m}}(x) e^{-im\Omega t},$$

where the Floquet mode $u_{\epsilon,m}^{\overline{m}}(x)$ of the photon sector m is the solution to the scattering problem at quasi-energy ϵ. We find that since $u_{\epsilon,m}^{\overline{m}}(x) \to 0$ already for moderately large m, the solution depends only weakly on time. Thus, for ease of illustration, we choose $t = 0$. The results are shown as a function of space and rescaled quasi-energy in Fig. 4.20. In the trivial regime (Fig. 4.20 (a)), the system is gapped and no mid-gap BSs appear. In turn, when the parameters are tuned to the topological regime, we find exponentially localized BSs at each end of the driven anti-wire (Fig. 4.20 (b)). Moreover, these topological boundary states possess a dominant spin projection perpendicular to the spin quantization axis of the underlying helical edge states (Fig. 4.20 (c)). Thus, when scattering into such states from the helical edge leads, the dominant process is not resonant tunneling but backscattering into the same channel. This is possible, since TR symmetry is explicitly broken in our system by the applied Zeeman field.
Although the Floquet topological BSs share some similarities with topological Majorana modes, they can only have a non-Abelian character under very specific conditions [KL13, TLK17]. Obviously, the most striking difference with respect to non-Abelian Majorana modes is that Floquet BSs are built from electrons of different bands, instead of electrons and holes in the Majorana case. Thus, in general, the operator γ_F, that is associated with such a BS, cannot obey $\gamma_F^\dagger = \gamma_F$ – the defining property of a non-Abelian Majorana. In other words, since zero-energy has no meaning in the absence of superconductivity, the Floquet BSs do, by no means, represent the ground state of the system. Hence, having such a state occupied or unoccupied makes a severe difference in contrast to the Majorana case. The only case, where a topological degeneracy is restored, is given when the chemical potential is exactly aligned with the quasi-energy of the topological Floquet BSs.

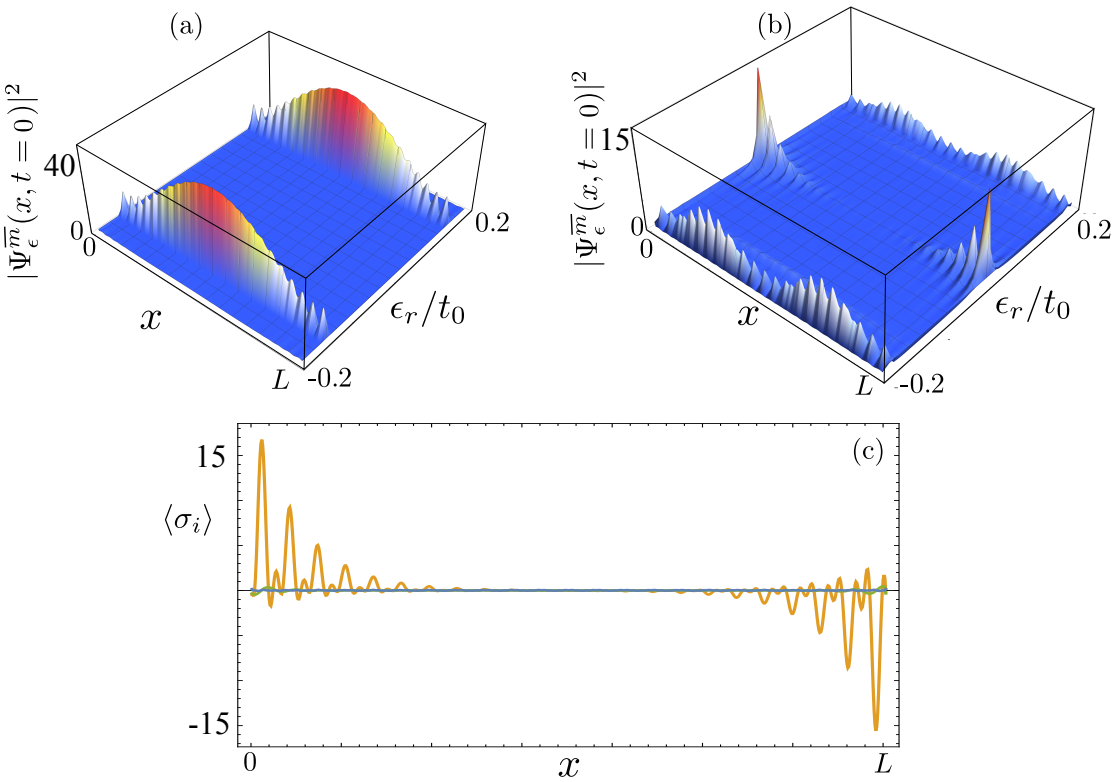

Figure 4.20: (a) Probability density according to Eq. (4.58) in units $t_0/(v_F)$, as a function of position and quasi-energy for $\overline{m} = 5$, $T_b = 5t_0$, $eA = 0.2t_0$, $B = 0.1t_0$, $t_c = t_0$ and $L = 35v_F/t_0$(b) Same as (a), with $\overline{m} = 5$, $T_b = 5t_0$, $eA = 0.1t_0$, $B = 0.2t_0$, $t_c = t_0$ and $L = 35v_F/t_0$ (c) Spin densities, green, orange and blue for the x, y, z components respectively, in units $t_0/(v_F)$, as a function of position. Other parameters as in panel (b). Reprinted figure with permission from Ref. [FZP+20]. Copyright 2020 by the American Physical Society.

4.6 $\mathbb{Z}_4$ parafermions in interacting superconducting quantum spin Hall quantum constrictions

The symmetries that are present in QSH edge theories take an important role not only for SP effects but in particular also when electronic interactions are considered. Notably, the existence of a Dirac point with $k_F = 0$ is a crucial property that leads to interesting physical implications. Namely, it allows the formation of interaction induced gaps for $k_F L \ll 1$, where L is the length on which a particular interaction term is present. Such interaction induced gaps can invoke high ground state degeneracies and eventually lead to parafermionic BSs in combination with s-wave SCs [OTMS15]. However, a central point of criticism that limits the experimental feasibility of parafermions is the required interaction strength. For instance, in Ref. [OTMS15] very strong interactions with a Luttinger parameter $K < 1/2$ are required to reach the regime where the desired gap terms constitute RG relevant perturbations. Even if such strong interactions could be reached at the helical edge, it is unlikely that it is possible to induce superconducting order, which is only RG relevant for $K > 1/2$.

Interestingly, QSH QCs provide room for an intriguing workaround of this problem. This ultimately originates from the increased number of fermionic fields that interact in the constricted region, which has two major effects: (i) TP scattering terms can now appear in various fashions. Typically, each of such terms gaps half of the free channels in the constriction. Thus, to entirely gap out the interacting constriction, at least two TP scattering terms of different kind will be needed. (ii) Each of these terms is RG relevant even for only weak repulsive electron-electron interactions. Consequently, weakly repulsive interacting QSH QCs simultaneously suffice as platform for both, superconducting order and TP scattering terms. In a hetero-junction built from superconducting and TP scattering regimes, a large ground state manifold forms, which eventually allows for a Majorana and a $\mathbb{Z}_4$ parafermion to form at interfaces.

While this looks very promising at first sight, there is a subtle point that needs to be treated carefully. Namely, from the analysis of the non-interacting QSH QC we know that, likely, there are naturally appearing TR invariant SP scattering terms (see Eqs. (4.2) and (4.3)). A RG analysis shows that in particular Eq. (4.2) also constitutes a relevant perturbation for weak repulsive interactions. This generates a problem: SP and TP terms invoke drastically different physical low energy properties (for instance in terms of ground state degeneracies). Thus, only one of the two kind of terms can dictate the low-energy properties. If both are RG relevant, typically the one that grows faster under RG flow dominates at low energies. In this naive ansatz, the SP terms dominate for most of the weakly interacting regime. However, the latter ansatz implies a roughly equal initial coupling strength of all terms under comparison. Fortunately, this does not have to be true here. The SP coupling terms emerge from wave function overlap. Thus, increasing the width of the constriction, they decay exponentially on length scales υ. The TP terms, on the other hand, emerge from long-range electron-electron interactions so that coupling constants decay only as a power-law. In that way, TP terms can dominate the SP hybridization terms in constrictions of width $w > \upsilon$. In the next sections we explain the underlying physics and mathematics of such systems carefully and follow closely the

analysis and results presented in Ref. [FTZT19].

4.6.1 Two-particle scattering in quantum spin Hall quantum constrictions

By definition, interactions always include at least two particles or, equivalently, four field operators. However, there are severe differences among the various possible TP interactions. The most common family of TP interactions are density-density interactions. In 1D systems of fermions, density-density interactions can be treated conveniently using bosonization (see Sec. 3.1). Then, the interacting theory of fermions becomes a non-interacting theory of bosons.
Due to the linear dispersion relation, QSH QCs, described by Eq. (4.1), are naturally predestined for bosonization. Using the formalism derived in Sec. 3.1 we can bosonize the effectively spinful fermionic theory of a QSH QC using the bosonization identity, written in terms of spin (σ) and charge (ρ) bosonic fields [Gia03]

$$\hat{\psi}_{r,\nu}(x) = \frac{\mathcal{F}_{r,\nu} e^{i\nu r k_F x}}{\sqrt{2\pi a}} e^{-\frac{i}{\sqrt{2}}\left[r\nu\hat{\phi}_\rho(x) - \hat{\theta}_\rho(x) + r\hat{\phi}_\sigma(x) - \nu\hat{\theta}_\sigma(x)\right]}, \tag{4.58}$$

where $r = 1,2 = +,-$ and $\nu = \uparrow,\downarrow = +,-$. $\mathcal{F}_{r,\nu}$ are Klein factors lowering the number of fermions by one. Moreover, a denotes a high-energy cutoff. The conjugate bosonic fields $\phi_{\rho/\sigma}(x)$, $\theta_{\rho/\sigma}(x)$ are linear combinations of bosonic fields on the upper and lower edge (designated by the indices 1 and 2): $\hat{\phi}_\rho = 1/\sqrt{2}(\hat{\phi}_1(x) + \hat{\phi}_2(x))$, $\hat{\phi}_\sigma = 1/\sqrt{2}(\hat{\theta}_2(x) - \hat{\theta}_1(x))$, $\hat{\theta}_\rho = 1/\sqrt{2}(\hat{\theta}_1(x) + \hat{\theta}_2(x))$, $\hat{\theta}_\sigma = 1/\sqrt{2}(\hat{\phi}_2(x) - \hat{\phi}_1(x))$. They obey the mutual commutation relations (compare also to Eq. (3.17))

$$\left[\hat{\phi}_\nu(x), \hat{\theta}_\mu(y)\right] = i\pi\ \theta(y-x)\delta_{\nu\mu}. \tag{4.59}$$

Including all kinds of density-density interactions, the Hamiltonian takes the form of Eq. (3.25)

$$H_{\mathrm{SLL}} = \frac{1}{2\pi} \sum_{\nu=\sigma,\rho} \int_{-L/2}^{L/2} \mathrm{d}x \left[\frac{u_\nu}{K_\nu} \left(\partial_x \hat{\phi}_\nu(x)\right)^2 + u_\nu K_\nu \left(\partial_x \hat{\theta}_\nu(x)\right)^2 \right]$$

with renormalized velocities u_ν and Luttinger interaction parameters K_ρ and K_σ characterizing the interaction strength. For helical Luttinger liquids, where spin-rotation invariance is broken, $K_\rho < 1$ and $K_\sigma > 1$ for repulsive interactions; likewise, $K_\rho > 1$ and $K_\sigma < 1$ for attractive interactions. For vanishing inter-edge interaction strength, the interaction parameters of both channels (charge and spin) are coupled to each other by $K_\rho = 1/K_\sigma \equiv K$ [HKC09]. If we switch on repulsive inter-edge interactions, we obtain $K_\rho < 1$ and $K_\sigma < 1/K$. On the other hand, if inter-edge interactions are equally strong compared to intra-edge interactions (this would correspond to the quantum wire situation), this implies $K_\sigma = 1$. Thus, as we deal with QCs of finite width, we expect to find K_σ ranging in between these two limits $1 < K_\sigma < 1/K$. Indeed, the fact that $K_\sigma \neq 1$ in our system has important implications for the formation of TP scattering terms that represent bosonic mass terms.

To be more concrete, there are two TP scattering terms that (i) preserve TR symmetry, (ii) are able to open a (partial) gap, and (iii) are relevant in the RG sense even for weak repulsive interactions. In fermionic representation, they are given by

$$H_{\text{um}} = \int \mathrm{d}x\ g_{\text{um}}(x)\hat{\psi}^{\dagger}_{R,\uparrow}(x)\hat{\psi}^{\dagger}_{R,\downarrow}(x)\hat{\psi}_{L,\downarrow}(x)\hat{\psi}_{L,\uparrow}(x) + \text{h.c.}, \tag{4.60}$$

$$H_{\text{pbs}} = \int \mathrm{d}x\ g_{\text{pbs}}(x)\hat{\psi}^{\dagger}_{R,\uparrow}(x)\hat{\psi}_{L,\downarrow}(x)\hat{\psi}^{\dagger}_{L,\uparrow}(x)\hat{\psi}_{R,\downarrow}(x) + \text{h.c.}. \tag{4.61}$$

Note that the Umklapp scattering term (4.60) [Gia03] is a spin-preserving process, while the pair backscattering term (4.61) [GJPB05, CT11, SKS13] requires breaking of axial spin symmetry [WBZ06]. Applying the bosonization identity (4.58) to Eqs. (4.60-4.61) and neglecting Klein factors, we obtain the bosonized Hamiltonians

$$H_{\text{um}} = \int \mathrm{d}x\ \tilde{g}_{\text{um}}(x)\cos[2\sqrt{2}\hat{\phi}_{\rho}(x) - 2\bar{k}_F x], \tag{4.62}$$

$$H_{\text{pbs}} = \int \mathrm{d}x\ \tilde{g}_{\text{pbs}}(x)\cos[2\sqrt{2}\hat{\theta}_{\sigma}(x) + 2\delta k_F x] \tag{4.63}$$

with $\tilde{g}_{\text{um}}(x) = g_{\text{um}}(x)/(2\pi^2 a^2)$, $\tilde{g}_{\text{pbs}}(x) = g_{\text{pbs}}(x)/(2\pi^2 a^2)$, $\bar{k}_F = (k_{F,1} + k_{F,2})$ and $\delta k_F = (k_{F,1} - k_{F,2})$, where $k_{F,1}$, $k_{F,2}$ represent the chemical potential in edge 1 and 2, respectively. Now, let us investigate the RG behavior of the above scattering terms. For that we can straightforwardly apply the perturbative RG approach for sine-Gordon models, described in detail in Sec. 3.1.6. Assuming that the couplings $\tilde{g}_{\text{um}}$ and $\tilde{g}_{\text{pbs}}$ are initially small, an one-loop RG analysis rescales them according to

$$\frac{\mathrm{d}y_{\text{um}}}{\mathrm{d}l} = (2 - 2K_{\rho})y_{\text{um}}, \tag{4.64}$$

$$\frac{\mathrm{d}y_{\text{pbs}}}{\mathrm{d}l} = (2 - 2/K_{\sigma})y_{\text{pbs}} \tag{4.65}$$

with the rescaled coupling constants $y_{\text{um}} = \tilde{g}_{\text{um}}/(\pi u_{\rho})$, $y_{\text{pbs}} = \tilde{g}_{\text{pbs}}/(\pi u_{\sigma})$, and the flow parameter l. Eq. (4.64) implies that H_{um} scales to strong coupling for the whole repulsively interacting regime $K_{\rho} < 1$. Likewise, Eq. (4.65) states the RG relevance of H_{pbs} for $K_{\sigma} > 1$. In the presence of electron-electron interactions, with the reasonable assumption that intra-edge interactions are stronger than inter-edge interactions, both conditions are satisfied.

4.6.2 Single-particle vs. two-particle scattering

From the discussions of the former sections, we know that there are two kinds of TR invariant SP scattering terms that are likely to appear in narrow QSH QCs. Thereby, Eq. (4.2) describes a hybridization of fermionic states with the same spin, that initially belong to different edges of the constriction. In contrast to that, Eq. (4.3) constitutes a forward scattering that allows particles to jump across the constriction, while keeping their propagation direction. In that sense, Eq. (4.3) might also be interpreted as an effective SOC term. The main difference between the two SP terms is that Eq. (4.2) opens a

spectral gap, while Eq. (4.3) does not.

In the language of bosonization, both terms resemble in a cosine form. However, this is not necessarily a contradiction to the behavior described above. Indeed, a cosine term in a bosonic theory does not a priori imply a spectral gap. Instead, what matters is whether the fields that are contained in the argument of the cosine can be pinned simultaneously in the same region of space, which is only possible if all contained fields commute[12]. Using the bosonization identity of Eq. (4.58) with neglecting Klein factors, we find

$$H_{t_0} = \int \mathrm{d}x\ \tilde{t}_0(x)\cos[\sqrt{2}\hat{\phi}_\rho(x) - \bar{k}_F x]\cos[\sqrt{2}\phi_\sigma(x)], \tag{4.66}$$

$$H_{t_c} = \int \mathrm{d}x\ \tilde{t}_c(x)\cos[\sqrt{2}\hat{\phi}_\sigma(x)]\cos[\sqrt{2}\hat{\theta}_\sigma(x)] \tag{4.67}$$

with $\tilde{t}_0(x) = 2t_0(x)/(\pi a)$ and $\tilde{t}_c(x) = 2t_c(x)/(\pi a)$. Evidently, while the fields in Eq. (4.66) can be pinned simultaneously in the same region of space, this is not equally possible for Eq. (4.67). In general, the pinning of bosonic fields is possible if the corresponding term constitutes a RG relevant perturbation and if it can be assumed that it dominates the low-energy physics (particularly in terms of ground states). In turn, terms that cannot be pinned are marginal for the low-energy properties of a system, especially in the presence of other terms that can be pinned. In that respect, we can exclude H_{t_c} from the following discussion of the ground states. H_{t_0}, on the other hand, cannot be excluded. In an one-loop RG analysis, we find for that term

$$\frac{\mathrm{d}y_\mathrm{t}}{\mathrm{d}l} = \left[2 - \frac{1}{2}(K_\rho + K_\sigma)\right] y_\mathrm{t} \tag{4.68}$$

with the rescaled coupling constant $y_\mathrm{t} = \tilde{t}_0/(\pi u_\sigma)$. Now, let us investigate the three first order RG equations (4.64) (4.65) and (4.68). First, let us assume we have $K_\sigma = 1/K_\rho$. Then, Eq. (4.68) flows to strong coupling provided $2 - \sqrt{3} < K_\rho < 2 + \sqrt{3}$. If we relax the relation of K_ρ and K_σ, we obtain the more general condition $K_\sigma + K_\rho < 4$. For instance, if $K_\sigma = 1$, which describes the situation in a quantum wire, we find $K_\rho < 3$ to obtain y_t as a relevant coupling. Apparently, however, there is a regime where all three scattering terms (Eqs. (4.62), (4.63) and (4.66)) simultaneously represent RG relevant perturbations.

This constitutes a problem because H_um and H_pbs commute with each other but both do not commute with H_{t_0}. Hence, they cannot be ordered simultaneously in the same region of space. Pinning of the bosonic fields in the strong coupling regime is thus only possible if either SP or TP scattering dominates the physics. In particular, for the emergence of parafermions, it is mandatory that at least one of the two TP scattering terms (H_um or H_pbs) provides the dominant interaction. As we will derive below, only then the required ground state degeneracy is present.

A convenient way to order the relative importance of different competing RG relevant perturbations is to compare their scaling dimensions. Under the assumption of initially small and roughly equal coupling constants, their growing rates, controlled by the scaling dimension, determine which term will dominate when the RG flow is eventually stopped.

[12] See also Sec. 2.4.4 for a detailed discussion on the pinning of bosonic fields.

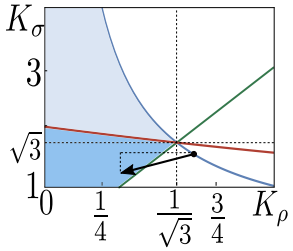

Figure 4.21: Illustration of the conditions obtained from the RG analysis of the various terms. The lines correspond to $K_\sigma = 3K_\rho$ (green), $K_\sigma = -K_\rho/2 + \sqrt{K_\rho^2/4+4}$ (red), $K_\sigma = 1/K_\rho$ (blue). The light and dark blue shaded areas mark the parameter regime where TP terms are RG-dominant. The black arrow indicates how the interaction parameters change when the case of isolated edge states is compared to the QC case. Reprinted figure with permission from Ref. [FTZT19]. Copyright 2020 by the American Physical Society.

This ordering produces the following inequalities between K_ρ and K_σ for the regime in parameter space where TP terms dominate the low-energy physics

$$K_\sigma > 3K_\rho, \tag{4.69}$$

$$K_\sigma > -K_\rho/2 + \sqrt{K_\rho^2/4+4}. \tag{4.70}$$

In particular, if Eq. (4.69) (Eq. (4.70)) is satisfied, then H_{um} (H_{pbs}) dominates over H_{t_0} in the RG sense. The conditions are illustrated in Fig. 4.21 in the K_ρ-K_σ plane. Together with the restrictions for K_σ ($1 < K_\sigma < 1/K_\rho$) as an additional bound, the shaded areas represent the parameter space for which at least one of the two TP processes dominates the low-energy physics. Remarkably, it is indeed sufficient that either H_{pbs} or H_{um} is more relevant than H_{t_0} to enable the formation of parafermions.
To be more precise, let us consider different scenarios. First, assume that H_{um} is the most relevant interaction, i. e. Eq. (4.69) is satisfied. Then, we first pin $\hat{\phi}_\rho(x)$ to minimize the contribution from the dominating term H_{um}. It turns out that for any eigenvalue of the resulting phase field $\hat{\phi}_\rho$, H_{t_0} vanishes exactly. Due to this property, we are subsequently also allowed to pin the bosonic field operators that characterize H_{pbs} .
For the second scenario, consider to have H_{pbs} stronger than H_{t_0}. Consequently, we introduce a phase field $\hat{\theta}_\sigma$. This in turn implies that H_{t_0} cannot be pinned anymore in the same region of space (on the basis of Eq. (4.59)) and eventually allows us to neglect H_{t_0} on the basis of energetics [KSYL13]. The lowest energy states, which are degenerate in the absence of H_{t_0}, are then obtained by pinning H_{um}.
Fig. 4.21 suggests that $K_\rho = 1/\sqrt{3}$ constitutes the upper bound such that TP backscattering dominates over SP scattering. This range of K_ρ still corresponds to rather strong Coulomb interactions. In particular, if this value is compared to the relevance condition of TP backscattering, which emerges at a single helical edge for $K < 1/2$ [OTMS15], we do not gain a significant advantage. However, note that we are comparing apples with oranges here, since K_ρ and K (the Luttinger parameter of single helical Luttinger liquid, i. e. a single helical edge) are different parameters. To actually compare the different relevance conditions, we need to reformulate all the conditions that ultimately result

in Fig. 4.21 in terms of K. In the absence of inter-edge interactions, K_ρ and K_σ are related by $K_\sigma = 1/K_\rho \equiv 1/K$ and are aligned on the blue curve in Fig. 4.21. By switching on the inter-edge interactions and starting from some point on the blue curve with $K = K_\rho > 1/\sqrt{3}$, we can at most reach the darker blue shaded region, since typically we expect to find $K_\rho < K$ and $K_\sigma < 1/K$ (Fig. 4.21). Thus, in principle, Eq. (4.69) can tolerate slightly larger values of K as compared to $1/\sqrt{3}$. To quantify this consideration, let us express the Luttinger parameters K_ρ and K_σ, given explicitly in Eq. (3.26), in terms of the Luttinger parameter K of an isolated helical edge

$$K_\rho = \sqrt{\frac{\tilde{g}_{4\perp} - \tilde{g}_{2\parallel} + (2 + \tilde{g}_{4\perp} - \tilde{g}_{2\parallel})K^2}{2 + \tilde{g}_{2\parallel} + \tilde{g}_{4\perp} + (\tilde{g}_{2\parallel} + \tilde{g}_{4\perp})K^2}}, \tag{4.71}$$

$$K_\sigma = \sqrt{\frac{2 - \tilde{g}_{2\parallel} - \tilde{g}_{4\perp} - (\tilde{g}_{2\parallel} + \tilde{g}_{4\perp})K^2}{\tilde{g}_{2\parallel} - \tilde{g}_{4\perp} + (2 + \tilde{g}_{2\parallel} - \tilde{g}_{4\perp})K^2}}, \tag{4.72}$$

where $\tilde{g}_\nu = g_\nu/(2\pi v_F)$ are the coupling constants of intra- and inter-edge interactions (see Eq. (3.24)). From inserting Eqs. (4.71) and (4.72) into Eq. (4.69), we obtain a relation for $g_{2\parallel}$ and $g_{4\perp}$ that depends on the initial value of K. Assuming $g_{2\parallel},\ g_{4\perp} \leq g_{2\perp}, g_{4\parallel}$ (i. e. $K_\sigma > 1$), we find that there is a parameter regime, such that Eq. (4.69) is fulfilled, up to $K \sim 0.65$. Nevertheless, there is still no substantial gain by these refined arguments in terms of a reduction of the required interaction strength.

Fortunately, there are two physical scenarios that lead to a dominance of TP backscattering over SP processes even in the regime $1/\sqrt{3} < K_\rho < 1$: (i) The coupling constants of the SP and TP terms have different physical origins. In fact it is very unlikely that the amplitude of all coupling constants are initially of the same magnitude, so that the simple comparison of the scaling dimensions remains a valid method to select the dominant scattering process. SP scattering is related to the overlap of the wave functions of edge states originating from different sides of the constriction. Thus, its coupling constant decays exponentially on length scales υ, which characterizes the decay of edges states towards the bulk of the QSH insulator. Contrary to that, the amplitude of TP scattering is related to Coulomb interactions following a power-law decay. Thus, we expect to find a geometric regime defined by the width w of the constriction such that $w > \upsilon$, where SP scattering can be neglected compared to TP scattering [DRT+10, BTM14]. Of course, this scenario requires sufficiently small chemical potentials, $\bar{k}_F \ll L^{-1}$ and $\delta k_F \ll L^{-1}$ with L being the length of the constriction, such that the effect of Eqs. (4.62-4.63) is not rendered ineffective due to spatial oscillations. (ii) In narrow QCs, the latter arguments do not apply. However, there we can profit from a finite $\bar{k}_F$. Assuming $w \leq \upsilon$, the electrostatic environment is expected to be approximately the same for both edges and consequently $\delta k_F = 0$. Then, a finite chemical potential only affects H_t and H_{um}, but leaves H_{pbs} invariant. If the flow is analyzed at fixed chemical potential, we find a finite chemical potential range in which H_t and H_{um} are still relevant [Gia03]. However, for $\bar{k}_F L \gtrsim \pi$ the energy contribution of these terms is reduced at least by a factor of $1/(\bar{k}_F L)$. This reduction shifts the power ratio of the different terms and can ultimately lead to a crossover for which H_{pbs} becomes the dominant scattering process.

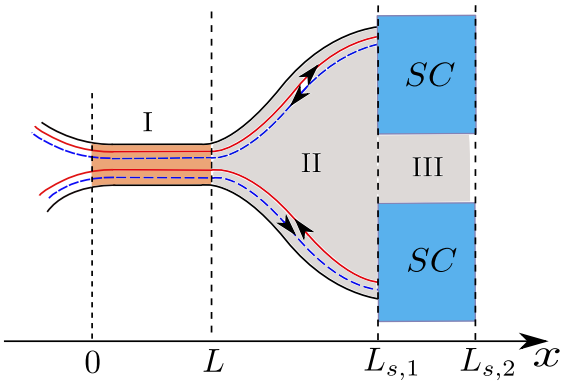

Figure 4.22: Schematic of the system: A QSH QC is brought in vicinity to two regions with proximity induced s-wave superconductivity. Reprinted figure with permission from Ref. [FTZT19]. Copyright 2020 by the American Physical Society.

4.6.3 Formation of $\mathbb{Z}_4$ parafermions

Ĺet us henceforth assume that TP scattering dominates the low-energy physics so that we can exclude SP scattering. For convenience and since the relative weight of $\tilde{g}_{\mathsf{um}}$ and $\tilde{g}_{\mathsf{pbs}}$ does not influence the number of existing minima of corresponding cosine potentials we choose $g_{\mathsf{pbs}}(x) = g_{\mathsf{um}}(x) = g(x)$. This allows us to reorganize Eqs. (4.62) and (4.63) into

$$H_{2\mathsf{p}} = H_{\mathsf{um}} + H_{\mathsf{pbs}} = \int \mathrm{d}x\ \tilde{g}(x) \cos[2\hat{\phi}_1(x)] \cos[2\hat{\phi}_2(x)] \tag{4.73}$$

with $\tilde{g}(x) = g(x)/(\pi^2 a^2)$. Let us focus on the setup sketched in Fig. 4.22. We consider three regimes characterized by different terms. The first regime extends from $x = 0$ to $x = L$ and defines the QSH QC. In this part of the system, TP scattering is active, and we assume $\tilde{g}(x) = \tilde{g}\theta(x)\theta(L-x)$. In the second regime with $L < x < L_{s,1}$, no gap-opening terms are present. Here the constriction evolves into isolated helical edge states. Finally, in the third regime, for $L_{s,1} < x < L_{s,2}$, we proximity induce s-wave superconductivity in each edge. In a BCS mean field approach, the latter is captured in fermionic form by Eq. (4.5) with $\Delta(x) = \Delta\theta(x - L_{s,1})\theta(L_{s,2} - x)$. In bosonic form, neglecting Klein factors, we obtain

$$H_\Delta = \int \mathrm{d}x\ \tilde{\Delta}(x) \Big\{ \cos\Big[2\hat{\theta}_1(x)\Big] + \cos\Big[2\hat{\theta}_2(x)\Big] \Big\} \tag{4.74}$$

with $\tilde{\Delta}(x) = \Delta(x)/(\pi a)$. For convenience, let us further assume the limit $L_{s,1} - L \to 0$. Then, assuming $1/2 < K, K_\rho < 1$, weak repulsive interactions i. e., both terms, Eq. (4.73) as well as Eq. (4.74), constitute RG relevant perturbations that each flow to strong coupling. Along the lines of the discussion presented in Sec. 2.4.4, the effective low-energy Hamiltonian then becomes[13]

$$H_{\mathsf{eff}} = H_{2\mathsf{p}} + H_\Delta = \int_0^L \mathrm{d}x\ \tilde{g} \cos[2\hat{\phi}_1] \cos[2\hat{\phi}_2] + \int_{L_{s,1}}^{L_{s,2}} \mathrm{d}x\ \tilde{\Delta} \Big\{ \cos\Big[2\hat{\theta}_1\Big] + \cos\Big[2\hat{\theta}_2\Big] \Big\},$$

[13] This assumes $L \to L_{s,1}$.

where we introduce the phase fields $\hat{\phi}_{1/2}$ and $\hat{\theta}_{1/2}$ that are defined on a circle $[0, 2\pi[$ (mod 2π) [ZK14]. Their eigenvalues correspond to the minima of the associated cosine. To find the ground state manifold, we have to count the different possibilities that *independently* minimize the above effective Hamiltonian. By doing so, we readily recognize that, since the TP scattering (present in region I) involves both edges, there is a strong correlation between $\hat{\phi}_1$ and $\hat{\phi}_2$. Indeed, minimization of Eq. (4.73) is achieved whenever one of the two cosines is maximized while the other is minimized. This constraint eventually condenses in the relation

$$\hat{\phi}_2 = -\hat{\phi}_1 - \pi/2 + \pi\hat{l}, \tag{4.75}$$

where $\hat{\phi}_1$ takes the eigenvalues $\phi_1 \in \{0, \pi/2, \pi, 3/2\pi\}$ and the integer valued operator $\hat{l}$ with eigenvalues $l \in \{1, 2\}$ (mod 2) relates $\hat{\phi}_1$ and $\hat{\phi}_2$. The commutation relations of the original fields (Eq. (4.59)) then imply

$$[\hat{l}, \hat{\theta}_1] = [\hat{l}, \hat{\theta}_2] = i, \quad [\hat{\phi}_1, \hat{\theta}_1] = i\pi, \quad [\hat{\phi}_1, \hat{\theta}_2] = 0, \quad [\hat{\phi}_1, \hat{l}] = [\hat{\phi}_2, \hat{l}] = 0.$$

Furthermore, with Eq. (4.75), the TP scattering term of Eq. (4.73) transforms into

$$H_{2p} = -\frac{\tilde{g}}{2} L \left(\cos[4\hat{\phi}_1 - 2\pi\hat{l}] + \cos[2\pi\hat{l}] \right).$$

Using the above form, the Hamiltonian looks familiar with respect to the ones that are typically required to design interface parafermionic BSs (compare for instance to Eq. (2.59)). The major difference in our case stems from the presence of the operator $\hat{l}$. Indeed, we can already guess the combined effect of $\hat{\phi}_1$ and $\hat{l}$ on the ground state manifold: Since $\hat{\phi}_1$ carries four eigenvalues it is likely that it will eventually invoke a $\mathbb{Z}_4$ parafermion. Likewise, $\hat{l}$ appears with two eigenvalues and, thus, this will result in an extra Majorana interface mode.

Let us be more concrete. We find that the operators $\{e^{i(\pi/2)\hat{S}}, e^{i\pi\hat{l}}\}$, where $\pi\hat{S} = \hat{\theta}_1 - \hat{\theta}_2$, commute with the Hamiltonian and among themselves. They induce the degenerate set of eigenstates $|s, l\rangle$, each of which obeying $e^{i(\pi/2)\hat{S}}|s, l\rangle = e^{i(\pi/2)s}|s, l\rangle$ and $e^{i\pi\hat{l}}|s, l\rangle = e^{i\pi l}|s, l\rangle$ with distinct eigenvalues $s \in \{0, 1, 2, 3\}$ (mod 4) and $l \in \{1, 2\}$ (mod 2). Given that, it is straightforward to demonstrate that the operators

$$\hat{\chi}_s = e^{i\pi/4} e^{i\hat{\phi}_1} e^{i\pi/2\hat{S}}, \quad \hat{\chi}_l = e^{-i/2(\hat{\theta}_1 + \hat{\theta}_2)} e^{i\pi\hat{l}} \tag{4.76}$$

commute with the effective Hamiltonian and describe creation operators on the ground state manifold spanned by the quantum numbers s and l

$$\hat{\chi}_s|s, l\rangle = e^{i(\pi/2)s}|s+1, l\rangle, \qquad \hat{\chi}_l|s, l\rangle = e^{-i(\pi/2)s} e^{i\pi l}|s, l+1\rangle. \tag{4.77}$$

In this representation, the operators obey the parafermionic exchange relations

$$\hat{\chi}_s \hat{\chi}_l = e^{i\pi/2} \hat{\chi}_l \hat{\chi}_s, \tag{4.78}$$

Then, from Eq. (4.77) we get that $\hat{\chi}_s^4 = 1$. Moreover, up to a $\hat{S}$ dependent phase, $\hat{\chi}_l^2$ acts as unity on the l-part of the ground state manifold. We can get rid of this phase by a

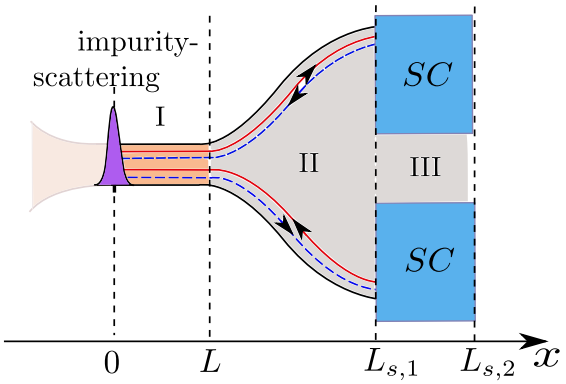

Figure 4.23: Schematic of the modified system: A QSH QC, pinched off by an impurity is brought in vicinity to two regions with proximity induced superconductivity. Reprinted figure with permission from Ref. [FTZT19]. Copyright 2020 by the American Physical Society.

simple gauge transformation $\hat{\chi}_l \to \tilde{\chi}_l = e^{-i(\pi/2)\hat{S}}\hat{\chi}_l$. Then, we also have $\tilde{\chi}_l^2 = 1$. Note that such a transformation does not change the role of $\tilde{\chi}_l$ as a creation operator of the quantum number l, however, the mutual exchange relation with $\hat{\chi}_s$ (Eq. (4.78)) transforms into the Majorana exchange relation

$$\hat{\chi}_s\tilde{\chi}_l = e^{i\pi}\tilde{\chi}\hat{\chi}_s.$$

The above relations imply the *simultaneous* presence of a $\mathbb{Z}_4$ parafermion ($\hat{\chi}_s$) as well as a Majorana mode ($\tilde{\chi}_l$). With $\hat{S}$ and $\hat{l}$, both operators contain phase fields that describe excitations on both edges of the constriction. Thus, the associated interface BSs constitute non-local objects, delocalized across the upper and lower edge of region II in Fig. 4.22.

Interestingly, we can get rid of this non-locality if we slightly modify the setup according to Fig. 4.23. The physical situation corresponds to a pinched off constriction, which is either realized by a strong impurity or a physical boundary of the structure. In either scenario, we can model it with a Hamiltonian similar to Eq. (4.6)

$$H_{\text{imp}}(x) = T_b \int \mathrm{d}x\ \delta(x) \sum_\sigma \left[\hat{\psi}^\dagger_{1,\sigma}(x)\hat{\psi}_{2,\sigma}(x) + \text{h.c.}\right].$$

In the limit $T_b \to \infty$, the above impurity Hamiltonian induces boundary conditions. Most conveniently, they can be derived in the fermionic picture, explicitly done in Sec. 4.3 (compare Eq. (4.9)). Eventually, we obtain

$$\hat{\psi}_{2,\uparrow}(x) = -i\hat{\psi}_{1,\uparrow}(-x), \qquad \hat{\psi}_{2,\downarrow}(x) = i\hat{\psi}_{1,\downarrow}(-x).$$

Adapting bosonization, the above relations imply that the number of Klein factors is reduced by half due to the boundary conditions. Then, together with the bosonization identity of Eq. (4.58), the above relations are straightforwardly translated into bosonic language as

$$\hat{\phi}_2(x) = -\hat{\phi}_1(-x) - \pi/2, \quad \hat{\theta}_2(x) = \hat{\theta}_1(-x). \tag{4.79}$$

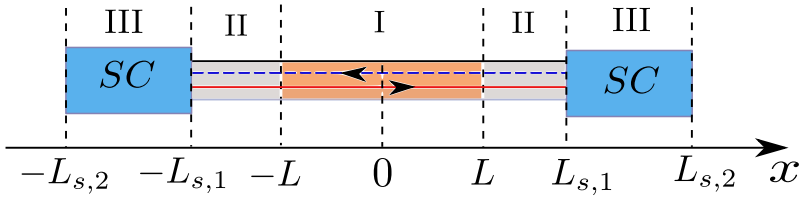

Figure 4.24: Schematic of the unfolded system in the presence of impurity scattering at $x = 0$. Reprinted figure with permission from Ref. [FTZT19]. Copyright 2020 by the American Physical Society.

Instead of the operator $\hat{l}$, now the boundary conditions enforce a correlation between the fields $\hat{\phi}_1(x)$ and $\hat{\phi}_2(x)$, however, the similarity to Eq. (4.75) is apparent.

Now, let us discuss the influence of Eq. (4.79) on the ground state manifold. The physical setup, depicted in Fig. 4.23, can be equivalently mathematically described by an *unfolded* model of the double system size sketched in Fig. 4.24. The resulting sine-Gordon model contains the following mass terms

$$\begin{aligned} H_\Delta &= H_{\Delta-} + H_{\Delta+} = \tilde{\Delta}\left[\int_{-L_{s,2}}^{-L_{s,1}} + \int_{L_{s,1}}^{L_{s,2}}\right] \mathrm{d}x \ \cos[2\hat{\theta}_1(x)], \\ H_{2\mathrm{p}} &= -\tilde{g}\int_{-L}^{L} \mathrm{d}x \ \cos[2\hat{\phi}_1(x)]\cos[2\hat{\phi}_1(-x)]. \end{aligned} \tag{4.80}$$

In general, Eq. (4.80) is difficult to treat due to its non-local nature. However, as we are only interested in the ground state properties of the system, the non-locality of Eq. (4.80) takes only a minor role. Indeed, minimization of Eq. (4.80) requires a constant field as any modulation as a function of space would add an energy $\propto \tilde{g}$ and push the system out of the ground state manifold. Thus, we have $\hat{\phi}_1(x) = \hat{\phi}_1(-x) = \hat{\phi}_1$. Hence, in combination with the superconducting phase fields $\hat{\theta}_\pm$, which refer to the SC right $(+)$ and left $(-)$ of the origin in Fig. 4.24, we obtain the effective Hamiltonians

$$\begin{aligned} H_{\Delta\pm} &= \tilde{\Delta}\,(L_{s,2} - L_{s,1})\cos[2\hat{\theta}_\pm], \\ H_{2\mathrm{p},j} &= -\tilde{g}_{\mathrm{pbs}} L\left(\cos[4\hat{\phi}_1] + 1\right). \end{aligned}$$

The relevant bosonic field operators obey the following commutation relations

$$[\hat{\phi}_1, \hat{\theta}_-] = 0, \qquad [\hat{\phi}_1, \hat{\theta}_+] = i\pi.$$

It is straightforward to demonstrate that the operators

$$\hat{\xi}_- = e^{i\hat{\phi}_1} e^{(i/2)\hat{\theta}_-}, \quad \hat{\xi}_+ = e^{i\hat{\phi}_1} e^{(i/2)\hat{\theta}_+}$$

commute with the Hamiltonian and obey the standard parafermionic exchange relations

$$\hat{\xi}_-\hat{\xi}_+ = e^{-i\pi/2}\hat{\xi}_+\hat{\xi}_-, \quad \hat{\xi}_\pm^4 = 1,$$

while they act as creation operators on the corresponding ground state manifold. In contrast to the case without boundary, the latter is reduced by a factor of two, which affects the operator $\hat{\chi}_l$ that is now obsolete. Indeed, the different ground states can be fully characterized by eigenstates of the fusion operator $\hat{\xi}_-^\dagger \hat{\xi}_+ = e^{(i/2)(\hat{\theta}_+ - \hat{\theta}_-)}$. Moreover, as a side effect, the parafermionic interface operators $\hat{\xi}_\pm$ are now purely local operators, bound in region II of Fig. 4.23 (Fig. 4.24 respectively), where each helical edge is occupied by a single parafermion.
From a more physical perspective, the change of the ground state manifold in the presence of an additional impurity can be understood as follows. In the scenario without boundary term, the system is actually not *complete* in the sense that we have neglected the discussion of a second Majorana-$\mathbb{Z}_4$-parafermion pair left of the constriction. This goes along the discussion of isolated Majorana modes (or likewise parafermionic modes) in heterojunctions. When we construct these exotic particles solely from (interacting) fermions, it is not possible to obtain an odd number of them, so that the total topological charge is fixed to an Abelian particle. In that sense, isolated non-Abelian excitations inevitably possess a displaced partner, which might eventually appear upon a compactification of the space. The addition of extra boundaries necessarily changes the way one can potentially compactify the space. For our specific case, this means that the world definitely ends at the impurity. Thus, one can only compactify the space towards the right. Eventually, we can adiabatically connect the (superconducting regions on the) upper and lower edge at $x \to \infty$ so that no extra boundaries emerge. Thus, the result of having two parafermions in the unfolded picture is reasonable.

4.6.4 Experimental signatures of interaction induced gaps

The immense comprehensiveness of QSH QCs and quantum point contacts (QPCs) equally inspires theorists and experimentalists. Recently, a very important step towards the understanding of such devices was accomplished by the experimental group of Laurens W. Molenkamp. They were able to use a novel nanostructuring method which allowed them to manufacture the first quantum point contact on the basis of HgTe based QSH insulators [SWF$^+$20]. This itself constitutes a major scientific breakthrough since the common way of designing QPCs, using purely electrostatic gating, is ineffective in QSH insulators due to Klein tunneling [KNG06]. Instead, one needs to physically carve the quantum point contact structure out of a homogeneous QSH insulator. To get to the interesting regime, i. e. the bulk band gap, where one expects to see the physics of the helical edge states, electrostatic gating is required. This, however, also hides some experimental impediments as the density of states strongly differs between the QPC region and the plain QSH insulator outside the quantum point contact. Thus, with a single gate extending over more than only the QPC, it is challenging to tune the parameters so that the chemical potential in the QPC and the surrounding QSH insulator are simultaneously positioned in the bulk band gap. This lead to the experimental setup, depicted in Fig. 4.25: A QPC on the basis of a QSH insulator that is gated in the regime of the QPC. This setup allows to measure the transport characteristics, such as the conductance, as a function of the applied gate voltage. Interestingly, this leads to three transport regimes for the two-terminal conductance (see Fig. 4.25 (c)): in the first, the typical QPC conductance steps in units of $2\mathrm{e}^2/\mathrm{h}$

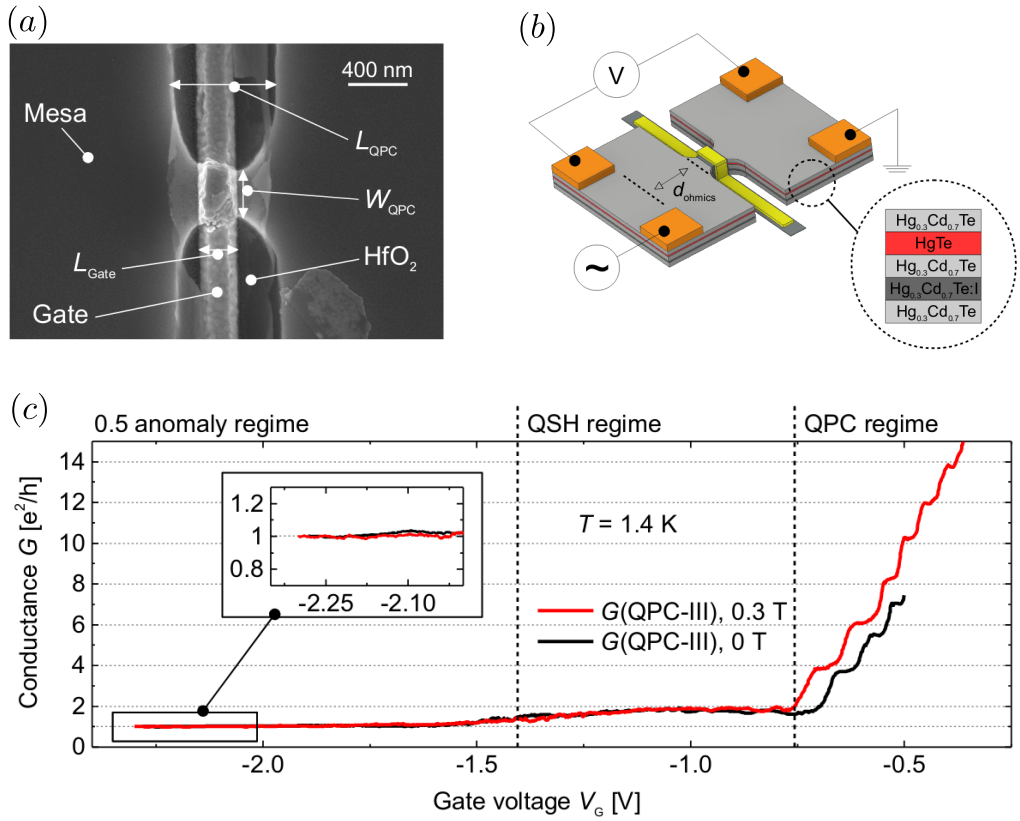

Figure 4.25: (a) SEM picture of the experimental system under investigation: A QSH QPC that is exposed to an externally applied gate over the extend of the QPC. (b) Schematic illustration of the QPC design and measurement setup. (c) Measured gate voltage dependence of the conductance at 1.4K performed on QPCs with quantum well thickness of $d_{\mathrm{QW}} = 10.5\mathrm{nm}$. Reprinted figure from Ref. [SWF+20].

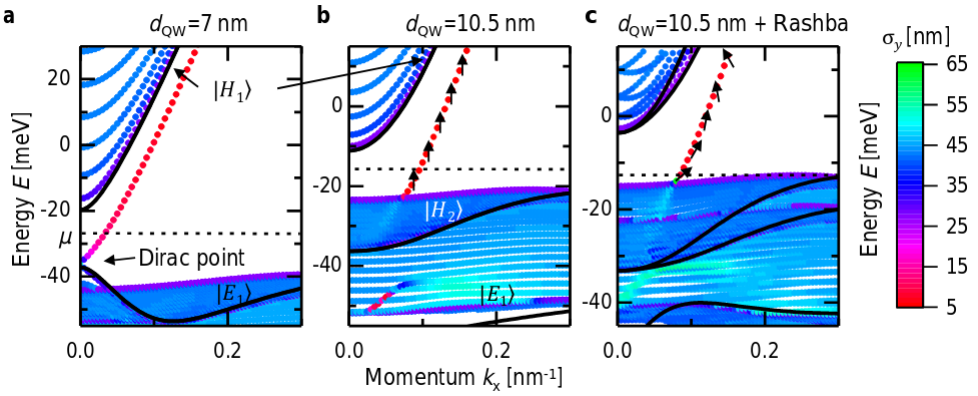

Figure 4.26: Band structure calculations for different quantum well thickness d_{QW}: black lines indicate the bulk band structure. The colored dots represent calculations performed on a finite ribbon with a width of 150nm in the y direction. The color code shows the wave function standard deviation σ_y in the y direction. Reprinted figure from Ref. [SWF+20].

(here we restore h for convenience) were observed [vWvHB+88]. With increasing applied gate voltage, consecutively less sub-bands contribute to the transport through the QPC. This continues until eventually the bulk band-gap is reached. There, as a characteristic of QSH insulators, the conductance is determined by the two remaining edge channels, resulting in a conductance of $2\mathrm{e}^2/\mathrm{h}$. Remarkably, as the gate voltage is further increased, an unexpected third transport regime is identified. There, the conductance drops to a stable value of $1\mathrm{e}^2/\mathrm{h}$ for a large regime of applied gate voltages[14]. As we will see below, this interesting and novel transport regime is difficult to explain on the SP level. However, there might be an explanation including interaction induced gaps.

The main reason why SP effects fail to explain the missing 1 e^2/h in the conductance is obtained from band structure calculations performed with realistic parameters on a HgTe based QSH insulator stripe that mimics the QPC (see Fig. 4.26). The main finding of this calculation is that the Dirac point of the helical edge states is buried deep inside the valence bulk bands, so that $k_F \sim 0.1$ nm^{-1} [15]. With a typical QPC length $L \sim 100 - 200$ nm, this implies that SP gap terms, such as for instance Eq. (4.2), cannot open a spectral gap as they should average out. Most prominently, this is seen from the bosonic form of Eq. (4.2), given in Eq. (4.66). H_{t_0} oscillates with a frequency of $2k_F$ as a function of space. Thus, having $k_F L \sim 10-20$ implies that 3-6 full periods fit in the gated QPC region. This renders SP gap-opening terms ineffective.

Indeed, this is a generic conclusion not specific to SP terms. Any gap-opening term that couples to k_F cannot be accountable for the conductance reduction. However, beyond SP physics, there are also gap-opening interaction terms that do *not* couple to k_F. Representatives of this class of interaction terms might thus be used to find an explanation of the

[14] A detailed discussion of the experiment is far beyond the scope of this thesis. Here we just summarize the main experimental results. For a more refined description, we refer the reader to Ref. [SWF+20].

[15] Note that $1\mathrm{e}^2/\mathrm{h}$ was only measured in samples with $d_{\mathrm{QW}} = 10.5$nm. A second series of samples with $d_{\mathrm{QW}} = 7$nm did not show this transport regime.

effect on the basis of helical edge states.

One of these terms is given by Eq. (4.61). It preserves the number of right- and left-movers and, hence, assuming the same chemical potential in each edge, effectively no momentum transfer emerges upon scattering according to Eq. (4.61). This is particularly evident from the bosonic form of Eq. (4.61), provided in Eq. (4.63). Assuming $\delta k_F \ll 1/L$, this term is insensitive to finite values of k_F and can, thus, also appear at large chemical potentials. Certainly, it is a necessary condition that a particular term can in principle appear, i. e. it is (for instance) not forbidden by symmetry constraints, yet this is not a sufficient condition on an equal footing. Interestingly, a sufficient condition for the presence of Eq. (4.63) can be directly deduced from the simultaneous presence of Rashba SOC within each edge in combination with ordinary inter-edge density-density interactions [Dol16]. Then, the coupling constant of Eq. (4.63) is related to the latter underlying effects by

$$g_{\text{pbs}} = \frac{1}{2}\sin^2\left[\arctan\left(\frac{\alpha_S}{v_F}\right)\right]\left(g_{2\parallel} - g_{4\perp}\right),$$

where α_S characterizes the coupling constant of Rashba SOC within each edge and $g_{2\parallel}$ and $g_{4\perp}$ are the corresponding inter-edge electron-electron interaction amplitudes (compare to Eq. (3.24)). Thus, in this approach, Eq. (4.61) only appears for $g_{2\parallel} \neq g_{4\perp}$ which relates to the absence of $SU(2)$ symmetry. More importantly, though, g_{pbs} grows for increasing Rashba SOC strength α_S. Rashba SOC, in turn, can emerge from externally applied electric fields. Thus, increasing the gate voltage enhances α_S and hence also g_{pbs}. To that effect, the band structures of Fig. 4.26 (b-c) hide an important subtlety: Increasing the gate voltage lowers the chemical potential until it eventually aligns with the bulk valence bands at high k_F. Then, due to the high density of states in those flat bands, a further increase of the gate voltage is pretty much ineffective and the chemical potential is pinned. Bulk-band transport in this regime is, however, sufficiently blocked due to the large momentum mismatch between valence and conduction bands, so that the only possible transport can happen via helical edge states.

This effect, typically coined *Fermi pinning* of the chemical potential, allows α_S and consequently g_{pbs} to grow significantly in the $d_{\text{QW}} = 10.5\text{nm}$ samples. Note in particular that in the $d_{\text{QW}} = 7\text{nm}$ samples, no such effect appears and also no conductance reduction to $1\text{e}^2/\text{h}$ emerges. But this is not the only consequence of the band structure calculations. A second conclusion that we obtain is that the localization length υ of the edge states is much smaller that than the width of the QPCs w. This subtle point ultimately allows us to recognize Eq. (4.63) in a charge transport experiment.

Eq. (4.63) depends only on the spin field $\hat{\theta}_\sigma(x)$. Thus, in a charge transport experiment performed on a quantum wire (or equivalently on a QPC with $\upsilon \sim w$) Eq. (4.63) does not lead to a conductance reduction although it blocks half of the channels. Here however, the situation is different. The strong localization of the edge states with $\upsilon \ll w$ allows us to treat each edge independently as particle transfer between the edges should be strongly suppressed. In this scenario, only correlated scattering processes that do not involve particle transfer among the edges matter. For Eq. (4.61), these describe backscattering processes: a right-mover in edge 1 is scattered into a left-mover of the same edge, where simultaneously in edge 2 a left-mover is scattered into a right-mover (see Fig. 4.27 (a)).

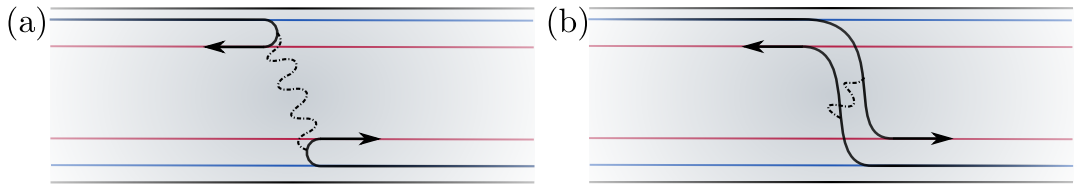

Figure 4.27: Schematic of the correlated scattering processes induced by Eq. (4.63). (a) correlated backscattering in each edge separately. (b) correlated forward scattering across the edges.

In turn, the second possible physical process, i. e. a right-mover in edge 1 is scattered into a right-mover in edge 2 and, simultaneously, a left-mover in edge 2 is scattered into a left-mover in edge 1 (see Fig. 4.27 (b)), should be suppressed. Then, the mass in half of the channels is indeed effective and reduces the conductance to $1\mathsf{e}^2/\mathsf{h}$.

5 Conclusion and outlook

5.1 Conclusion

In this thesis, we have demonstrated that QSH QCs are a powerful and comprehensive alternative to SOC quantum wires and are an eligible platform to show profound physics. In particular, such devices might be interpreted as symmetry enriched versions of quantum wires. In an effective low-energy theory, they are described by a $1+1$ dimensional Dirac theory of four fermions, distinguished by moving-direction and spin. Their main advantage over quantum wires originates from the existence of a charge-conjugation symmetric point in combination with the helical nature of isolated edge states. Eventually, this not only allows for a number of profound physical effects, but also to detect them by virtue of novel transport experiments, which directly make use of the helical nature of the leads.
On the SP level, TR invariant hybridization gaps can induce spectral properties that are closely related to the ones found in SOC quantum wires. Including s-wave superconductivity and magnetic Zeeman fields, this eventually leads to the formation of a topological superconducting phase. Such a phase typically comes along with isolated Majorana modes, located at the boundaries of the corresponding system. In QSH QCs, such boundaries can be constructed for a device design which we call QSH anti-wire – a narrow trench that is carved in an elsewhere homogeneous QSH sheet. Notably, it is not only possible to design topological superconductivity in QSH anti-wires, but also to unambiguous detect it by means of a simple transport experiment: the non-local conductance in a helical edge that is weakly coupled to the topological superconducting anti-wire. In particular, when it is coupled to a Majorana mode at *zero-energy*, where spin-up and spin-down states couple differently, then the non-local conductance changes sign and becomes negative. Essentially, this means that an incoming electron is transmitted as a hole, or in other words, an equal spin Cooper pair is injected into the superconducting condensate. Such a Cooper pair can possess very interesting and unconventional superconducting pairing symmetries. Indeed, topological superconductivity is inextricably linked with the appearance of unconventional superconductivity. In particular, odd-frequency pairing is profoundly related to Majorana modes. However, the relation is unilateral: the presence of Majorana modes implies the presence of odd-frequency pairing, but odd-frequency pairing is not sufficient to provide for isolated Majoranas. Nevertheless, odd-frequency superconductivity (i. e. superconducting pairing that behaves odd in its temporal arguments) already itself constitutes an intriguing piece of physics. In particular, a proof of odd-frequency superconductivity in a certain system certifies its potential for the formation of exotic quantum matter from many perspectives. Since we know that superconducting QSH QCs can serve as a platform for topological superconductivity, we expect to also find odd-frequency components. More unexpectedly, we can even find a transport signature that is related to this unconventional superconducting pairing regardless of the presence of Majorana modes: the non-local con-

ductance in a single edge, measured across a hetero-junction which is built from a s-wave SC and a QSH QC including SP scattering. By virtue of spin momentum locking, this transport channel is directly related to the creation of an equal spin Cooper pair in the hetero-junction. A symmetry analysis of the pairing amplitudes then shows that such a Cooper pair carries an even- as well as an odd-frequency component. In analogy to this finding, it is very likely that also the conductance signature used to identify the Majorana mode in the anti-wire model can equivalently serve as a direct evidence of odd-frequency pairing. The necessary step to prove this hypothesis is to explicitly compute the systems Green function and perform a full symmetry analysis of the pairing amplitudes.
Although topological superconductivity is a stationary phase of matter, by virtue of the existence of charge-conjugation symmetry, it is possible to mimic this intriguing phase of matter in QSH QCs in a non-stationary ansatz. The presence of a time-periodic electromagnetic field with the right frequency excites electronic states in the conduction band with negative energies to their charge-conjugated partner in the valence band with positive energies. In that way, particle-hole symmetry can be imitated. Then, the role of superconductivity is replaced by non-stationary Floquet hybridization gaps. In combination with applied (stationary) Zeeman fields, this eventually evokes to the formation of a Floquet topological phase, characterized by the presence of topologically protected Floquet end states. As zero-energy has no meaning in the absence of superconductivity, it is hardly surprising that these topological states appear at finite quasi-energy. In particular, they form at the quasi-energy of the dynamically created charge-conjugation symmetric point. Notably, the presence of these states can be directly seen in simple conductance measurements. Namely, as the Floquet topological states possess a dominant spin-projection perpendicular to the spin quantization axis of the helical edge states to which they are coupled from the outside, a backscattering appears, signaling their presence.
Electronic interactions significantly complexify the study of (topological) BSs in hetero-systems. This happens as a consequence of the reorganization of the Fock space. Relevant interactions are no longer of fermionic kind but carry a bosonic character. Isolated fermionic (bound) states are thus difficult to describe. However, the inclusion of electronic interactions also contains enormous potential, especially for the formation of more complex anyons beyond the Majorana. Thereby, the limiting factor is given by the ground state degeneracy. Without electronic interactions, 1D systems cannot show any other non-Abelian anyonic excitation than the Majorana. Even in the presence of interactions, this can be challenging for *purely* 1D systems (such as quantum wires are) by fundamental considerations as demonstrated by Fidkowski and Kitaev [FK11]. In turn, systems that emerge as a boundary theory from topological properties of a higher dimensional system are not constrained by Ref. [FK11]. In the latter scenario, interaction terms can induce a high, symmetry protected ground state manifold that enables the formation of parafermionic BSs in proximity to s-wave superconductivity. However, the typically strong interactions that are required to obtain the latter interactions as RG relevant perturbations often times constitutes a challenge and a main point of criticism. In QSH QCs, this criticism is definitely inappropriate. There, due to the increased number of fermions, gap-inducing interaction terms can appear as RG relevant perturbations even for only weak repulsive electron-electron interactions. In combination with superconductivity, this leads to the formation of an eightfold ground state degeneracy that makes room for the formation of

one parafermion and one Majorana mode, bound at the interfaces. Interestingly, recent transport experiments, performed on QSH QPCs indeed indicate the presence of interaction induced gaps in the form of a conductance reduction of an integer conductance quantum e^2/h. In particular, the term that we associate with this reduction takes also a central role for the formation of parafermions.

5.2 Outlook

Despite the findings presented in this thesis, many questions still search for their answers. QSH anti-wires constitute an eligible alternative platform for the formation of topological superconductivity. Moreover, we were able to find an unambiguous transport signature that proves the presence of Majorana modes. However, the immense potential of such nanostructures is by far not exhausted with these results. An open and interesting question would for instance be, whether one can find a signature that proves the topological separation of the Majorana modes (located at the ends of the anti-wire). Such a proof would clearly constitute a powerful proposal that goes far beyond existing ones. When it comes to the formation of parafermions in such structures it would further be an interesting question if (at all) there exists a transport signature that discriminates them from Majoranas. So far the only existing proposal addressing this question is given in Ref. [ZK14], where the authors describe a 8π-periodic Josephson effect in the presence of $\mathbb{Z}_4$ parafermions. The main reason for the lack of proposals in this direction is that parafermions are typically constructed as interface BSs and not as end modes of topological system. This emerges only partially from computational reasons. More conceptually, it is difficult to engineer ends in edge state based systems, inherent to a higher dimensional topological system. The anti-wire model constitutes an exception from that. Thus, from a conceptional point of view, one could consider the QSH anti-wire toy model setup (see Fig. 4.6), where the Majorana is replaced by a parafermion, and compute the conducting properties of this structure.

Acronyms

1D	one-dimensional
2D	two-dimensional
BCS	Bardeen-Cooper-Schrieffer (theory)
BdG	Bogoliubov-De-Gennes
BS	bound state
CAR	crossed Andreev reflection
EC	electron co-tunneling
PH	particle-hole
QC	quantum constriction
QPC	quantum point contact
QSH	quantum spin Hall
RG	renormalization group
SC	superconductor
SOC	spin-orbit coupled/coupling
SP	single-particle
TI	topological insulator
TP	two-particle
TR	time-reversal

Bibliography

[AAB+19] F. Arute, K. Arya, R. Babbush, D. Bacon, J. C. Bardin, R. Barends, R. Biswas, S. Boixo, F. G. S. L. Brandao, D. A. Buell, B. Burkett, Y. Chen, Z. Chen, B. Chiaro, R. Collins, W. Courtney, A. Dunsworth, E. Farhi, B. Foxen, A. Fowler, M. Gidney, C.and Giustina, R. Graff, K. Guerin, S. Habegger, M. P. Harrigan, M. J. Hartmann, A. Ho, M. Hoffmann, T. Huang, T. S. Humble, S. V. Isakov, E. Jeffrey, Z. Jiang, D. Kafri, K. Kechedzhi, J. Kelly, P. V. Klimov, S. Knysh, A. Korotkov, F. Kostritsa, D. Landhuis, M. Lindmark, E. Lucero, D. Lyakh, S. Mandrà, J. R. McClean, M. McEwen, A. Megrant, X. Mi, K. Michielsen, M. Mohseni, J. Mutus, O. Naaman, M. Neeley, C. Neill, M. Y. Niu, E. Ostby, A. Petukhov, J. C. Platt, C. Quintana, E. G. Rieffel, P. Roushan, N. C. Rubin, D. Sank, K. J. Satzinger, V. Smelyanskiy, K. J. Sung, M. D. Trevithick, A. Vainsencher, B. Villalonga, T. White, Z. J. Yao, P. Yeh, A. Zalcman, H. Neven, and J. M. Martinis. Quantum supremacy using a programmable superconducting processor. *Nature*, 574:505–510, 2019. doi:https://doi.org/10.1038/s41586-019-1666-5.

[AB59] Y. Aharonov and D. Bohm. Significance of Electromagnetic Potentials in the Quantum Theory. *Phys. Rev.*, 115:485–491, Aug 1959. doi:10.1103/PhysRev.115.485.

[ABC17a] J. Atteia, J. H. Bardarson, and J. Cayssol. Ballistic transport through irradiated graphene. *Phys. Rev. B*, 96:245404, Dec 2017. doi:10.1103/PhysRevB.96.245404.

[ABC17b] M. Avgerinou, P. Bertoldi, and L. Castellazzi. Trends in Data Centre Energy Consumption under the European Code of Conduct for Data Centre Energy Efficiency. *Energies*, 10:1470–1488, 2017. doi:10.3390/en10101470.

[ADB14] A. Alexandradinata, X. Dai, and B. A. Bernevig. Wilson-loop characterization of inversion-symmetric topological insulators. *Phys. Rev. B*, 89:155114, Apr 2014. doi:10.1103/PhysRevB.89.155114.

[ADH+11] A. R. Akhmerov, J. P. Dahlhaus, F. Hassler, M. Wimmer, and C. W. J. Beenakker. Quantized Conductance at the Majorana Phase Transition in a Disordered Superconducting Wire. *Phys. Rev. Lett.*, 106:057001, Jan 2011. doi:10.1103/PhysRevLett.106.057001.

[Adl69] S. L. Adler. Axial-Vector Vertex in Spinor Electrodynamics. *Phys. Rev.*, 177:2426–2438, Jan 1969. doi:10.1103/PhysRev.177.2426.

[AF16] J. Alicea and P. Fendley. Topological Phases with Parafermions: Theory and Blueprints. *Annual Review of Condensed Matter Physics*, 7(1):119–139, 2016. doi:10.1146/annurev-conmatphys-031115-011336.

[AGC+10] P. Adroguer, C. Grenier, D. Carpentier, J. Cayssol, P. Degiovanni, and E. Orignac. Probing the helical edge states of a topological insulator by Cooper-pair injection. *Phys. Rev. B*, 82:081303, Aug 2010. doi:10.1103/PhysRevB.82.081303.

[AGW09] A. Ahlbrecht, L. S. Georgiev, and R. F. Werner. Implementation of Clifford gates in the Ising-anyon topological quantum computer. *Phys. Rev. A*, 79:032311, Mar 2009. doi:10.1103/PhysRevA.79.032311.

[AHM+16a] D. Aasen, M. Hell, R. V. Mishmash, A. Higginbotham, J. Danon, M. Leijnse, T. S. Jespersen, J. A. Folk, C. M. Marcus, K. Flensberg, and J. Alicea. Milestones Toward Majorana-Based Quantum Computing. *Phys. Rev. X*, 6:031016, Aug 2016. doi:10.1103/PhysRevX.6.031016.

[AHM+16b] S. M. Albrecht, A. P. Higginbotham, M. Madsen, F. Kuemmeth, T. S. Jespersen, J. Nygård, P. Krogstrup, and C. M. Marcus. Exponential protection of zero modes in Majorana islands. *Nature*, 531(7593):206–209, Mar. 2016. doi:10.1038/nature17162.

[Ali12] J. Alicea. New directions in the pursuit of Majorana fermions in solid state systems. *Rep. Prog. Phys.*, 75:076501, 2012. doi:10.1088/0034-4885/75/7/076501.

[AOR+11] J. Alicea, Y. Oreg, G. Refael, F. von Oppen, and M. P. A. Fisher. Non-Abelian statistics and topological quantum information processing in 1D wire networks. *Nat. Phys.*, 7(5):412–417, May 2011. doi:10.1038/nphys1915.

[AT13] Y. Asano and Y. Tanaka. Majorana fermions and odd-frequency cooper pairs in a normal-metal nanowire proximity-coupled to a topological superconductor. *Phys. Rev. B*, 87:104513, Mar 2013. doi:10.1103/PhysRevB.87.104513.

[AZ97] A. Altland and M. R. Zirnbauer. Nonstandard symmetry classes in mesoscopic normal-superconducting hybrid structures. *Phys. Rev. B*, 55:1142–1161, Jan 1997. doi:10.1103/PhysRevB.55.1142.

[BBS10] M. Baraban, N. E. Bonesteel, and S. H. Simon. Resources required for topological quantum factoring. *Phys. Rev. A*, 81:062317, Jun 2010. doi:10.1103/PhysRevA.81.062317.

[BCNS10] P. Bonderson, D. J. Clarke, C. Nayak, and K. Shtengel. Implementing Arbitrary Phase Gates with Ising Anyons. *Phys. Rev. Lett.*, 104:180505, May 2010. doi:10.1103/PhysRevLett.104.180505.

[BCS57] J. Bardeen, L. N. Cooper, and J. R. Schrieffer. Theory of Superconductivity. *Phys. Rev.*, 108:1175–1204, Dec 1957. doi:10.1103/PhysRev.108.1175.

[BD07] C. J. Bolech and E. Demler. Observing Majorana bound States in p-Wave Superconductors Using Noise Measurements in Tunneling Experiments. *Phys. Rev. Lett.*, 98:237002, Jun 2007. doi:10.1103/PhysRevLett.98.237002.

[BDD+02] M. J. Bremner, C. M. Dawson, J. L. Dodd, A. Gilchrist, A. W. Harrow, D. Mortimer, M. A. Nielsen, and T. J. Osborne. Practical Scheme for Quantum Computation with Any Two-Qubit Entangling Gate. *Phys. Rev. Lett.*, 89:247902, Nov 2002. doi:10.1103/PhysRevLett.89.247902.

[Bee13] C. W. J. Beenakker. Search for Majorana Fermions in Superconductors. *Annual Review of Condensed Matter Physics*, 4(1):113–136, 2013. doi:10.1146/annurev-conmatphys-030212-184337.

[Bee15] C. W. J. Beenakker. Random-matrix theory of Majorana fermions and topological superconductors. *Rev. Mod. Phys.*, 87:1037–1066, Sep 2015. doi:10.1103/RevModPhys.87.1037.

[Ber74] V. L. Berezinskii. New model of the anisotropic phase of superfluid He^3. *JETP Lett.*, 20:287–289, 1974.

[Ber84] M. V. Berry. Quantal Phase Factors Accompanying Adiabatic Changes. *Proc. R. Soc. London A*, 392:45–57, Mar 1984. doi:10.1098/rspa.1984.0023.

[BF28] M. Born and V. Fock. Beweis des Adiabatensatzes. *Zeitschrift für Physik*, 51:165–180, Jan 1928. doi:10.1007/BF01343193.

[BHM11] D. M. Badiane, M. Houzet, and J. S. Meyer. Nonequilibrium Josephson Effect through Helical Edge States. *Phys. Rev. Lett.*, 107:177002, Oct 2011. doi:10.1103/PhysRevLett.107.177002.

[BHZ06] B. A. Bernevig, T. L. Hughes, and S.-C. Zhang. Quantum spin Hall effect and topological phase transition in HgTe quantum wells. *Science*, 314:1757–1761, 2006. doi:10.1126/science.1133734.

[BHZS05] N. E. Bonesteel, L. Hormozi, G. Zikos, and S. H. Simon. Braid Topologies for Quantum Computation. *Phys. Rev. Lett.*, 95:140503, Sep 2005. doi:10.1103/PhysRevLett.95.140503.

[BIS+18] S. Boixo, S. V. Isakov, V. N. Smelyanskiy, R. Babbush, N. Ding, Z. Jiang, M. J. Bremner, J. M. Martinis, and H. Neven. Characterizing quantum supremacy in near-term devices. *Nat. Phys.*, 14:595–600, Jun 2018. doi:10.1038/s41567-018-0124-x.

[BJ69] J. S. Bell and R. Jackiw. A PCAC puzzle: $\pi^0 \to \gamma\gamma$ in the σ-model. *Il Nuovo Cimento A (1965-1970)*, 60:47–61, 1969. doi:10.1007/BF02823296.

[Bog58] N. Bogoljubov. On a new method in the theory of superconductivity. *Nuovo Cimento*, 7:794–805, 1958. doi:10.1007/BF02745585.

[Bra06] S. Bravyi. Universal quantum computation with the $\nu = 5/2$ fractional quantum Hall state. *Phys. Rev. A*, 73:042313, Apr 2006. doi:10.1103/PhysRevA.73.042313.

[BSH+18] K. Bendias, S. Shamim, O. Herrmann, A. Budewitz, P. Shekhar, P. Leubner, J. Kleinlein, E. Bocquillon, H. Buhmann, and L. W. Molenkamp. High Mobility HgTe Microstructures for Quantum Spin Hall Studies. *Nano Letters*, 18(8):4831–4836, Aug 2018. doi:10.1021/acs.nanolett.8b01405.

[BTM14] J. C. Budich, B. Trauzettel, and P. Michetti. Time Reversal Symmetric Topological Exciton Condensate in Bilayer HgTe Quantum Wells. *Phys. Rev. Lett.*, 112:146405, Apr 2014. doi:10.1103/PhysRevLett.112.146405.

[BVE01] F. S. Bergeret, A. F. Volkov, and K. B. Efetov. Josephson current in superconductor-ferromagnet structures with a nonhomogeneous magnetization. *Phys. Rev. B*, 64:134506, Sep 2001. doi:10.1103/PhysRevB.64.134506.

[BVE05] F. S. Bergeret, A. F. Volkov, and K. B. Efetov. Odd triplet superconductivity and related phenomena in superconductor-ferromagnet structures. *Rev. Mod. Phys.*, 77:1321–1373, Nov 2005. doi:10.1103/RevModPhys.77.1321.

[Bü86] M. Büttiker. Four-Terminal Phase-Coherent Conductance. *Phys. Rev. Lett.*, 57:1761–1764, Oct 1986. doi:10.1103/PhysRevLett.57.1761.

[Bü92] M. Büttiker. Scattering theory of current and intensity noise correlations in conductors and wave guides. *Phys. Rev. B*, 46:12485–12507, Nov 1992. doi:10.1103/PhysRevB.46.12485.

[CAJ+15] W. Chang, S. M. Albrecht, T. S. Jespersen, F. Kuemmeth, P. Krogstrup, J. Nygård, and M. C. M. Hard gap in epitaxial semiconductor–superconductor nanowires. *Nature Nanotechnology*, 10:231–236, Mar 2015. doi:10.1038/nnano.2014.306.

[Car96] J. Cardy. *Scaling and Renormalization in Statistical Physics*. Cambridge University Press, 1996.

[CAS13] D. J. Clarke, J. Alicea, and K. Shtengel. Exotic non-Abelian anyons from conventional fractional quantum Hall states. *Nat. Comm.*, 4:1348, Aug 2013. doi:10.1038/ncomms2340.

[CBT15] F. Crépin, P. Burset, and B. Trauzettel. Odd-frequency triplet superconductivity at the helical edge of a topological insulator. *Phys. Rev. B*, 92:100507, Sep 2015. doi:10.1103/PhysRevB.92.100507.

[CMA18] A. Chew, D. F. Mross, and J. Alicea. Fermionized parafermions and symmetry-enriched Majorana modes. *Phys. Rev. B*, 98:085143, Aug 2018. doi:10.1103/PhysRevB.98.085143.

[CMSS18] A. Calzona, T. Meng, M. Sassetti, and T. L. Schmidt. $\mathbb{Z}_4$ parafermions in one-dimensional fermionic lattices. *Phys. Rev. B*, 98:201110, Nov 2018. doi:10.1103/PhysRevB.98.201110.

[CMT93] P. Coleman, E. Miranda, and A. Tsvelik. Possible realization of odd-frequency pairing in heavy fermion compounds. *Phys. Rev. Lett.*, 70:2960–2963, May 1993. doi:10.1103/PhysRevLett.70.2960.

[CO14] E. Cobanera and G. Ortiz. Fock parafermions and self-dual representations of the braid group. *Phys. Rev. A*, 89:012328, Jan 2014. doi:10.1103/PhysRevA.89.012328.

[CSH+18] D. Chevallier, P. Szumniak, S. Hoffman, D. Loss, and J. Klinovaja. Topological phase detection in Rashba nanowires with a quantum dot. *Phys. Rev. B*, 97:045404, Jan 2018. doi:10.1103/PhysRevB.97.045404.

[CT11] M. Cheng and H.-H. Tu. Majorana edge states in interacting two-chain ladders of fermions. *Phys. Rev. B*, 84:094503, Sep 2011. doi:10.1103/PhysRevB.84.094503.

[CT17] G. Carleo and M. Troyer. Solving the quantum many-body problem with artificial neural networks. *Science*, 355:602–606, 2017. doi:10.1126/science.aag2302.

[CTSR16] C.-K. Chiu, J. C. Y. Teo, A. P. Schnyder, and S. Ryu. Classification of topological quantum matter with symmetries. *Rev. Mod. Phys.*, 88:035005, Aug 2016. doi:10.1103/RevModPhys.88.035005.

[DGY+74] R. Dennard, F. Gaensslen, H.-N. Yu, V. Rideout, E. Bassous, and A. Leblanc. Design of Ion-Implanted MOSFET's with Very Small Physical Dimensions. *Solid-State Circuits, IEEE*, 9, 10 1974. doi:10.1109/JSSC.1974.1050511.

[Dol11] F. Dolcini. Full electrical control of charge and spin conductance through interferometry of edge states in topological insulators. *Phys. Rev. B*, 83:165304, Apr 2011. doi:10.1103/PhysRevB.83.165304.

[Dol16] Dolcetto, G. and Sassetti, M. and Schmidt, T. L. Edge physics in two-dimensional topological insulators. *Riv. Nuovo Cim.*, 39:113–154, 2016. doi:10.1393/ncr/i2016-10121-7.

[DRT+10] F. Dolcini, D. Rainis, F. Taddei, M. Polini, R. Fazio, and A. H. MacDonald. Blockade and Counterflow Supercurrent in Exciton-Condensate Josephson Junctions. *Phys. Rev. Lett.*, 104:027004, Jan 2010. doi:10.1103/PhysRevLett.104.027004.

[DSFN05] S. Das Sarma, M. Freedman, and C. Nayak. Topologically Protected Qubits from a Possible Non-Abelian Fractional Quantum Hall State. *Phys. Rev. Lett.*, 94:166802, Apr 2005. doi:10.1103/PhysRevLett.94.166802.

[DSFN15] S. Das Sarma, M. Freedman, and C. Nayak. Majorana zero modes and topological quantum computation. *npj Quantum Inf.*, 1:15001, Oct 2015. doi:10.1038/npjqi.2015.1.

[DSNT06] S. Das Sarma, C. Nayak, and S. Tewari. Proposal to stabilize and detect half-quantum vortices in strontium ruthenate thin films: Non-Abelian braiding statistics of vortices in a $p_x + ip_y$ superconductor. *Phys. Rev. B*, 73:220502, Jun 2006. doi:10.1103/PhysRevB.73.220502.

[EA15] A. Eckardt and E. Anisimovas. High-frequency approximation for periodically driven quantum systems from a Floquet-space perspective. *New Journal of Physics*, 17(9):093039, sep 2015. doi:10.1088/1367-2630/17/9/093039.

[Ein24] A. Einstein. Quantentheorie des einatomigen idealen Gases. *Königliche Preußische Akademie der Wissenschaften. Sitzungsberichte*, pages 261–267, 1924.

[FDG10] Z. Fan and H. De Garis. Braid matrices and quantum gates for Ising anyons topological quantum computation. *Eur. Phys. J. B*, 74:419–427, Mar 2010. doi:10.1140/epjb/e2010-00087-4.

[FDTZT18] C. Fleckenstein, F. Domínguez, N. Traverso Ziani, and B. Trauzettel. Decaying spectral oscillations in a Majorana wire with finite coherence length. *Phys. Rev. B*, 97:155425, Apr 2018. doi:10.1103/PhysRevB.97.155425.

[FGSJ18] F. Finocchiaro, F. Guinea, and P. San-Jose. Topological π Junctions from Crossed Andreev Reflection in the Quan-

tum Hall Regime. *Phys. Rev. Lett.*, 120:116801, Mar 2018. doi:10.1103/PhysRevLett.120.116801.

[FJK11] L. Fidkowski, T. S. Jackson, and I. Klich. Model Characterization of Gapless Edge Modes of Topological Insulators Using Intermediate Brillouin-Zone Functions. *Phys. Rev. Lett.*, 107:036601, Jul 2011. doi:10.1103/PhysRevLett.107.036601.

[FK06] L. Fu and C. L. Kane. Time reversal polarization and a Z_2 adiabatic spin pump. *Phys. Rev. B*, 74:195312, Nov 2006. doi:10.1103/PhysRevB.74.195312.

[FK07] L. Fu and C. L. Kane. Topological insulators with inversion symmetry. *Phys. Rev. B*, 76:045302, Jul 2007. doi:10.1103/PhysRevB.76.045302.

[FK08] L. Fu and C. L. Kane. Superconducting Proximity Effect and Majorana Fermions at the Surface of a Topological Insulator. *Phys. Rev. Lett.*, 100:096407, Mar 2008. doi:10.1103/PhysRevLett.100.096407.

[FK09] L. Fu and C. L. Kane. Josephson current and noise at a superconductor/quantum-spin-Hall-insulator/superconductor junction. *Phys. Rev. B*, 79:161408, Apr 2009. doi:10.1103/PhysRevB.79.161408.

[FK11] L. Fidkowski and A. Kitaev. Topological phases of fermions in one dimension. *Phys. Rev. B*, 83:075103, Feb 2011. doi:10.1103/PhysRevB.83.075103.

[FKM07] L. Fu, C. L. Kane, and E. J. Mele. Topological Insulators in Three Dimensions. *Phys. Rev. Lett.*, 98:106803, Mar 2007. doi:10.1103/PhysRevLett.98.106803.

[FKTTZ18] C. Fleckenstein, F. Keidel, B. Trauzettel, and N. Traverso Ziani. The invisible Majorana bound state at the helical edge. *Eur. Phys. J. Spec. Top.*, 227:1377–1386, 2018. doi:10.1140/epjst/e2018-800093-5.

[Fra13] E. Fradkin. *Field Theories of Condensed Matter Physics*. Camebridge University Press, 2013.

[FTZCT20] C. Fleckenstein, N. Traverso Ziani, A. Calzona, and B. Trauzettel. Majorana bound states in quantum spin Hall slits. *arXiv:2001.03475*, 2020.

[FTZT19] C. Fleckenstein, N. Traverso Ziani, and B. Trauzettel. $\mathbb{Z}_4$ parafermions in Weakly Interacting Superconducting Constrictions at the Helical Edge of Quantum Spin Hall Insulators. *Phys. Rev. Lett.*, 122:066801, Feb 2019. doi:10.1103/PhysRevLett.122.066801.

[FW02] M. J. L. Freedman, M. H. and Z. Wang. A modular functor which is universal for quantum computation. *Commun. Math. Phys.*, 227:605–622, Jun 2002. doi:10.1007/s002200200645.

[FZP+20] C. Fleckenstein, N. T. Ziani, L. Privitera, M. Sassetti, and B. Trauzettel. Transport signatures of a Floquet topological transition at the helical edge. *Phys. Rev. B*, 101:201401, May 2020. doi:10.1103/PhysRevB.101.201401.

[FZT18] C. Fleckenstein, N. T. Ziani, and B. Trauzettel. Conductance signatures of odd-frequency superconductivity in quantum spin Hall systems using a quantum point contact. *Phys. Rev. B*, 97:134523, Apr 2018. doi:10.1103/PhysRevB.97.134523.

[Geo08] S. L. Georgiev. Towards a universal set of topologically protected gates for quantum computation with Pfaffian qubits. *Nuc. Phys. B*, 789:552–590, Feb 2008. doi:10.1016/j.nuclphysb.2007.07.016.

[Gia03] T. Giamarchi. *Quantum Physics in One Dimension*. Oxford University Press, 2003.

[GJPB05] V. Gritsev, G. Japaridze, M. Pletyukhov, and D. Baeriswyl. Competing Effects of Interactions and Spin-Orbit Coupling in a Quantum Wire. *Phys. Rev. Lett.*, 94:137207, Apr 2005. doi:10.1103/PhysRevLett.94.137207.

[GNT98] A. O. Gogolin, A. A. Nerseyan, and A. M. Tsvelik. *Bosonization and Strongly Correlated Systems*. Camebridge University Press, 1998.

[GRA05] V. Gurarie, L. Radzihovsky, and A. V. Andreev. Quantum Phase Transitions across a p-Wave Feshbach Resonance. *Phys. Rev. Lett.*, 94:230403, Jun 2005. doi:10.1103/PhysRevLett.94.230403.

[GWW91] M. Greiter, X.-G. Wen, and F. Wilczek. Paired Hall state at half filling. *Phys. Rev. Lett.*, 66:3205–3208, Jun 1991. doi:10.1103/PhysRevLett.66.3205.

[GWW92] M. Greiter, X.-G. Wen, and F. Wilczek. Paired Hall states. *Nuc. Phys. B*, 374:567–614, May 1992. doi:10.1016/0550-3213(92)90401-V.

[Hal81a] F. D. M. Haldane. Effective Harmonic-Fluid Approach to Low-Energy Properties of One-Dimensional Quantum Fluids. *Phys. Rev. Lett.*, 47:1840–1843, Dec 1981. doi:10.1103/PhysRevLett.47.1840.

[Hal81b] F. D. M. Haldane. 'Luttinger liquid theory' of one-dimensional quantum fluids. I. Properties of the Luttinger model and their extension to the general 1D interacting spinless Fermi gas. *Journal of Physics*

C: Solid State Physics, 14(19):2585–2609, jul 1981. doi:10.1088/0022-3719/14/19/010.

[Hal82] B. I. Halperin. Quantized Hall conductance, current-carrying edge states, and the existence of extended states in a two-dimensional disordered potential. *Phys. Rev. B*, 25:2185–2190, Feb 1982. doi:10.1103/PhysRevB.25.2185.

[Hal88] F. D. M. Haldane. Model for a Quantum Hall Effect without Landau Levels: Condensed-Matter Realization of the "Parity Anomaly". *Phys. Rev. Lett.*, 61:2015–2018, Oct 1988. doi:10.1103/PhysRevLett.61.2015.

[HBvOO15] A. Haim, E. Berg, F. von Oppen, and Y. Oreg. Current correlations in a Majorana beam splitter. *Phys. Rev. B*, 92:245112, Dec 2015. doi:10.1103/PhysRevB.92.245112.

[HBY10] W. J. Herrera, P. Burset, and A. L. Yeyati. A Green function approach to graphene–superconductor junctions with well-defined edges. *Journal of Physics: Condensed Matter*, 22(27):275304, Jun 2010. doi:10.1088/0953-8984/22/27/275304.

[HK10] M. Z. Hasan and C. L. Kane. Colloquium: Topological insulators. *Rev. Mod. Phys.*, 82:3045–3067, Nov 2010. doi:10.1103/RevModPhys.82.3045.

[HKC09] C.-Y. Hou, E.-A. Kim, and C. Chamon. Corner Junction as a Probe of Helical Edge States. *Phys. Rev. Lett.*, 102:076602, Feb 2009. doi:10.1103/PhysRevLett.102.076602.

[HL16] A. Hutter and D. Loss. Quantum computing with parafermions. *Phys. Rev. B*, 93:125105, Mar 2016. doi:10.1103/PhysRevB.93.125105.

[HMBG13] M. Houzet, J. S. Meyer, D. M. Badiane, and L. I. Glazman. Dynamics of Majorana States in a Topological Josephson Junction. *Phys. Rev. Lett.*, 111:046401, Jul 2013. doi:10.1103/PhysRevLett.111.046401.

[HNW13] M. B. Hastings, C. Nayak, and Z. Wang. Metaplectic anyons, Majorana zero modes, and their computational power. *Phys. Rev. B*, 87:165421, Apr 2013. doi:10.1103/PhysRevB.87.165421.

[HRC02] A. W. Harrow, B. Recht, and I. L. Chuang. Efficient discrete approximations of quantum gates. *J. Math. Phys.*, 43:4445, 2002. doi:10.1063/1.1495899.

[HTZC+17] S. Heedt, N. Traverso Ziani, F. Crépin, W. Prost, S. Trellenkamp, J. Schubert, D. Grützmacher, B. Trauzettel, and T. Schäpers. Signatures of interaction-induced helical gaps in nanowire quantum point contacts. *Nat. Phys.*, 13:563–567, Mar 2017. doi:10.1038/nphys4070.

[HWB15] Z. Huang, P. Wölfle, and A. V. Balatsky. Odd-frequency pairing of interacting Majorana fermions. *Phys. Rev. B*, 92:121404, Sep 2015. doi:10.1103/PhysRevB.92.121404.

[HWL15] A. Hutter, J. R. Wootton, and D. Loss. Parafermions in a Kagome Lattice of Qubits for Topological Quantum Computation. *Phys. Rev. X*, 5:041040, Dec 2015. doi:10.1103/PhysRevX.5.041040.

[HXQ+09] D. Hsieh, Y. Xia, D. Qian, L. Wray, F. Meier, J. H. Dil, J. Osterwalder, L. Patthey, A. V. Fedorov, H. Lin, A. Bansil, D. Grauer, Y. S. Hor, R. J. Cava, and M. Z. Hasan. Observation of Time-Reversal-Protected Single-Dirac-Cone Topological-Insulator States in Bi_2Te_3 and Sb_2Te_3. *Phys. Rev. Lett.*, 103:146401, Sep 2009. doi:10.1103/PhysRevLett.103.146401.

[HZBS07] L. Hormozi, G. Zikos, N. E. Bonesteel, and S. H. Simon. Topological quantum compiling. *Phys. Rev. B*, 75:165310, Apr 2007. doi:10.1103/PhysRevB.75.165310.

[IMR+15] F. Iemini, L. Mazza, D. Rossini, R. Fazio, and S. Diehl. Localized Majorana-Like Modes in a Number-Conserving Setting: An Exactly Solvable Model. *Phys. Rev. Lett.*, 115:156402, Oct 2015. doi:10.1103/PhysRevLett.115.156402.

[Jos62] B. D. Josephson. Possible new effects in superconductive tunnelling. *Phys. Lett.*, 1:251–253, Jul 1962. doi:10.1016/0031-9163(62)91369-0.

[JPA+11] L. Jiang, D. Pekker, J. Alicea, G. Refael, Y. Oreg, and F. von Oppen. Unconventional Josephson Signatures of Majorana Bound States. *Phys. Rev. Lett.*, 107:236401, Nov 2011. doi:10.1103/PhysRevLett.107.236401.

[JR76] R. Jackiw and C. Rebbi. Solitons with fermion number ½. *Phys. Rev. D*, 13:3398–3409, Jun 1976. doi:10.1103/PhysRevD.13.3398.

[Kat50] T. Kato. On the Adiabatic Theorem of Quantum Mechanics. *Journal of the Physical Society of Japan*, 5:435, 1950.

[KBM+08] M. König, H. Buhmann, L. W. Molenkamp, T. Hughes, C.-X. Liu, X.-L. Qi, and S.-C. Zhang. The Quantum Spin Hall Effect: Theory and Experiment. *Journal of the Physical Society of Japan*, 77(3):031007, 2008. doi:10.1143/JPSJ.77.031007.

[KBS14] V. Kliuchnikov, A. Bocharov, and K. M. Svore. Asymptotically Optimal Topological Quantum Compiling. *Phys. Rev. Lett.*, 112:140504, Apr 2014. doi:10.1103/PhysRevLett.112.140504.

[KDP80] K. v. Klitzing, G. Dorda, and M. Pepper. New Method for High-Accuracy Determination of the Fine-Structure Constant Based on Quantized Hall Resistance. *Phys. Rev. Lett.*, 45:494–497, Aug 1980. doi:10.1103/PhysRevLett.45.494.

[KDS11] I. Knez, R.-R. Du, and G. Sullivan. Evidence for Helical Edge Modes in Inverted InAs/GaSb Quantum Wells. *Phys. Rev. Lett.*, 107:136603, Sep 2011. doi:10.1103/PhysRevLett.107.136603.

[Kit01] A. Y. Kitaev. Unpaired Majorana fermions in quantum wires. *Physics-Uspekhi*, 44(10S):131–136, oct 2001. doi:10.1070/1063-7869/44/10s/s29.

[Kit03] A. Y. Kitaev. Fault-tolerant quantum computation by anyons. *Ann. Phys. (N.Y.)*, 303:2–30, 2003. doi:10.1016/S0003-4916(02)00018-0.

[Kit06] A. Kitaev. Anyons in an exactly solved model and beyond. *Ann. Phys. (N.Y.)*, 321:2–111, 2006. doi:10.1016/j.aop.2005.10.005.

[KL12] J. Klinovaja and D. Loss. Composite Majorana fermion wave functions in nanowires. *Phys. Rev. B*, 86:085408, Aug 2012. doi:10.1103/PhysRevB.86.085408.

[KL13] J. Klinovaja and D. Loss. Fractional Fermions with Non-Abelian Statistics. *Phys. Rev. Lett.*, 110:126402, Mar 2013. doi:10.1103/PhysRevLett.110.126402.

[KL14] J. Klinovaja and D. Loss. Time-reversal invariant parafermions in interacting Rashba nanowires. *Phys. Rev. B*, 90:045118, Jul 2014. doi:10.1103/PhysRevB.90.045118.

[KM05a] C. L. Kane and E. J. Mele. Quantum Spin Hall Effect in Graphene. *Phys. Rev. Lett.*, 95:226801, Nov 2005. doi:10.1103/PhysRevLett.95.226801.

[KM05b] C. L. Kane and E. J. Mele. Z_2 Topological Order and the Quantum Spin Hall Effect. *Phys. Rev. Lett.*, 95:146802, Sep 2005. doi:10.1103/PhysRevLett.95.146802.

[KMB12] G. Kells, D. Meidan, and P. W. Brouwer. Near-zero-energy end states in topologically trivial spin-orbit coupled superconducting nanowires with a smooth confinement. *Phys. Rev. B*, 86:100503, Sep 2012. doi:10.1103/PhysRevB.86.100503.

[KMP+19] D. M. Kennes, N. Müller, M. Pletyukhov, C. Weber, C. Bruder, F. Hassler, J. Klinovaja, D. Loss, and H. Schoeller. Chiral one-dimensional Floquet topological insulators beyond the rotating wave approximation. *Phys. Rev. B*, 100:041103, Jul 2019. doi:10.1103/PhysRevB.100.041103.

[KNG06] M. I. Katsnelson, K. S. Novoselov, and A. K. Geim. Chiral tunnelling and the Klein paradox in graphene. *Nat. Phys.*, 2:620–625, Jun 2006. doi:10.1038/nphys384.

[KPRvO15] T. Karzig, F. Pientka, G. Refael, and F. von Oppen. Shortcuts to non-Abelian braiding. *Phys. Rev. B*, 91:201102, May 2015. doi:10.1103/PhysRevB.91.201102.

[KSBT17] O. Kashuba, B. Sothmann, P. Burset, and B. Trauzettel. Majorana STM as a perfect detector of odd-frequency superconductivity. *Phys. Rev. B*, 95:174516, May 2017. doi:10.1103/PhysRevB.95.174516.

[KSV99] A. Y. Kitaev, A. H. Shen, and M. N. Vyalyi. *Classical and Quantum Computation*. American Mathematical Society, 1999.

[KSYL13] J. Klinovaja, P. Stano, A. Yazdani, and D. Loss. Topological Superconductivity and Majorana Fermions in RKKY Systems. *Phys. Rev. Lett.*, 111:186805, Nov 2013. doi:10.1103/PhysRevLett.111.186805.

[KT00] S. Kashiwaya and Y. Tanaka. Tunnelling effects on surface bound states in unconventional superconductors. *Reports on Progress in Physics*, 63(10):1641–1724, sep 2000. doi:10.1088/0034-4885/63/10/202.

[KWB+07] M. König, S. Wiedmann, C. Brüne, A. Roth, H. Buhmann, L. W. Molenkamp, X.-L. Qi, and S.-C. Zhang. Quantum spin Hall insulator state in HgTe quantum wells. *Science*, 318(5851):766–770, 2007. doi:10.1126/science.1148047.

[KYL14] J. Klinovaja, A. Yacoby, and D. Loss. Kramers pairs of Majorana fermions and parafermions in fractional topological insulators. *Phys. Rev. B*, 90:155447, Oct 2014. doi:10.1103/PhysRevB.90.155447.

[Lan57a] L. D. Landau. Oscillations in a Fermi Liquid. *Soviet Phys. JETP*, 5:101, 1957.

[Lan57b] L. D. Landau. The Theory of a Fermi Liquid. *Soviet Phys. JETP*, 3:920, 1957.

[Lau83] R. B. Laughlin. Anomalous Quantum Hall Effect: An Incompressible Quantum Fluid with Fractionally Charged Excitations. *Phys. Rev. Lett.*, 50:1395–1398, May 1983. doi:10.1103/PhysRevLett.50.1395.

[LB19] J. Linder and A. V. Balatsky. Odd-frequency superconductivity. *Rev. Mod. Phys.*, 91:045005, Dec 2019. doi:10.1103/RevModPhys.91.045005.

[LBRS12] N. H. Lindner, E. Berg, G. Refael, and A. Stern. Fractionalizing Majorana Fermions: Non-Abelian Statistics on the Edges of Abelian Quantum Hall States. *Phys. Rev. X*, 2:041002, Oct 2012. doi:10.1103/PhysRevX.2.041002.

[LBRT11] C.-X. Liu, J. C. Budich, P. Recher, and B. Trauzettel. Charge-spin duality in nonequilibrium transport of helical liquids. *Phys. Rev. B*, 83:035407, Jan 2011. doi:10.1103/PhysRevB.83.035407.

[LCD+14] J. Li, H. Chen, I. K. Drozdov, A. Yazdani, B. A. Bernevig, and A. H. MacDonald. Topological superconductivity induced by ferromagnetic metal chains. *Phys. Rev. B*, 90:235433, Dec 2014. doi:10.1103/PhysRevB.90.235433.

[LCL15] D. E. Liu, M. Cheng, and R. M. Lutchyn. Probing Majorana physics in quantum-dot shot-noise experiments. *Phys. Rev. B*, 91:081405, Feb 2015. doi:10.1103/PhysRevB.91.081405.

[LHQ+08] C. Liu, T. L. Hughes, X.-L. Qi, K. Wang, and S.-C. Zhang. Quantum Spin Hall Effect in Inverted Type-II Semiconductors. *Phys. Rev. Lett.*, 100:236601, Jun 2008. doi:10.1103/PhysRevLett.100.236601.

[LLM17] S.-P. Lee, R. M. Lutchyn, and J. Maciejko. Odd-frequency superconductivity in a nanowire coupled to Majorana zero modes. *Phys. Rev. B*, 95:184506, May 2017. doi:10.1103/PhysRevB.95.184506.

[LLN09] K. T. Law, P. A. Lee, and T. K. Ng. Majorana Fermion Induced Resonant Andreev Reflection. *Phys. Rev. Lett.*, 103:237001, Dec 2009. doi:10.1103/PhysRevLett.103.237001.

[LM77] J. M. Leinaas and J. Myrheim. On the theory of identical particles. *Il Nuovo Cimento B (1971-1996)*, 37:1–23, Jan 1977. doi:10.1007/BF02727953.

[LP93] H.-K. Lo and J. Preskill. Non-Abelian vortices and non-Abelian statistics. *Phys. Rev. D*, 48:4821–4834, Nov 1993. doi:10.1103/PhysRevD.48.4821.

[LP17] V. Lahtinen and J. K. Pachos. A Short Introduction to Topological Quantum Computation. *SciPost Phys.*, 3:021, 2017. doi:10.21468/SciPostPhys.3.3.021.

[LPBL16] J. Li, W. Pan, B. A. Bernevig, and R. M. Lutchyn. Detection of Majorana Kramers Pairs Using a Quantum Point Contact. *Phys. Rev. Lett.*, 117:046804, Jul 2016. doi:10.1103/PhysRevLett.117.046804.

[LSDS10] R. M. Lutchyn, J. D. Sau, and S. Das Sarma. Majorana Fermions and a Topological Phase Transition in Semiconductor-Superconductor Heterostructures. *Phys. Rev. Lett.*, 105:077001, Aug 2010. doi:10.1103/PhysRevLett.105.077001.

[LSDS18] C.-X. Liu, J. D. Sau, and S. Das Sarma. Distinguishing topological Majorana bound states from trivial Andreev bound states: Proposed tests through differential tunneling conductance spectroscopy. *Phys. Rev. B*, 97:214502, Jun 2018. doi:10.1103/PhysRevB.97.214502.

[Lut63] J. M. Luttinger. An Exactly Soluble Model of a Many-Fermion System. *J. Math. Phys.*, 4:1154–1162, 1963. doi:10.1063/1.1704046.

[Maj37] E. Majorana. Teoria simmetrica dell'elettrone e del positrone. *Il Nuovo Cimento (1924-1942)*, 14:171, 1937.

[Mal13] M. Malard. Sine-Gordon Model: Renormalization Group Solution and Applications. *Braz. J. Phys.*, 43:182–198, Mar 2013. doi:10.1007/s13538-013-0123-4.

[MB02] M. Moskalets and M. Büttiker. Floquet scattering theory of quantum pumps. *Phys. Rev. B*, 66:205320, Nov 2002. doi:10.1103/PhysRevB.66.205320.

[MB07] J. E. Moore and L. Balents. Topological invariants of time-reversal-invariant band structures. *Phys. Rev. B*, 75:121306, Mar 2007. doi:10.1103/PhysRevB.75.121306.

[MBB06] J. P. Morten, A. Brataas, and W. Belzig. Circuit theory of crossed Andreev reflection. *Phys. Rev. B*, 74:214510, Dec 2006. doi:10.1103/PhysRevB.74.214510.

[MCA+14] R. S. K. Mong, D. J. Clarke, J. Alicea, N. H. Lindner, P. Fendley, C. Nayak, Y. Oreg, A. Stern, E. Berg, K. Shtengel, and M. P. A. Fisher. Universal Topological Quantum Computation from a Superconductor-Abelian Quantum Hall Heterostructure. *Phys. Rev. X*, 4:011036, Mar 2014. doi:10.1103/PhysRevX.4.011036.

[McM68] W. L. McMillan. Theory of Superconductor—Normal-Metal Interfaces. *Phys. Rev.*, 175:559–568, Nov 1968. doi:10.1103/PhysRev.175.559.

[Moo69] G. E. Moore. Cramming more components onto integrated circuits. *Electronics*, 38:114–117, 1969.

[Mos11] M. V. Moskalets. *Scattering Matrix Approach to Non-Stationary Quantum Transport*. Imperial College Press, 2011.

[MR91] G. Moore and N. Read. Nonabelions in the fractional quantum hall effect. *Nuc. Phys. B*, 360:362–396, 1991. doi:10.1016/0550-3213(91)90407-O.

[MS89] G. Moore and N. Seiberg. Classical and quantum conformal field theory. *Comm. Math. Phys.*, 123:177–254, 1989. doi:10.1007/BF01238857.

[MST18] C. Moore, T. D. Stanescu, and S. Tewari. Two-terminal charge tunneling: Disentangling Majorana zero modes from partially separated Andreev bound states in semiconductor-superconductor heterostructures. *Phys. Rev. B*, 97:165302, Apr 2018. doi:10.1103/PhysRevB.97.165302.

[MZF+12] V. Mourik, K. Zuo, S. M. Frolov, S. R. Plissard, E. P. A. M. Bakkers, and L. P. Kouwenhoven. Signatures of Majorana Fermions in Hybrid Superconductor-Semiconductor Nanowire Devices. *Science*, 336:1003–1007, Mar 2012. doi:10.1126/science.1222360.

[MZST18] C. Moore, C. Zeng, T. D. Stanescu, and S. Tewari. Quantized zero-bias conductance plateau in semiconductor-superconductor heterostructures without topological Majorana zero modes. *Phys. Rev. B*, 98:155314, Oct 2018. doi:10.1103/PhysRevB.98.155314.

[NC00] M. A. Nielsen and I. L. Chuang. *Quantum Computation and Quantum Information*. Cambridge University Press, 2000.

[NPDBY13] S. Nadj-Perge, I. K. Drozdov, B. A. Bernevig, and A. Yazdani. Proposal for realizing Majorana fermions in chains of magnetic atoms on a superconductor. *Phys. Rev. B*, 88:020407, Jul 2013. doi:10.1103/PhysRevB.88.020407.

[NS18] T. Neupert and F. Schindler. Topological Crystalline Insulators. In *Topological Matter: Lectures from the Topological Matter School 2017*, pages 31–61. Springer International Publishing, Cham, 2018. doi:10.1007/978-3-319-76388-0_5.

[NSS+08] C. Nayak, S. H. Simon, A. Stern, M. Freedman, and S. Das Sarma. Non-Abelian anyons and topological quantum computation. *Rev. Mod. Phys.*, 80:1083–1159, Sep 2008. doi:10.1103/RevModPhys.80.1083.

[NW96] C. Nayak and F. Wilczek. 2n-quasihole states realize 2^{n-1}-dimensional spinor braiding statistics in paired quantum Hall states. *Nuc. Phys. B*, 479:529–553, Nov 1996. doi:10.1016/0550-3213(96)00430-0.

[ORvO10] Y. Oreg, G. Refael, and F. von Oppen. Helical Liquids and Majorana Bound States in Quantum Wires. *Phys. Rev. Lett.*, 105:177002, Oct 2010. doi:10.1103/PhysRevLett.105.177002.

[OTMS15] C. P. Orth, R. P. Tiwari, T. Meng, and T. L. Schmidt. Non-Abelian parafermions in time-reversal-invariant interacting helical systems. *Phys. Rev. B*, 91:081406, Feb 2015. doi:10.1103/PhysRevB.91.081406.

[PASJ17] E. Prada, R. Aguado, and P. San-Jose. Measuring Majorana nonlocality and spin structure with a quantum dot. *Phys. Rev. B*, 96:085418, Aug 2017. doi:10.1103/PhysRevB.96.085418.

[PGvO13] F. Pientka, L. I. Glazman, and F. von Oppen. Topological superconducting phase in helical Shiba chains. *Phys. Rev. B*, 88:155420, Oct 2013. doi:10.1103/PhysRevB.88.155420.

[PKA16] D. I. Pikulin, Y. Komijani, and I. Affleck. Luttinger liquid in contact with a Kramers pair of Majorana bound states. *Phys. Rev. B*, 93:205430, May 2016. doi:10.1103/PhysRevB.93.205430.

[PN12] D. I. Pikulin and Y. V. Nazarov. Phenomenology and dynamics of a Majorana Josephson junction. *Phys. Rev. B*, 86:140504, Oct 2012. doi:10.1103/PhysRevB.86.140504.

[PSJA12] E. Prada, P. San-Jose, and R. Aguado. Transport spectroscopy of NS nanowire junctions with Majorana fermions. *Phys. Rev. B*, 86:180503, Nov 2012. doi:10.1103/PhysRevB.86.180503.

[QZ11] X.-L. Qi and S.-C. Zhang. Topological insulators and superconductors. *Rev. Mod. Phys.*, 83:1057–1110, Oct 2011. doi:10.1103/RevModPhys.83.1057.

[RG00] N. Read and D. Green. Paired states of fermions in two dimensions with breaking of parity and time-reversal symmetries and the fractional quantum Hall effect. *Phys. Rev. B*, 61:10267–10297, Apr 2000. doi:10.1103/PhysRevB.61.10267.

[RLD+17] F. Reis, G. Li, L. Dudy, M. Bauernfeind, G. Glass, W. Hanke, R. Thomale, J. Schäfer, and R. Claessen. Bismuthene on a SiC substrate: A candidate for a high-temperature quantum spin Hall material. *Science*, 357:287–290, Jul 2017. doi:10.1126/science.aai8142.

[RO10] G. Rigolin and G. Ortiz. Adiabatic Perturbation Theory and Geometric Phases for Degenerate Systems. *Phys. Rev. Lett.*, 104:170406, Apr 2010. doi:10.1103/PhysRevLett.104.170406.

[Roy09] R. Roy. Z_2 classification of quantum spin Hall systems: An approach using time-reversal invariance. *Phys. Rev. B*, 79:195321, May 2009. doi:10.1103/PhysRevB.79.195321.

[RR96] N. Read and E. Rezayi. Quasiholes and fermionic zero modes of paired fractional quantum Hall states: The mechanism for non-Abelian statistics. *Phys. Rev. B*, 54:16864–16887, Dec 1996. doi:10.1103/PhysRevB.54.16864.

[RR99] N. Read and E. Rezayi. Beyond paired quantum Hall states: Parafermions and incompressible states in the first excited Landau level. *Phys. Rev. B*, 59:8084–8092, Mar 1999. doi:10.1103/PhysRevB.59.8084.

[RS15] E. I. Rashba and V. I. Sheka. Symmetry of Energy Bands in Crystals of Wurtzite Type II. Symmetry of Bands with Spin-Orbit Interaction Included. *New. J. Phys.*, 17:050202, 2015. Originally published in Fiz. Tverd. Tela: Collected Papers 2: 62–76, 1959.

[RSW09] E. Rowell, R. Stong, and Z. Wang. On Classification of Modular Tensor Categories. *Commun. Math. Phys.*, 292:343–389, 2009. doi:10.1007/s00220-009-0908-z.

[SBF+06] S. H. Simon, N. E. Bonesteel, M. H. Freedman, N. Petrovic, and L. Hormozi. Topological Quantum Computing with Only One Mobile Quasiparticle. *Phys. Rev. Lett.*, 96:070503, Feb 2006. doi:10.1103/PhysRevLett.96.070503.

[SCMA15] E. M. Stoudenmire, D. J. Clarke, R. S. K. Mong, and J. Alicea. Assembling Fibonacci anyons from a $\mathbb{Z}_3$ parafermion lattice model. *Phys. Rev. B*, 91:235112, Jun 2015. doi:10.1103/PhysRevB.91.235112.

[SCT11] J. D. Sau, D. J. Clarke, and S. Tewari. Controlling non-Abelian statistics of Majorana fermions in semiconductor nanowires. *Phys. Rev. B*, 84:094505, Sep 2011. doi:10.1103/PhysRevB.84.094505.

[SH16] B. Sothmann and E. M. Hankiewicz. Fingerprint of topological Andreev bound states in phase-dependent heat transport. *Phys. Rev. B*, 94:081407, Aug 2016. doi:10.1103/PhysRevB.94.081407.

[Sha94] R. Shankar. Renormalization-group approach to interacting fermions. *Rev. Mod. Phys.*, 66:129–192, Jan 1994. doi:10.1103/RevModPhys.66.129.

[Shi65] J. H. Shirley. Solution of the Schrödinger Equation with a Hamiltonian Periodic in Time. *Phys. Rev.*, 138:B979–B987, May 1965. doi:10.1103/PhysRev.138.B979.

[Sim83] B. Simon. Holonomy, the Quantum Adiabatic Theorem, and Berry's Phase. *Phys. Rev. Lett.*, 51:2167–2170, Dec 1983. doi:10.1103/PhysRevLett.51.2167.

[SJPA12] P. San-Jose, E. Prada, and R. Aguado. ac Josephson Effect in Finite-Length Nanowire Junctions with Majorana Modes. *Phys. Rev. Lett.*, 108:257001, Jun 2012. doi:10.1103/PhysRevLett.108.257001.

[SKS13] N. Sedlmayr, P. Korell, and J. Sirker. Two-band Luttinger liquid with spin-orbit coupling: Applications to monatomic chains on surfaces. *Phys. Rev. B*, 88:195113, Nov 2013. doi:10.1103/PhysRevB.88.195113.

[SLTDS10] J. D. Sau, R. M. Lutchyn, S. Tewari, and S. Das Sarma. Generic New Platform for Topological Quantum Computation Using Semiconductor Heterostructures. *Phys. Rev. Lett.*, 104:040502, Jan 2010. doi:10.1103/PhysRevLett.104.040502.

[SND+14] E. M. Spanton, K. C. Nowack, L. Du, G. Sullivan, R.-R. Du, and K. A. Moler. Images of Edge Current in InAs/GaSb Quantum Wells. *Phys. Rev. Lett.*, 113:026804, Jul 2014. doi:10.1103/PhysRevLett.113.026804.

[SPAW18] R. Skolasinski, D. I. Pikulin, J. Alicea, and M. Wimmer. Robust helical edge transport in quantum spin Hall quantum wells. *Phys. Rev. B*, 98:201404, Nov 2018. doi:10.1103/PhysRevB.98.201404.

[SRvOG12] T. L. Schmidt, S. Rachel, F. von Oppen, and L. I. Glazman. Inelastic Electron Backscattering in a Generic Helical Edge Channel. *Phys. Rev. Lett.*, 108:156402, Apr 2012. doi:10.1103/PhysRevLett.108.156402.

[Ste08] A. Stern. Anyons and the quantum Hall effect—A pedagogical review. *Ann. Phys. (N.Y.)*, 323:204–249, 2008. doi:10.1016/j.aop.2007.10.008.

[STG99] H. L. Stormer, D. C. Tsui, and A. C. Gossard. The fractional quantum Hall effect. *Rev. Mod. Phys.*, 71:S298–S305, Mar 1999. doi:10.1103/RevModPhys.71.S298.

[STL08] Z. W. S. Trebst, M. Troyer and A. W. Ludwig. A short introduction to Fibonacci anyon models. *Prog. Theor. Phys. Supp.*, 176:384–407, Jun 2008. doi:10.1143/PTPS.176.384.

[STL+10] J. D. Sau, S. Tewari, R. M. Lutchyn, T. D. Stanescu, and S. Das Sarma. Non-Abelian quantum order in spin-orbit-coupled semiconductors: Search for topological Majorana particles in solid-state systems. *Phys. Rev. B*, 82:214509, Dec 2010. doi:10.1103/PhysRevB.82.214509.

[Sto39] E. C. Stoner. Collective electron ferromagnetism. *Proc. R. Soc. London Ser. A*, 165:372–414, 1939. doi:10.1098/rspa.1938.0066.

[SWF+20] J. Strunz, J. Wiedenmann, C. Fleckenstein, L. Lunczer, W. Beugeling, V. L. Müller, P. Shekhar, N. Traverso Ziani, S. Shamim, J. Kleinlein, H. Buhmann, B. Trauzettel, and L. W. Molenkamp. Interacting topological edge channels. *Nat. Phys.*, 16(1):83–88, Jan. 2020. doi:10.1038/s41567-019-0692-4.

[TDSN+07] S. Tewari, S. Das Sarma, C. Nayak, C. Zhang, and P. Zoller. Quantum Computation using Vortices and Majorana Zero Modes of a $p_x + ip_y$ Superfluid of Fermionic Cold Atoms. *Phys. Rev. Lett.*, 98:010506, Jan 2007. doi:10.1103/PhysRevLett.98.010506.

[TG07] Y. Tanaka and A. A. Golubov. Theory of the proximity effect in junctions with unconventional superconductors. *Phys. Rev. Lett.*, 98:037003, Jan 2007. doi:10.1103/PhysRevLett.98.037003.

[TGKU07] Y. Tanaka, A. A. Golubov, S. Kashiwaya, and M. Ueda. Anomalous josephson effect between even- and odd-frequency superconductors. *Phys. Rev. Lett.*, 99:037005, Jul 2007. doi:10.1103/PhysRevLett.99.037005.

[TK09] J. C. Y. Teo and C. L. Kane. Critical behavior of a point contact in a quantum spin Hall insulator. *Phys. Rev. B*, 79:235321, Jun 2009. doi:10.1103/PhysRevB.79.235321.

[TLK17] M. Thakurathi, D. Loss, and J. Klinovaja. Floquet Majorana fermions and parafermions in driven Rashba nanowires. *Phys. Rev. B*, 95:155407, Apr 2017. doi:10.1103/PhysRevB.95.155407.

[Tom50] S.-I. Tomonaga. Remarks on Bloch's method of sound waves applied to many-fermion problems. *Prog. Theor. Phys.*, 5:544–569, Jul 1950. doi:10.1143/ptp/5.4.544.

[TPB11] A. M. Turner, F. Pollmann, and E. Berg. Topological phases of one-dimensional fermions: An entanglement point of view. *Phys. Rev. B*, 83:075102, Feb 2011. doi:10.1103/PhysRevB.83.075102.

[TSG82] D. C. Tsui, H. L. Stormer, and A. C. Gossard. Two-Dimensional Magnetotransport in the Extreme Quantum Limit. *Phys. Rev. Lett.*, 48:1559–1562, May 1982. doi:10.1103/PhysRevLett.48.1559.

[TSN12] Y. Tanaka, M. Sato, and N. Nagaosa. Symmetry and topology in superconductors –odd-frequency pairing and edge states–. *Journal of the Physical Society of Japan*, 81(1):011013, 2012. doi:10.1143/JPSJ.81.011013.

[TTG07] Y. Tanaka, Y. Tanuma, and A. A. Golubov. Odd-frequency pairing in normal-metal/superconductor junctions. *Phys. Rev. B*, 76:054522, Aug 2007. doi:10.1103/PhysRevB.76.054522.

[vDS98] J. von Delft and H. Schoeller. Bosonization for Beginners –Refermionization for Experts. *Ann. Phys.*, 7:225–305, 1998. doi:10.1002/(SICI)1521-3889(199811)7:4<225::AID-ANDP225>3.0.CO;2-L.

[VNAW19] A. Vuik, B. Nijholt, A. R. Akhmerov, and M. Wimmer. Reproducing topological properties with quasi-Majorana states. *SciPost Phys.*, 7:61, 2019. doi:10.21468/SciPostPhys.7.5.061.

[Vol94] G. E. Volovik. *The Universe in a Helium Droplet*. Oxford University Press, 1994.

[vOPP14] F. von Oppen, Y. Peng, and F. Pientka. Topological superconducting phases in one dimension. In *Topological Aspects of Condensed Matter Physics: Lecture Notes of the Les Houches Summer School*, pages 387–450. Oxford University Press, 2014.

[vWvHB+88] B. J. van Wees, H. van Houten, C. W. J. Beenakker, J. G. Williamson, L. P. Kouwenhoven, D. van der Marel, and C. T. Foxon. Quantized conductance of point contacts in a two-dimensional electron gas. *Phys. Rev. Lett.*, 60:848–850, Feb 1988. doi:10.1103/PhysRevLett.60.848.

[WADB11] M. Wimmer, A. R. Akhmerov, J. P. Dahlhaus, and C. W. J. Beenakker. Quantum point contact as a probe of a topological superconductor. *New Journal of Physics*, 13(5):053016, May 2011. doi:10.1088/1367-2630/13/5/053016.

[Wal16] M. M. Waldrop. More than Moore. *Nature*, 530:144–147, 2016. doi:10.1038/530144a.

[WAM+10] M. Wimmer, A. R. Akhmerov, M. V. Medvedyeva, J. Tworzydło, and C. W. J. Beenakker. Majorana Bound States without Vortices in Topological Superconductors with Electrostatic Defects. *Phys. Rev. Lett.*, 105:046803, Jul 2010. doi:10.1103/PhysRevLett.105.046803.

[WAvH+19] G. W. Winkler, A. E. Antipov, B. van Heck, A. A. Soluyanov, L. I. Glazman, M. Wimmer, and R. M. Lutchyn. Unified numerical approach to topological semiconductor-superconductor heterostructures. *Phys. Rev. B*, 99:245408, Jun 2019. doi:10.1103/PhysRevB.99.245408.

[WBZ06] C. Wu, B. A. Bernevig, and S.-C. Zhang. Helical Liquid and the Edge of Quantum Spin Hall Systems. *Phys. Rev. Lett.*, 96:106401, Mar 2006. doi:10.1103/PhysRevLett.96.106401.

[Wen91] X. G. Wen. Non-Abelian statistics in the fractional quantum Hall states. *Phys. Rev. Lett.*, 66:802–805, Feb 1991. doi:10.1103/PhysRevLett.66.802.

[Wen04] X.-G. Wen. *Quantum Field Theory of Many-Body Systems*. Oxford University Press, 2004.

[Wil82a] F. Wilczek. Magnetic Flux, Angular Momentum, and Statistics. *Phys. Rev. Lett.*, 48:1144–1146, Apr 1982. doi:10.1103/PhysRevLett.48.1144.

[Wil82b] F. Wilczek. Quantum Mechanics of Fractional-Spin Particles. *Phys. Rev. Lett.*, 49:957–959, Oct 1982. doi:10.1103/PhysRevLett.49.957.

[Wil90] F. Wilczek. *Fractional Statistics and Anyon Superconductivity*. World Scientific, 1990. doi:10.1142/0961.

[WZ84] F. Wilczek and A. Zee. Appearance of Gauge Structure in Simple Dynamical Systems. *Phys. Rev. Lett.*, 52:2111–2114, Jun 1984. doi:10.1103/PhysRevLett.52.2111.

[XCN10] D. Xiao, M.-C. Chang, and Q. Niu. Berry phase effects on electronic properties. *Rev. Mod. Phys.*, 82:1959–2007, Jul 2010. doi:10.1103/RevModPhys.82.1959.

[XQH+09] Y. Xia, D. Qian, D. Hsieh, L. Wray, A. Pal, H. Lin, A. Bansil, D. Grauer, Y. S. Hor, R. J. Cava, and M. Z. Hasan. Observation of a large-gap topological-insulator class with a single Dirac cone on the surface. *Nat. Phys.*, 5:398–402, May 2009. doi:10.1038/nphys1274.

[YTN11] T. Yokoyama, Y. Tanaka, and N. Nagaosa. Anomalous Meissner Effect in a Normal-Metal–Superconductor Junction with a Spin-Active Interface. *Phys. Rev. Lett.*, 106:246601, Jun 2011. doi:10.1103/PhysRevLett.106.246601.

[Zak89] J. Zak. Berry's phase for energy bands in solids. *Phys. Rev. Lett.*, 62:2747–2750, Jun 1989. doi:10.1103/PhysRevLett.62.2747.

[Zir96] M. R. Zirnbauer. Riemannian symmetric superspaces and their origin in random-matrix theory. *J. Math. Phys.*, 37:4986, 1996. doi:10.1063/1.531675.

[ZK14] F. Zhang and C. L. Kane. Time-Reversal-Invariant Z_4 Fractional Josephson Effect. *Phys. Rev. Lett.*, 113:036401, Jul 2014. doi:10.1103/PhysRevLett.113.036401.

[ZR99] P. Zanardi and M. Rasetti. Holonomic quantum computation. *Phys. Lett. A*, 264:94–99, 1999. doi:10.1016/S0375-9601(99)00803-8.

[ZS20] G. Zhang and C. Spånslätt. Distinguishing between topological and quasi Majorana zero modes with a dissipative resonant level. *Phys. Rev. B*, 102:045111, Jul 2020. doi:10.1103/PhysRevB.102.045111.

Acknowledgments

I like to thank all my colleagues from the group TP IV in Würzburg, who created a very pleasant social and professional atmosphere. In particular my supervisor Prof. Björn Trauzettel for continuous guidance and support even beyond scientific questions. My long year office mate and friend Niccoló Traverso Ziani for all our fruitful scientific collaborations, sustained support, numerous interesting discussions and a great hospitality at the University of Genova. Further, I wish to thank all my colleagues I had the chance to collaborate with, in particular, Fernando Dominguez, Alessio Calzona, Lorenzo Privitera, Jonas Strunz, Jonas Wiedenmann, Marin Bukov and Maura Sassetti. It was a pleasure to participate in international conferences and schools such as for instance the Topological Matter School in San Sebastian. Moreover, I will always gratefully remember the time I spent at the University of California in Berkeley, mainly made possible by the commitment of Prof. Trauzettel and Prof. Joel Moore. Last but not least I would like to thank all my family and friends, which encouraged and supported me throughout the years of my PhD. Especially, I wish to name my girlfriend Nina Lichtenberger for unconditional support in any situation.
Financial support was thankfully granted by the DFG (SFB 1170 and SPP 1666), the Helmholtz Foundation (VITI), the Elitenetzwerk Bayern (ENB graduate school on topological insulators) and the Studienstiftung des Deutschen Volkes.

List of publications

1. *Charge and spin density in the helical Luttinger liquid*, N. Traverso Ziani, C. Fleckenstein, F. Crépin, B. Trauzettel, Europhys. Lett. **113**, 37002 (2016).

2. *Chiral anomaly in real space from stable fractional charges at the edge of a quantum spin Hall insulator*, C. Fleckenstein, N. Traverso Ziani, B. Trauzettel, Phys. Rev. B **94**, 241406 (2016).

3. *Fractional charge oscillations in quantum dots with quantum spin Hall effect*, N. Traverso Ziani, C. Fleckenstein G. Dolcetto, B. Trauzettel, Phys. Rev. B **95**, 205418 (2017).

4. *Decaying spectral oscillations in a Majorana wire with finite coherence length*, C. Fleckenstein, F. Dominguez, N. Traverso Ziani, B. Trauzettel, Phys. Rev. B **97**, 155425 (2018).

5. *Conductance signatures of odd-frequency superconductivity in quantum spin Hall systems using a quantum point contact*, C. Fleckenstein, N. Traverso Ziani, B. Trauzettel, Phys. Rev. B **97**, 134523 (2018).

6. *Detection of fractional solitons in quantum spin Hall systems*, C. Fleckenstein, N. Traverso Ziani, B. Trauzettel, Europhys. Lett. **121**, 57003 (2018).

7. *The invisible Majorana bound state at the helical edge*, C. Fleckenstein, F. Keidel, B. Trauzettel, N. Traverso Ziani, Eur. Phys. J. Spec. Top. **227**, 1377 (2018).

8. *$\mathbb{Z}_4$ parafermions in Weakly Interacting Superconducting Constrictions at the Helical Edge of Quantum Spin Hall Insulators*, C. Fleckenstein, N. Traverso Ziani, B. Trauzettel, Phys. Rev. Lett. **122**, 066801 (2019).

9. *Interacting topological edge channels*, J. Strunz, J. Wiedenmann, C. Fleckenstein, L. Lunczer, W. Beugeling, V. L. Müller, P. Shekhar, N. Traverso Ziani, S. Shamim, J. Kleinlein, H. Buhmann, B. Trauzettel, L. W. Molenkamp, Nat. Phys. **16**, 83 (2020).

10. *Transport signatures of a Floquet topological transition at the helical edge*, C. Fleckenstein, N. Traverso Ziani, L. Privitera, M. Sassetti, B. Trauzettel, Phys. Rev. B **101**, 201401 (2020).

11. *From fractional solitons to Majorana fermions in a paradigmatic model of topological superconductivity*, N. Traverso Ziani, C. Fleckenstein, L. Vigliotti, B. Trauzettel, M. Sassetti, Phys. Rev. B **101**, 195303 (2020).